Università degli studi di Salerno

DIPARTIMENTO DI MEDICINA, CHIRURGIA E ODONTOIATRIA
"SCUOLA MEDICA SALERNITANA"

Dottorato di Ricerca in
Medicina Traslazionale Dello Sviluppo e dell'Invecchiamento Attivo

XXXII ciclo

Tesi di Dottorato in

Clinical characterization, genetic screening and genotype-phenotype associations in cerebellar and brainstem congenital defects

Coordinatore:

Prof. Palmiero Monteleone

Tutor:

Prof. Pietro Vajro

Candidata:

Dott.ssa Sara Nuovo

Anno Accademico 2018-2019

SUMMARY

OVERVIEW

Cerebellar and brainstem congenital defects (CBCDs) represent a wide spectrum of malformative disorders resulting from abnormal development of midbrain-hindbrain and characterised by high clinical and genetic heterogeneity. Due to the uncommonness of these conditions and the substantial under-recognition on brain imaging studies, limited information is available on their prevalence, genetic causes, natural history, and genotype-phenotype associations. Such a contingency of factors leads to uncertain prognosis and wrong counselling.

The aim of this thesis was to improve current knowledge of CBCDs through the creation of a multidisciplinar European network, involved in the collection of clinical-neuroradiological data and biological samples of the affected individuals. The genetic basis of mendelian CBCDs have been investigated through complementary molecular approaches, including Sanger sequencing, multiplex ligation-dependent probe amplification (MLPA), next-generation sequencing (NGS) techniques, and high-resolution targeted array comparative genomic hybridization (aCGH). Multivariate statistical methods have been applied to analyse genotype-phenotype associations and define predictors of disease progression. Bioinformatics modeling and functional studies have been performed to investigate the effect of genomic variants affecting known genes and to confirm the pathogenic role of new candidate disease-genes identified through whole exome sequencing (WES).

Among CBCDs-associated diseases, Joubert syndrome (JS), pontocerebellar hypoplasia (PCH), tubulinopathies and shrunken cerebellum have been explored in more detail and are discussed in distinct sections.

i. Population-based prevalence rates of JS in Italy have been estimated applying the standards of descriptive epidemiology. Mutational frequency and phenotypic spectrum of JS have been defined through collection and targeted resequencing of over 400 patients followed by aCGH analysis of selected cases. A retrospective collection of biochemical and clinical data of a subset of JS patients has been conducted to assess the frequency of chronic kidney disease (CKD) and identify a quantitative biomarker of the risk of CKD progression. A new JS-causing gene has been identified through WES analysis and confirmed by functional studies.
ii. Genetic causes of PCH have been investigated in more than 50 patients by Sanger sequencing, MLPA and targeted resequencing. Genotype-phenotype associations have been

explored through a statistical approach combining unsupervised hierarchical clustering and logistic regression analysis.

iii. Frequency and type of CBCDs have been investigated in 20 patients with mutations in tubulin genes through magnetic resonance and diffusion tensor imaging. A new gene has been identified by WES causing an autosomal recessive tubulinopathy-like disorder.

iv. Two patients presenting with shrunken cerebellum and non-progressive congenital ataxia due to mutations in different genes have been identified. In the first case, the existence of a mutation-specific atypical inheritance pattern has been ascertained; in the second case, an expansion of clinical and mutational spectrum has been observed.

Altogether, the results of our study demonstrate that the creation of a clinical and research network represents a valuable strategy for the study of rare diseases such as CBCDs, providing expertise for patient assessment, genetic characterization and functional validation of new candidate genes. Furthermore, the proposed molecular workflow has proved to be a successful, cost-effective strategy for the identification of the genetic cause in many different CBCDs, showing detection rates equal to or greater than values reported in the literature. Besides increasing knowledge about the genetic causes of CBCDs, our findings give new insight on the epidemiology, phenotypic spectrum, natural history, and inheritance pattern of this group of disorders.

ABBREVIATIONS

CA: cerebellar atrophy; CBCDs: cerebellar and brainstem congenital defects; CCD: cortical cerebellar dysplasia; CD: cerebellar dysplasia; CDG: Congenital disorders of glycosylation; CKD: chronic kidney disease; CNVs: Copy Number Variants; CSTs: corticospinal tracts; DCCMs: dynamic cross correlation maps; DDAVP: 1- deamino-arginine vasopressin; DEC: directionally encoded colour; DTI: diffusion tensor imaging; DWM: Dandy-Walker malformation; EEG: electroencephalogram; eGFR: estimated glomerular filtration rate; gnomAD: Genome Aggregation Database; HGPPS: horizontal gaze palsy and progressive scoliosis; HGVS: Human Genome Variation Society; IQR: interquartile range; JS: Joubert syndrome; MCDs: malformations of cortical development; MCPs: middle cerebellar peduncles; MLPA: multiple ligation probe amplification; MRI: magnetic resonance imaging; MTS: molar tooth sign; NGS: next-generation sequencing; NPCA: nonprogressive congenital ataxia; NPH: nephronophthisis; NRF: normal renal function; PCH: Pontocerebellar hypoplasia; PCR: polymerase chain reaction; PF: posterior fossa; PMG: polymicrogyria; PTMs: posttranslational modifications; RMSD: root mean square deviation; RMSF: root mean square fluctuation; SD: standard deviation; SHH: Sonic Hedgehog; TPF: transverse pontine fibers; UCD: urinary concentration defect; UPS: ubiquitin-proteasome system; US: ultrasound; WB: Western Blot; WES: whole exome sequencing

BACKGROUND

Cerebellar and brainstem congenital defects (CBCDs) represent a wide spectrum of malformative disorders resulting from abnormal development of midbrain-hindbrain, characterised by high clinical and genetic heterogeneity.

The embryology of these structures begins approximately at 3 weeks gestation continuing until 20 months of postnatal life [1], and is finely regulated by overlapping sets of genes **(Fig.1)** [2].

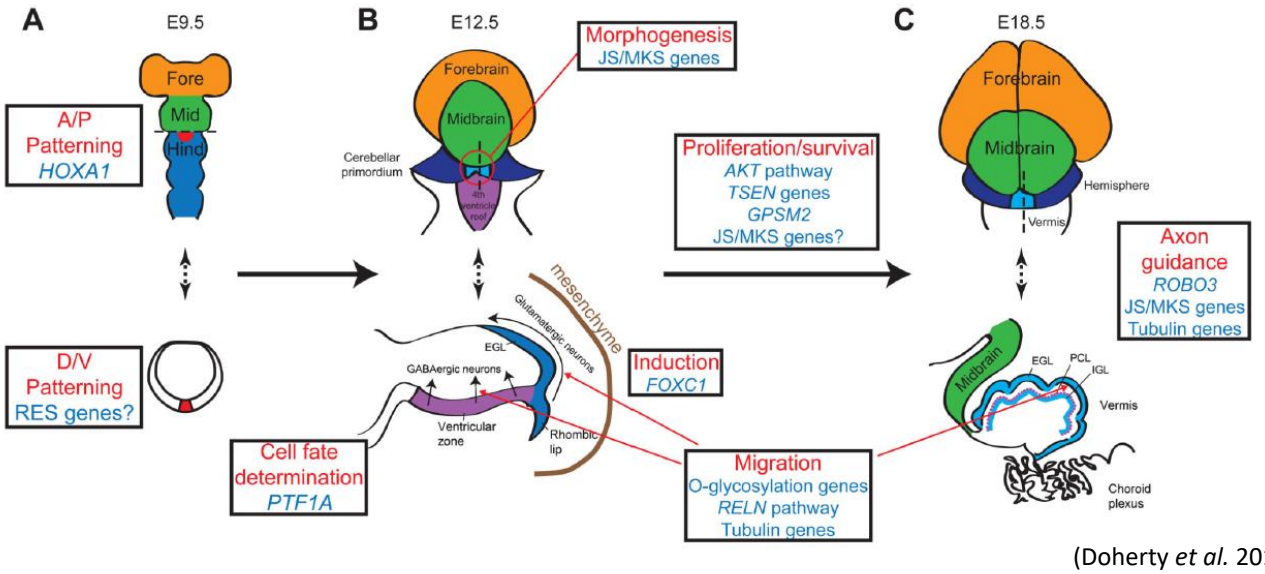

(Doherty *et al.* 2013)

Fig.1. Midbrain-hindbrain development and genes associated with human mid-hindbrain malformations. Representative stages of midbrain-hindbrain development in mouse embryo. The upper diagrams depict dorsal views at E9.5, E12.5 and E18.5 (days after conception). Dotted lines in the upper diagrams indicate the position of the axial (A) or sagittal (B and C) cross sections depicted in the lower diagrams. **(A)** *HOXA1* is involved in Anterior/Posterior (A/P) patterning of the mid-hindbrain, while rhombencephalosynapsis may be due to defects in Dorsal/Ventral (D/V) patterning at the most dorsal and rostral portion of the hindbrain (red area), where the cerebellar vermis is formed. **(B)** The upper diagram shows the location of early vermis formation (red circle), that may require the genes involved in Joubert/Meckel syndromes. Lower image shows *PTF1A* expressed in the cerebellar ventricular zone is required for GABAergic Purkinje cell precursor fate, *FOXC1* is necessary for induction between mesenchyme and rhombic lip, while the *RELN* pathway, O-glycosylation genes, and tubulin genes are likely required for migration of precursors out of the rhombic lip and ventricular zone. **(C)** By E18.5, the cerebellar hemispheres (blue in upper figure) and the vermis (light blue in upper figure) have partially formed. The midline sagittal (lower) diagram depicts early foliation and cortical lamination. Multiple pathways are likely involved in proliferation, migration, and survival of neuronal precursors and other cell types. *ROBO3*, Joubert/Meckel and tubulin genes are required for axon guidance to establish connections with cerebellar and brainstem nuclei. Fore: Forebrain, Hind: Hindbrain, Mid: Midbrain, RES: rhombencephalosynapsis.

The brainstem is composed of the midbrain, derived from the embryonic mesencephalon, the pons, formed from the rostral part of the hindbrain (metencephalon), and the medulla, formed from the caudal part of the hindbrain (myelencephalon). The cerebellum, which is a dorsal extension of the rostral hindbrain, is composed of the midline vermis and the bilateral hemispheres [2]. Conventional magnetic resonance imaging (MRI) sequences allow detailed evaluation of the anatomy of the posterior fossa (PF) and its contents. A midline sagittal T1-weighted or T2-weighted sequence is ideal for showing the overall size of the PF, the shape and size of the vermis, and the size and morphology of the fourth ventricle and brainstem **(Fig.2A)** [3]. The vermis is divided into three sections by the primary and prepyramidal fissures. The rostrocaudal length of the ventral pons at its largest point should be approximately twice that of the midbrain from the isthmus (ventral midbrain-pons junction) to the third ventricle, whereas the rostrocaudal length of the midbrain should be roughly the same as that of the medulla (from the obex to the ventral pontomedullary junction). The posterior margin of the brainstem (from the caudal sylvian aqueduct to the obex) should be a straight line. The fastigium (or summit of the fourth ventricle), should lie just below the midpoint of the ventral pons on sagittal images **(Fig.2A)**. Parasagittal sections are useful for evaluating the cerebellar hemispheres and peduncles, whereas the size and morphology of the vermis, cerebellar hemispheres, dentate nuclei, and superior and middle cerebellar peduncles can be best evaluated on axial images. In particular, the hemispheric folia of the inferior half of the

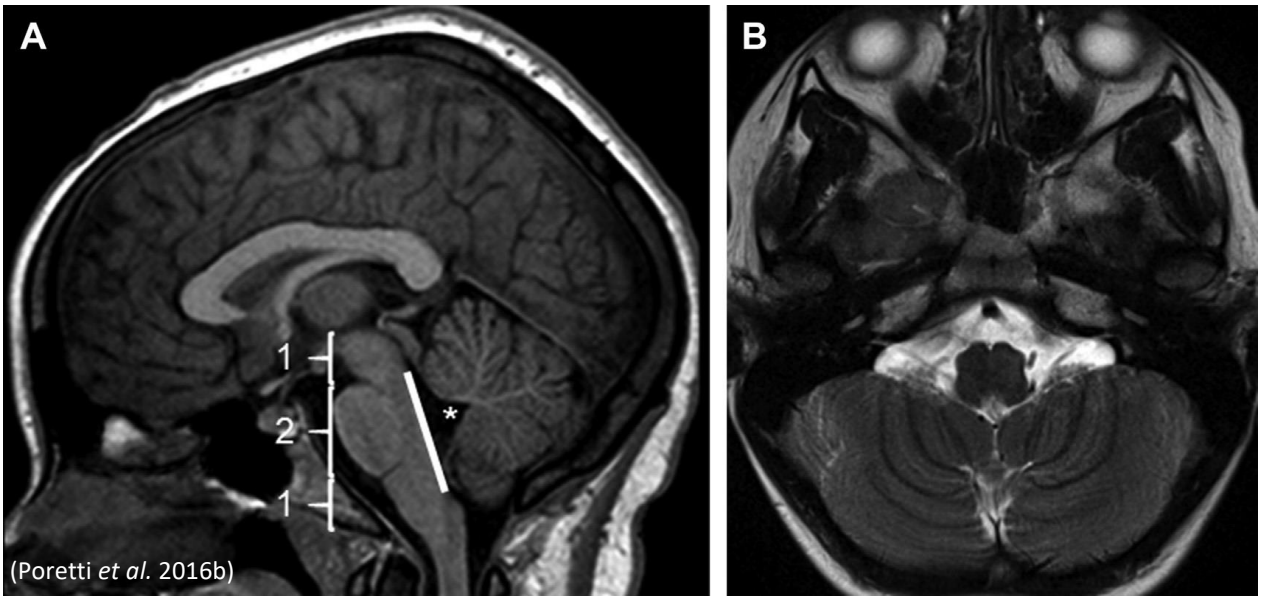

Fig.2. Normal MRI images of the posterior fossa. (A) Midsagittal T1-weighted MR image shows a normal-sized posterior fossa, a normal vermis, right-sized pons (the rostrocaudal length is approximately twice [2] that of the midbrain [1] and medulla [1]), a flat dorsal surface of the brainstem (*line*) and an appropriately positioned fastigium just below the midpoint of the ventral pons (*asterisk*). **(B)** Axial T2-weighted MR image shows normal orientation of the cerebellar folia, running parallel to the calvaria (onionlike orientation).

cerebellum run parallel to the calvarium (onionlike configuration) **(Fig.2B)**. On coronal sections, the cerebellar hemispheres are characterized by fissures radiating towards the cerebellar nuclei, especially at the level of the vermian nodulus. In the end, the superior, middle, and inferior cerebellar peduncles should be evaluated for size, contour, and location [2,3].

Only a few prevalence data are available on CBCDs, due to the uncommonness of these conditions and the substantial under-recognition on brain imaging studies. In particular, the estimated prevalence for Dandy-Walker malformation (DWM) ranges from ∼1 per 30,000 to 1 per 5,000 population [2,4], while a birth prevalence of 1.30 per 100,000 was found for cerebellar hypoplasia [5].

Due to the increasing use of prenatal ultrasound (US) and MRI to evaluate the fetal brain, CBCDs are often diagnosed before birth [6], with variable outcome [7,8]. Specifically, prenatal US can identify cerebellar hypoplasia, abnormal fluid collections in the PF or poor delineation of PF landmarks, while fetal MRI is required to appreciate more subtle morphological anomalies [2].

Postnatal clinical presentation of CBCDs is variable and typically non-specific. The most frequently observed features include hypotonia, motor delay, ataxia, nystagmus, and decreased visual attention [2]. Cognitive impairment is common, occasionally associated with autistic spectrum disorder [2,9,10]. Cranial nerve involvement can also be present, resulting in abnormal eye movements, ptosis, facial palsy, hearing loss or facial and corneal anesthesia. Some patients are more severely affected, presenting with apnea, dysphagia, aspiration, spasticity, epilepsy, or lack of developmental progress. Conversely, neurodevelopmental outcome can also be favorable, and mildly affected patients may have subtle manifestations, such as isolated cranial nerve dysfunction [2]. In addition to features shared by different CBCDs, peculiar clinical signs have been identified, prompting towards a specific diagnosis. For instance, alternating tachypnea or apnea, polydactyly, coloboma, retinal dystrophy, and kidney or liver disease can be observed in a subset of patients with Joubert Syndrome (JS). Analogously, most patients with rhombencephalosynapsis have persistent head-shaking, while others present with scalp alopecia, trigeminal anesthesia and hyperactivity [2]. Furthermore, laboratory testing can be useful in the differential diagnosis: elevated blood creatine kinase levels are often detected in patients with cobblestone malformations, abnormal transferrin glycosylation is typical of Congenital Disorders of Glycosylation (CDG), while low to undetectable insulin levels in the presence of hyperglycemia are suggestive for *PTF1A*-related cerebellar and pancreatic agenesis [2].

The widespred diffusion of next-generation sequencing (NGS) techniques has considerably increased the diagnostic rate of CBCDs, allowing the identification of the underlying genetic defect in many families [11,12]. Furthermore, chromosomal aneuploidies and Copy Number Variants (CNVs) can explain an additional part of CBCDs cases [6,13–16], especially in patients presenting with DWM [17–20]. Although many of these conditions are caused by parentally inherited or *de novo* occurring mutations, for some others the genetic etiology still remains unknown.

Different classification schemes for CBCDs have been proposed over time including both genetic and acquired forms [1,3,21–24]. The first comprehensive categorization was performed by Barkovich and colleagues [23], relying on known embryologic, genetic, imaging, and pathophysiologic information. Basing on these data, the following macro-categories have been identified: (i) malformations secondary to early anteroposterior and dorsoventral patterning defects, or to misspecification of mid-hindbrain germinal zones; ii) malformations associated with later generalized developmental disorders that significantly affect the brainstem and cerebellum (and have a pathogenesis that is at least partly understood); (iii) localized brain malformations that significantly affect the brainstem and cerebellum (pathogenesis partly or largely understood, including local proliferation, cell specification, migration and axonal guidance); and (iv) combined hypoplasia and atrophy in putative prenatal onset degenerative disorders [23]. Nevertheless, the practical "every day" approach to a patient with a midbrain-hindbrain malformation is based mainly on the neuroimaging "pattern recognition" approach, initially introduced by Doherty and collaborators [2] and further developed by Bosemani and colleagues [24]. According to this classification system, CBCDs fall within one of the following groups, each including distinct nosological entities: (i) predominantly cerebellar malformations; (i) cerebellar and brainstem malformations; (iii) predominantly brainstem malformations; (iv) predominantly midbrain malformations **(Tab.1)**. Based on this scheme, Poretti *et al* accurately defined the characteristic neuroimaging features of a variety of cerebellar and brainstem malformations, in order to improve the diagnostic work-up of these conditions [3,25].

This thesis mainly focuses on specific CBCDs-associated diseases, that will be discussed in more detail.

Tab.1. Neuroimaging-based differential diagnosis for congenital posterior fossa abnormalities

Neuroimaging Pattern	Malformations
Predominantly cerebellar Involvement	
Predominantly vermian	DWM and other cystic lesions of the posterior fossa, including Blake pouch cyst, mega cisterna magna, and arachnoid cysts; isolated vermian hypoplasia; rhombencephalosynapsis
Global cerebellar	Malformations of cortical development: lissencephaly (*RELN*, *VLDRL*, tubulin genes), polymicrogyria (tubulin genes, *GPR56*), periventricular nodular heterotopia (*FLNA*), and primary microcephaly; macrocerebellum; cerebellar dysplasia, including Chudley-McCullough syndrome; global cerebellar hypoplasia in multiple genetic syndromes (e.g. Ritschcer-Schinzel syndrome, CHARGE syndrome, Delleman syndrome); congenital CMV infection
Unilateral cerebellar	Isolated unilateral cerebellar hypoplasia, PHACES syndrome, *COL4A1* mutations, cerebellar cleft
Cerebellar and brainstem involvement	PCH type 1–10; glycosylation type 1a congenital disorder; *CASK* mutations; Joubert syndrome; cerebellar agenesis caused by a disruptive lesion or representing a malformation due to *PTF1A* mutations; congenital muscular dystrophies due to defective dystroglycan O-glycosylation; vanishing cerebellum in Chiari 2 malformation; cerebellar disruption secondary to prematurity
Predominantly brainstem involvement	Pontine tegmental cap dysplasia; horizontal gaze palsy and progressive scoliosis (*ROBO3* mutations)
Predominantly midbrain involvement	Dysplasia of the diencephalic-mesencephalic junction

CHARGE: coloboma, heart defect, choanal atresia, retarded growth and development, genital abnormality, and ear abnormality, CMV: cytomegalovirus, DWM: Dandy-Walker malformation, PCH: pontocerebellar hypoplasia.

(Bosemani *et al.* 2015)

JOUBERT SYNDROME

Joubert syndrome (JS) is an autosomal or X-linked recessive congenital ataxia whose diagnosis is based on the presence of a unique cerebellar and brainstem malformation recognisable on brain imaging, known as *molar tooth sign* (MTS) [26] **(Fig.3)**.

To date, descriptive epidemiology data such as population-based prevalence rates are almost completely lacking. The commonly reported range of 1:80,000-100,000 livebirths [27] is probably underestimated due to low awareness of MTS in historical texts [26]. Furthermore, it does not reflect the presence of the disease at later ages, since medical complications in JS can lead to early death [28]. A recent systematic review attempted to estimate the prevalence of childhood ataxia across World Health Organization regions. Among the 115 articles included, only one referred to JS: the estimated prevalence in Swedish children at 31 December 1992 was 0.17 per 100,000 (based on a single JS case) [29].

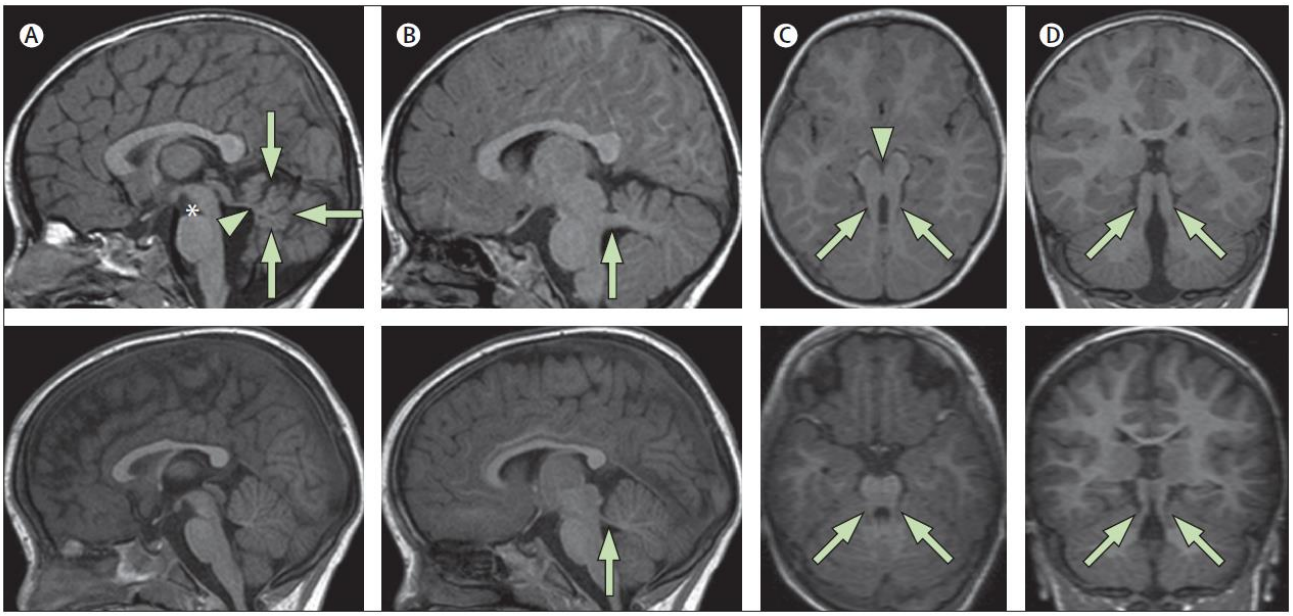

(Romani *et al.* 2013)

Fig.3. Neuroimaging findings in a 2-year-old child with Joubert Syndrome (upper panels) compared with a healthy control child (lower panels). (A) Midsagittal T1-weighted image shows a moderate hypoplasia and dysplasia of the cerebellar vermis (arrows) with secondary distortion and enlargement of the fourth ventricle with rostral shifting of the fastigium (arrowhead). A deepened interpeduncular fossa is also noted (asterisk). **(B)** Parasagittal T1-weighted image shows the thickened, elongated, and horizontally orientated superior cerebellar peduncles (arrow). **(C)** Axial T1-weighted image at the pontomesencephalic junction shows the molar tooth sign with a deepened interpeduncular fossa (arrowhead) and elongated, thickened, and horizontally orientated superior cerebellar peduncles (arrows). Additionally, the cerebellar vermis seems to be hypoplastic and its remnants dysplastic. **(D)** Coronal T1-weighted image reveals the thickened superior cerebellar peduncles (arrows).

Neurological signs appear in the neonatal period and include hypotonia progressing to ataxia, developmental delay, oculomotor apraxia, and breathing dysregulation. In addition, a wide spectrum of organ defects can be observed at different ages. Among these, the most common are retinal defects (from Leber congenital amaurosis to slowly progressive retinopathy), renal disease, and congenital liver fibrosis. Rarer features include chorioretinal or optic nerve colobomas, congenital heart malformations, situs inversus, scoliosis, skeletal dysplasia, Hirschsprung disease, and midline orofacial defects. In particular, the association of JS with polydactyly and midline oral and facial defects defines the so-called orofaciodigital type VI syndrome **(Fig.4)** [26]. With respect to neuropsychological phenotype, 65% of cases present with intellectual disability, and abnormal electroencephalogram (EEG) seems to predict lower neuropsychological functions [30]. Among JS patients, the leading causes of death are respiratory failure (35%) before 6 years of age, and kidney failure (37.5%), which is more common in older individuals [28]. An additional life-threatening complication is liver fibrosis [31,32], requiring surgical or pharmacological early intervention [33–36].

JS presents high genetic heterogeneity, with over 40 causative genes identified [37–45]. All the genes code for proteins of the primary cilium **(Fig.5)**, a ubiquitous subcellular organelle involved in embryonic development and in many cellular functions, including signal transduction, as well as regulation of tissue maintenance, polarity, and proliferation. This makes JS part of an expanding group of disorders known as ciliopathies, characterised by a marked phenotypic and genetic overlap **(Fig.6)** [26,37]. Despite the acceleration in gene discovery enabled by NGS, the overall detection rate for JS is estimated at ~60% [11], suggesting further genetic heterogeneity. Genotype–phenotype correlations are known only for few genes. The most relevant one has been established between *TMEM67* and JS with liver involvement [11,46,47]. In particular, *TMEM67* accounts for about 80% of individuals with this rare phenotype, whereas only a few have mutations in other genes such as *CC2D2A* or *RPGRIP1L* [48]. Another statistically significant association has been drawn between *CEP290* and retinal dystrophy [11,49]. Additional genotype-phenotype correlations have been proposed for *TMEM67* with coloboma [11,46], *CEP290* with kidney disease [11,49], *CPLANE1* (previously referred to as *C5orf42*) with polydactyly and hypothalamic hamartoma [11,50], *OFD1* with encephalocele [11], *TCTN2* with encephalocele and polydactyly [11], *AHI1* with retinal disease [11,51], and *CC2D2A* with ventriculomegaly and seizures [52]. Nevertheless, genotype–phenotype correlations remain problematic. For example, the founder mutation Arg73Cys in *TMEM216* causes a JS phenotype that can be pure or variably associated with polydactyly, renal disease, orofaciodigital features, and retinopathy [53]. This evidence, together with the lack of reliable prognostic indicators,

make it difficult to predict organ damage in young JS patients. An extra layer of complexity is represented by the identification of single heterozygous variants affecting JS-causative genes in many patients analyzed trough NGS approach, the pathogenic significance of which still remains unclear [26,54]. These variants could be hypothesised to act as genetic modifiers of the phenotype, and mutations in more than one gene have indeed been reported in some patients with JS who underwent several screenings or whole-exome sequencing (WES) [26]. Alternatively, they could represent one of the two mutated alleles expected for an autosomal recessive condition; in this case, the second mutation might consist of a deep-intronic variant, an intragenic rearrangement or a CNV, not easily detectable trough conventional NGS and requiring different molecular approaches, as showed by many recent publications [55–57]. All these evidences make JS an interesting model for understanding mendelian disorders characterised by high clinical and genetic heterogeneity, highlighting the need for additional studies.

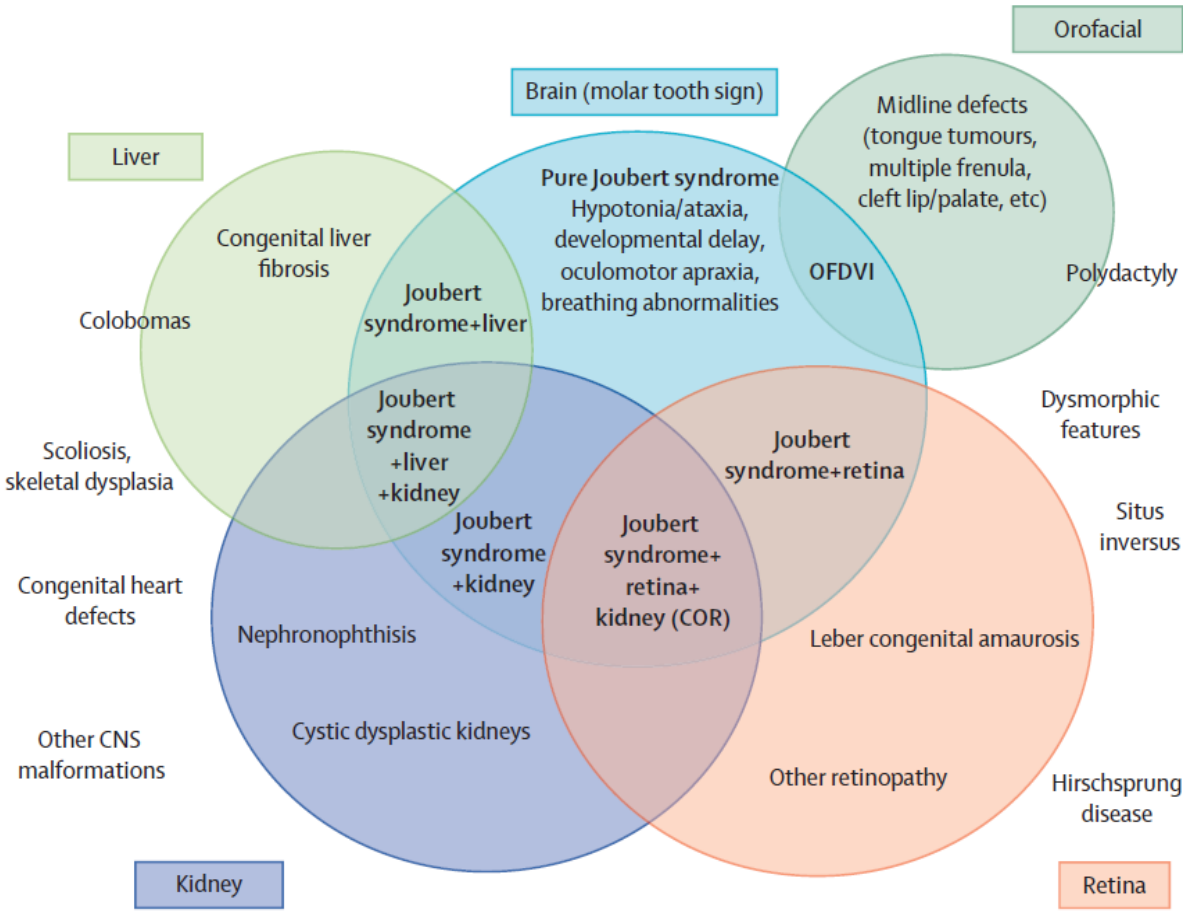

(Romani *et al.* 2013)

Fig.4. Clinical subgroups in Joubert syndrome. Colobomas are more frequent in patients with Joubert syndrome and hepatopathy but can also be present in other subgroups. Similarly, polydactyly (especially pre-axial or meso-axial) is invariably present in the OFDVI subgroup, but post-axial polydactyly is also frequent in other Joubert syndrome phenotypes. Clinical features outside the circles occur rarely, without a specific association with a clinical subgroup. COR: cerebello-oculo-renal. OFDVI: orofaciodigital type VI syndrome.

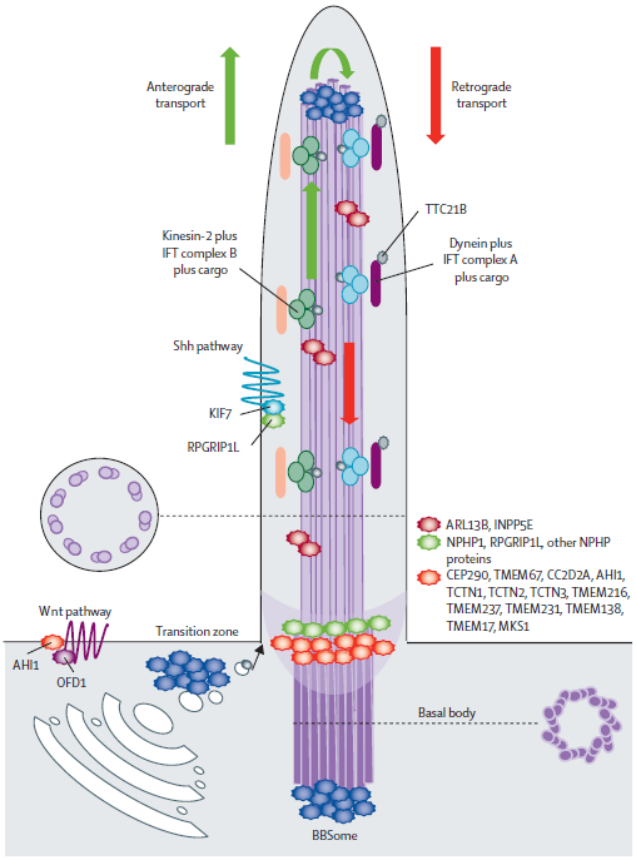

(Romani *et al.* 2013)

Fig.5. Schematic representation of the structure of the primary cilium depicting the main subciliary compartments. The image clearly shows the localization of BBSome, transition zone, NPH complex (light green), as well as IFT subcomplexes IFT-A and IFT-B (mediating retrograde and anterograde transport, respectively). Most proteins that are mutated in Joubert syndrome and Meckel syndrome cluster in large complexes at the basal body or the transition zone of the cilium. These complexes participate in the regulation of ciliogenesis, control the trafficking of specific pools of molecules targeted to the cilium, and are implicated in signalling pathways mediated by the cilium. Other Joubert syndrome proteins are also found along the ciliary axoneme or interact with Shh or Wnt pathways, which have crucial roles in embryonic development. BBS: Bardet–Biedl syndrome; IFT: intraflagellary transport; NPH: Nephronophthisis Shh: Sonic Hedgehog Homolog; Wnt: Wingless-related integration site.

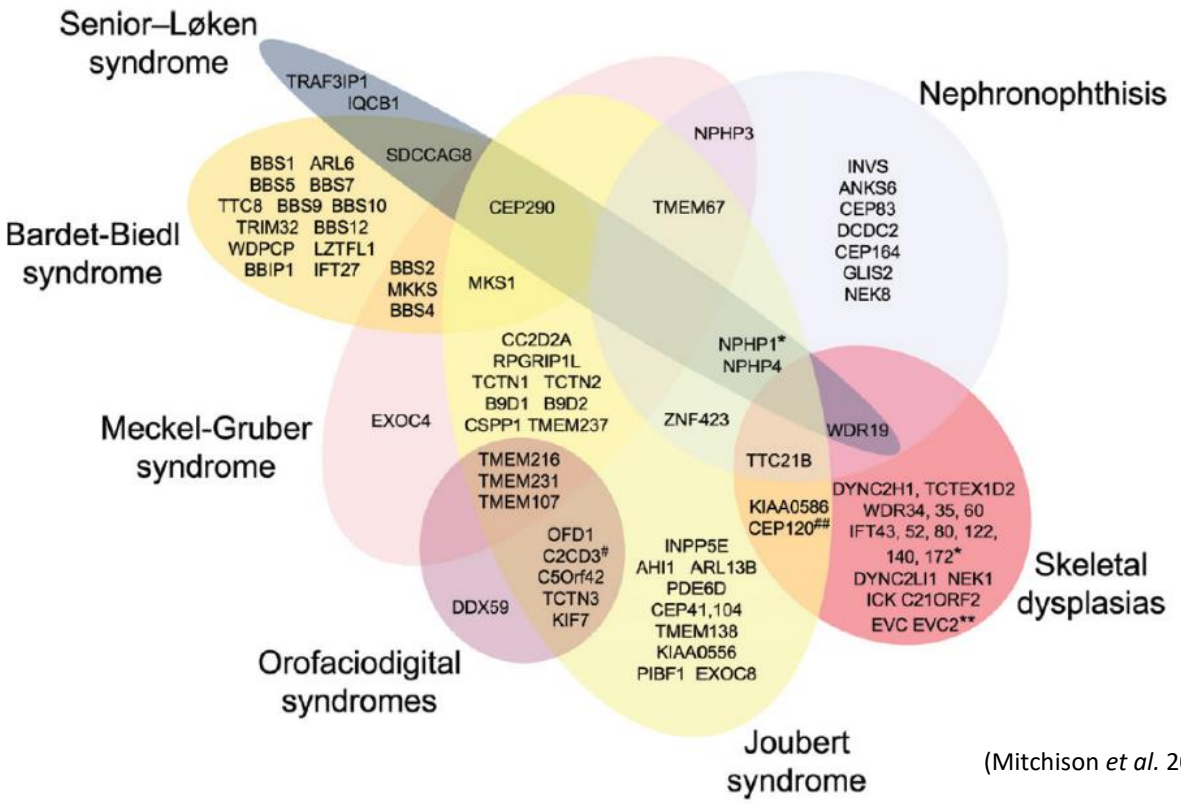

(Mitchison *et al.* 2017)

Fig.6. Clinical and genetic variability of primary ciliopathies. Venn diagram summarizing the genetic overlap among distinct ciliopathies. *Also found mutated in a single family with Bardet Biedl Syndrome; **Also proposed as a novel candidate gene for Meckel Syndrome; #Also found mutated in a single family with skeletal dysplasia; ##Also found mutated in a fetus resembling Meckel Syndrome.

PONTOCEREBELLAR HYPOPLASIA

Pontocerebellar hypoplasia (PCH) represents a heterogeneous group of inherited neurodegenerative disorders usually with prenatal onset, primarily affecting cerebellum and pons, possibly associated with supratentorial involvement. In particular, hypoplasia with superimposed atrophy of the cerebellum and absence or significant reduction of the pontine prominence are characteristic findings of PCH [3]. Clinical consequences include global developmental delay and a variable association of additional features, mainly neurological [58,59]. To date, 13 different subtypes have been described, based on clinical, neurological and biochemical features, as well as on the underlying genetic defect (https://www.omim.org/phenotypicSeries/PS607596) [59,60] (**Tab.2**).

Tab.2. Overview of pontocerebellar hypoplasia subtypes with associated gene defect

Subtype	Symptoms/ distinctive features in addition to PCH	Subcategory and gene	Gene function
PCH1	Motor neuron degeneration, muscle weakness, hypotonia, respiratory insufficiency, congenital contractures	PCH1A: *VRK1*	Neuronal migration
		PCH1B: *EXOSC3*	mRNA degradation
		PCH1C: *EXOSC8*	mRNA degradation
		PCH1D: *SLC25A46*	Mitochondrial fission and fusion
PCH2	Generalized clonus, impaired swallowing, dystonia, chorea, progressive microcephaly	PCH2A: *TSEN54*	tRNA splicing
		PCH2B: *TSEN2*	tRNA splicing
		PCH2C: *TSEN34*	tRNA splicing
		PCH2D*: *SEPSECS*	Selenocysteine synthesis
		PCH2E: *VPS53*	Unknown
		PCH2F: *TSEN15*	tRNA splicing
PCH3	Facial dysmorphism, optic atrophy, cerebellar atrophy	*PCLO**	Regulation synaptic protein & vesicle formation
PCH4	Severe form of PCH2 with congenital contractures and polyhydramnios	*TSEN54*	tRNA splicing

PCH5	Severe form of PCH2 with congenital contractures and polyhydramnios (identical to PCH4)	*TSEN54*	tRNA splicing
PCH6	Hypotonia, seizures, elevated CSF lactate, progressive supratentorial atrophy	*RARS2**	Arginyl tRNA synthetase
PCH7	disorders of sex development, thin corpus callosum, enlarged ventricles	*TOE1*	RNA processing
PCH8	Abnormal muscle tone, dystonia, ataxia, no/little disease progression. Non-degenerative.	*CHMP1A*	Regulation INK4A
PCH9	Abnormal muscle tone, impaired swallowing, corpus callosum agenesis and “Fig. 8” configuration of brainstem	*AMPD2*	Regulation GTP synthesis
PCH10	Abnormal muscle tone, seizures, motor neuron degeneration, mild cerebellar hypoplasia/atrophy	*CLP1*	tRNA splicing
PCH11	Non-progressive/ non-degenerative PCH	*TBC1D23*	Intracellular vesicle transport
PCH12	PCH with microcephaly and multiple contractures	*COASY*	CoA synthesis pathway
PCH13	PCH with feeding difficulties, dysmorphic features, thin corpus callosum	*VPS51*	canonical membrane fusion events in the process of endocytic recycling

PCH: pontocerebellar hypoplasia; *Imaging suggests postnatal onset of neurodegeneration in (a subset of) patients in this group

(adapted from Van Dijk et al. 2018)

PCH is an extremely rare disorder, whose overall incidence is unknown. PCH2A caused by homozygosity for the p.A307S mutation in *TSEN54* is the most frequent type of PCH, with an estimated incidence < 1:200.000 [61].

An autosomal recessive inheritance has been reported for almost all the 21 PCH genes identified so far [59,60,62–65] with the exception of *KIF26B*, described with a heterozygous *de novo* variant in a single PCH patient [66]. Moreover, mutations in the *CASK*, *RELN*, and *VLDLR* genes may also result in severe cerebellar and pontine hypoplasia [3]. While *RELN* and *VLDLR* are recessive genes, *CASK* mutations are inherited with an X-linked pattern, usually occurring *de novo*, and more commonly affect female patients, which display intellectual disability and microcephaly [67]. Interestingly, a certain number of PCH males with *CASK* mutations have also been identified [67–72], with the less severe cases displaying germline hypomorphic variants or inactivating variants in a mosaic state [67,68,71,72].

Many genotype-phenotype correlations have been hypothesized, especially for the earliest identified and most frequently mutated genes [58]. In particular, Namavar and collaborators [73] showed that the common homozygous p.A307S variant in *TSEN54* is clinically associated with dyskinesia and/or dystonia and variable degrees of spasticity. In addition, they found a strong statistically significant association between the above-mentioned variant and a dragonfly-like cerebellar pattern on magnetic resonance imaging (MRI), characterized by flat and severely undersized cerebellar hemispheres with a relatively spared vermis **(Fig.8A-B)**.

With regard to *CASK* gene, the largest case series [68,69,72] describe progressive microcephaly and severe developmental delay as almost invariably traits, often associated with feeding difficulties, muscular hypotonia, extrapyramidal signs or spasticity. Additional features such as epilepsy, ophthalmologic abnormalities, sensorineural hearing loss and facial dysmorphisms have also been observed. MRI images often display a butterfly-like pattern (with cerebellar hemispheres and vermis similarly involved), in addition to a variable grade of pons hypoplasia and a normal-sized corpus callosum [68,69,72,74] **(Fig.8C-D)**. Lastly, mutations in *EXOSC3* are commonly responsible for PCH combined with spinal muscular atrophy, characterized by generalized muscle weakness and profound psychomotor retardation. Moreover, a genotype-related variability in survival, clinical severity and neuroimaging pattern has been reported [75–78].

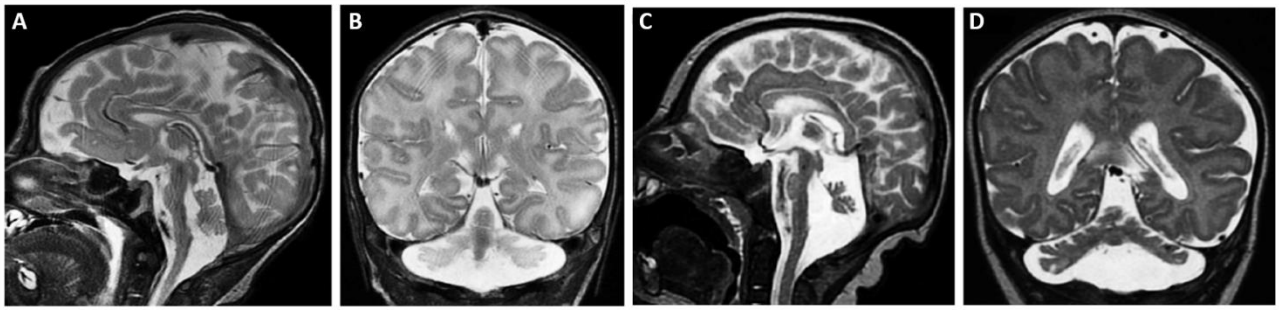

(Poretti *et al.* 2016)

Fig.8 MRI variable patterns of pontocerebellar hypoplasia. (A) Midsagittal and **(B)** coronal T2-weighted MR images of a child with pontocerebellar hypoplasia type 2 and *TSEN54* mutations show hypoplasia of the pons and cerebellum with more severe involvement of the cerebellar hemispheres compared with the vermis (dragonfly appearance). The structure of the cerebellar hemispheres appears to be melting, representing the degenerative nature of the disease. Microcephaly and thin corpus callosum are also noted. **(C)** Midsagittal and **(D)** coronal T2-weighted MR images of a girl with *CASK* mutation reveal hypoplasia of the pons and cerebellum with proportionate involvement of the cerebellar hemispheres compared with the vermis (butterfly appearance). Microcephaly is also noted.

Despite the increasing development and appliance of NGS techniques, there are still many patients with a clinical diagnosis of PCH, in whom no mutations in any of the known PCH related genes are identified. On the other end, the investigated clinical features of mutated patients differ among studies, and MRI description usually focuses on PF abnormalities, making it difficult to delineate the full clinical spectrum associated to each gene and to draw reliable genotype-phenotype associations. In order to address these issues, collection and systematic clinical and genetic characterizations of large patient cohorts would be advisable.

TUBULINOPATHIES

Tubulinopathies are a recently reported group of brain malformations caused by mutations in genes involved in microtubule formation and function. Up until now, mutations in seven tubulin genes encoding different α- and β-tubulin isotypes (*TUBA1A*, *TUBA8* and *TUBB2A*, *TUBB2B*, *TUBB3*, *TUBB5*) and more recently ϒ-tubulin (*TUBG1*) have been identified [79,80]. While most occurrences are sporadic and due to *de novo* mutations, recurrences have been reported due to germline mosaicism and autosomal recessive inheritance [2].

The spectrum of associated phenotypes ranges from isolated congenital fibrosis of the extraocular muscles to severe intellectual disability, quadriplegic cerebral palsy, postnatal microcephaly, seizures, cranial neuropathies and hydrocephalus. Dysmorphic features are infrequently reported and other organs are not affected [2,3].

The neuroimaging phenotype is broad and overlapping between different genetic causes. Cortical malformations include lissencephaly (commonly showing an anterior-to-posterior gradient), simplified gyral pattern and polymicrogyria (generalized, asymmetric with left-side prevalence, or restricted to the perisylvian region). Dysmorphic basal ganglia (especially putamen and caudate) with absence of the anterior limb of the internal capsule are the most typical and consistent finding. Furthermore, malformation of the cranial nerves and ventriculomegaly with abnormal shape of the frontal horns have also been described, as well as agenesis/dysgenesis of the corpus callosum and anterior commissure [3]. PF abnormalities include PCH of variable severity, cerebellar and tectal dysplasia, and asymmetric brainstem. Cerebellar dysplasia usually involves the upper portion of the vermis, and is characterised by diagonal folia (crossing the midline at an oblique angle), best visible on axial images [3] **(Fig.7)**. More recently, diffusion tensor imaging (DTI) and fiber tractography studies revealed tubulinopathies-associated anomalies of different white matter tracts, suggesting a role of tubulin genes in axonal pathfinding. In particular, the anterior commissure is usually missing, while fornices may be thin or present a more flattened course. In the PF, the transverse pontine fibers may be markedly thin and have a more slanting course. In addition, the corticospinal tracts may also be thin and asymmetric in size [3].

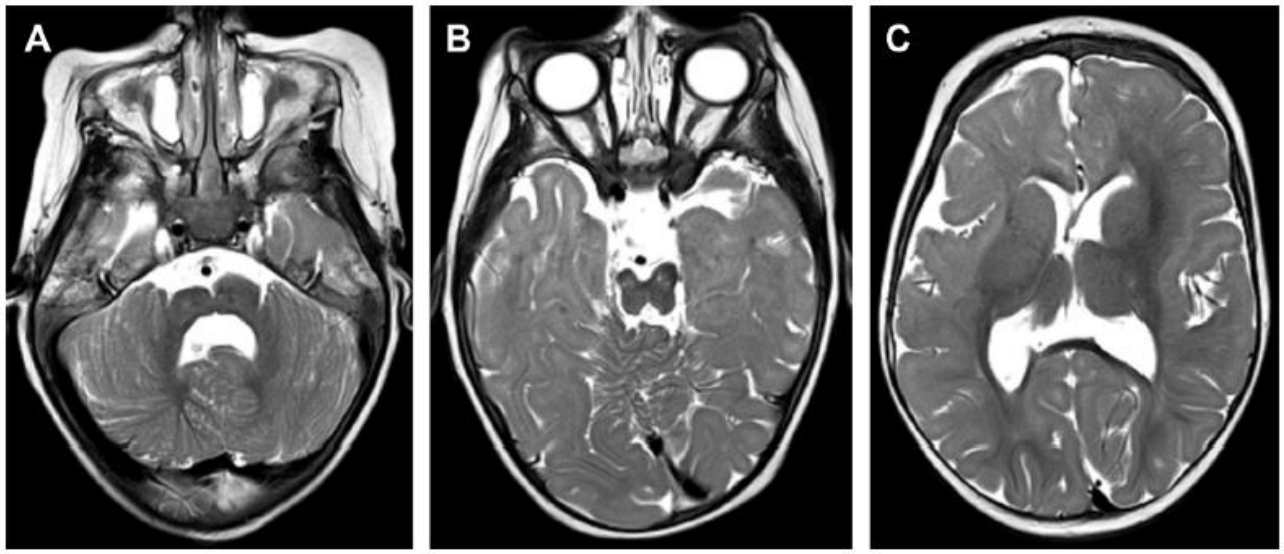

(Poretti *et al.* 2016)

Fig.7. MRI typical features of tubulinopathy. (A–C) Axial T2-weighted MR images of a 15-month-old child with *TUBA1A* mutation reveal marked asymmetry of the brainstem, cerebellar dysplasia involving mostly the superior part of the vermis, a dysmorphic appearance of the bilateral putamen and caudate nucleus with absence of the anterior limb of the internal capsule, and mild ventriculomegaly with abnormal shape of the frontal horns.

NON-PROGRESSIVE CONGENITAL ATAXIA

Nonprogressive congenital ataxias (NPCAs) represent a clinically and genetically heterogeneous group of conditions, all sharing the early evidence of cerebellar ataxia, without progression on follow-up or tending to gradual improvement. The prevalence of NPCAs in general population is not recorded, but it is likely to be underestimated. The earliest clinical manifestations consist in muscle hypotonia and delayed motor (and often language) milestones, while obvious truncal and/or limb ataxia is usually not seen before 2-3 years of age [81]. Quadrupedal gait has been exceptionally reported. Patients with NPCA present an increased prevalence of nystagmus, strabismus, microcephaly, autistic features, and seizures (usually responsive to treatment). Besides neurologic deficits, cognitive impairment is a common finding [81].

During infancy and preschool age, motor impairment is usually predominant. Ataxia persists at later ages but becomes less significant and tends not to be the primary difficulty in daily life. Conversely, linguistic and cognitive deficits, although not consistent, become more evident as children get older, often hindering their scholastic and professional achievements. On long-term follow-up, a small percentage of patients develop spasticity, or focal dystonia [81].

Neuroimaging pattern in NPCA is variable and characterised by both inter- and intrafamiliar variability. A minor part of cases shows cerebellar hypoplasia, defined as a reduction in cerebellar volumes with preserved architecture in a normal-sized or small PF. Hypoplasia can be occasionally unilateral or show a marked asymmetry between cerebellar hemispheres. In a further patient subgroup, neuroimaging reveals a progressive enlargement of cerebellar fissures resembling cerebellar atrophy (CA), although associated with clinical improvement **(Fig.9A-B)**. In some other cases, the enlargement of interfolial spaces is stable or slowly progressive; in view of the static clinical course, some authors inappropriately call this cerebellar appearance “hypoplasia”, leading to confusion in terminology and increasing the risk of misdiagnoses [25,81]. For this reason, we propose to use the term “shrunken cerebellum” to indicate a neuroimaging pattern characterised by enlarged cerebellar sulci mimicking CA but displaying a stable course over time [82] **(Fig.9C-D)**. This observation implies that a single neuroimaging study may not be able to distinguish reliably “degenerative” CA from the “developmental” nonprogressive situation represented by “shrunken

cerebellum", highlighting the need for an adequate follow-up. Lastly, MRI is normal in a considerable proportion of patients, contributing to under-recognition of NPCA among physicians [81].

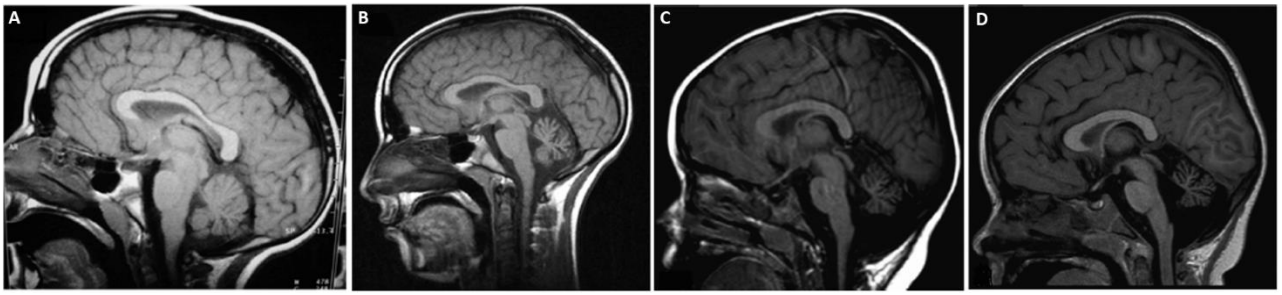

(Bertini *et al.* 2018)

Fig.9 MRI variable patterns in non-progressive congenital ataxia. (A–B) Female patient with motor delay and the heterozygous p.S218L *de novo* missense mutation in *CACNA1A*. Brain MRI was performed at the age of 3 years **(A)** and repeated at 10 years **(B)**. Notice the prominence of interfolial spaces, although the patient is clinically improving **(C–D)** Male patient with congenital strabismus and motor delay, carrying the heterozygous p.R1352Q *de novo* missense mutation in *CACNA1A*. Brain MRI was performed at 3 years **(C)** and 4 years **(D)** appearing relatively unchanged (possible slight worsening of vermian atrophy). Although patient is still not able to walk alone at age 4 years, he is slowly improving.

AIMS AND OBJECTIVES

This thesis aims at improving current knowledge of CBCDs through clinical, neuroradiological and molecular characterization of a large cohort of affected individuals. Phenotypic data and biological samples have been collected over the past ten years by a multidisciplinar network involving more than 50 Italian and International centers active in diagnosis, care and research of CBCDs, in the context of various research projects coordinated by Prof. Enza Maria Valente.

The work described in this PhD thesis has been conducted within the network project "Pediatric ataxias and Public Health: epidemiological studies and disease registry, characterization of genetic determinants and implementation of protocols for diagnosis, management, and rehabilitation using innovative low cost, widely accessible technologies", funded by the Italian Ministry of Health and focused on the following aims: 1) epidemiology: creation of a national registry of pathology; evaluation of clinical paths and costs management; definition and dissemination of guidelines for diagnostic/care; 2) diagnosis: rapid and cost-effective genetic analysis; identification of novel genes; genotype-phenotype correlates; innovative neuroimaging studies; 3) rehabilitation: development of novel low-cost home-based technologies for quantitative motor evaluation and for motor, cognitive and behavioral rehabilitation using virtual reality platforms.

This thesis will focus on the results of aim 2, investigating the molecular basis, genotype-phenotype associations and neuroimaging patterns of CBCDs.

PATIENTS AND METHODS

PATIENT RECRUITMENT AND CLINICAL ASSESSMENT

Patients have been referred from several diagnostic and research centers belonging to 27 countries (Austria, Belgium, Croatia, Egypt, United Arab Emirates, France, Germany, Greece, India, United Kingdom, Hungary, Ireland, Iceland, Israel, Italy, Lithuania, Malta, the Netherlands, Norway, Pakistan, Portugal, Romania, Spain, Switzerland, Serbia, Sweden and Turkey). After giving their informed consent, both probands and their relatives have been identified by a unique alphanumeric code and included in a dedicated, encrypted database. To date, more than 550 JS probands and over 650 probands with other CBCDs have been collected.

For each affected individual, a deepened clinical questionnaire has been filled, including separate sections for neuropsychological development, neurological assessment, and multi-organ involvement **(Appendix, Clinical questionnaire)**. In up to 50% of cases, a ≥18 months follow-up has been obtained.

NEUROIMAGING STUDIES

Neuroimaging phenotype has been investigated through brain MRI examination (performed either on a 1.5 T or a 3 T) including morphological sequences (T1 and/or T2-weighted) in at least two orthogonal planes, comprehensive of axial sections. Images have been systematically reviewed by a team of physicians with documented experience in paediatric neuroradiology. The morphology and size of the cerebellar vermis and hemispheres has been evaluated, together with rotation of the cerebellar vermis. The presence of a median cleft or asymmetry involving the brainstem has been investigated on axial images. The volume of the pons has been assessed on both sagittal and axial scans. The size of the middle cerebellar peduncles (MCPs) and IV ventricle, the depth of the ponto-mesencephalic junction, and the size and symmetry of the mesencephalon (especially the cerebral peduncles) have also been evaluated. Moreover, the presence of morphological abnormalities of the corpus callosum, basal ganglia and cranial and optic nerves as well as malformations of cortical development (MCDs) have been investigated. The identified anatomical malformations have been carefully inspected, reported in consensus and classified according to a shared assessment sheet **(Appendix, MRI assessment sheet)**. In a subset of patients, DTI sequences were also acquired by using different protocols and processed through TORTOISE software [83], obtaining mean diffusivity, fractional anisotropy [84] and directionally encoded colour (DEC) [85] maps.

After correcting raw data for motion and distortion artefacts (e.g. eddy current, B0 susceptibility, echo-planar imaging distortion), the DTI tensor was computed by using a non-linear least square estimator [86] and the final parametric maps were derived. As for conventional MR images, also DTI maps were systematically reviewed and reported in consensus.

PADAPORT (Pediatric Ataxia DAtabase and PORTal) PROJECT

In order to collect longitudinal data of patients with pediatric ataxias (including those presenting with CBCDs) the PADAPORT online database was created. The project was funded from the Mariani Foundation and developed thanks to collaborative efforts with IRCCS Eugenio Medea (Bosisio Parini). The database includes different sections for anagraphic, anamnestic, clinical, neuroimaging and genetic data and can be updated after each follow-up visit by the referring clinicians. The use of a shared online database will consent harmonization of data among centers and facilitate searching for patients based on single, or combinations of, features, with the aim to identify subgroups of patients sharing peculiar constellations of clinical and/or imaging signs. A beta version of PADAPORT is available at the following address: www.padaport.it.

MOLECULAR ANALYSES

For each family, samples were obtained from proband, parents and healthy/affected siblings (if available). Genomic DNA was extracted from peripheral blood (2-10 ml) collected in EDTA vacutainer tubes. DNA concentration and absorbance values at 260, 280 e 230 nm have been assessed using NanoDrop® ND-1000 UV-Vis Spectrophotometer (Thermo Fisher Scientific). For NGS protocols, a further and more accurate DNA quantification was performed through Qubit® 2.0 Fluorometer (Invitrogen). DNA degradation was evaluated by electrophoresis in a 0.8% agarose gel.

Different molecular methods have been applied in variable combinations, depending on the investigated phenotype. Diagnostic flow-chart is shown in **Fig.10**. Pathogenic variants in tubulin genes and p.A307S founder variant in *TSEN54* gene have been investigated through polymerase chain reaction (PCR) and Sanger sequencing. Specifically, coding regions and exon-intron boundaries of candidate genes were amplified using specific primer pairs for each DNA fragment. Bidirectional sequencing reaction was performed by using Big Dye terminator cycle sequencing kit (Applied BioSystems, USA) and was followed by capillary electrophoresis on ABI Prism 3130 Genetic Analyser sequencer (Applied Biosystems). The same approach has been used for validation of candidate variants identified by NGS method and for familial segregation analysis.

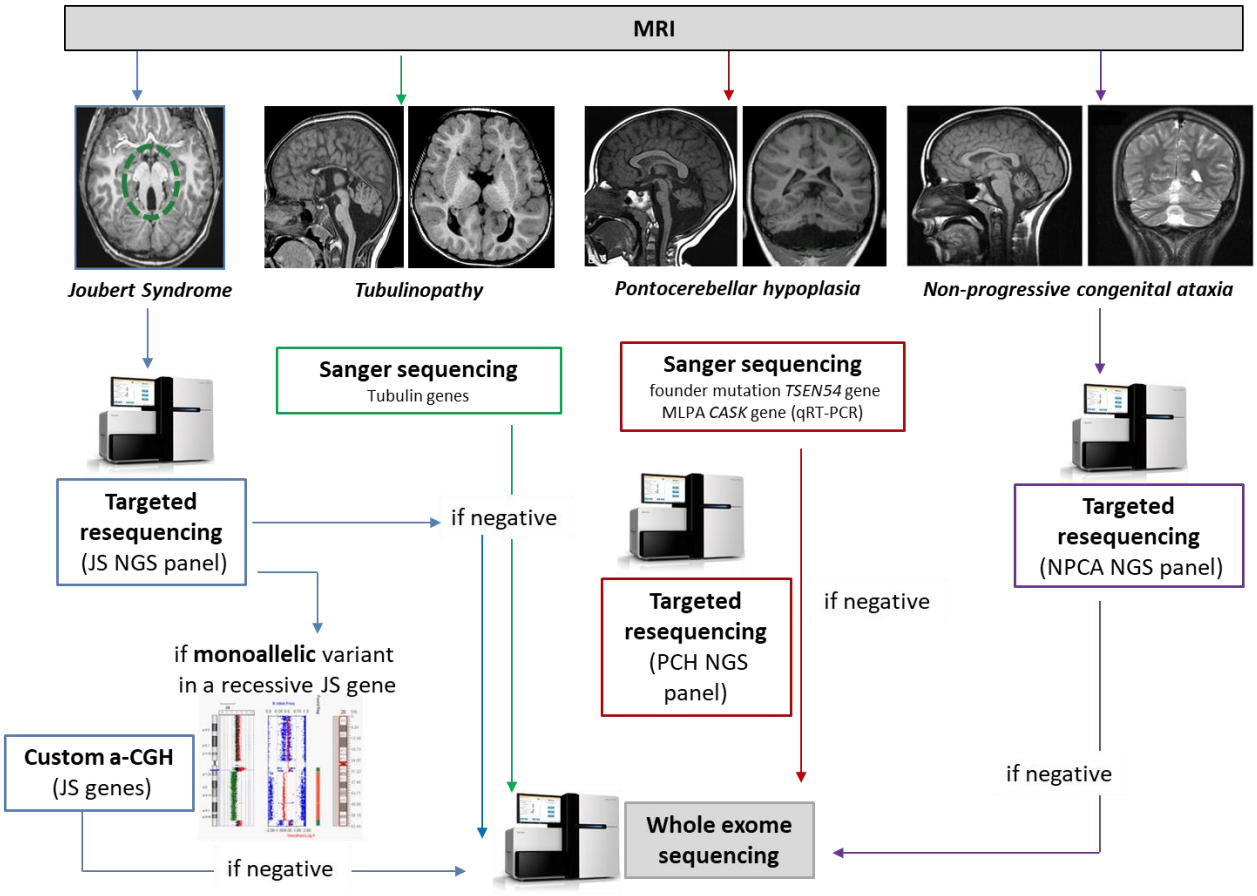

Fig.10. Molecular workflow. The sequence of the applied molecular techniques changes according to the investigated phenotype and consists in a variable combination of Sanger sequencing, MLPA (and qRT-PCR), targeted resequencing and whole exome sequencing.

Exonic deletions or duplications of *CASK* gene were investigated by using SALSA MLPA Probemix P398-A1 CASK (MRC-Holland, Amsterdam, The Netherlands) and confirmed by quantitative real-time PCR (qRT-PCR) on genomic DNA.

Targeted NGS has been carried out in JS patients, in PCH patients negative for the p.A307S founder variant in *TSEN54* gene and without intragenic rearrangements in *CASK* gene, as well as in NPCA patients. SureSelect^{QXT} Target Enrichment Protocol (Agilent Technologies) was used for the enrichment of genomic regions of interest. Two different gene panels were designed through SureDesign Software (Agilent Technologies), including known genes causative for JS **(Appendix, Tab.A1)**, PCH and other CBCDs (including NPCA) **(Appendix, Tab.A2)**. Sequencing was performed on MiSeq 2500 platform (Illumina).

WES analysis was carried out on selected families (trios, quads or sibling pairs) with negative result of targeted NGS or without pathogenic variants in tubulin genes after Sanger sequencing. For this purpose, SureSelect^{XT} Target Enrichment System (CRE V1- Agilent Technologies) was used on a HiSeq 2500 sequencing platform (Illumina).

In both targeted resequencing and WES, a hybrid capture-based target enrichment protocol was used**,** together with a solid phase amplification-based technology, and a sequencing method based on cyclic reversible termination**.**

In a subset of JS patients, intragenic rearrangements have been assessed in detail. Since NGS is not the optimal technique for CNVs detection, a custom high density comparative genomic hybridisation (HD-CGH) microarray 8x15k (Agilent Technologies) was designed with SureDesign software, in order to investigate intragenic deletions/duplications affecting the most frequent JS causative genes **(Appendix, Tab.A1)**. HD-CGH microarray analysis was performed on probands showing a pathogenic or likely pathogenic monoallelic variant in a known JS recessive gene identified through NGS. In positive cases, segregation analysis was performed on parents and available relatives.

During my PhD project I have not performed molecular assays firsthand. Instead, I have dealt with bioinformatic analysis and interpretation of NGS data, whose steps are as follows.

BIOINFORMATIC NGS DATA ANALYSIS

Bioinformatic analysis was carried out mapping sequences against the human reference genome (GRCh37) using BWA v0.7.5 as a first step. Variants were called through GATK Unified Genotyper and annotated by the eVANT v1.3 software (enGenome). Only variants predicted to affect the protein sequence or splicing, with reported frequency <1% in publicly available population databases (dbSNP, 1000 Genomes, Exome Aggregation Database (gnomAD), and NHLBI Exome Sequencing Project Exome Variant Server (EVS)) were retained. For each variant, *in silico* prediction of functional effects and evolutionary conservation of the involved amino acids were investigated by using different tools (including DANN, dbscSNV, PaPI, PolyPhen-2, SIFT, Mutation Assessor, MutationTaster, Provean, CADD phyloP, GERP++, SiPhy). Candidate variants identified through genetic testing were confirmed by Sanger sequencing and described according to Human Genome Variation Society guidelines (HGVS) (http://varnomen.hgvs.org/) (with nucleotide +1 corresponding to the A of the ATG translation initiation codon). Variants pathogenicity was assessed according to American College of Medical Genetics and Genomics (ACMG) criteria **(Figg.11,12)** [87].

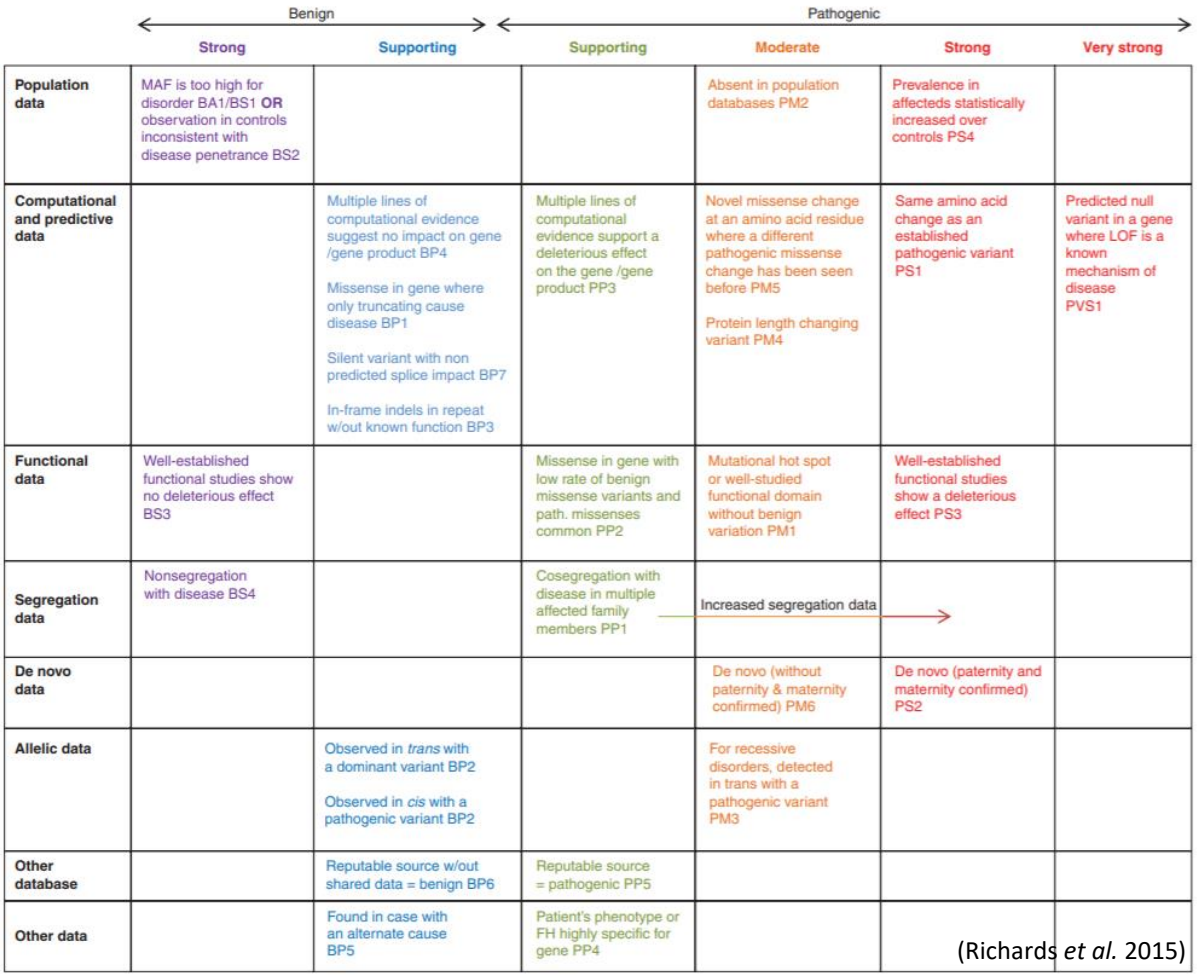

	Benign		Pathogenic			
	Strong	**Supporting**	**Supporting**	**Moderate**	**Strong**	**Very strong**
Population data	MAF is too high for disorder BA1/BS1 **OR** observation in controls inconsistent with disease penetrance BS2			Absent in population databases PM2	Prevalence in affecteds statistically increased over controls PS4	
Computational and predictive data		Multiple lines of computational evidence suggest no impact on gene /gene product BP4 Missense in gene where only truncating cause disease BP1 Silent variant with non predicted splice impact BP7 In-frame indels in repeat w/out known function BP3	Multiple lines of computational evidence support a deleterious effect on the gene /gene product PP3	Novel missense change at an amino acid residue where a different pathogenic missense change has been seen before PM5 Protein length changing variant PM4	Same amino acid change as an established pathogenic variant PS1	Predicted null variant in a gene where LOF is a known mechanism of disease PVS1
Functional data	Well-established functional studies show no deleterious effect BS3		Missense in gene with low rate of benign missense variants and path. missenses common PP2	Mutational hot spot or well-studied functional domain without benign variation PM1	Well-established functional studies show a deleterious effect PS3	
Segregation data	Nonsegregation with disease BS4		Cosegregation with disease in multiple affected family members PP1	Increased segregation data →		
De novo data				De novo (without paternity & maternity confirmed) PM6	De novo (paternity and maternity confirmed) PS2	
Allelic data		Observed in *trans* with a dominant variant BP2 Observed in *cis* with a pathogenic variant BP2		For recessive disorders, detected in trans with a pathogenic variant PM3		
Other database		Reputable source w/out shared data = benign BP6	Reputable source = pathogenic PP5			
Other data		Found in case with an alternate cause BP5	Patient's phenotype or FH highly specific for gene PP4			

(Richards *et al.* 2015)

Fig.11. Evidence Framework. The chart organizes each of the criteria by the type of evidence as well as the strength of the criteria for a benign (left side) or pathogenic (right side) assertion. BS: benign strong; BP: benign supporting; FH: family history; LOF: loss-of-function; MAF: minor allele frequency; path: pathogenic; PM: pathogenic moderate; PP: pathogenic supporting; PS: pathogenic strong; PVS: pathogenic very strong.

Pathogenic	(i) 1 Very strong (PVS1) *AND* (a) ≥1 Strong (PS1–PS4) *OR* (b) ≥2 Moderate (PM1–PM6) *OR* (c) 1 Moderate (PM1–PM6) and 1 supporting (PP1–PP5) *OR* (d) ≥2 Supporting (PP1–PP5) (ii) ≥2 Strong (PS1–PS4) *OR* (iii) 1 Strong (PS1–PS4) *AND* (a)≥3 Moderate (PM1–PM6) *OR* (b)2 Moderate (PM1–PM6) *AND* ≥2 Supporting (PP1–PP5) *OR* (c)1 Moderate (PM1–PM6) *AND* ≥4 supporting (PP1–PP5)
Likely pathogenic	(i) 1 Very strong (PVS1) *AND* 1 moderate (PM1–PM6) *OR* (ii) 1 Strong (PS1–PS4) *AND* 1–2 moderate (PM1–PM6) *OR* (iii) 1 Strong (PS1–PS4) *AND* ≥2 supporting (PP1–PP5) *OR* (iv) ≥3 Moderate (PM1–PM6) *OR* (v) 2 Moderate (PM1–PM6) *AND* ≥2 supporting (PP1–PP5) *OR* (vi) 1 Moderate (PM1–PM6) *AND* ≥4 supporting (PP1–PP5)
Benign	(i) 1 Stand-alone (BA1) *OR* (ii) ≥2 Strong (BS1–BS4)
Likely benign	(i) 1 Strong (BS1–BS4) and 1 supporting (BP1–BP7) *OR* (ii) ≥2 Supporting (BP1–BP7)
Uncertain significance	(i) Other criteria shown above are not met OR (ii) the criteria for benign and pathogenic are contradictory

(adapted from Richards *et al.* 2015)

Fig.12. Rules for Combining Criteria to Classify Sequence Variants. Combination of criteria (shown in Fig.11) defining pathogenic, likely pathogenic, benign, likely benign, and uncertain significance variants.

RESULTS

CHAPTER 1: JOUBERT SYNDROME

In this Chapter, clinical and molecular spectrum of JS will be described, and prevalence data for the Italian population will be provided for the first time. Furthermore, urinary concentration ability will be presented as a potential predictor of renal insufficiency in JS patients. Lastly, a new JS causing gene will be described in detail. My personal contribution consisted in the evaluation of clinical questionnaires and brain MRI of patients, bioinformatic analysis and interpretation of NGS data, collection of demographic and genetic data required for the epidemiological study, acquisition of baseline and follow-up clinical information related to renal function in JS patients and application of univariate and multivariate statistical methods for data analysis.

1.1 DETECTION RATE AND MUTATIONAL SPECTRUM

Considering the partial clinical and neuroimaging overlap between JS and other neurodevelopmental syndromic disorders such as CGD [88], molecular analysis has been performed after a critical neuroradiological evaluation. In particular, patients selected for NGS showed not only vermis hypoplasia/agenesis, but also a deepened interpeduncular fossa and thickening of the superior cerebellar peduncles (SCPs), responsible for MTS-appearance. Furthermore, clinical questionnaire also comprised a section for blood testing (included transferrin isoelectric focusing), in order to improve differential diagnosis with CDG.

To date, 447 probands with neuroradiological evidence of MTS have been screened through NGS techniques. Biallelic variants in autosomal recessive genes or hemizygous variants in the X-linked recessive *OFD1* gene have been identified in 257 patients (~58%) **(Appendix, Tab.A3)**. 43 probands presenting with monoallelic pathogenic or likely pathogenic variants in at least one recessive JS gene have been further analyzed through HD-CGH microarray approach. In 5 out of 43 cases (~12%), a CNV affecting genes previously identified with a point mutation on the other allele has been detected, allowing to reach a genetic diagnosis **(Appendix, Tab.A4)**.

Specifically, CNVs explaining the phenotype have been observed in *AHI1* (n=1), *CEP290* (n=1), *CPLANE1* (n=1), and *KIAA0586* (n=2). Moreover, one patient has been identified with a homozygous deletion encompassing *NPHP1* gene using real-time PCR. Overall, predicted causative variants have been identified in 263 patients out of 447 screened probands, corresponding to a detection rate of ~59%. The most frequent mutated genes are *CPLANE1* (also known as *C5orf42*) (9.4%), *CEP290*

(8.1%), *AHI1* (6.5%), *CC2D2A* (6.5%), *TMEM67* (6.3%), *KIAA0586* (3.8%), *RPGRIP1L* (2.7%), *MKS1* (2.5%), *INPP5E* (2.0%), *OFD1* (1.8%), and *CSPP1* (1.6%) **(Fig.13)**. One proband (COR322) has been identified with both the homozygous missense variant p.(R1622C) in *CEP290* gene and the truncating hemizygous variant p.(Q870Lfs*2) in *OFD1* gene.

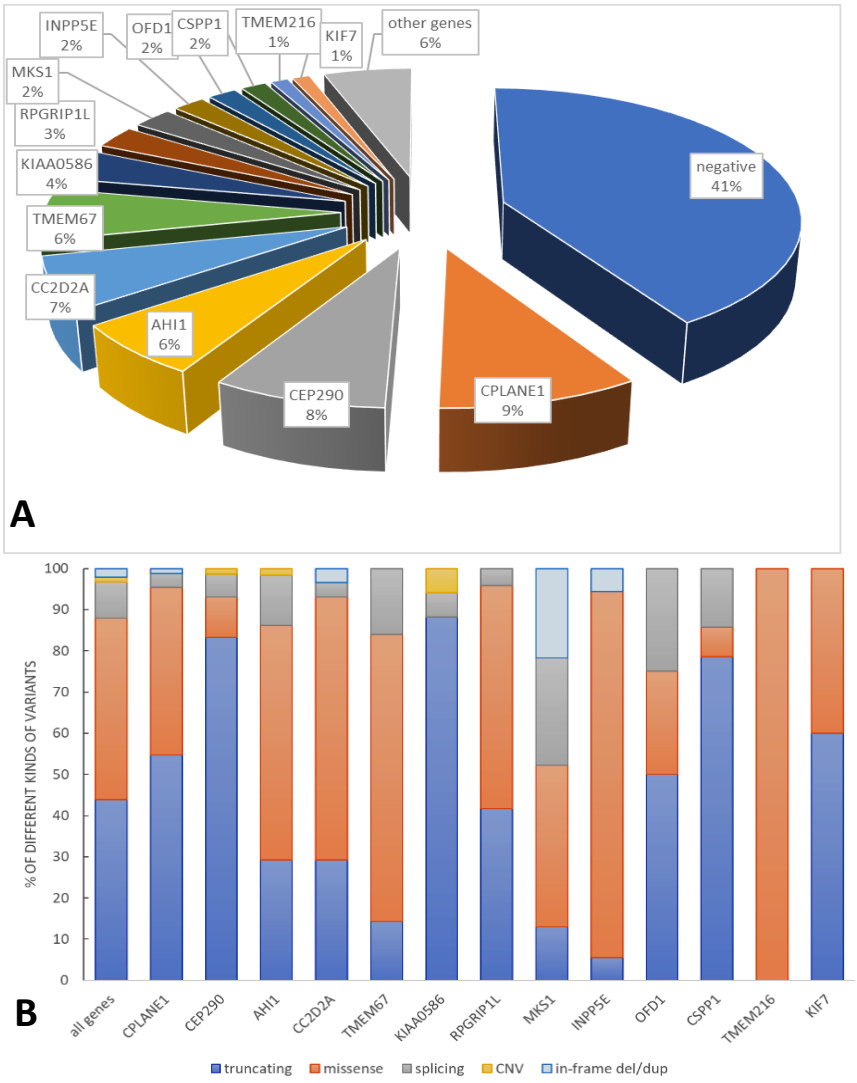

Fig.13. Genetic architecture of Joubert Syndrome. (A) Mutational spectrum identified in the investigated cohort **(B)** Differential contribution of mutation types across the 13 genes most commonly associated with Joubert Syndrome.

When considering all the mutated genes identified in the investigated cohort, truncating and missense variants result to be equally represented, while splicing variants, in-frame deletions/duplications and CNVs account for a smaller percentage of cases. The proportion of each variant type considerably changes from gene to gene. In particular, *CEP290*, *KIAA0586* and *CSPP1* have been more frequently found to carry truncating variants, while *AHI1*, *CC2D2A*, *TMEM67* and *INPP5E* more often show missense changes. Moreover, missense variants are the only mutation type identified in *TMEM216* gene in the screened cohort. Also, the percentage of splice site variants substantially varies across genes, mainly involving *MKS1* and *OFD1*. Lastly, in-frame deletions or duplications have more frequently been detected in *MKS1* gene.

With respect to patient clinical features **(Appendix, Tab.A3)**, some previously described associations seem to be confirmed in our cohort. Specifically, ~79% of *TMEM67*-mutated probands presented

with liver disease (associated with coloboma in approximately half of cases), while no signs of hepatopathy have been identified in *RPGRIP1L*- nor in *CC2CD2A*-mutated probands. Conversely, 70% of cases with pathogenic variants in *RPGRIP1L* have been identified with renal involvement. *CEP290* gene has resulted to be associated with oculo-renal phenotype: in fact, kidney disease and retinopathy have been detected in 50% and 75% of cases, respectively (with ~43% of probands showing both renal and ocular manifestations). Lastly, polydactyly has been observed in 50% of probands with *CPLANE1* mutations, while 79% of cases due to *AHI1* gene have been identified with retinal dystrophy. Despite these preliminary data, genotype-phenotype associations are fare from being definitively established. In fact, clinical information are missing for many patients; in other cases, last follow-up dates back to very early ages, when children are still at risk of developing organ complications. For all these reasons, additional efforts would be necessary for investigating the causal relationship between clinical outcome and the underlying genotype.

1.2 AGE AND SEX ESTIMATE OF JOUBERT SYNDROME IN ITALY [89]

In order to estimate the prevalence of JS in Italy applying standards of descriptive epidemiology, clinical and anagraphic data of the collected patients have been revised, to ascertain the number of cases resident in Italy (60,483,973 inhabitants as of 2018) on October 8, 2018.

All the data were double-checked with the aid of a network of 46 Italian centers active in diagnosis, care and research of JS and connected to the Italian Association for Joubert syndrome and congenital ataxias (AISJAC). Age at diagnosis among probands, inferred from both medical records and brain MRIs, has been defined as age at first detection of the MTS. The crude age- and sex-specific prevalence has been calculated, assuming a Poisson distribution. The 95% CI have been computed with the formula: $\pi \pm 1.96\sqrt{\pi(1-\pi)/n}$, where π means the prevalence and n the absolute number of inhabitants [90]. The database of the Italian National Institute of Statistics (ISTAT) has provided population data for 2018 (http://demo.istat.it/pop2018/index.html).

Statistical analyses have been performed using t-test for age comparison. Linear regression analysis has been used to test the relationship between age at point prevalence and age at diagnosis. Data have been analyzed with SPSS (v.25.0). A p-value of ≤ 0.05 has been considered statistically significant, with Bonferroni correction for multiple comparisons.

Tab.3. Population-based prevalence rate of Joubert Syndrome in Italy (per 100,000 population, year 2018)

Age	Males			Females			Total	
(yrs)	cases	Population	rate (95% CI)	cases	population	rate (95% CI)	cases	rate (95% CI)
0-4	10	1,249,919	0.80 (0.30-1.30)	10	1,181,740	0.85 (0.32-1.37)	20	0.82 (0.46-1.18)
5-9	32	1,432,161	2.23 (1.46-3.01)	31	1,351,543	2.29 (1.49-3.10)	63	2.26 (1.70-2.82)
10-14	33	1,475,522	2.24 (1.47-3.00)	24	1,389,291	1.73 (1.04-2.42)	57	1.99 (1.47-2.51)
15-19	27	1,504,897	1.79 (1.12-2.47)	21	1,393,182	1.51 (0.86-2.15)	48	1.66 (1.19-2.12)
20-24	20	1,557,238	1.28 (0.72-1.85)	14	1,429,282	0.98 (0.47-1.49)	34	1.14 (0.76-1.52)
25-29	11	1,661,411	0.66 (0.27-1.05)	16	1,587,513	1.01 (0.51-1.50)	27	0.83 (0.52-1.14)
30-34	9	1,712,078	0.53 (0.18-0.87)	9	1,682,623	0.53 (0.19-0.88)	18	0.53 (0.29-0.78)
35-39	5	1,911,532	0.26 (0.03-0.49)	3	1,901,851	0.16 (0.00-0.34)	8	0.21 (0.06-0.36)
>40	9	16,922,849	0.05 (0.02-0.09)	0	19,139,341	0.00 (0.00-0.00)	9	0.02 (0.01-0.04)
total	156	29,427,607	0.53 (0.45-0.61)	128	31,056,366	0.41 (0.34-0.48)	284	0.47 (0.41-0.52)

284 JS patients (220 Caucasian) resident in Italy have been identified, originating from 251 families. M/F ratio was 1.22 (156/128). The overall mean age at point prevalence was 16.7±10.4 years (median 14.7; range 1-60; interquartile range-IQR 8.3-23.2). The mean male- and female-specific ages at point prevalence were 17.5±11.2 years (median 15; range 2-60; IQR 8.8-23.5) and 15.7±9.2 years (median 14.1; range 1-39; IQR 8.8-23.5), respectively, without significant differences between sexes. Among patients, 124 (44%) presented exclusive neurological manifestations and 134 (47%) had additional multiorgan involvement, while data were missing in 26 cases (9.1%).

The crude prevalence rates of JS in Italy on October 8, 2018 for total, females and males were 0.47 (95% CI 0.41-0.53), 0.41 (95% CI 0.32-0.49) and 0.53 (95% CI 0.45-0.61) per 100,000 population, respectively **(table 3)**. When focusing on patients aged 0-19 years, the crude prevalence estimates for total, females and males increased to 1.7 (95% CI 1.49-1.97), 1.62 (95% CI 1.31-1.99) and 1.80 (95% CI 1.49-2.18) per 100,000 population **(Tab.3).**

200 out of the 251 (80%) probands had both parents of Italian origin, 44 (17.5%) had at least one non-Italian parent; 23 (9.1%) descended from consanguineous unions. NGS panel analysis of JS genes has been conducted on 219 probands. **Tab.4** summarizes the proband genetic status. Among the 219 tested probands, 131 had a confirmed molecular diagnosis, resulting in a mutation rate of 60%.

Tab.4. Categories of probands with Joubert Syndrome, based on their genetic status

Group 1[a] (N, %)	Group 2[b] (N, %)	Group 3[c] (N, %)	Group 4[d] (N, %)	Total (N, %)
32 (13%)	131 (52%)	35 (14%)	53 (21%)	251 (100%)

[a]Genetic testing not performed; [b]Confirmed molecular diagnosis of Joubert Syndrome; [c]Monoallelic pathogenic or likely pathogenic variant in at least one autosomal Joubert Syndrome gene; [d]Negative testing

The commonest mutated genes were *AHI1* (9.1%), *CPLANE1* (8.7%), *TMEM67* (8.2%) and *CEP290* (6.9%), similarly distributed between sexes **(Fig.14)**. When considering also affected siblings, molecularly confirmed cases increased to 152. In this latter group, the crude prevalence rates for total, females and males were 0.25 (95% CI 0.21-0.29), 0.24 (95% CI 0.20- 0.31) and 0.26 (95% CI 0.21-0.32) per 100,000 population **(Tab.5).** Interestingly, single heterozygous pathogenic or likely

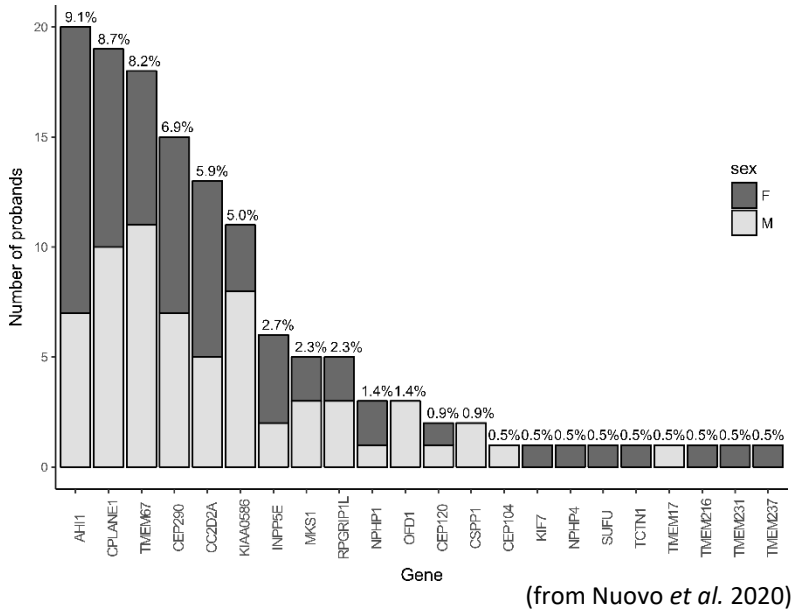

(from Nuovo *et al.* 2020)

Fig.14. Mutational frequency in probands. Absolute number and percentage of probands mutated in different Joubert genes. For each gene, the percentage was calculated on the total number of tested probands (n=219)

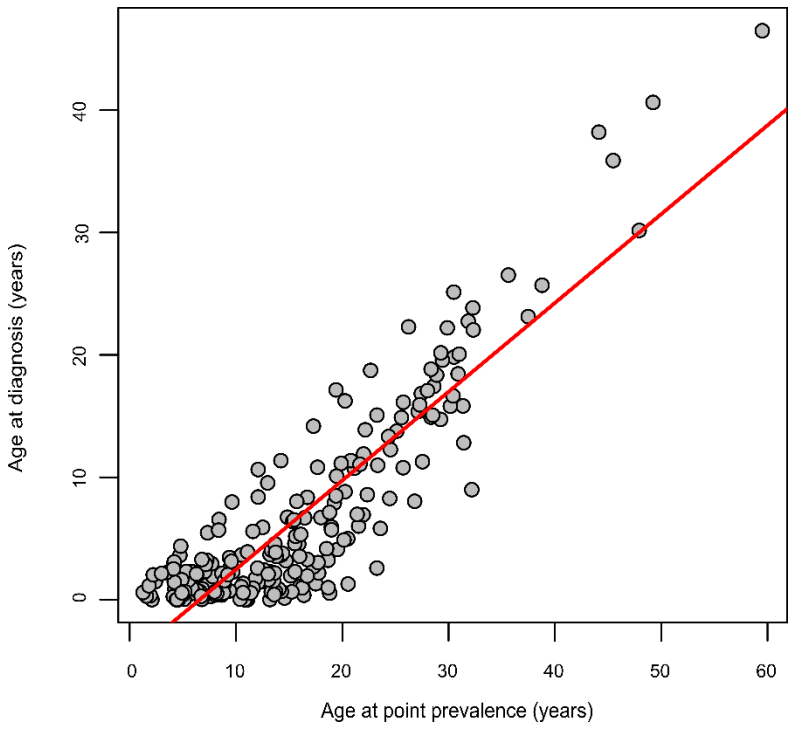

(from Nuovo *et al.*2020)

Fig.15. Age at point prevalence vs age at diagnosis in probands. Linear regression analysis between age at point prevalence and age at diagnosis. Data refer to the 223 probands for whom both ages were available, independently of their genetic status

pathogenic variants have been detected in 35 probands (16% of tested cases). For these patients, the potential role of variants of unknown significance, as well as the existence of a second variant missed by NGS (e.g. variants outside coding regions or large rearrangements) should be considered, requiring complementary diagnostic strategies.

Age at diagnosis was available for 223 probands, with a mean of 6.67±8.10 years (median 3.18; range 0-46.49; IQR 1.06-10.37). The mean sex-specific age at diagnosis was 7.24±9.08 years for males and 6.01±6.76 years for females, without statistically significant difference between groups. Finally, the linear relationship between age at point prevalence and age at diagnosis was statistically significant (r^2=0.79; p<0.001) **(Fig.15)**.

This study considerably increases knowledge of JS epidemiology, demonstrating an overall population-based crude prevalence rate of 0.47 per

100,000 population. This rate is approximately halved for molecularly confirmed cases (ratio 0.5=0.25/0.47 per 100,000 population) **(Tab.3,5)**. When considering pediatric age, JS prevalence was 1.7 per 100,000 population, 10 times higher than the single report published to date (0.17 per 100,000 population) [91]. However, this comparison is not completely appropriate because the latter study was performed before the MTS identification. Also a comparison with the figure reported by Parisi and collaborators [27] may be complicated, because it describes an incidence for live-birth.

Since the network has not been created for epidemiological purposes, the main limitation of this approach consists in a possible underrepresentation of JS patients. Firstly, we were not able to provide information about the referring process or the systematic use of MRI in ataxic patients diagnosed outside the Italian network. Furthermore, we may have missed some other cases, due to the wide clinical variability of the disease. Indeed, patients with a very mild phenotype might not undergo brain MRI, remaining undiagnosed. For all these reasons, these data should be considered as minimum prevalence estimates. However, it must be noted that the distribution of JS cohort among the three macro-areas (North, Center, South-Islands) is in accordance with that reported in the general population.

As the probability of diagnosis might increase with a previously identified case in the family, age at diagnosis was considered only for probands, showing a linear relationship with age at point prevalence. A possible explanation is that elderly patients exhibited first signs of disease at a time of lower awareness of JS, leading to delayed diagnosis. However, such delay could also relate to the existence of mild phenotypes, not recognizable until later ages. A detailed clinical characterization of patients will be necessary to clarify this issue.

Tab.5. Population-based prevalence rate of molecularly confirmed Joubert Syndrome in Italy (per 100,000 population, year 2018)

Age	Males			Females			Total	
(yrs)	cases	Population	rate (95% CI)	cases	population	rate (95% CI)	cases	rate (95% CI)
0-4	1	1,249,919	0.08 (0.00-0.24)	6	1,181,740	0.51 (0.10-0.91)	7	0.29 (0.07-0.50)
5-9	16	1,432,161	1.12 (0.57-1.66)	14	1,351,543	1.04 (0.49-1.58)	30	1.08 (0.69-1.46)
10-14	16	1,475,522	1.08 (0.55-1.62)	14	1,389,291	1.01 (0.48-1.54)	30	1.05 (0.67-1.42)
15-19	11	1,504,897	0.73 (0.30-1.16)	11	1,393,182	0.79 (0.32-1.26)	22	0.76 (0.44-1.08)
20-24	12	1,557,238	0.77 (0.33-1.21)	11	1,429,282	0.77 (0.31-1.22)	23	0.77 (0.46-1.08)
25-29	8	1,661,411	0.48 (0.15-0.82)	11	1,587,513	0.69 (0.28-1.10)	19	0.58 (0.32-0.85)
30-34	5	1,712,078	0.29 (0.04-0.55)	8	1,682,623	0.48 (0.15-0.80)	13	0.38 (0.17-0.59)
35-39	2	1,911,532	0.10 (0.00-0.25)	1	1,901,851	0.05 (0.00-0.16)	3	0.08 (0.00-0.17)
>40	5	16,922,849	0.03 (0.00-0.06)	0	19,139,341	0.00 (0.00-0.00)	5	0.01 (0.00-0.03)
total	76	29,427,607	0.26 (0.20-0.32)	76	31,056,366	0.24 (0.19-0.30)	152	0.25 (0.21-0.29)

1.3 PREDICTOR OF RENAL DISEASE PROGRESSION IN JOUBERT SYNDROME [92]

Kidney involvement is a frequent complication of JS, occurring in 25–30% of patients [11,26,93,94]. In a recent study on 97 JS individuals, 29 (30%) presented renal phenotypes, including nephronophthisis (NPH) (20%), unilateral cystic dysplastic kidneys (3%) or undetermined cystic kidney disease (7%). Most of these phenotypes were detected by ultrasound, and only 18 of 29 (62%) patients had a confirmed diagnosis of chronic kidney disease (CKD) [94]. NPH is a distinctive clinical–pathological entity characterized by disruption of tubular basement membranes, progressive tubular atrophy, interstitial fibrosis and small corticomedullary cysts, within small or normal-sized kidneys [95]. In most cases, NPH remains asymptomatic or paucisymptomatic in the first decade, manifesting only with polyuria, polydipsia and mild anaemia, but it inexorably progresses during adolescence or early adulthood to CKD, and finally to end-stage renal disease (CKD5). Renal failure is a frequent cause of death in JS, as dialysis and renal transplantation may be hindered by the occurrence of severe comorbidities [28]. Since JS is mostly diagnosed in very young children with neurological symptoms, when their renal function is still normal, tests to predict the risk of developing progressive renal disease would be extremely useful, to allow an early diagnosis and management of patients at risk [26,96,97]. Kidney US is sensitive in diagnosing cystic kidney diseases while, in isolated NPH, it may show increased echogenicity and/or small corticomedullary cysts, or it may remain negative. Moreover, this test relies on the operator's experience and does not predict the risk of developing CKD. To date, a reliable early quantitative biomarker for renal insufficiency in JS is lacking. In order to address this issue, a comprehensive assessment and long term follow-up of renal functioning in a large cohort of Italian JS subjects has been conducted, and the prognostic value of urine osmolality in predicting the risk of developing adverse renal outcome has been assessed.

Ninety-three Italian JS children (55 males) from 76 families were selected. Inclusion criteria were (i) a neuroradiologically confirmed diagnosis of JS; and (ii) a complete investigation of renal function at first examination, including (a) serum and urine electrolytes and (b) two-step assessment of urinary concentration ability, as follows. First, spontaneous urine osmolality was measured on the first-morning urine sample. If osmolality was ≥800 mOsm/kg H_2O, no further tests were performed. Otherwise, patients underwent a challenging test with 1- deamino-arginine vasopressin (DDAVP) [98]. Briefly, hourly urine samples were collected over a 4-h period after 20 mg intranasal administration of DDAVP. The highest value among four was used to define the maximum urinary osmolality. During the test, patients had free access to water and were monitored and weighed. Children were

not given water unless they clearly expressed thirst. The test was not performed in patients presenting with renal insufficiency or unable to exhibit thirst. Serum electrolytes were tested at the beginning and end of the test. A urinary concentration defect (UCD) was diagnosed when maximum urine osmolality was <600 mOsm/kg H_2O, whereas values between 600 and 800 mOsm/kg H_2O were considered borderline [99]. Estimated glomerular filtration rate (eGFR) was calculated by using appropriate formulas according to age, namely the Schwartz formula in children and the Modification of Diet in Renal Disease equation in adults [100–102]. CKD categories were classified using KDOQI guidelines [96]. Most patients underwent kidney ultrasound, either at first examination or at follow-up. Owing to intellectual impairment, polyuria could not be measured accurately in most patients and was broadly defined as the passage of large volumes of urine with increased frequency, associated with nycturia, enuresis and polydipsia. Retinopathy was diagnosed based on abnormal findings at fundus oculi and/or electroretinogram. Liver involvement was defined as any type of liver abnormality, including repeatedly altered liver function tests, abnormal liver ultrasound or hepatic fibrosis detected with liver biopsy. Sixty patients were followed-up one or more times over the years.

Continuous variables were analysed with two-sided t-test if they passed the Kolmogorov–Smirnov normality test, and with two-sided Mann–Whitney U test otherwise. The normally and non-normally distributed variables were described by using mean and standard deviation (SD), or median and interquartile range (IQR), respectively. A logistic regression model was used to estimate the probability of developing decreased eGFR based on the presence of UCD (adjusting for age at osmolality assessment). A similar approach was employed to investigate the probability of presenting with polyuria, kidney ultrasound abnormalities and extra-renal signs as a function of CKD, and to explore genotype–phenotype correlations. Binomial-response general linear models were fit using the bias-reduction method [103]. Results were statistically significant for $p < 0.05$. Survival analysis was performed with Kaplan–Meier estimator. A receiver operating characteristic (ROC) curve was used to determine the diagnostic accuracy of urine osmolality assessment and to calculate the cut-off value for optimal sensitivity and specificity. Statistical analysis was performed using R [104].

The 93 recruited patients were divided in five subgroups: (i) ≥18 years with normal renal function (NRF≥18); (ii) <18 years with normal renal function (NRF<18); (iii) isolated UCD with normal eGFR (iUCD); (iv) mildly to severely decreased eGFR (CKD2–CKD4); and (v) end-stage renal disease (CKD5). The age cut-off was chosen as juvenile NPH mostly becomes symptomatic in the late first or early second decade, and therefore we assumed that subjects ≥18 years with normal renal function had negligible risk of kidney disease.

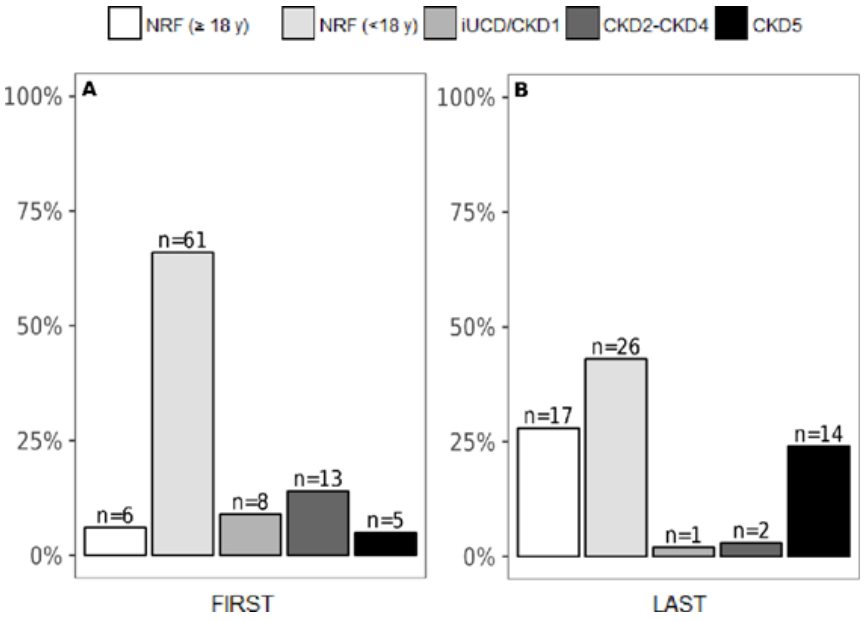

Fig.16. Assessment of renal function at first and last examination. (A) Renal status of all 93 patients at first evaluation. **(B)** Renal status of 60 patients with available follow-up data at last examination. NRF: normal renal function; iUCD/CKD1: isolated urinary concentration defect with normal eGFR; CKD2–CKD4: CKD with mildly to severely decreased eGFR; CKD5: end-stage renal disease.

(from Nuovo *et al.* 2018a)

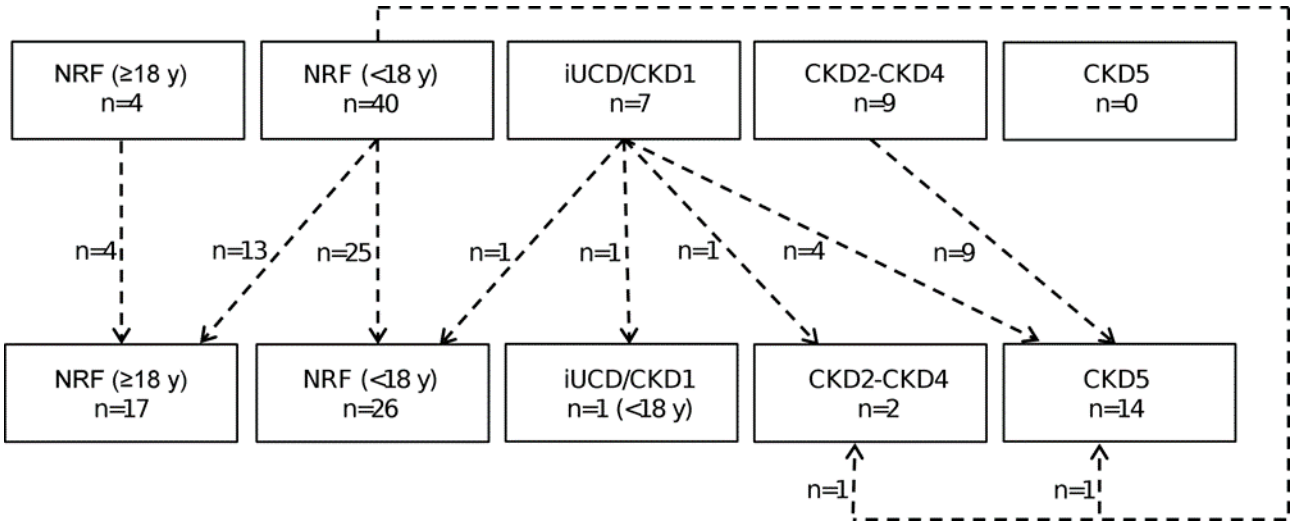

(from Nuovo *et al.* 2018a)

Fig.17. Follow-up of renal function. Evolution of renal function in the 60 patients for whom at least one follow-up visit was available. iUCD/CKD1: isolated urinary concentration defect with normal GFR (CKD1); CKD2-CKD4: CKD with mildly to severely decreased GFR; CKD5: end-stage renal disease

Tab.6. Clinical and laboratory features of patients at last follow-up

	Total	NRF	CKD	Coefficient (95% CI)[a]	p-value
Number of patients, n/N (%)	93	66/93 (71%)	27/93 (29%)[b]	-	-
Age (years)	14±9[c]	15±10[c]	12±6[c]	-	0.16
Kidney assessment, n/N (%)					
Polyuria	22/88 (25%)	2/62 (3%)	20/26 (77%)	4.34 (2.95 to 6.60)	<0.001***
Abnormal kidney ultrasound	23/85 (27%)[d]	2/62 (3%)	21/23 (91%)	5.34 (3.72 to 8.14)	<0.001***
Other features					
Retinopathy	33/92 (36%)	17/65 (26%)	16/27 (59%)	1.38 (0.46 to 2.39)	0.004**
Coloboma	12/93 (13%)[e]	9/66 (14%)	3/27 (11%)	-0.15 (-1.80 to 1.10)	0.83
Liver involvement	17/91 (19%)[e]	12/65 (19%)	5/26 (19%)	0.09 (-1.19 to 1.18)	0.88

For each variable, the % is calculated on the effective number of patients for whom information was available. [a]the coefficient stands for the regression coefficient b between renal function and each independent variable; [b]including two patients with isolated urinary concentration defect and 25 with decreased eGFR; [c]values are expressed as mean±SD; [d]including three patients with cystic kidney dysplasia; [e]6 Joubert patients presented with both coloboma and liver disease (COACH syndrome) **p-value ≤0.01; ***p-value ≤0.001. CKD: chronic kidney disease; NRF: normal renal function

At first examination, median (IQR) age was 8 years (9; min: 1; max: 52; 14 patients ≥18 years). Sixty-seven patients had NRF, 8 had iUCD and 18 patients had CKD2–CKD5 **(Fig.16A)**. Sixty patients were evaluated more than once, with median (IQR) follow-up of 9 years (6; min: 1; max: 14). At their last examination [median (IQR) age: 15 years (11); min: 4; max: 36], 43 out of 44 patients still had NRF (although those ≥18 years had raised from 4 to 17), 1 patient <18 years had iUCD, and the number of subjects with CKD2–CKD5 had increased from 9 to 16 **(Fig.16B, Fig.17)**. The remaining 33 subjects were assessed only once. Overall, the prevalence of CKD at last available examination was 29% (27/93).

When comparing clinical and instrumental findings between subjects with NRF and those with renal involvement (iUCD, CKD2–CKD4 and CKD5), the prevalence of polyuria and of abnormal kidney ultrasound was significantly higher in the second group, as expected. In particular, US was pathological in 21 of 23 subjects with CKD, showing isolated kidney hyperechogenicity in 18 and bilateral cysts in 3 (of whom 2 also presented increased echogenicity). Conversely, US was unremarkable in 60 subjects with NRF, whereas the remaining 2 (aged 5.9 and 14 years at last examination) presented kidney hyperechogenicity **(Tab.6)**. In respect of extra-renal involvement, only retinopathy significantly associated with renal impairment, with a frequency more than twice as high as in NRF subjects. Genetic tests revealed mutations in 38 out of 70 analysed probands (54%). Genes mutated in both CKD and NRF groups include *CEP290* (n=5 CKD, 1 NRF), *RPGRIP1L* (n=2 CKD, 1 NRF), *TMEM67* (n=1 CKD, 4 NRF) and *AHI1* (n=1 CKD, 3 NRF). Genes whose mutations were found only in the NRF group are *CPLANE1* (n=5) and *CC2D2A* (n=4). Other genes (*NPHP1*, *NPHP4*, *KIAA0586*, *INPP5E*, *TMEM17*, *TMEM216*, *TMEM237* and *TCTN1*) were mutated only in single probands, of whom only those with *NPHP4* or *TMEM216* mutations had CKD. The evolution of renal function was assessed by Kaplan– Meier survival curves **(Fig.18)**.

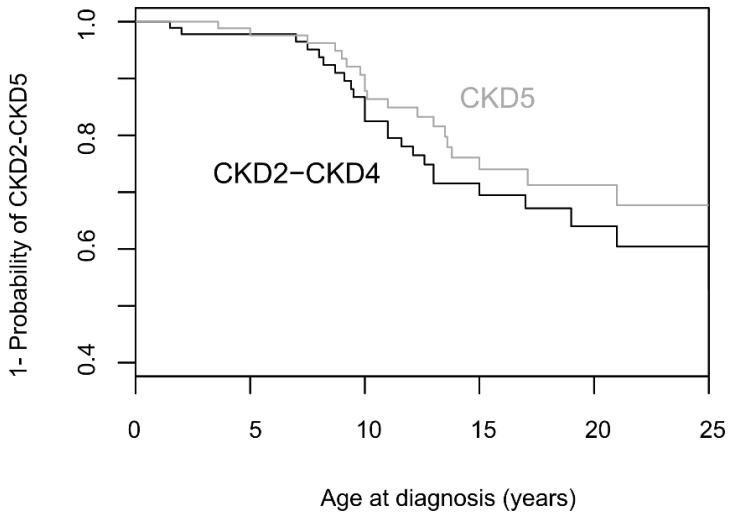

Fig.18. **Survival analysis.** Kaplan–Meyer curves representing the disease-free survival for CKD2–CKD4 and CKD5, respectively. The figure shows age at first diagnosis, which does not necessarily correspond to the actual age at onset. CKD2–CKD4: CKD with mildly to severely decreased eGFR; CKD5: end-stage renal disease

(from Nuovo *et al.*, 2018a)

Because in most patients renal function was not evaluated before JS diagnosis, the age of each CKD category corresponds to the first available medical records, and does not always represent the actual age of onset of renal damage. Specifically, some patients were recruited after developing CKD5. With these limitations, patients developed CKD (CKD2–CKD5) at median age of 10 years. In the 15 families with multiple affected members, the renal phenotype was fully concordant (NRF in 10 families and renal involvement in 5) **(Fig.19)**.

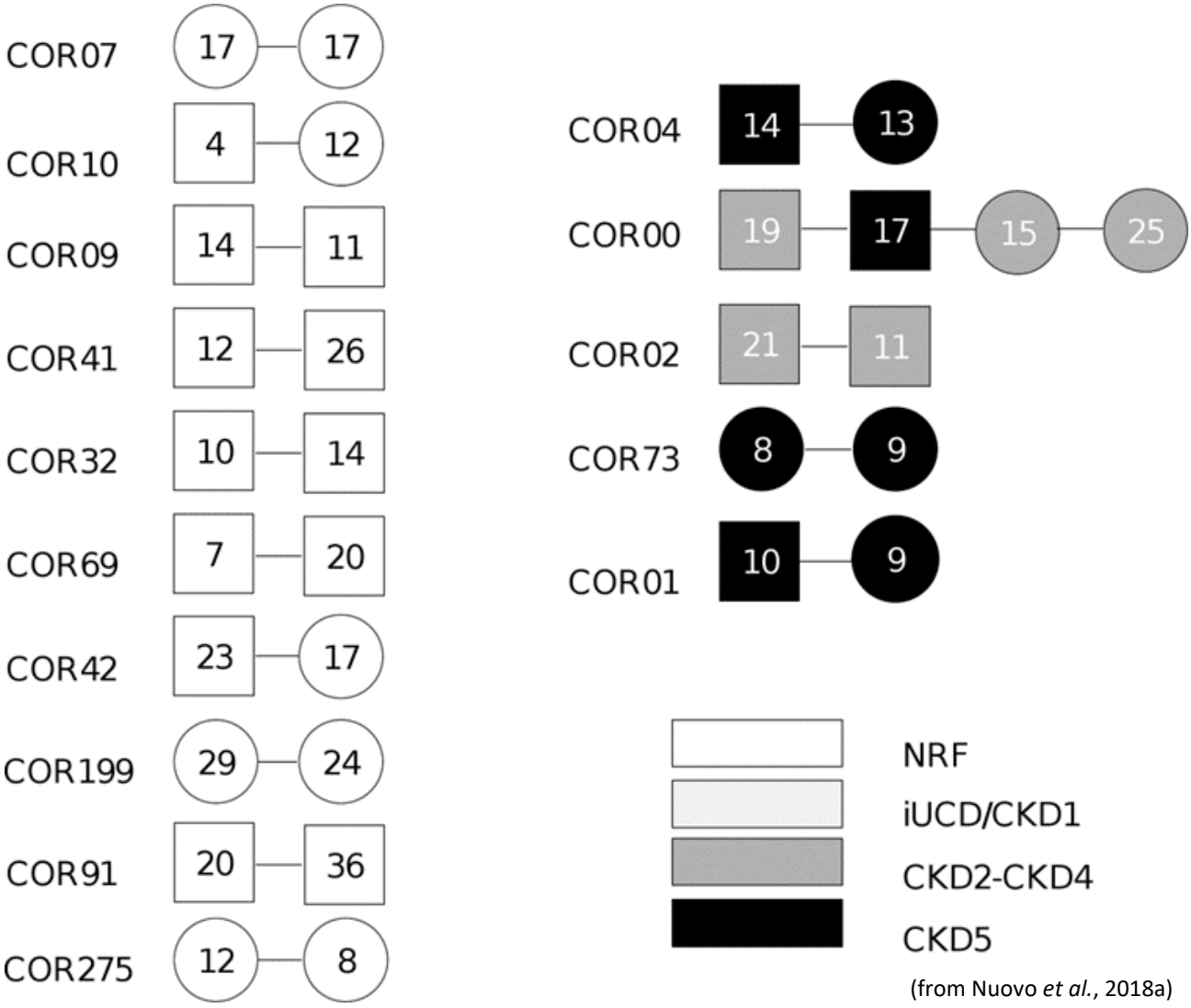

(from Nuovo *et al.*, 2018a)

Fig19. Familial segregation of renal phenotypes. All Joubert families with multiple affected members are reported. Circles and squares represent females and males, respectively. Numbers inside each symbol indicate the age at diagnosis (for subjects within CKD2-CKD5) or the age at last examination (for subjects with NRF). iUCD was not detected in these families. CKD2-CDK5: chronic kidney disease stage 2-5; iUCD: isolated urinary concentration defect; NRF: normal renal function

To evaluate the significance of isolated tubular defects in JS, we focused on the 77 patients who at first examination had either NRF (n=67) or iUCD (n=8). Their urine osmolality values at first

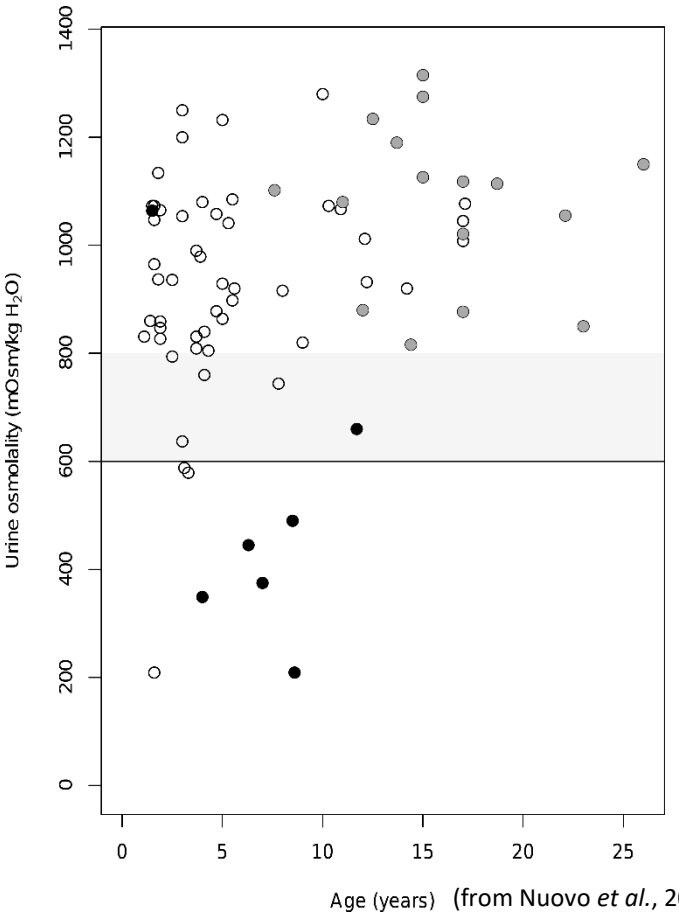

Fig.20. Assessment of urine osmolality and evolution of renal function. For each patient, urine osmolality at first examination was plotted against age. Normality values are set at or >600 mOsm/kg H_2O (black line). The grey zone between 600 and 800 mOsm/kg H_2O defines borderline values. Only subjects with normal eGFR at first examination were included. Grey circles represent patients with NFR who were ≥18 years at time of last examination. Black circles represent patients with normal, borderline or abnormal urinary osmolality at first examination who later developed overt renal insufficiency with abnormal eGFR (CKD2–CKD5). White circles represent patients with NRF who were still <18 years at time of last examination. CKD2-CDK5: chronic kidney disease stage 2-5; NRF: normal renal function (from Nuovo *et al.*, 2018a)

examination were plotted against their age **(Fig.20)**. Notably, UCD was already detectable in very young children, the youngest being 2 years old. Patients with iUCD had significantly higher magnesuria compared with those with NRF. No other differences were observed between the two groups **(Tab.7)**. In 18 patients, urine osmolality was reassessed after 5±3 years (range: 2–12 years). None of the 12 patients with first values ≥800 mOsm/kg H_2O had a pathological test when re-evaluated. Three of four patients with first osmolality <600 mOsm/kg H_2O showed abnormal results in subsequent tests. The fourth patient (first value 579 mOsm/kg H_2O at 3 years) had normal urine osmolality 4 years later. Two children with initial borderline results (aged 3 and 12 years) underwent a second test after about 4 years: the follow-up osmolality was normal in one, borderline in the second patient **(Fig.21)**.

A main aim of this study was to assess the validity of urine osmolality in predicting the risk of developing CKD in JS. We therefore focused on a subset of 23 patients with normal eGFR at the first examination, who either developed CKD2–CKD5 later or maintained NRF in adulthood. Seven subjects had abnormal eGFR at follow-up (CKD2– CKD5). Of them, five had iUCD at their first examination, one had borderline osmolality values and one had normal osmolality **(Fig.20, black circles)**. Conversely, all 16 patients who maintained preserved eGFR after age 18 years had normal

osmolality at first examination **(Fig.20, grey circles)**. In these two groups (7 CKD2–CKD5 versus 16 NRF≥18), we compared the distribution of urine osmolality values at first examination. In line with the above results, data did not overlap, with the exception of a single patient with normal initial urinary concentration ability that later developed CKD5. Mean osmolality values significantly differed between the two groups (513 mOsm/kg H_2O versus 1102 mOsm/kg H_2O, $p<0.001$) **(Fig.22A)**. Logistic regression analysis showed that the probability of developing CKD2–CKD5 significantly correlated with the initial urine osmolality values [β-coefficient =-0.007, 95% confidence interval (95% CI) -0.023 to -0.003; $p<0.01$], with only a small confounding effect of age at osmolality testing. Specifically, the probability of adverse renal outcome was >50% for values <749 mOsm/kg H_2O, and >75% for values <596 mOsm/kg H_2O **(Fig.22B)**. Finally, ROC analysis demonstrated a high diagnostic accuracy of urine osmolality (AUC=0.96, 95% CI 0.86–1.00). The optimal cut-off value for predicting progression to CKD2–CKD5 was 738 mOsm/kg H_2O, corresponding to 86% sensitivity and 100% specificity **(Fig.22C)**. All these results remained significant after including in the calculations the 26 NRF patients <18 years at last follow-up.

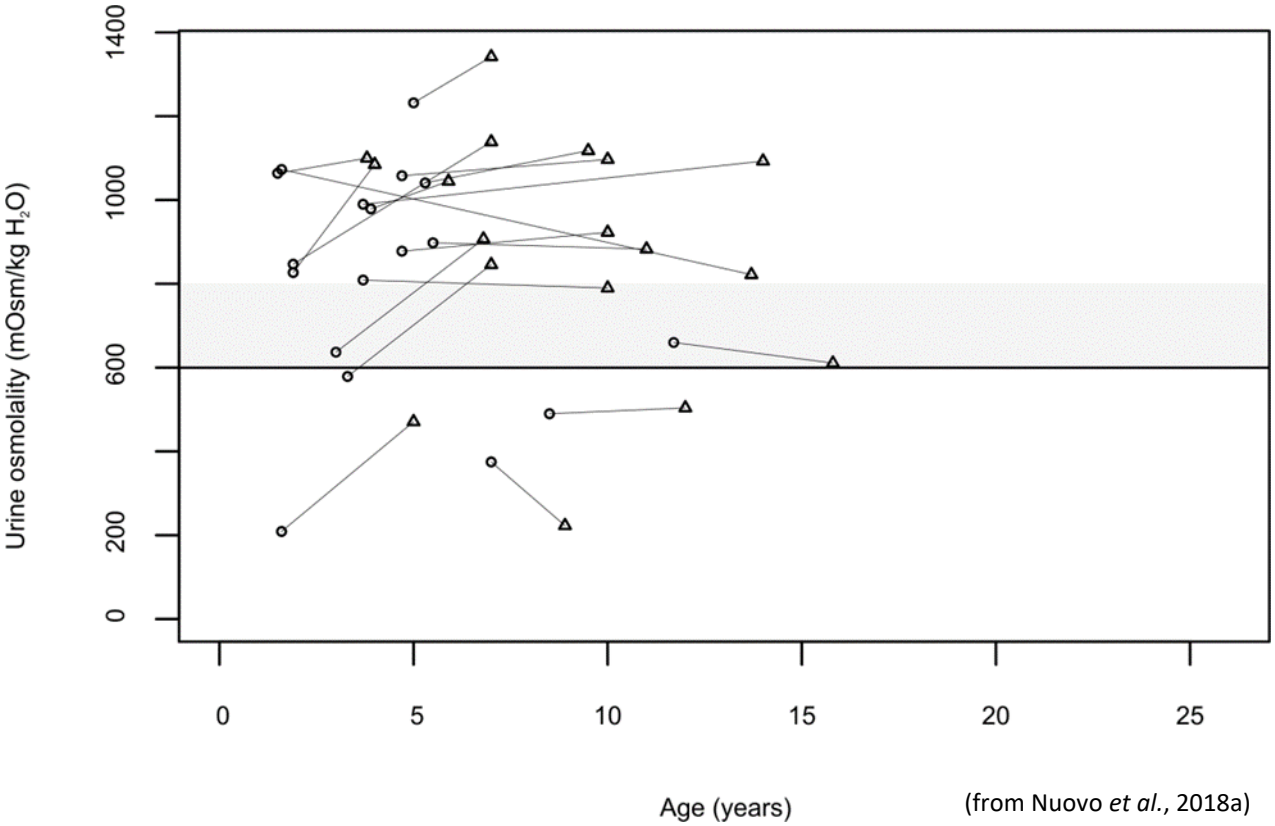

(from Nuovo *et al.*, 2018a)

Fig.21. Repeated osmolality values. Only patients with repeated measurements of urinary osmolality are included in this graph. Each osmolality value is plotted against the corresponding age at measurement. Normality values are set at or above 600 mOsm/Kg H_2O (black line). The shaded zone between 600 and 800 mOsm/Kg H_2O defines borderline values.

Tab.7. Biochemical profile of patients with normal eGFR, with and without urine concentration defect

	Units	NRF (n=67)	iUCD (n=8)	p-value
Age, median (IQR), years	Years	5 (3-13)	5 (3-7)	0.45
Serum Na, mean±SD, mEq/L	mEq/l	140.0±2.5	139.9±1.9	0.88
Serum K, mean±SD, mEq/L	mEq/l	4.4±0.5	4.1±0.6	0.21
Serum Cl, mean±SD, mEq/L	mEq/l	104.3±3.0	103.1±1.4	0.08
Serum Ca, median (IQR), mg/dL	mg/dl	9.6 (9.1-10.0)	9.4 (9.4-9.7)	0.78
Serum P, mean±SD, mg/dL	mg/dl	4.9±0.8	5.1±1.0	0.55
Serum Mg, mean±SD, mg/dL	mg/dl	2.2±0.2	2.1±0.3	0.48
Serum UA, mean±SD, mg/dL	mg/dl	4.1±1.2	4.4±1.2	0.44
FeNa, median (IQR), %	%	0.5 (0.3-0.7)	0.8 (0.5-2.1)	0.13
FeUA, mean±SD, %	%	9.4±4.1	8.8±4.5	0.73
Ca/Cr, mean±SD, mg/mg	mg/mg	0.14±0.12	0.09±0.09	0.36
Mg/Cr, mean±SD, mg/mg	mg/mg	0.15±0.08	0.22±0.08	0.04*
TRP, median (IQR), %	%	91.0 (88.0-93.0)	90.0 (88.0-92.0)	0.68
Tmp/eGFR, mean±SD, mg/dL	mg/dl	4.3±1.1	4.6±1.1	0.51
CrCl, mean±SD, mL/min/1.73 m^2	ml/min/1.73m^2	122.1±30.6	107.7±20.5	0.24

Italics are used for not-normally distributed variables. *p-value ≤0.05. Ca/Cr: urinary calcium/creatinine ratio; CrCl: creatinine clearance; FeNa: fractional excretion of sodium; FeUA: fractional excretion of uric acid; iUCD: isolated urine concentration defect; Mg/Cr: urinary magnesium/creatinine ratio; NRF: normal renal function; TmP/eGFR: maximum reabsorption of phosphates per unit volume of glomerular filtration rate; TRP: tubular reabsorption of phosphates.

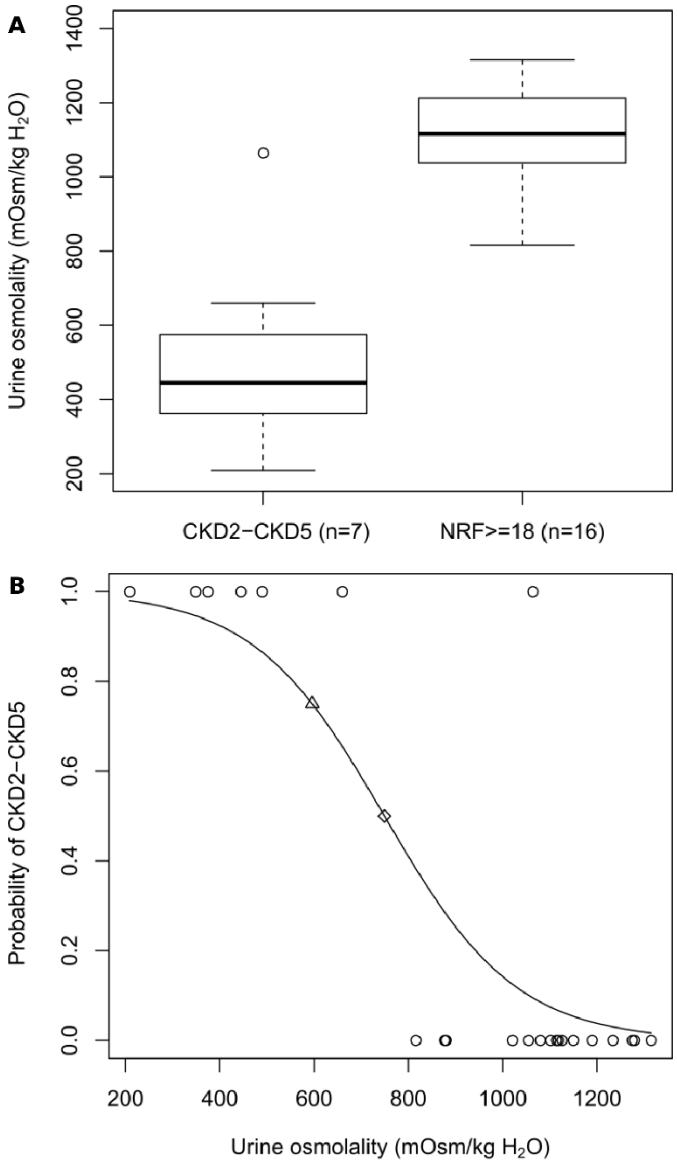

Fig.22. Predictive value of urinary osmolality. **(A)** Box and whisker plots of urine osmolality for patients with normal eGFR at first examination who at follow-up fell in the two following groups: NRF ≥18 (≥18 years with normal renal function); CKD2–CKD5. The central box represents the distance between the lower and the upper quartiles, the middle line is the median and the whiskers extend from the minimum to the maximum osmolality value, excluding outside and far out values, which are displayed as separate points. **(B)** Probability of developing adverse renal outcome (CKD2–CKD5) based on prediction from logistic regression model. Each circle represents a single patient. The risk is predicted to be >50% for urine osmolality values <749 mOsm/kg H_2O (diamond) and >75% for urine osmolality values <596 mOsm/kg H_2O (triangle). **(C)** ROC plot for urine osmolality comparing NRF ≥18 and CKD2–CKD5 groups. The area under the curve is 0.96 (95% CI 0.86–1.00). The value of 738 mOsm/kg H_2O is the best threshold for urine osmolality (defined as the value associated with minimum false-negative and false-positive rates). All figures refer to a subset of 23 patients with normal eGFR at the first examination, who either developed CKD2–CKD5 later or maintained normal NRF in adulthood. CKD2-CDK5: chronic kidney disease stage 2-5; NRF: normal renal function

(from Nuovo *et al.*, 2018a)

Our data demonstrate that kidney involvement is a severe and insidious complication of JS. Since renal disease was not fully recognized until recently, JS patients were frequently diagnosed with advanced CKD. The probability curves for CKD2–CKD4 and for CKD5 observed in our cohort are similar in slope and are separated only by 1–2 years **(Fig.18)**, suggesting that once renal impairment develops, patients progress relatively quickly to end-stage renal disease. A recent study reported renal abnormalities in

30% children with JS, of whom only ~60% (i.e. 18% of the whole cohort) had developed CKD [94]. The latter finding is likely an underestimation as, similar to other studies, this cohort included many young children, at risk of developing CKD later in life [11,105]. Accordingly, when considering only 60 subjects for whom renal follow-up was available in our study, the number of patients with reduced eGFR approximately doubled between the first and the last examination, rising from 15% to 27% **(Fig.17)**. Hypothetically, this estimation could have also been biased by the fact that patients with abnormal renal findings were more likely to be followed-up over time. However, due to the severity of their disease, very few patients were lost at follow-up and the remaining patients were reanalysed irrespectively of the initial finding. Another potential bias of our study relates to the referral of some patients by nephrologists, which may have enriched the population in subjects with NPH. Yet, the majority of patients enrolled by nephrologists had been referred to them by neurologists to perform systematic evaluations of the renal function. We cannot rule out, however, that this may have marginally influenced the observed frequencies. Overall, it appears reasonable to estimate that renal insufficiency will occur in ~25–30% of patients with JS.

The present study clearly shows that low urine osmolality after DDAVP stimulation identifies patients at risk of developing progressive CKD. Notably, a recent work from Rinschen and colleagues [106] identified the urine concentration deficit as a precocious manifestation of autosomal dominant polycystic kidney disease; they also provided exciting evidence that blockade of the vasopressin-2 receptor, probably acting on the distal section of the collecting duct, represents a promising therapeutic strategy, confirming the importance of urine osmolality as a biomarker in different ciliopathies. In our cohort, an iUCD could be detected in patients as young as 2–3 years of age. These children showed no other pathological glomerular or tubular finding, but had on average higher magnesuria, compared with patients with normal concentration ability. This finding is particularly interesting since magnesium handling is nearly exclusively operated at the distal tubule, and isolated magnesuria have been reported in other conditions characterized by abnormalities in tubulointerstitial development, such as in *HNF1B* mutations [107]. In principle, other markers of tubular dysfunction such as NGAL could also be useful for identifying patients at risk, but these could not be assessed in this study. Also, we could not collect enough data about low-molecular weight proteinuria, which would have indicated a proximal tubular dysfunction. Nonetheless, patients with iUCD did not present proteinuria by standard urine analysis, suggesting that proximal tubular reabsorption of proteins was preserved, and that initial tubular defect was more distal.

When available, follow-up assessment of urinary osmolality showed that most normal and pathological values, even if obtained in very young children, remained in the same normal or pathological ranges after several years. Values within or close to the borderline range (600–800 mOsm/kg H_2O) had a less predictable outcome. These observations reflect well the clinical evolution in the long term. Specifically, five out of seven subjects with iUCD at first examination (as well as one patient with borderline values) developed CKD at follow-up. Conversely, of the 17 subjects with normal osmolality that were reassessed in adult age, all but one had normal renal function. This single outliner was diagnosed with JS at age 2 months, had normal urinary concentration ability tested at 3 years and was then lost at follow-up. When re-evaluated at 11 years, he was found to have CKD3 and progressed to CKD5 one year later.

Overall, our study indicates that urine osmolality is a good predictor of the probability of developing renal insufficiency. In practical terms, we propose to measure the first-morning urine osmolality in all JS patients around the age of 3 years. If urine osmolality is repeatedly found <800 mOsm/kg H_2O, then a DDAVP test is useful to assess the renal concentration ability. Although exceptions cannot be excluded, when patients can concentrate their urine >800 mOsm/kg H_2O, the family can be reassured, as long as a control test is planned later (around 8 years of age). Borderline osmolality values (600–800 mOsm/kg H_2O) should be rechecked earlier, as some patients may develop renal disease. Conversely, values <600 mOsm indicate a probable nephropathy. A confirmatory test should be planned in the following months and, if abnormal, appropriate water intake and renal monitoring should be started.

Our data also confirms the previously reported association of retinal and renal involvement in JS [11,105], and the concordance of renal phenotype within families [105]. Pathogenic mutations in known JS-associated genes were identified in ~54% probands with renal disease, with a high prevalence of mutations in *CEP290*, a gene that we first reported to be significantly associated to the retinal–renal phenotype [49]. This is also in line with a recent study describing the clinical and genetic correlates of a large cohort of 440 JS patients [11]. In our cohort, mutations in *TMEM67* and *AHI1* seem to be slightly overrepresented in patients with NRF compared with those with renal disease, at difference to what shown by Fleming and collaborators [94], who reported a similar mutation frequency of these genes in the two groups. A possible explanation for this discrepancy could lie in the definition of "kidney disease" used by the authors, which also include subjects with abnormal renal US as an isolated finding, regardless of kidney function. However, these differences between studies can also be

explained by the small number of patients with mutations in a given gene. Hence, comparison did not reach statistical significance.

In conclusion, we observed that nearly 30% patients with JS eventually develop renal insufficiency. Besides ultrasound abnormalities, an iUCD often represents the earliest sign of an underlying renal disease and predicts evolution towards CKD. A positive family history for renal disease and the presence of retinopathy also convey a high risk of renal involvement. These findings are relevant for the clinical management and genetic counselling of JS patients, and we suggest that urinary osmolality should be included in the diagnostic work-up of children with JS.

1.4 HYPOMORPHIC RECESSIVE VARIANTS IN *SUFU* IMPAIR THE SONIC HEDGEHOG PATHWAY AND CAUSE JOUBERT SYNDROME WITH CRANIO-FACIAL AND SKELETAL DEFECTS [108]

The use of WES in families with no identified mutations in known JS causative genes after targeted resequencing has allowed to identify *SUFU*, coding for the main negative regulator of the Sonic Hedgehog (SHH) pathway, as a new JS-associated gene. In addition to our JS patient cohort, a second JS cohort recruited at the University of California San Diego (La Jolla, CA, United States) has been considered for this project.

Homozygous missense variants in this gene have been identified in four children from two unrelated families (originating from Italy and Egypt, respectively). All affected subjects presented peculiar facial dysmorphisms (hypertelorism, broad and depressed nasal bridge, frontal bossing), oculomotor apraxia, developmental delay with mild intellectual impairment, gait ataxia, and dysarthria. Three of them had post-axial polydactyly and two had global macrosomia with

Fig.23. Patient clinical and neuroimaging features. (A–D) Pictures of the four children from families COR369 **(A,B)** and MTI2023 **(C,D)**. Note hypertelorism, frontal bossing, and broad, depressed nasal bridge. **(E and F)** Bilateral hand post-axial polydactyly **(E)** and plantar dyskeratotic pits **(F)** in the boy from COR369. **(G)** Right hand post-axial polydactyly in the boy from MTI-2023. **(H–O)** Brain MRI of girl **(H–K)** and boy **(L–O)** from COR369. Note mild vermis hypoplasia **(H,L)** and thickened, horizontally orientated superior cerebellar peduncles **(**mild *molar tooth*, **I,M)**, associated with polymicrogyria **(arrows in J,K,N,O)**. Also note the megacisterna magna in the sagittal image of the girl **(H)**. **(P–S)** Brain MRI in the proband from MTI-2023. Note vermis hypoplasia, megacisterna magna **(P,Q)**, dysplastic folia **(curved arrows in R)**, deep interpeduncular fossa, and thickened horizontally orientated superior cerebellar peduncles **(**mild *molar tooth*, **Q)**. All subjects show lateral ventricular enlargement and shrunken white matter in the posterior regions **(K,N,O,S)**.

(from De Mori *et al.*, 2017)

macrocephaly. One child also showed a few small dyskeratotic pits on the foot soles **(Fig.23A-G)**. There were no other signs of systemic involvement, except for mild retinopathy in one sibling from family COR369. Brain imaging showed cerebellar vermis hypoplasia with elongated superior cerebellar peduncles and deepened interpeduncular fossa (mild MTS) in all children; in addition, the two siblings from family COR369 had bilateral polymicrogyria mainly involving the perisylvian regions **(Fig.23H–S)**.

In family COR369, two distinct homozygous missense variants survived the steps of stringent filtering of WES data, Sanger validation, and segregation analysis: c.1217T>C (p.(I406T)) in *SUFU* (GenBank: NM_016169.3) and c.2146A>T (p.(T716S)) in *CDHR1* (MIM: 609502; GenBank: NM_033100) **(Fig.24)**. Both variants were absent from all public databases and from in-house WES databases consisting of more than 6,000 samples and were unanimously predicted to be deleterious. Only one individual in the gnomAD database carried a heterozygous missense variant affecting the same *SUFU* residue but resulting in a different amino acid change (c.1218C>G; p.(I406M)). *CDHR1* (also termed *PCDH21*) is expressed only in the outer nuclear layer of the retina and encodes for protocadherin 21. Recessive variants of this gene are known to cause a form of cone-rod dystrophy with onset in the late second decade of life (MIM: 613660).

In family MTI-2023, only the c.527A>G (p.(H176R)) variant in *SUFU* survived bioinformatic filtering of WES data and segregation analysis **(Fig.24)**. This variant was absent from public databases and from in-house dataset, including sequencing data from more than 3,000 Egyptian individuals, and was predicted to have a deleterious impact on the protein function.

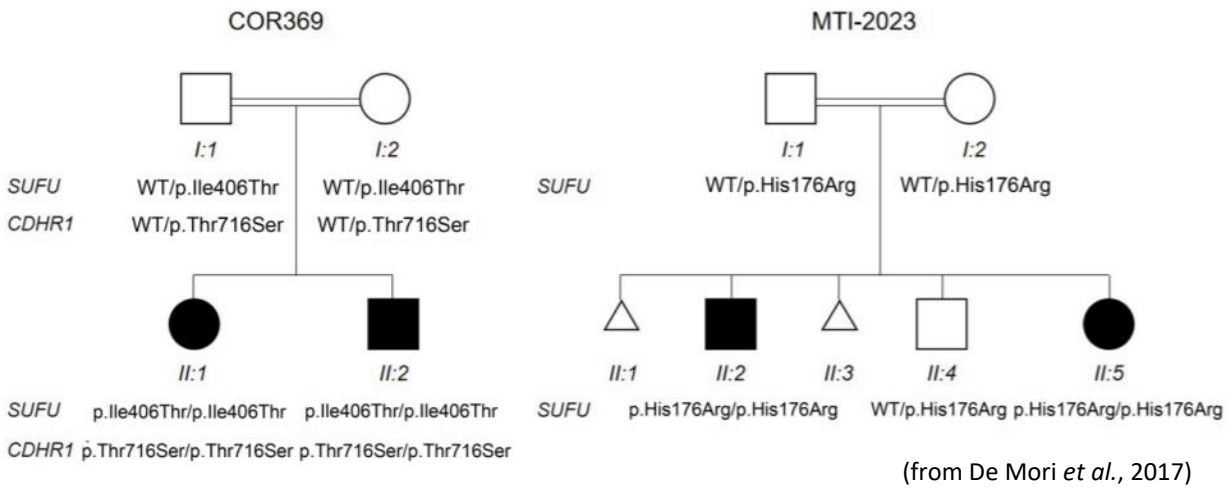

(from De Mori *et al.*, 2017)

Fig.24. Simplified pedigrees of families COR369 and MTI-2023. Genotypes of the identified variants is reported below the symbols. Black symbols denote affected individuals.

In order to confirm the pathogenic effect of *SUFU* mutations, both bioinformatic modeling and functional studies have been performed.

(i) Dynamic Properties of Mutant SUFU Protein

The SUFU protein alternates between ‘‘open’’ and “closed’’ conformations. The closed form is stabilized by the binding with GLI proteins, whereas the open state is caused by the dissociation from GLI. Changes of critical residues on the interface between SUFU and GLI proteins may disrupt their complex and prevent SUFU from repressing GLI-mediated transcription. To assess the pathogenic effect of the identified missense variants, we first investigated their structural and dynamic impact on the SUFU protein **(Fig.25)**. In particular, the following measures were calculated in WT and mutant proteins: (1) root mean square deviation (RMSD), that measures the average distance between all heavy atoms (in this case Cα atomic coordinates) with respect to the X-ray structure; (2) root mean square fluctuation (RMSF), measuring the deviation over time between the positions of the Cα atomic coordinates of each residue with respect to the X-ray structure; and (3) dynamic cross correlation maps (DCCMs), that allow investigation of the long-range interactions of atoms.

Globally, mutant proteins showed higher RMSD levels and turned out to be more flexible than WT, with SUFU$^{p.H176R}$ mainly affecting the region involved in the formation of the GLI3-binding pocket **(Fig.25A-C)**. DCCMs of both mutants versus WT showed a dramatic change in the protein dynamics. In the WT model, the linker domain moved in a highly anti-correlated way with both the C-terminal and the N-terminal regions of the core domain. Instead, both mutants displayed random movements of the residues within the C-terminal domain and loss of the native enveloping movement of the binding site around GLI3 protein **(Fig.25D)**. To confirm the observed major perturbation of SUFU-GLI3 complex activity, we analyzed the modification of hydrogen bonds (h-bonds) between residues that constitute the SUFU-GLI3 binding site, as well as the size of the binding pocket. During 200 ns simulation time, the WT protein repeatedly changed the size of the binding site and the number of h-bonds depending on the alternative open or closed conformations, while both mutants kept an almost stable distance between amino acids constituting the binding site and an almost constant number of h-bonds with GLI3 **(Fig.25E,F)**. Overall, these findings suggest that both mutants hamper significantly the functional open/close states of the protein to different extents.

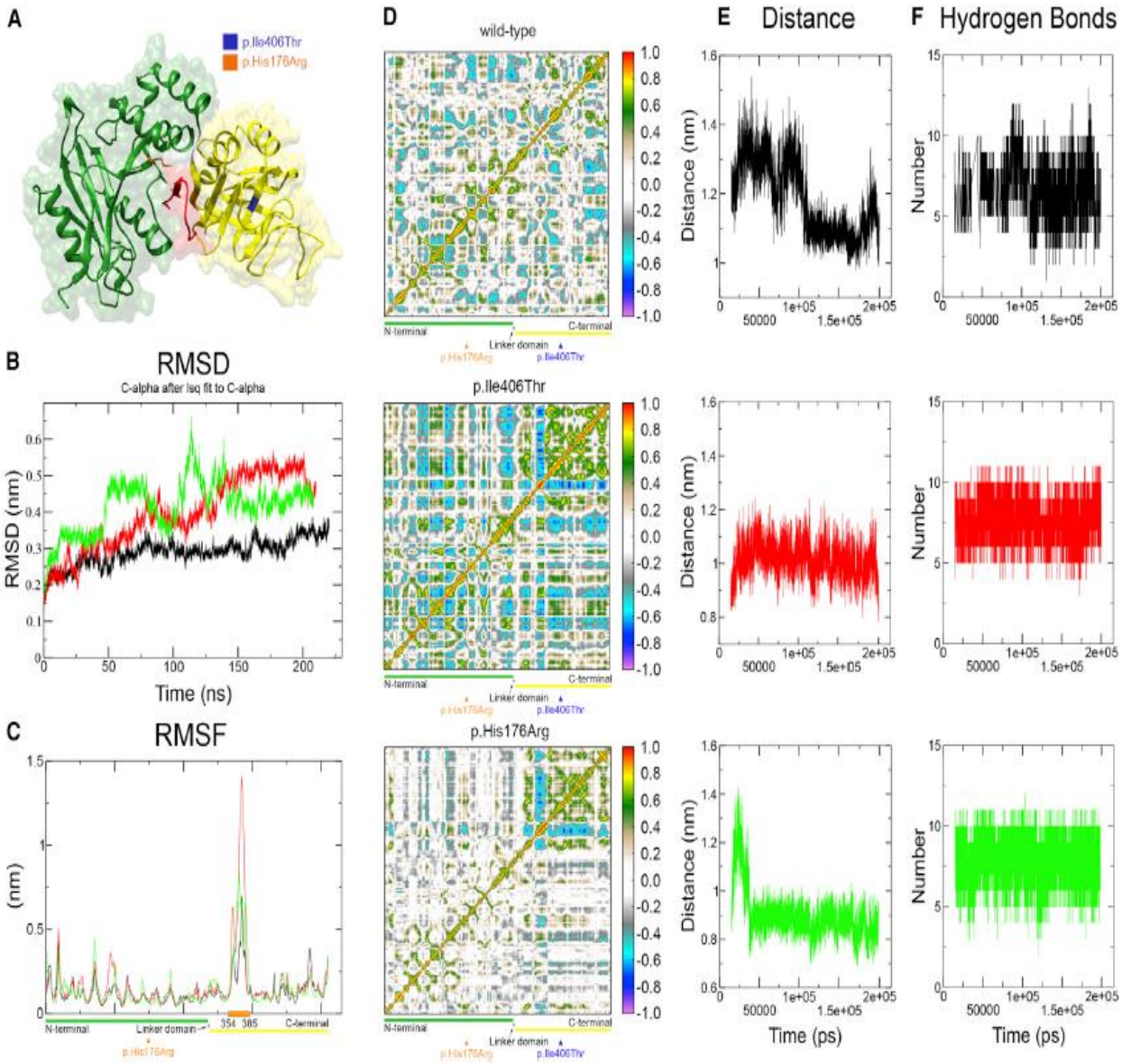

from De Mori *et al.*, 2017

Fig.25. Analysis of Molecular Dynamics Simulations of wild-type and mutant SUFU Proteins

(A) 3D structure of SUFU-GLI complex. The N-terminal, C-terminal, and linked domains are colored green, yellow, and gray, respectively, while the GLI3 protein is colored in red. p.I406T is highlighted in blue and p.H176R in orange.

(B) SUFU wild-type reaches a stable state after 60 ns of simulation, recording an RMSD of ~0.3 nm. Conversely, both SUFU mutants exhibits root mean square deviation (RMSD) levels around 0.5 nm, after a longer stabilization stage of 150 ns.

(C) SUFU$^{p.H176R}$ shows altered root mean square fluctuation (RMSF) values compared to wild type, mainly affecting the region nearby the mutation, which is known to participate in the formation of the GLI3-binding pocket.

(D) Covariance matrix for SUFU wild-type (top), SUFU$^{p.I406T}$ (center), and SUFU$^{p.H176R}$ (bottom). Perfect direct or inverse correlations are highlighted in red or violet, respectively.

(E) Distances between amino acids forming the binding site for GLI3.

(F) H-bonds established during simulation between the residues forming the ligand binding pocket and GLI3.

In **(B)–(F)** graphs, SUFU wild-type is colored in black, SUFU$^{p.I406T}$ in red, and SUFU$^{p.H176R}$ in green.

(ii) *SUFU* Missense Variants Reduce Protein Stability

To evaluate whether *SUFU* variants could impact protein stability, IMCD3 cells were transfected with HA-tagged SUFU WT, SUFU$^{p.I406T}$, or SUFU$^{p.H176R}$ for 24, 48, and 72 hr and processed by Western Blot (WB). Mutant SUFU protein levels were significantly lower than WT already at 24 hr and decreased rapidly, with SUFU$^{p.I406T}$ almost disappearing at 72 hr after transfection **(Fig.26)**. Moreover, confocal microscopy analysis showed an abnormal subcellular localization of SUFU$^{p.I406T}$, which tended to form intracytoplasmic aggregates, while SUFU WT and SUFU$^{p.H176R}$ had uniform cytoplasmic and nuclear localization **(Fig.27)**.

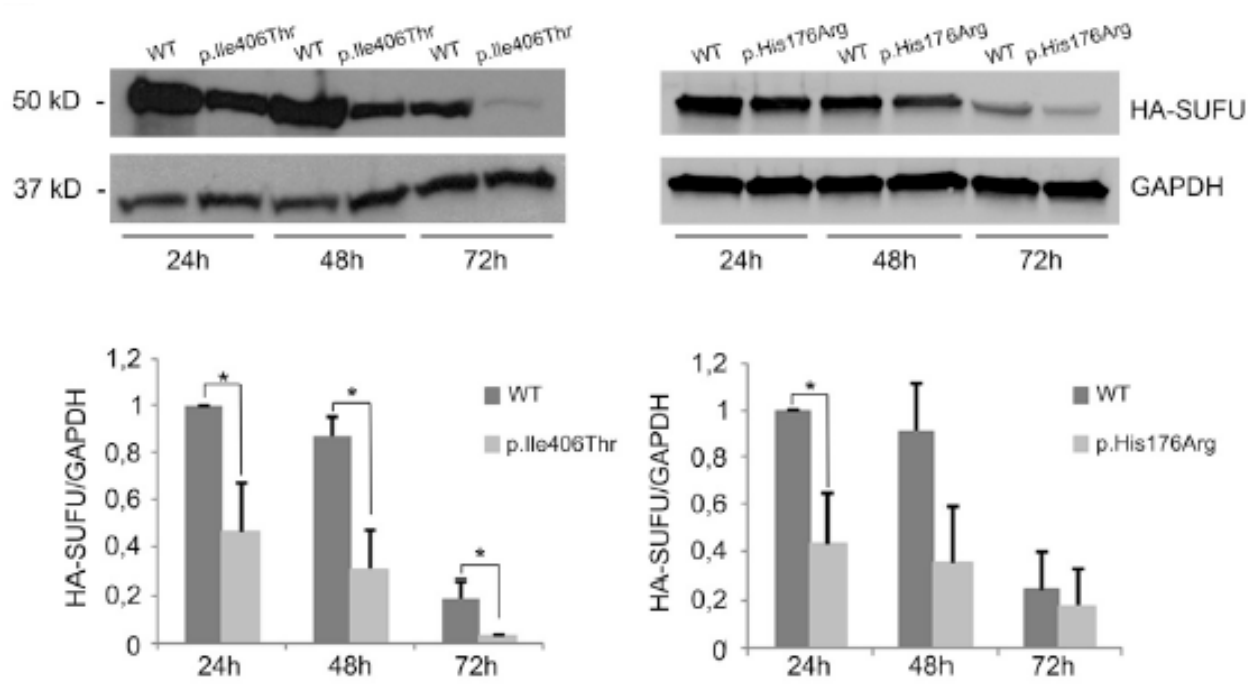

(from De Mori *et al.* 2017)

Fig.26. *SUFU* Missense Variants Reduce Protein Stability
IMCD3 cells transfected with hemagglutinin (HA)-tagged SUFU WT, SUFU$^{p.I406T}$, and SUFU$^{p.H176R}$ for 24, 48, and 72 hr show a more rapid decrease of mutant SUFU protein levels compared to WT (quantified by densitometry in the corresponding graphs). Graphs represent means ± standard errors. *$p < 0.05$.

SUFU protein levels are regulated within the cell mainly by degradation through the ubiquitin-proteasome system (UPS). To test whether the observed reduction in SUFU levels was due to increased UPS-mediated degradation, transfected IMCD3 cells were treated with the proteasomal inhibitor MG132 for 6 hr and analyzed by WB. Proteasomal blockage induced the accumulation of both WT and mutant SUFU proteins, confirming that mutant proteins are processed through the UPS **(Fig.28)**.

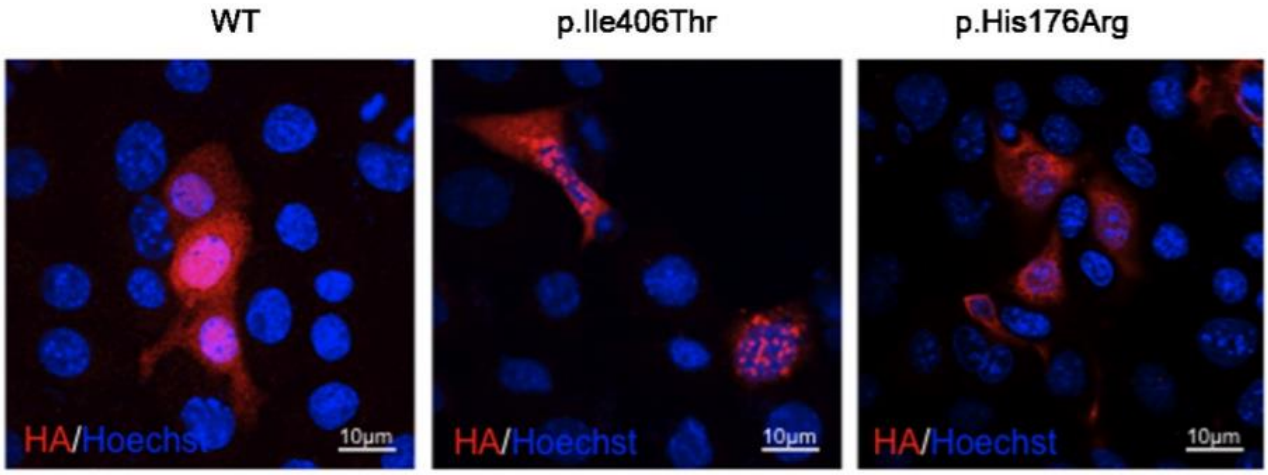

(from De Mori *et al.* 2017)

Fig.27. Subcellular localization of mutant SUFU within cells. Representative images of IMCD3 cells transfected with hemagglutinin (HA)-tagged SUFU WT, SUFU$^{p.I406T}$ or SUFU$^{p.H176R}$ for 24 hours and processed for immunofluorescence. Both SUFU wild-type and SUFU$^{p.H176R}$ distributed uniformly throughout the cytoplasm and the nucleus, while SUFU$^{p.I406T}$ showed the tendency to form aggregates.

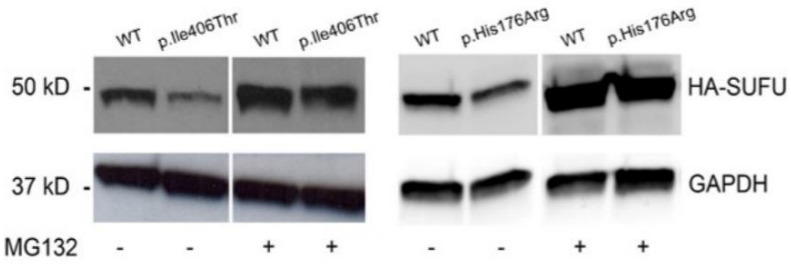

(from De Mori *et al.* 2017)

Fig.28. Wild-type and mutant SUFU proteins are degraded by the ubiquitin-proteasome pathway. IMCD3 cells were transfected with HA-tagged SUFU wild-type, SUFU$^{p.I406T}$ and SUFU$^{p.H176R}$ and treated with the proteasomal inhibitor MG132 for 6 hours. Treatment induced accumulation of both wild-type and mutant SUFU proteins.

(iii) *SUFU* Missense Variants Impair the Binding with GLI3 and Its Proteolytic Cleavage

Next, we focused on the interaction between SUFU and GLI3, since it is known that the major contribution to the repressor forms of GLI comes from GLI3. Indeed, cleaved GLI3R suppresses SHH target genes when the pathway is inactive, while activated GLI2 triggers target gene expression upon stimulation of the pathway [109]. To examine whether the identified missense variants could affect SUFU-GLI3 binding, as suggested by molecular dynamics simulations, co-immunoprecipitation experiments were performed on total protein extracts of IMCD3 cells transfected with either HA-tagged SUFU WT, SUFU$^{p.I406T}$, or SUFU$^{p.H176R}$. The binding of unprocessed GLI3 was significantly higher with SUFU WT than with either of the two mutant proteins, suggesting that both missense variants impaired the ability of SUFU to bind GLI3 **(Fig.29)**.

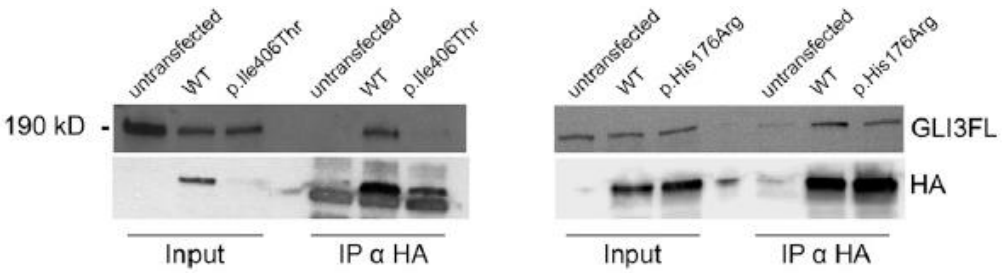

(from De Mori *et al.* 2017)

Fig.29. SUFU Missense Variants Impair Binding to GLI3. Co-immunoprecipitation experiments in IMCD3 cells transfected with either hemagglutinin (HA)-tagged SUFU WT, SUFU$^{p.I406T}$, or SUFU$^{p.H176R}$, showing reduced binding of GLI3 to mutant SUFU.

(iv) *SUFU* Missense Variants Impair Repression of the SHH Pathway

In light of the previous results, we sought to assess whether the SHH pathway was deregulated in the presence of mutant SUFU. To this aim, we evaluated by quantitative real-time PCR in control and mutant fibroblasts the expression levels of 14 genes, including several target genes of the SHH pathway and representative genes of other developmental pathways such as BMP, canonical Wnt, and noncanonical Wnt/planar cell polarity (PCP) pathways. Interestingly, the basal expression levels of the key SHH target genes *BCL2*, *GLI1*, and *PTCH1* were significantly higher in both mutant fibroblasts compared to control, with a limited further increase upon stimulation with SAG, SMO agonist able to activate the SHH pathway. Conversely, mutant cells showed markedly lower basal expression levels of VANGL2 (involved in the PCP pathway), which were only minimally perturbed after SAG treatment **(Fig.30)**. These altered expression levels could be partially rescued by overexpression of SUFU WT in mutant fibroblasts (data not shown). These findings confirm the previous observations that the identified missense variants impair the ability of SUFU to constitutively repress the SHH pathway, which results in deregulation of target gene expression especially in unstimulated conditions.

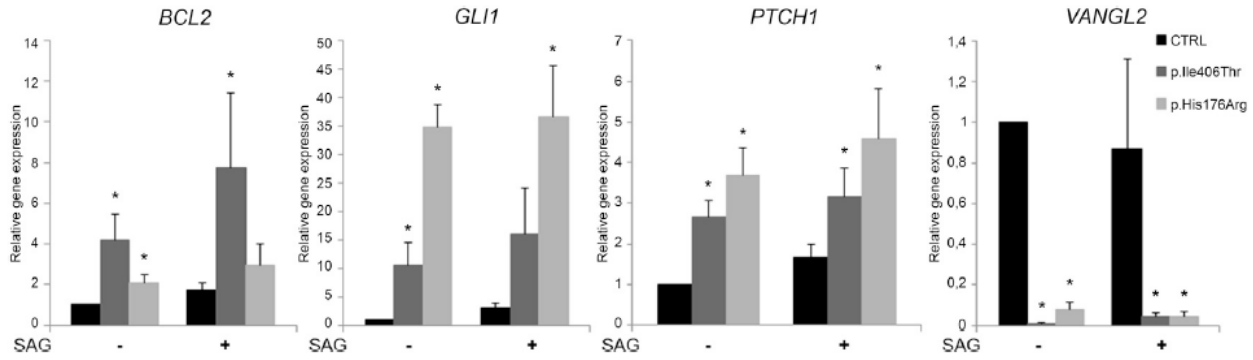

Fig.30. The Sonic Hedgehog pathway is deregulated in mutant fibroblasts. (from De Mori *et al.* 2017)
Histograms show the expression levels of four target genes that in basal conditions are either significantly overexpressed (*BCL2*, *GLI1*, and *PTCH1*) or under-expressed (*VANGL2*) in fibroblasts from the two probands compared to control subjects. Results are representative of three independent experiments. Graphs represent means 5 standard errors. *$p < 0.05$.

The SHH pathway plays a central role in controlling cell patterning and differentiation of several embryonic structures, such as the central nervous system and the limbs. In vertebrates, SHH signaling is critically mediated by the primary cilium, a microtubule-based organelle protruding from the surface of nearly all cell types. Many components of the SHH pathway are variably localized within the cilia at different steps of pathway activation [110,111], and the malfunctioning of many ciliary genes is known to impair SHH signaling [112–115]. On the other hand, ciliopathies such as JS, acrocallosal syndrome and oral-facial-digital syndromes frequently present with congenital defects of the CNS midline facial anomalies and polydactyly, which are at least partially attributed to altered SHH signaling [26,116–118]. An aberrant activity of the SHH pathway has also been firmly associated with increased risk of developing cancer. Germline heterozygous loss-of-function variants of either *PTCH1* or *SUFU* may cause a complex condition termed nevoid-basal-cell carcinoma syndrome (Gorlin syndrome [MIM: 109400]), characterized by the occurrence of several basal cell carcinomas and other cancers at a young age (<20 years), variably associated with developmental and skeletal abnormalities [119,120]. Moreover, somatic variants of *PTCH1*, and both germinal and somatic variants of *SUFU*, have been found to predispose to a variety of tumors, such as basal cell carcinoma, meningioma, and cerebellar medulloblastoma (MIM: 605462, 607174, 155255) [121–125]. To date, germline recessive pathogenic variants of *SUFU* had never been reported in human subjects, supporting the essential role of SUFU in embryonic development.

Our findings suggest that both the identified variants are hypomorphic alleles, resulting only in a partial loss of the normal gene function. This is in line with the previous observations that complete Sufu knock-out is lethal in mouse embryos [126] and that human *SUFU* is extremely intolerant to loss of function and generally intolerant to variation. In fact, homozygous loss-of-function variants were never observed in more than 138,000 individuals from the gnomAD database (pLI score = 1) [127], and even synonymous and missense variants were observed at significantly lower frequency than expected (positive Z scores of 1.82 and 2.54, respectively) and nearly always in the heterozygous state. Of note, the Geno2MP database reports the occurrence of a rare, potentially harmful homozygous missense variant in *SUFU* (p.A425V, CADD score 18.38) in a single subject with reported cerebellar anomalies. Although we were not able to get in touch with the referring clinician, this individual may represent yet another case of *SUFU* recessive hypomorphic mutations giving rise to a neurodevelopmental phenotype. Intriguingly, limb-specific conditional deletion of Sufu in mouse model results in polydactyly due to a block in Gli3R processing [128,129], whereas mouse embryos with conditional knock-out of Sufu in the mid-hindbrain show altered morphology of the brainstem and

cerebellum and delayed differentiation and abnormal migration of most cerebellar cell types [130], resembling clinical features of those of our affected children.

Functional studies performed on patient fibroblasts demonstrate that deregulation of the SHH pathway induced by *SUFU* hypomorphic recessive variants occurs through two distinct mechanisms: on one hand by reducing SUFU half-life within cells, on the other hand by selectively impairing its interaction with GLI3 and the subsequent formation of GLI3R. Further support to the link between the identified *SUFU* variants and a deregulation of SHH signaling comes from the observed phenotype, which is mainly characterized by (1) typical cranio-facial dysmorphisms (hypertelorism, depressed nasal bridge, frontal bossing, macrocephaly); (2) developmental delay, mild intellectual impairment, ataxia, and ocular-motor apraxia; (3) cerebellar vermis hypoplasia with dysplastic foliar pattern and mildly elongated superior cerebellar peduncles (mild MTS); and (4) postaxial polydactyly. This clinical presentation shares features both with ciliopathies (such as JS and acrocallosal syndrome) and with syndromes characterized by impaired repression of the SHH pathway (for example Greig cephalopolysyndactyly syndrome [MIM: 175700], caused by heterozygous *GLI3* variants). Moreover, a proportion of subjects with Gorlin syndrome, caused by heterozygous loss-of-function variants of either *PTCH1* or *SUFU*, variably exhibit macrocephaly, hypertelorism, depressed nasal bridge, post-axial polydactyly, as well as macrosomia and dyskeratotic plantar pits (present in family COR369). Such observations suggest that these peculiar cranio-facial and digit anomalies are strictly related to abnormal activation of the SHH pathway, caused either by reduced levels (or functioning) of repressor proteins or by the constitutive activation of proteins that transduce SHH signaling.

In conclusion, we report that germline recessive hypomorphic variants in *SUFU* may alter its stability and function as repressor of the SHH pathway, giving rise to a peculiar spectrum of developmental defects sharing features of ciliopathies such as JS and of SHH-related disorders. The occurrence of specific cranio-facial and digit abnormalities should represent red flags implicating an underlying defect of genes involved in the SHH pathway.

CHAPTER2: PONTOCEREBELLAR HYPOPLASIA

In this Chapter, clinical and molecular spectrum of PCH will be presented, together with genotype-phenotype associations. I was personally involved in the revision of clinical and neuroimaging features of patients, in the analysis and interpretation of NGS data, as well as and in the statistical analyses.

2.1 DETECTION RATE AND MUTATIONAL SPECTRUM

To date, 63 probands referred for molecular genetic testing of PCH-causative genes have been screened through targeted resequencing. Biallelic variants in autosomal recessive genes or heterozygous/hemizygous variants in the X-linked *CASK* gene have been identified in 46 patients (~73%) **(Appendix, Tab.A5) (Fig.31)**. The most frequently mutated gene is *CASK*, accounting for 43% of the screened probands. Notably, four out of the 27 *CASK*-positive cases were males, showing a hemizygous genotype for a nonsense variant in mosaic state (c.82C>T), a missense variant (c.1852A>G), a two-exons deletion ((c.831+1_832-1)_(1015+1_1016-1)del) and a single-amino-acid deletion (c.2174_2176del), respectively. *CASK* variants identified in the whole cohort occurred *de novo*, with the exception of the in-frame deletion c.2174_2176del, which resulted to be maternally inherited. An additional percentage of probands presents with mutations in *TSEN54*, which explains 16% of PCH cases. All the identified *TSEN54*-patients presented the missense founder variant c.919G>T (p.(A307S)) in homozygous state [131]. The third more frequently mutated gene is *EXOSC3*, detected in 8% of probands and mostly identified with the missense variant c.395A>C (p.(D132A)). Lastly, a minor percentage of probands has been diagnosed with pathogenic variants in *PMM2* (2%), *RARS2* (1%), *TOE1* (1%) and *VLDLR* (1%).

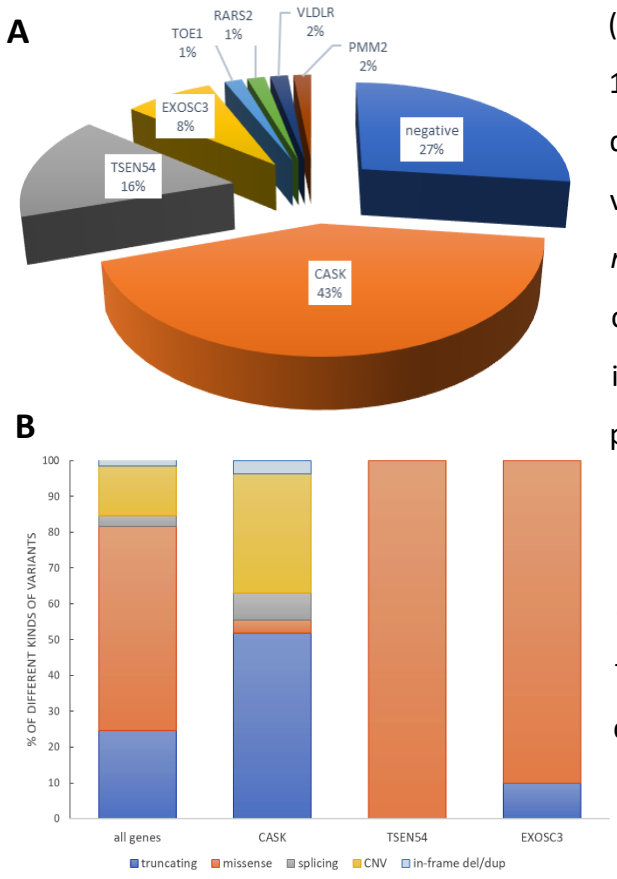

Fig.31. Genetic architecture of pontocerebellar hypoplasia. (A) mutational spectrum identified in the investigated cohort **(B)** differential contribution of mutation types across the 3 genes most commonly associated with pontocerebellar hypoplasia.

When considering all the mutated genes, the prevalent kind of variants is represented by

missense changes (56.9%), followed by truncating variants (24.6%) and CNVs (13.9%), while splicing variants and in-frame deletions/duplications account for a minimal percentage of cases. A clear prevalence of missense variants has been observed also for *TSEN54* and *EXOSC3* genes, taken individually. Conversely, *CASK* is mainly affected by truncating variants (51.6%) and CNVs (33.3%) spanning across the whole gene.

2.2 GENOTYPE-PHENOTYPE ASSOCIATIONS

In most of available publications reporting large patients cohorts, the analytic approach consists in assessing the frequency of single clinical features within specific PCH subtypes [68,69,71–73,77,131,132]. Moreover, the investigated features differ among studies, and MRI description usually focuses on PF abnormalities.

In order to improve phenotypic characterization of PCH patients, we performed a systematic assessment of our patient cohort as a whole. A comprehensive phenotypic and neuroradiological characterization has been obtained for 53 PCH individuals, recruited as part of a multicenter research project. We also proposed a phenotype-based cluster analysis for investigating associations between genes and specific PCH subphenotypes.

MRI studies have been performed either on a 1.5 T or a 3 T MR scanner. In addition to MRI scans, detailed clinical data (including ancestry, sex, family history, pregnancy and delivery, occipito-frontal-circumference measurements at birth and later ages, psychomotor development, cerebellar signs, cognitive and motor changes, epilepsy, vision and hearing) have been retrospectively collected by physicians. Head circumference was measured and plotted on CDC charts and expressed as SD. For patients repeatedly assessed over time, clinical status at last follow-up was considered.

One-way analysis of variance was used to compare age at last follow-up between the patient groups. In order to explore genotype-phenotype correlations, a subset from the original dataset was created, containing clinical and neuroradiological features of the mutated patients. Unsupervised hierarchical cluster analysis was performed to identify homogeneous subphenotypes; since mixed types of variables have been considered (i.e. continuous and categorical), Gower's distance was used as a similarity index. Then, potential associations between genes and clusters were investigated through a baseline-category logistic regression model. A p-value of ≤0.05 was

considered statistically significant, with Benjamini & Hochberg correction for multiple comparisons. Statistical analyses were performed using R [133].

Among the 53 probands with available detailed clinical information, causative variants have been identified in *CASK* (n=25), *TSEN54* (n=10) and *EXOSC3* (n=5), while 13 patients had a negative genetic test result.

Tab.8. Comprehensive clinical and neuroradiological features of patients with pontocerebellar hypoplasia

	CASK	***TSEN54***	***EXOSC3***	**NEGATIVE**
Clinical features*				
M:F	0.2	1.0	0.7	0.9
age at last follow-up	5.9±5.7	3.6±5.6	3.2±3.6	7.7±7.6
term pregnancy	18/25 (72%)	8/10 (80%)	5/5 (100%)	9/13 (69%)
polyhydramnios	0/25 (0%)	1/10 (10%)	0/5 (0%)	1/13 (7.7%)
OFC at birth (mean±SD)	-2.0±1.2	-1.1±0.6	-1.2±1.4	-1.8±2.3
OFC at last FU (mean±SD)	-4.2±2.1	-3.8±1.92	-3.4±2.6	-3.0±2.3
microcephaly at last FU	21/24 (87.5%)	8/9 (88.9%)	3/5 (60%)	9/12 (75%)
neurodevelopmental delay	25/25 (100%)	10/10 (100%)	5/5 (100%)	13/13 (100%)
ataxia	14/23 (60.9%)	2/9 (22.2%)	0/4 (0%)	2/13 (15.4%)
dyskinesias	10/21 (47.6%)	7/10 (70%)	1/4 (25%)	7/12 (58.3%)
jitteriness, clonus	0/25 (0%)	3/10 (30%)	0/5 (0%)	0/13 (0%)
other involuntary movements	7/24 (29.2%)	4/10 (40%)	0/3 (0%)	2/13 (15.4%)
hypotonia				
diffuse	5/23 (21.7%)	2/10 (20%)	3/5 (60%)	0/12 (0%)
proximal	15/23 (65.2%)	7/10 (70%)	2/5 (40%)	9/12 (75%)
hypertonia				
diffuse	2/22 (9.1%)	0/10 (0%)	0/5 (0%)	1/12 (8.3%)
distal	10/22 (45.5%)	8/10 (80%)	0/5 (0%)	9/12 (75%)
deep tendon reflexes				
hyperelicitable	13/20 (65%)	8/10 (80%)	0/5 (0%)	10/12 (83.3%)
hypoelicitable	3/20 (15%)	1/10 (10%)	5/5 (100%)	0/12 (0%)
lower motor neuron signs	1/23 (4.4%)	0/10 (0%)	5/5 (100%)	0/13 (0%)
epilepsy	9/22 (40.9%)	2/10 (20%)	0/5 (0%)	8/13 (61.5%)
central visual impairment	1/24 (4.2%)	2/10 (20%)	0/5 (0%)	1/13 (7.7%)
abnormal fundus, retinopathy	9/19 (47.4%)	1/9 (11.1%)	1/5 (20%)	3/11 (27.3%)
nystagmus	5/18 (27.8%)	2/9 (22.2%)	2/3 (66.7%)	2/10 (20%)
strabismus	11/19 (57.9%)	6/10 (60%)	4/4 (100%)	7/11 (63.6%)
oculomotor apraxia	4/19 (21.1%)	3/9 (33.3%)	2/3 (66.7%)	0/9 (0%)
impaired swallowing	6/23 (26.1%)	5/10 (50%)	2/5 (40%)	0/13 (0%)
deafness	6/25 (24%)	0/10 (0%)	1/4 (25%)	3/11 (27.3%)
dysmorphisms	15/24 (62.5%)	8/10 (80%)	2/4 (50%)	8/13 (61.5%)
Neuroradiological features				
cerebellar pattern				
dragonfly	21/25 (84%)	8/10 (80%)	3/5 (60%)	9/13 (69.2%)

butterfly	4/25 (16%)	2/10 (20%)	2/5 (40%)	3/13 (23.1%)
cerebellar vermis hypoplasia				
mild	1/25 (4%)	5/10 (50%)	1/5 (20%)	5/13 (38.5%)
moderate	12/25 (48%)	4/10 (40%)	2/5 (40%)	3/13 (23.1%)
severe	12/25 (48%)	1/10 (10%)	2/5 (40%)	5/13 (38.5%)
cerebellar hemispheres involvement	24/25 (96%)	10/10 (100%)	4/5 (80%)	11/13 (84.6%)
cerebellar cortical hyperintense signal	1/25 (4%)	2/10 (20%)	1/5 (20%)	2/13 (15.4%)
cerebellar subcortical hyperintense signal	1/25 (4%)	1/10 (10%)	1/5 (20%)	1/13 (7.7%)
dentate nuclei alterations	0/25 (0%)	0/10 (0%)	3/5 (60%)	1/13 (7.7%)
cerebellar cysts	0/25 (0%)	2/10 (20%)	0/5 (0%)	0/13 (0%)
pons hypoplasia				
very mild	0/25 (0%)	0/10 (0%)	1/5 (20%)	1/13 (7.7%)
mild	3/25 (12%)	0/10 (0%)	4/5 (80%)	1/13 (7.7%)
moderate	11/25 (44%)	0/10 (0%)	0/5 (0%)	3/13 (23.1%)
severe	10/25 (40%)	10/10 (100%)	0/5 (0%)	8/13 (61.5%)
cerebral atrophy	3/25 (12%)	1/10 (10%)	2/5 (40%)	3/13 (23.1%)
normosized corpus callosum	12/25 (48%)	10/10 (100%)	5/5 (100%)	8/13 (61.5%)
ventriculomegaly	7/25 (28%)	6/10 (60%)	3/5 (60%)	4/13 (30.8%)
delayed mielination/hypomielination	0/25 (0%)	1/10 (10%)	0/5 (0%)	4/13 (30.8%)
small posterior fossa	1/25 (4%)	7/10 (70%)	2/5 (40%)	5/13 (38.5%)
microcephaly at MRI	11/25 (44%)	2/10 (20%)	0/5 (0%)	5/11 (45.5%)
MPC thinning				
mild	6/25 (24%)	0/10 (0%)	2/5 (40%)	0/13 (0%)
moderate	10/25 (40%)	1/10 (10%)	2/5 (40%)	3/13 (23.1%)
severe	9/25 (36%)	9/10 (90%)	0/5 (0%)	9/13 (69.2%)

For each variable, the % is calculated on the effective number of patients for whom information was available

MCP: middle cerebellar peduncles; OFC: occipito-frontal circumference

Clinical features and brain MRI patterns of patients are summarized in **Tab.8**, showing the main findings for each genotype-based group (carrying *TSEN54*, *CASK* and *EXOSC3* variants or resulting with negative molecular result). The mean age at last follow-up is 5.7 years (range 0.2-29 years), with no statistically significant difference between groups (p-value= 0.322). Pregnancy and delivery were often uneventful. All children presented with neurodevelopmental delay. Patients with assessable cognitive function showed variable degree of intellectual disability, mostly severe. Some features are highly gene specific, including jitteriness or clonus (detected exclusively in the *TSEN54*-group) and lower motor neuron signs (identified almost only in patients with *EXOSC3* variants). Analogously, cerebellar cysts have been observed only in *TSEN54* patients, while altered signal in

the dentate nuclei are prevalent in the *EXOSC3*-group. Other clinical and neuroimaging features are variably represented in different patient groups.

CASK group also included four male probands, whose clinical features are as follows:

Patient 1 (CCM195) was born at 40 weeks from Italian non-consanguineous parents after an uneventful pregnancy. Birth weight and length were 4.07 kg and 51.5 cm, respectively. Head circumference at birth was in the normal range (35.5 cm, -0.18 SD). He started sitting independently at 12 months and standing without support at 18 months. Last follow-up dates back to 22 months. At that age, he was able to babble, while walking was not achieved. Progressive microcephaly became evident, with a head circumference of 43.5 cm (-3.5 SD). Furthermore, he presented with proximal hypotonia and distal hypertonia, hyperelicitable osteotendinous reflexes, truncal ataxia, motor stereotypies involving the upper limbs and drooling. Examination of the fundus oculi showed mild retinal depigmentation. Brain MRI, performed at 21 months of age, revealed mild hypoplasia of the pons, dragonfly appearance of the cerebellum and mild thinning of middle cerebellar peduncles **(Fig.32A,B)**. Molecular analysis revealed the nonsense variant c.82C>T (p.(R28*)) in mosaic state **(Fig.32C)**.

Patient 2 (CCM510) was born at term from Albanian non-consanguineous parents after normal pregnancy. Apgar score was 10 at both 1 and 5 minutes, and birth weight was 3.03 kg. At the age of 5 months, he presented with seizures, characterized by paroxysmal extension of four limbs and head movements, lasting a few minutes with spontaneous resolution. Both awake and sleep electroencephalogram (EEG) performed at 2 years of age showed epileptic activity in the bilateral posterior regions, mainly starting from the right side with contralateral spread. Less frequently, epileptiform discharges occurred asynchronously over both hemispheres, with right predominance. Background activity was only occasionally recorded on awake EEG, while cyclic organization of sleep was absent. Although head circumference at birth was unknown, following measurements revealed a progressive microcephaly (42.3 cm at 12 months and 43.5 cm at 24 months, corresponding to -3.2 and -3.6 SD, respectively). At the age of 3 years and 4 months, he completely lacked postural and kinetics achievements, and also cognitive development appeared severely compromised. Neurological assessment showed reduced muscle strength, drooling, fluctuating muscular tone with predominant proximal hypotonia and distal hypertonia, hyperelicitable osteotendinous reflexes of lower limbs with spontaneous Babinski sign and dystonia. Ophthalmological evaluation revealed bilateral ptosis, oculomotor apraxia with erratic eye movements, small and pale optic discs with

pseudo-colobomatous excavation, as well as abnormal ERG findings. Furthermore, VEP displayed alterations in both retinal functions and retro-retinal visual pathway. Additional clinical features were dysphagia, bilateral sensorineural hearing loss caused by retrocochlear impairment, recurrent aspiration pneumonia, as well as reduced complex II activity in muscle biopsy. Brain MRI, dating back to 1 year and 5 months, was characterized by dragonfly-like pattern of the cerebellum with severe pontine hypoplasia, cerebral atrophy, ventriculomegaly, and severe thinning of middle cerebellar peduncles **(Fig.32D,E)**. Genetic testing identified the hemizygous c.2174_2176del variant, segregating from the healthy mother and resulting in a single-amino-acid deletion (p.(E725del)) **(Fig.32F)**.

Patient 3 (BR1) was born at term from Caucasian parents. No significant events occurred during pregnancy. He presented with neurodevelopmental delay and progressive reduction of head circumference (34 cm at birth and 44 cm at the age of 1 year, corresponding to -0.83 and -1.83 SD, respectively). At 12 years of age (corresponding to last follow-up), walking ability was only partially acquired, and the patient showed severe intellectual disability and epilepsy. Neurological features included proximal hypotonia associated with distal spasticity, hyperactive osteotendinous reflexes, gait ataxia and dyskinesias. Strabismus emerged from eye examination, while there was no evidence of retinopathy. Brain MRI showed a butterfly-shaped cerebellum with normal pons, as well as mild thinning of middle cerebellar peduncles. Molecular exams detected the hemizygous missense variant c.1852A>G (p.(R618G)), maternally inherited.

Patient 4 (CCM395) was born from Italian parents after an uneventful at term pregnancy. He suffered from fetal distress and presented with a plurimalformative syndrome, characterized by severe microcephaly (34.6 cm at 6 months, equivalent to -6.68 SD), dolicocephaly, microretrognathia, low-set years, palatoschisis, dental agenesis and bilateral cryptorchidism. Abnormal findings were shown on ERG and PEV, performed at 1 year of age. Besides severe psychomotor delay, the patient developed drug-resistant tonic-clonic seizures associated with a burst suppression pattern on both awake and sleep EEG. Clinical manifestations also included dysphagia (treated with percutaneous endoscopy gastrostomy), chronic respiratory failure (requiring tracheostomy), and sensorineural hearing loss. At last assessment, dating back to the age of 4 years and 2 months, physical examination showed tetraparesis, diffuse hypotonia and hyporeflexia. Brain MRI confirmed microcephaly and displayed extremely severe cerebellar hypoplasia with dragonfly appearance, marked pons hypoplasia and cerebral atrophy. Additional

findings were cerebellar cortical and subcortical hyperintense signal, a longer corpus callosum relative to head size, ventriculomegaly, small posterior fossa, and severe middle cerebellar peduncles thinning **(Fig.32G,H)**. Genetic analysis showed the hemizygous deletion (c.831+1_832-1)(1015+1_1016-1)del, involving exons 9-10 **(Fig.32I)**.

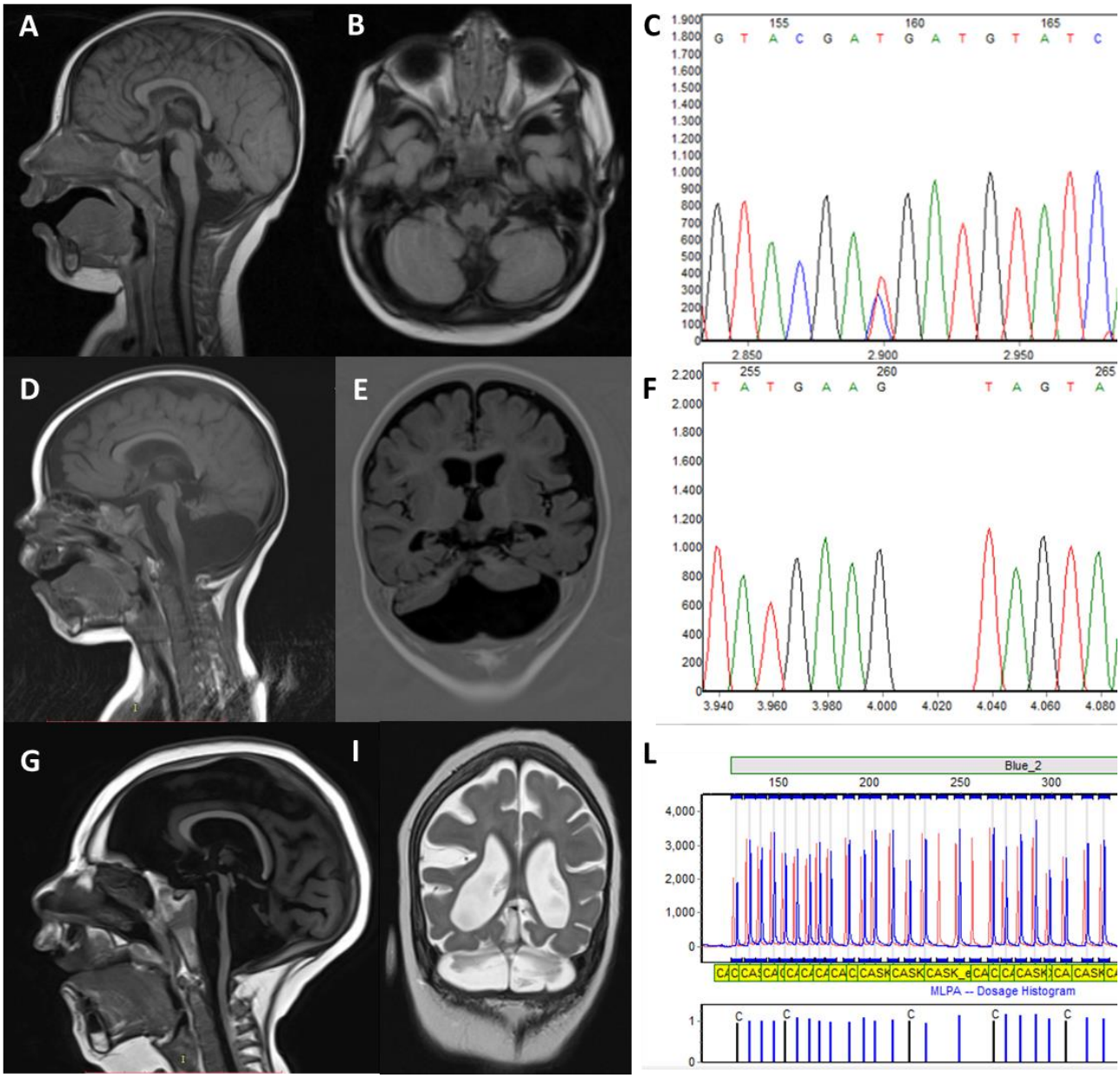

Fig.32.Male CASK probands. MRI sagittal **(A)** and axial **(B)** scans and electropherogram **(C)** of proband CCM195; sagittal **(D)** and coronal **(E)** sections and electropherograms **(F)** of proband CCM510; sagittal **(G)** and coronal **(H)** scans and MLPA graphic analysis **(I)** of proband CCM395.

A three-cluster model best fits the dataset of mutated patients, as evidenced by the generated dendrogram **(Fig.33A)**. A detailed representation of clusters is shown in **Fig.33B**. Members of cluster

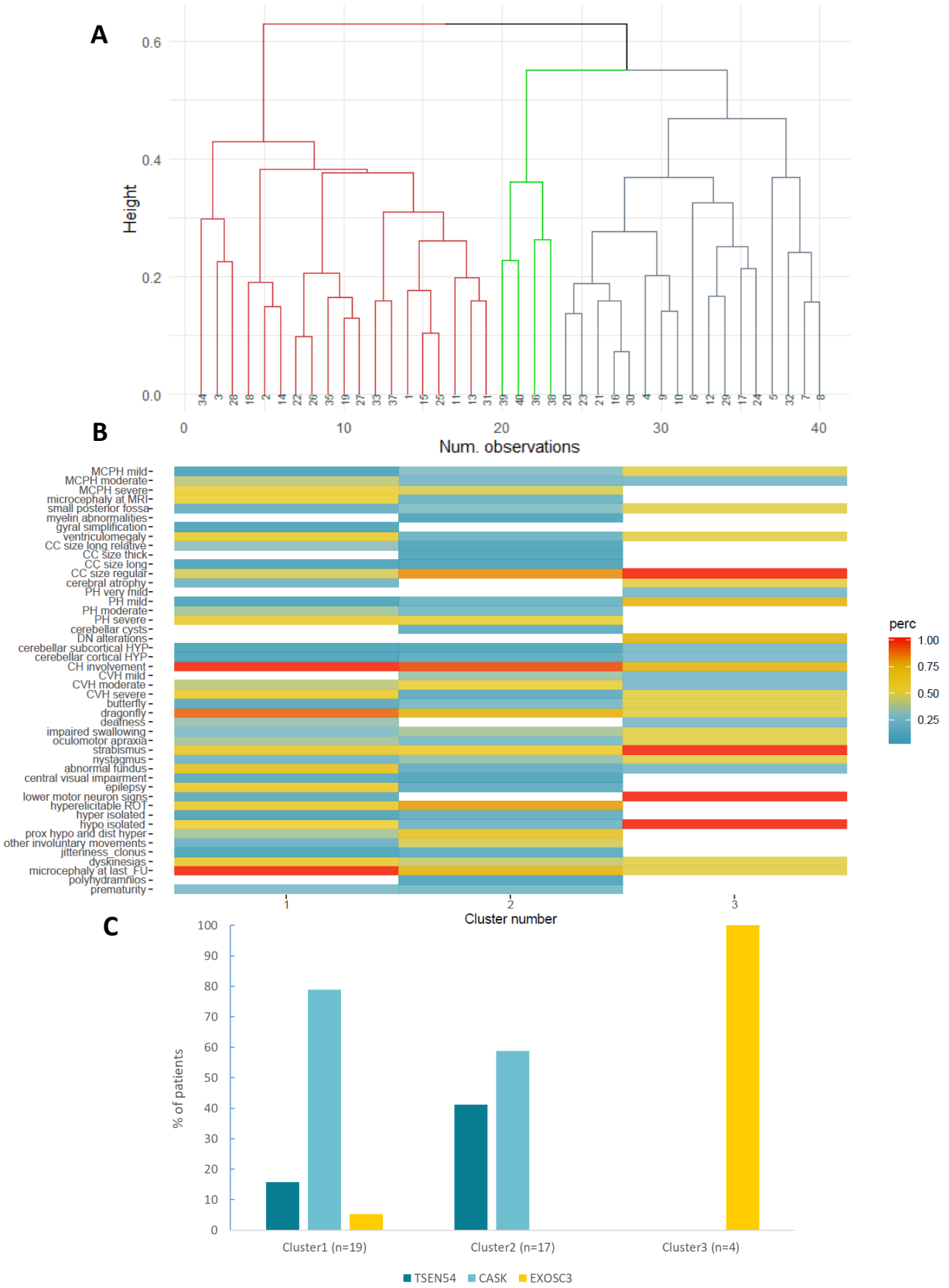

Fig.33. Hierarchical cluster analysis results. (A) Dendrogram showing the three-cluster model best fitting the dataset of mutated probands; **(B)** Heatmap displaying the percentage frequency distribution of features within each cluster; **(C)** Histograms sowing the percentage frequency of mutated genes within each cluster. CC: corpus callosum; CH: cerebellar hemispheres; CVH: cerebellar vermis hypoplasia; dist: distal; DN: dentate nuclei; FU: follow-up; HYP: hyperintense signal; MCPH: middle cerebellar peduncles hypoplasia; PH: pons hypoplasia; prox: proximal; ROT: osteotendinous reflexes.

1 typically present with progressive microcephaly (often visible by MRI), and a dragonfly-like cerebellar pattern, frequently associated with dyskinesias, hypotonia (diffuse or combined with distal spasticity and hyperelicitable deep tendon reflexes) epilepsy, abnormal fundus oculi, strabismus, moderate-severe pontine hypoplasia, normosized corpus callosum, ventriculomegaly and moderate-severe MCPs hypoplasia. Characterising features of cluster 2 are progressive microcephaly (although less frequent compared to cluster 1), a dragonfly appearance of the cerebellum and regularly sized corpus callosum, followed by dyskinesias or other involuntary movements, proximal hypotonia with distal hypertonia (associated with hyperelicitable deep tendon reflexes), strabismus, severe pontine hypoplasia and severe MCPs hypoplasia. Lastly, members of cluster 3 typically show diffuse hypotonia, lower motor neuron signs, normal corpus callosum appearance and strabismus; additional frequent features are represented by dentate nuclei alterations and mild hypoplasia of the pons, followed by progressive microcephaly, oculomotor apraxia, impaired swallowing, dragonfly or butterfly-like cerebellar pattern, cerebral atrophy, ventriculomegaly, small PF and mild MCPs hypoplasia.

While cluster 3 included exclusively patients with mutations in *EXOSC3*, clusters 1 and 2 show a more heterogeneous composition **(Fig.33C)**. Specifically, although *CASK* mutations are overrepresented in both cluster 1 and 2, their percentage almost approaches that of *TSEN54* mutations in cluster 2. Baseline-category logistic regression model analysis showed a statistically significant enrichment of *EXOSC3* mutations in cluster 3 with respect to cluster 1 ($\beta = 2.50$, $p = 0.012$) and cluster 2 ($\beta = 2.56$, $p = 0.0098$). After Benjamini & Hochberg correction for multiple hypothesis testing, a trend toward significance is observed ($p=0.055$ for both comparisons).

Our data contribute to expand the phenotypic spectrum associated with the most common PCH causative genes. Some previously described associations (including jitteriness, clonus, dyskinesias and other involuntary movements in *TSEN54* patients, epilepsy and ophthalmologic abnormalities in *CASK* patients and generalized muscle hypotonia with lower motor neuron signs in *EXOSC3* patients) have been confirmed in our investigated cohort. Also, the association between milder phenotypes and germline hypomorphic variants or inactivating variants in a mosaic state in *CASK* male patients has been observed in our patient group. Conversely, the dragonfly-like cerebellar pattern on MRI has not resulted to be strictly associated with the homozygous p.A307S founder variant in *TSEN54* gene, as it has been also identified in 84% and 60% of *CASK* and *EXOSC3*-mutated patients, respectively. On the other hand, 2 out of 10 patients with the founder *TSEN54* variant in a

homozygous state presented with a butterfly-like appearance of the cerebellum. Furthermore, a normosized corpus callosum has been identified only in 48% of our *CASK* group, while it seems to be a constant feature in the other patient groups.

The comprehensive neuroradiological assessment of our cohort has allowed to identify additional features, including dentate nuclei abnormalities (detected in most of *EXOSC3* patients), cerebellar cysts (affecting 20% of *TSEN54* patients), ventriculomegaly (often observed in *TSEN54* and *EXOSC3* groups), and small PF (detected in the majority of *TSEN54* patients). Also, the degree of pons and MCPs hypoplasia seems to depend on genotype, showing greater severity in the *TSEN54* group and resulting to be more attenuated in *EXOSC3* patients.

Many studies reporting genotype-phenotype correlations are based on comparison of each individual trait between patient groups. This approach could not be statistically convenient for studying complex phenotypes (characterised by tens of clinical-neuroradiological features), due to the reduction of significance after correction for multiple tests. Moreover, it does not reflect the real condition of syndromic patients, typically showing a constellation of signs and symptoms. For this reason, the present study also provides a new approach for genotype-phenotype associations, focusing on phenotypic clusters instead of individual clinical features and investigating the prevalence of mutated genes in each cluster. However, more studies conducted on large patient cohorts will be necessary to confirm our results.

CHAPTER3: TUBULINOPATHIES

In this Chapter, cerebellar and brainstem abnormalities associated with tubulinopathies will be explored. Furthermore, a new disease gene responsible for an autosomal recessive *tubulinopathy-like* disorder will be described. I was personally involved in critical revision of genetic data and genotype-phenotype associations, as well as in the analysis and interpretation of NGS data.

3.1 TUBULIN-RELATED CEREBELLAR DYSPLASIA: DEFINITION OF A DISTINCT PATTERN OF CEREBELLAR MALFORMATION [134]

Cerebellar dysplasia (CD) is characterised by abnormal cerebellar foliation and fissuration, white matter arborisation and an abnormal grey-white matter junction [3], with many existing classification schemes based either on the cerebellar region involved or the side of abnormal foliation [21,135]. Focal CD may be seen in prenatal cerebellar disruptions such as unilateral cerebellar cleft and unilateral cerebellar hypoplasia [24]. In addition, CD and/or hypoplasia have been described in the context of some inherited PF malformations, including tubulinopathies. Recently, Oegema *et al* [136] identified heterozygous mutations in tubulin genes in six patients with superior vermis hypoplasia and normal or mildly hypoplastic cerebellar hemispheres, in the absence of obvious MCDs. Nevertheless, a detailed characterization of CD in an unselected cohort of tubulin-mutated patients, has not been performed to date.

In order to determine the neuroimaging pattern of cerebellar dysplasia (CD) and other PF morphological anomalies associated with mutations in tubulin genes, a comprehensive neuroimaging study with focus on the PF has been performed. A cohort of 28 patients (14 females; age range 5 months–11 years in 24 children and 22–52 years in four adults) from 25 families has been investigated, with pathogenic or likely pathogenic heterozygous variants in a tubulin gene (*TUBA1A*, *TUBB2* or *TUBB3*). Mutated cases have been identified after Sanger sequencing analysis on a larger cohort, which included patients: (a) recruited within the CBCD research project; (b) referred for a second opinion; (c) referred for molecular genetic testing upon suspicion of tubulinopathy. Review of clinical-neurological data and follow-up examinations provided information on neurological features and extracerebral findings. MRI examination has been performed as previously described (see *Patients and methods* section). In addition to other neuroimaging features, the presence of CD has been investigated in detail. Specifically, cortical CD has been defined as abnormal orientation or arborisation of the cerebellar folia visible on two

different planes. Moreover, cerebellar vermis was considered dysplastic if lobules were incomplete or showed an irregular arborisation.

Clinical-genetic and neuroimaging findings of the 28 mutated patients are summarized in **Tab.A6 of Appendix**. Twenty-three distinct heterozygous variants were detected in 25 probands, affecting either *TUBA1A* (n = 10), *TUBB2B* (n = 8) or *TUBB3* gene (n = 5). Variants p.(R390H) in *TUBA1A* and p.(E288K) in *TUBB3* were each identified in two unrelated probands, while the remaining 21 variants occurred in single probands or families. Segregation could be verified in 19 families: all variants resulted to be *de novo* except for *TUBA1A* p.(S54N), which was inherited by twin sisters from their affected father (family P113708). The detected variants were scattered across the three main domains (GTPase domain, intermediate domain and C-terminus domain) for *TUBB2B* and *TUBB3*, while they clustered in the GTPase and intermediate domains for *TUBA1A*.

Cerebellar anomalies were detected in 24/28 (86%) patients. Of these, the most common was CD, which was observed in 19/28 (68%) patients. Interestingly, only one patient presented isolated vermian dysplasia, while all the remaining 18 patients showed involvement of the hemispheric cerebellar cortex (cortical cerebellar dysplasia, CCD), either associated with vermian dysplasia (n = 6), hypoplasia and/or rotation of the vermis without dysplastic features (n = 8), or without any vermis involvement (n = 4) **(Figg.34,35,36)**. The postero-superior region of the cerebellar hemisphere was most frequently affected (n = 15). Despite the presence of CCD, the overall volume of cerebellar hemispheres was always preserved. Moreover, except for the abnormal orientation of the folia, the cerebellar cortex had a regular aspect, without cysts, thickenings or signal alterations **(Figg.34,35,36)**. Patients with CCD showed frequent brainstem involvement, without a typical pattern. The observed defects included ventral brainstem cleft and variable abnormalities of the pons, of the MCPs and of the pontine-mesencephalic junction **(Appendix, Tab.A7)**. If comparing clinical and other neuroimaging findings in patients with and without CCD, the only significant difference was the more frequent involvement of MCPs in patients with CCD (p-value < 0.05). As expected, supratentorial malformations involving the basal ganglia and/or the corpus callosum were detected in most patients, regardless of the presence or absence of CCD **(Figg.34,35,36)**. In 26/28 patients, basal ganglia presented the anterior limb of the internal capsule as thinned or absent, causing a fusion between the head of the caudate nuclei and lenticular nuclei. In 21 cases thalami were small with a “rounded” shape. One patient had normal basal ganglia and one showed only a

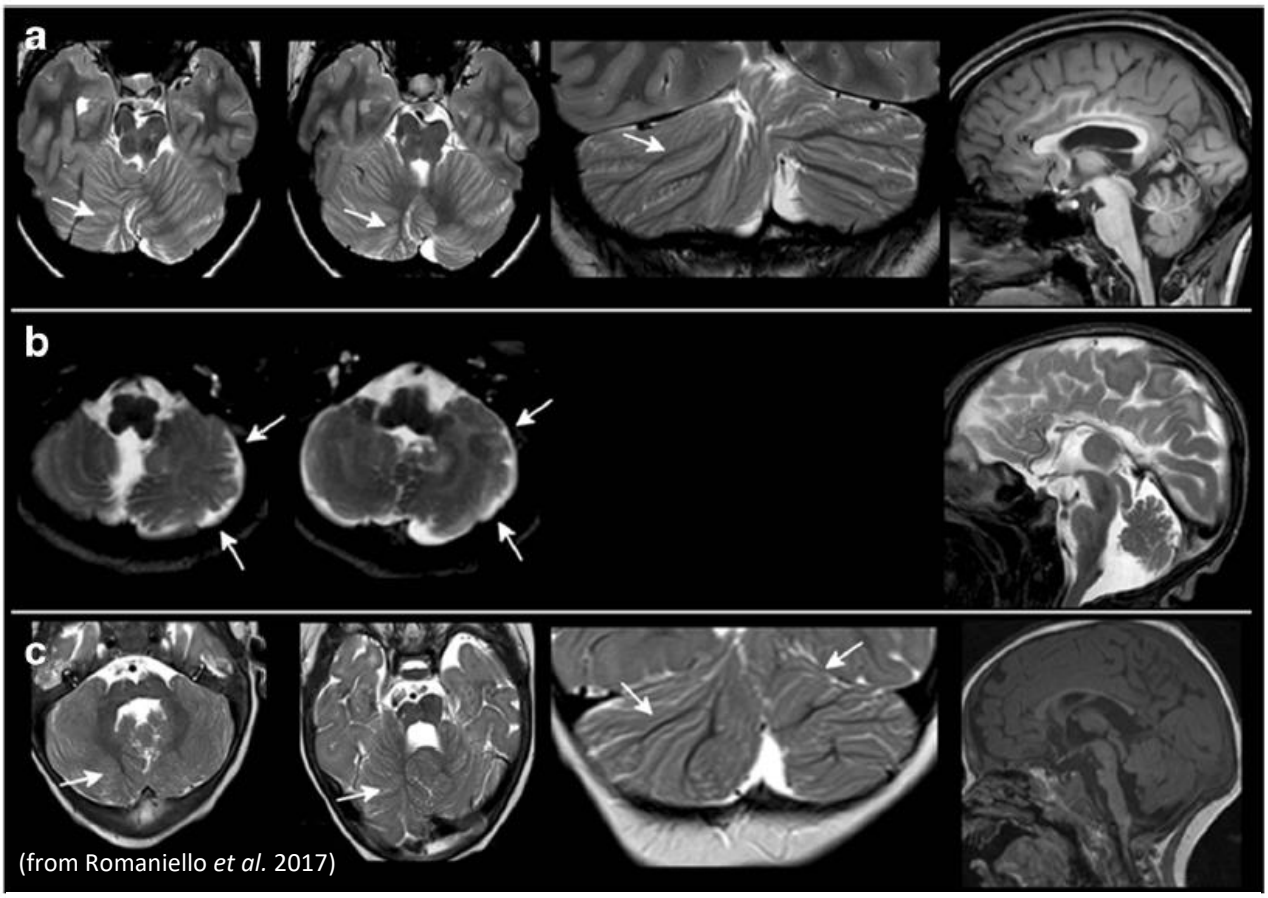

Fig.34. MRI findings in patients with mutations in TUBA1A gene. Representative MRI findings from three patients. **(A)** Irregular orientation of cerebellar folia in the right hemisphere and dysplastic vermis **(B)** Severe dysplasia of the left cerebellar hemisphere and vermis hypoplasia **(C)** Involvement of the right and the posterior left hemispheres and pontine hypoplasia. In all three patients, corpus callosum anomalies are also evident on sagittal planes.

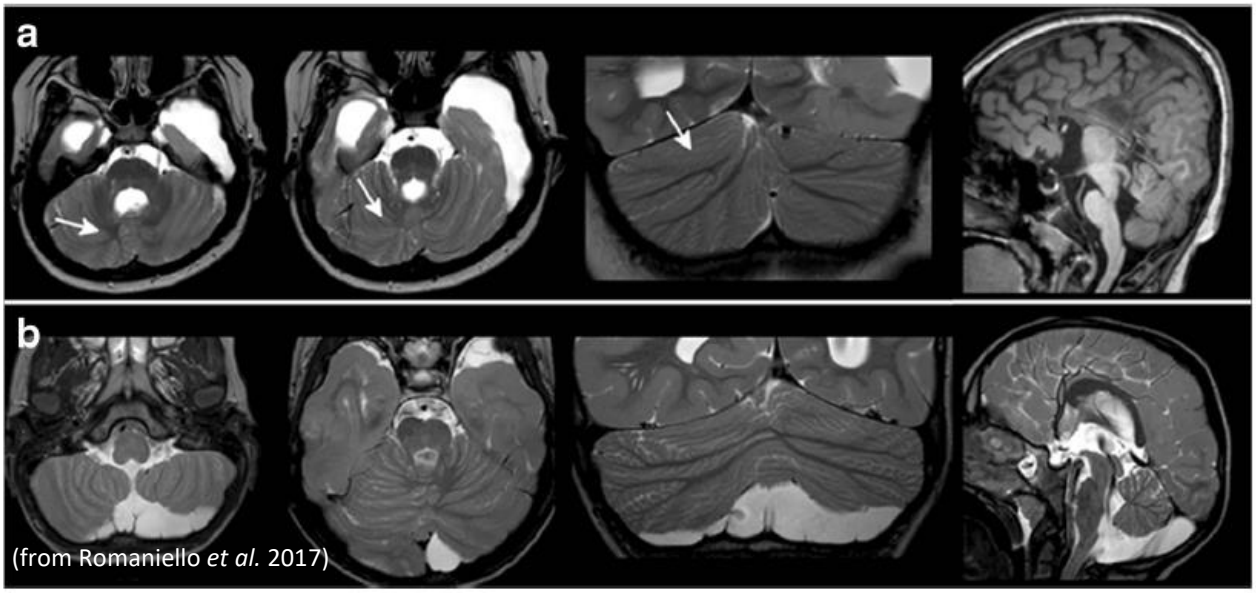

Fig.35. MRI findings in patients with mutations in *TUBB2B* gene. Representative MRI findings from two patients. **(A)** Right cortical cerebellar dysplasia involving the posterosuperior cerebellar hemisphere (arrows), small vermis, thin ponto-mesencephalic junction and corpus callosum agenesis **(B)** Normal cerebellum with supratentorial and brainstem involvement.

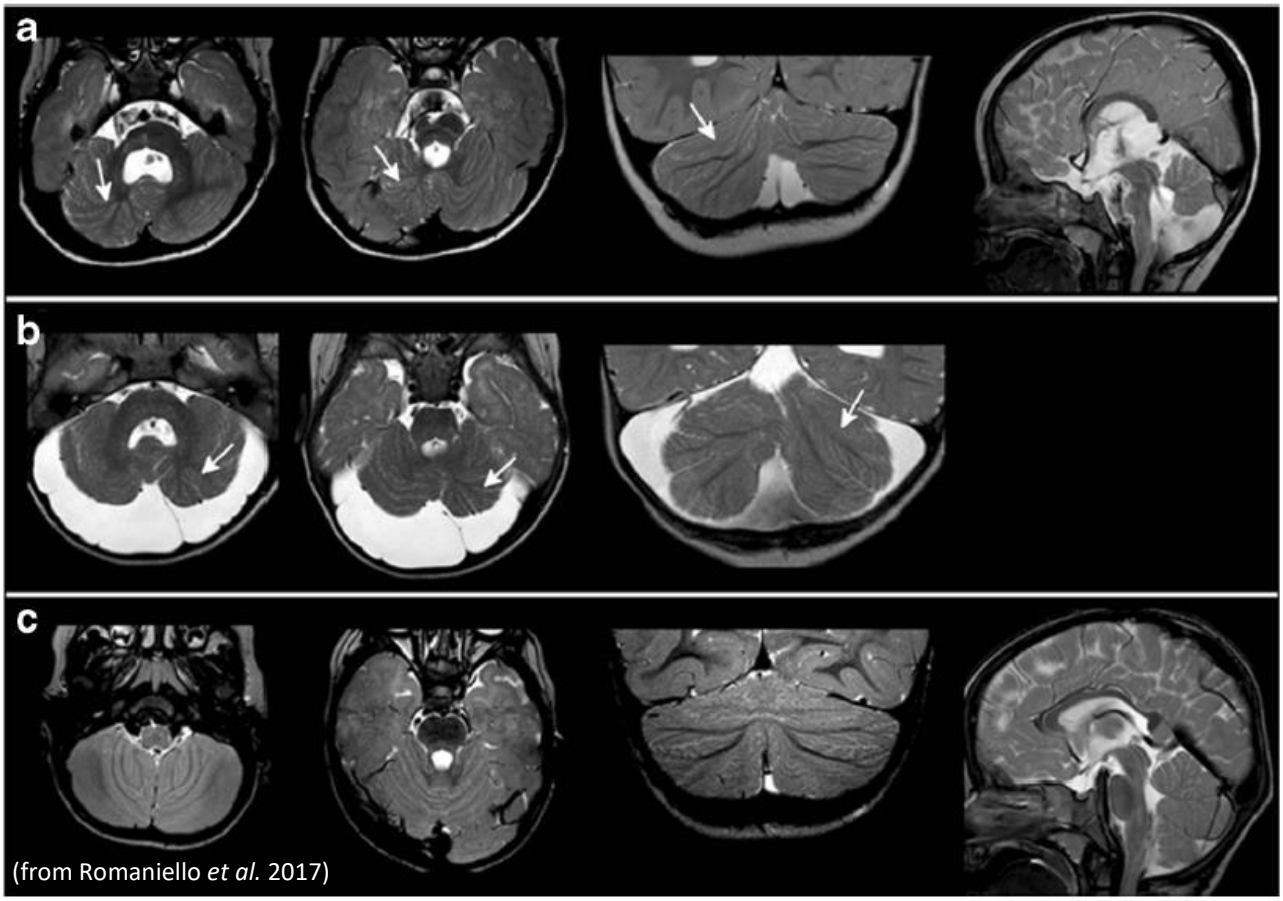

Fig.36. MRI findings in patients with mutations in *TUBB3* gene. Representative MRI findings from two patients. **(A)** Right cortical cerebellar dysplasia with vermis hypoplasia and rotation, small brainstem cleft, thick left malformation of cortical development (MCP) and short pons **(B)** Left cortical cerebellar dysplasia **(C)** Normal orientation of cerebellar folia.

mild deep nuclei asymmetry. The corpus callosum was thin (n = 12), thin and partially agenetic (n = 2), agenetic and/or or partially agenetic (n = 7), dysgenetic (n = 3), short (n = 1) and irregular (n = 2). In one patient the corpus callosum was normal. Malformations of cortical development (MCDs) including perysilvian, multifocal or generalized polymicrogyria (PMG), schizencephaly, simplified gyral pattern with focal PMG, periventricular heterotopias and subcortical linear heterotopia were observed in 14/28 patients (50%): eight patients with CCD (44%) and six without CCD (60%).

Tab.9 summarizes differences of clinical and neuroimaging findings among the three gene subgroups (*TUBA1A*, *TUBB2* and *TUBB3*). Epilepsy, congenital microcephaly and MCDs were absent or very rare in *TUBB3*-mutated patients, while they occurred frequently as part of the *TUBB2* phenotype; basal ganglia involvement prevailed in *TUBA1A* and *TUBB2B*-mutated patients (100%). In addition, in all *TUBB2B* and *TUBB3* mutated patients CCD was located only in the right cerebellar

Tab.9 Genotype-phenotype correlations of the 28 mutated patients

Clinical features	*TUBA1A* (n = 14)	*TUBB2B* (n = 8)	*TUBB3* (n = 6)	All patients (n = 28)	p-value
Developmental delay	13/13 (100%)	8 (100%)	6 (100%)	27/27 (100%)	ns
Intellectual disability	14 (100%)	5/5 (100%)	5/5 (100%)	24/24(100%	ns
Congenital microcephaly	12 (86%)	8 (100%)	1 (17%)	21 (75%)	< .05
Neuro-ophthalmic findings[a]	11 (79%)	5 (62.5%)	3/5 (60%)	19/27 (70%)	Ns
Epilepsy	6 (43%)	7 (87.5%)	0	13 (46%)	< .05
Extra-cerebral findings[b]	8 (57%)	5 (62.5%)	2 (33%)	15 (54%)	ns
Infratentorial defects					
Hemispheric CCD	10 (71%)	4 (50%)	4 (67%)	18 (64%)	ns
Only right	5	4	4	13	
Only left	2	0	0	2	
Bilateral	3	0	0	3	
Vermis	11 (78%)	6 (75%)	3 (50%)	20 (71%)	ns
Dysplastic	4	0	0	4	
Dysplastic and rotated	1	2	0	3	
Hypoplastic	3	2	2	7	
Hypoplastic and rotated	2	2	1	5	
Rotated	1	0	0	1	
Ventral brainstem cleft	6 (43%)	0	3 (50%)	9 (32%)	ns
Pons	8 (57%)	6 (75%)	5 (83%)	19 (68%)	ns
Hypoplastic	1	2	2	5	
Asymmetric	2	0	1	3	
Hypoplastic and asymmetric	5	3	2	10	
Short and thin posterior cap	0	1	0	1	
Middle cerebellar peduncles	7 (50%)	1 (12%)	3 (50%)	11 (39%)	ns
Short	4	0	0	4	
Thick right	1	0	0	1	
Thick left	2	1	3	6	
Ponto-mesencephalic junction	3 (21%)	3 (37%)	1 (16%)	7 (25%)	ns
Narrow	2	1	1	4	
Thick	1	1	0	2	
Shallow inter-peduncular fossa	0	1	0	1	
Mesencephalon	3 (21%)	2 (25%)	0	5 (18%)	ns
Asymmetrical	3	1		4	
Thick	0	1		1	
Enlarged IV ventricle	8 (57%)	7 (87%)	3 (50%)	18 (64%)	ns
Supratentorial defects					
Corpus callosum	14 (100%)	7 (87%)	6 (100%)	27 (96%)	ns
Basal ganglia	14 (100%)	8 (100%)	4 (67%)	26 (93%)	< .05
MCDs	7 (50%)	7 (87%)	0	14 (50%)	< .05
Cranial/optic nerves	0	2 (25%)	1 (16%)	3 (11%)	ns

Fisher's exact test; CCD: cortical cerebellar dysplasia; MCDs: malformation of cortical development.
[a]Nystagmus, oculomotor apraxia, strabismus, ptosis, central visual impairment, blindness, depigmented fundus oculi, optic atrophy, optic nerve hypoplasia
[b]Cyclic vomiting, facial dysmorphisms, obesity, scoliosis, sensorineural deafness

hemisphere, while it could also be bilateral or located only in the left cerebellar hemisphere in *TUBA1A*. Finally, vermis dysplasia was not seen in *TUBB3*. Mutations in tubulin genes have been

described in a large spectrum of developmental brain disorders involving the cerebral cortex, basal ganglia, commissures, cerebellum and brainstem [79,137,138]. The occurrence of cerebellar hypoplasia or dysplasia, mainly affecting the vermis, has often been reported in tubulin-mutated patients with typical basal ganglia and commissural abnormalities as well as malformations of the cerebral cortex [136,139,140]. Nevertheless, a detailed characterization of the spectrum and prevalence of cerebellar and brainstem morphological anomalies in tubulinopathies was still lacking. The present study identifies cerebellar anomalies in 24 subjects (86%), matching previous reports (e.g. 84% in the largest cohort of tubulin-mutated patients published to date) [79], and confirming that cerebellar involvement in tubulinopathies is nearly as common as abnormalities of the basal ganglia and commissures. Upon a detailed analysis of cerebellar structures, CD was observed in 19 patients (68%), including one patient (mutated in *TUBB2B*) with isolated dysplasia and rotation or the vermis and 18 subjects with cortical hemispheric involvement. This neuroimaging phenotype represents a recurrent and well recognizable pattern that may be labelled as "tubulin-related cerebellar dysplasia". It is characterised by: (a) consistent involvement of the hemispheres with or without associated vermian dysplasia; (b) prevalent unilateral pattern (right > > left), often localized in the postero-superior hemispheric region; (c) regular aspect of the cerebellar cortex with abnormal orientation of the folia but without cysts, thickening of the cerebellar folia or signal alterations. This pattern clearly differs from other genetic conditions responsible for CD (Chudley-McCullogh syndrome, α-dystroglycanopathies, *GPR56*-related polymicrogyria, Poretti-Boltshauser syndrome, JS and Lhermitte-Duclos disease) that are generally bilateral and show associated cortical signal alterations, cysts or folial thickening [3].

While asymmetrical defects of the cerebral cortex and brainstem have been frequently described in tubulin-related conditions [137,141] a mild, asymmetrical involvement of cerebellar hemispheres has only been reported by Oegema and collaborators [136]. Our frequent observation of focal, unilateral cortical dysplasia is a novel important finding, as it partially refutes the tendency to consider a focal cerebellar lesion as suggestive of a prenatal acquired (disruptive) origin [3,24]. The mechanism underlying such asymmetry in tubulinopathies remains unexplained, although a different left–right expression of tubulin genes has been suggested [137,142].

The slightly higher occurrence of CD in our cohort (64%) compared to that reported by Bahi-Buisson and collaborators (58% of patients with mutations in the same three tubulin genes) [79], and especially the more frequent observation of asymmetrical hemispheric involvement, may be related to several

factors. Firstly, the focus of the present study on cerebellar defects may have helped to disclose a larger proportion of focal areas of CCD than previously observed. Secondly, there are significant phenotypic differences among the two groups. The Bahi- Buisson cohort included a large proportion of patients with lissencephaly, a cortical malformation that is more likely to be associated with vermis hypoplasia than CCD. In our study, however, MCDs were characterised in all 14 patients either by perysilvian, multifocal or generalized PMG or simplified gyral patterns, two conditions that were also more commonly associated with cerebellar dysplasia in the other cohort (67% and 79%, respectively) [79,136]. In the present series, no striking phenotypic or neuroimaging differences could be observed among the three tubulin genes. Nevertheless, some considerations are possible: in *TUBA1A*- mutated patients, bilateral and unilateral left CCD, vermis dysplasia or rotation, absence of associated cranial and/or optic nerves defects were observed. Only unilateral right CCD, less common MCP involvement, predominance of MCDs, congenital microcephaly and epilepsy were more frequently noticed in association with *TUBB2B* mutations. Lastly, unilateral right CCD, lower vermis and basal ganglia involvement, as well as rare occurrence of MCDs, epilepsy and congenital microcephaly are more typical of *TUBB3* mutations. Clinical and supratentorial neuroimaging findings support previous observations implicating *TUBA1A* and *TUBB2B* in neuronal migration and proliferation mechanisms and *TUBB3* in axonal guidance [137]. Moreover, the observation that 12 out of 14 patients with MCDs also present with cerebellar dysplasia suggests common underlying pathomechanisms for abnormal cerebellar foliation and cortical maldevelopment, consisting of abnormalities of neuronal migration and proliferation.

All identified variants in our cohort, including ten novel variants, fall within exons that are commonly mutated in tubulinopathies (*TUBA1A* exons 2 to 4, *TUBB2* and *TUBB3* exon 4) [79,136,140,141,143–148]. Although some genotype-phenotype correlations have been proposed [79], it remains largely unexplained how mutations affecting the same protein domains, and even the same amino acid residues, may result in a wide spectrum of clinical and neuroimaging phenotypes [137].

3.2 THE SPECTRUM OF BRAINSTEM MALFORMATIONS ASSOCIATED TO MUTATIONS OF THE TUBULIN GENES FAMILY: MRI AND DTI ANALYSIS[149]

Supratentorial and cerebellar malformations caused by mutations in tubulin genes have been extensively described with conventional/anatomical MRI; conversely, brainstem abnormalities have never been extensively investigated in tubulinopathies. The occurrence of brainstem hypoplasia or asymmetry has been reported with variable frequencies (31-80%) [79,136,140]; however, further morphological characterisation has not been provided. Similarly, advanced MRI (including DTI), has been used to elucidate the pattern of the supratentorial anomalies [143,150,151], but not for investigating infratentorial anomalies. As demonstrated for other brainstem malformations (e.g. JS, horizontal gaze palsy with progressive scoliosis, pontine tegmental cap dysplasia, diencephalic–mesencephalic junction dysplasia) [3,152–161], DTI may provide valuable structural and architectural information about the normal and abnormal course and organisation of white matter tracts within the brainstem.

For these reasons, a neuroradiological study has been performed in a cohort of children with confirmed tubulinopathies, to fully characterise the spectrum of brainstem malformations by conventional/ anatomical MRI and to investigate the morphology of white matter tracts within the brainstem by DTI.

A cohort of 15 patients (male/female ratio, 6:9; mean age, 4.7 ± 8.2 years; median age, 1.25 years; range, 1 month to 31 years) was collected from the MRI database of E. Medea Research Institute and from other institutes involved in the CBCD research project. The inclusion criteria were: (a) proven mutation on peripheral blood cells in a gene of the tubulin family; (b) brain MR examination including morphological sequences (T1 and/or T2-weighted) in at least two orthogonal planes, including axial sections; (c) DTI sequence with at least 32 directions acquired with b values of at least 700 s/mm2.

Clinical, genetic and neuroimaging data are shown in **Tab.A8 and A9 of Appendix**. Among patients, eight carried mutations in *TUBA1A* gene, four in *TUBB2B* gene and three in *TUBB3* gene. The genetic study on patients' parents showed that all variants occurred *de novo*. All patients showed developmental delay and motor impairment signs. Present or past history of epileptic seizures was documented in six cases, four of which had associated MCDs. Disturbances of ocular movements (strabismus and/ or nystagmus) affected eight patients.

In 14/15 cases (93%) the brainstem showed malformative features on T1- and T2-weighted sequences **(Fig.37)**. Twelve patients had a moderate to marked brainstem asymmetry that in two cases involved only the pons and in ten involved more than one segment including pons + medulla oblongata and/or mesencephalon. In five out of twelve cases, the asymmetry was crossed between medulla and pons (i.e. hypertrophic right medulla and hypertrophic left pons). Five patients with asymmetry and one with no asymmetry had an anterior brainstem cleft. On midsagittal planes, the pons appeared short and small in ten cases. In one of ten, a small posterior pontine cap was observed **(Fig.38)**. The middle cerebellar peduncles appeared short in five children and asymmetric in two. The ponto-mesencephalic junction was thin in four children and thick in one child, while the mesencephalon appeared thick in one child and clearly asymmetric in three other children.

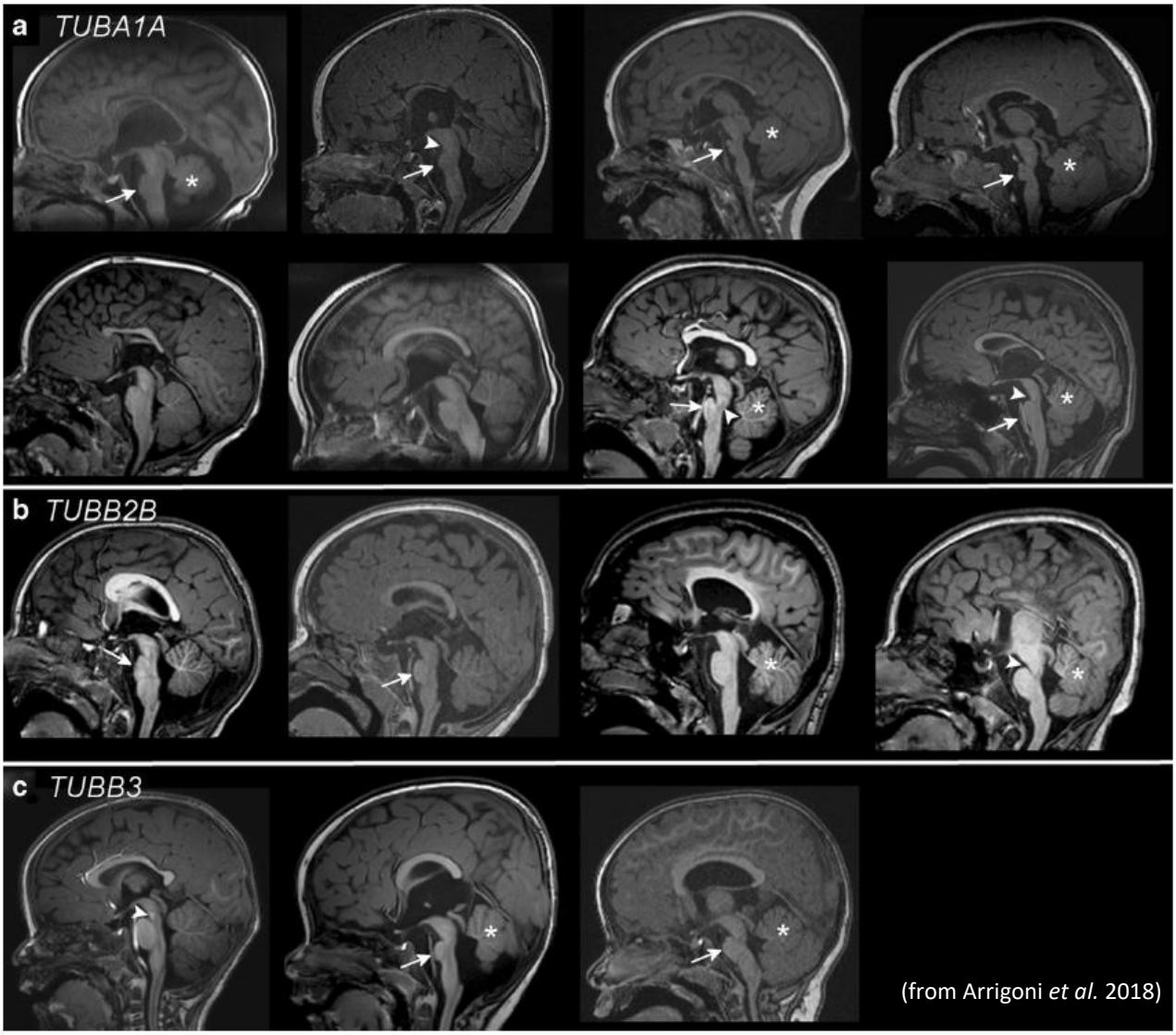

Fig.37. Brainstem appearance on sagittal sections. Midline T1-weighted sections show the heterogeneity of midbrain-hindbrain dysmorphisms in patients with mutations in *TUBA1A* **(a)**, *TUBB2B* **(b)** and *TUBB3* **(c)** genes. Pons hypoplasia (arrows), irregular ponto-mesencephalic junction (arrowheads) and vermis hypoplasia (stars) could be noted in several patients. Corpus callosum malformations are also evident in all patients.

A thickened tectum was observed in two cases. Vermis hypoplasia or rotation could be detected in ten cases and cerebellar dysplasia (i.e. folia malorientation) was present in nine cases **(Appendix, Tab.A9)**. All patients had malformations of the supratentorial brain involving the corpus callosum, anterior commissure, basal ganglia and thalami. MCDs, including polymicrogyria and schizencephaly, were detected in eight children.

The inspection of the fractional anisotropy and DEC maps revealed valuable information about the structure and organisation of the main white matter tracts within the malformed brainstems **(Appendix, Tab.A9)**. The inferior cerebellar peduncles could easily be detected in eight patients while in seven children their integrity could not be assessed due to limited resolution. The MCPs

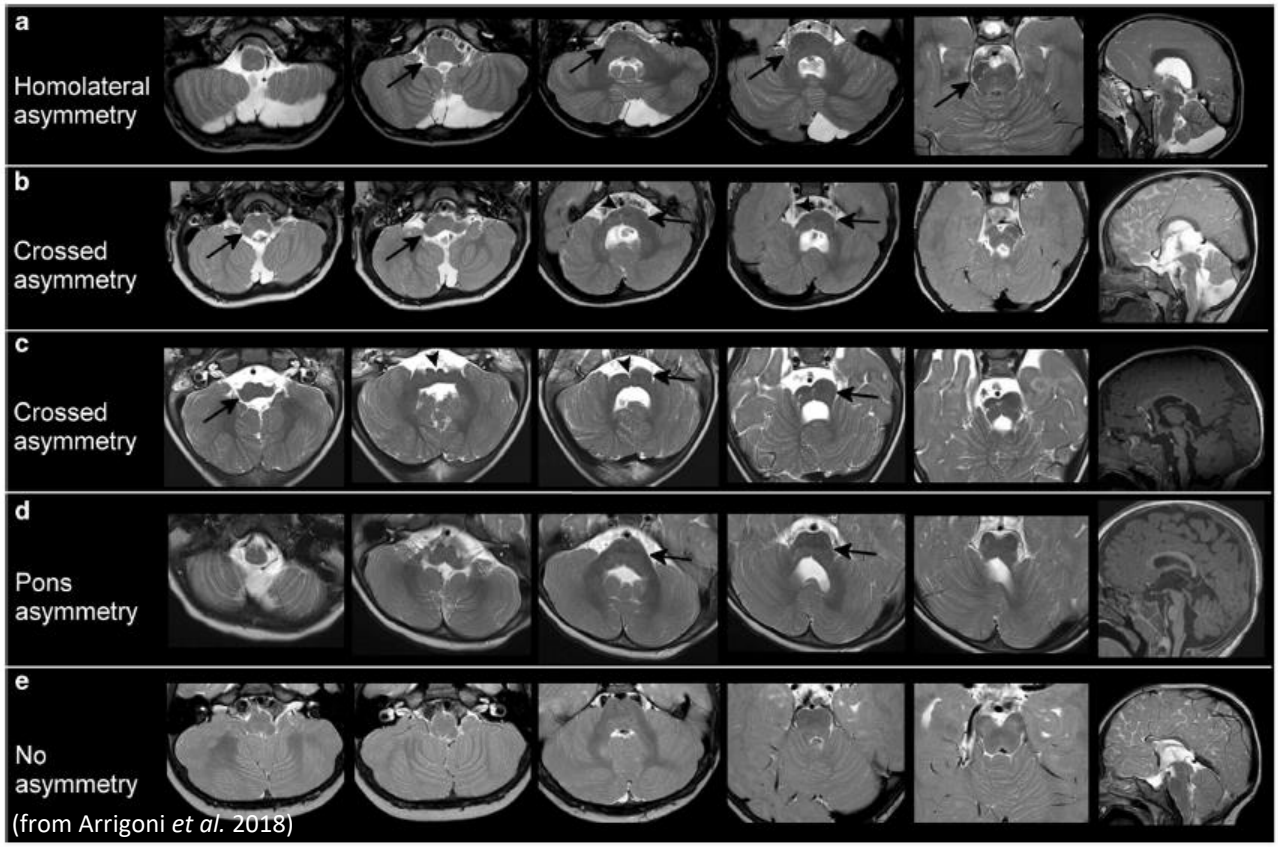

Fig.38. Patterns of brainstem asymmetry. Midline Axial T2-weighted sections of the brainstem, from the medulla to the mesencephalon, of five patients with different patterns of brainstem asymmetry are shown in each row. Sagittal T1 and T2-weighted sections are shown in the last column of each row. Patient A has an ipsilateral asymmetry with an enlargement of the right portion of medulla, pons and right cerebral peduncle (arrows in **a**). Patients B and C carry mutations on different genes (*TUBB3* and *TUBA1A* respectively) but share the same pattern of crossed brainstem asymmetry (right medulla > left medulla; right pons < left pons) (arrows in **b** and **c**) and an anterior midline cleft (arrowheads in b and c). Patient D shows an isolated pontine asymmetry (arrow in **d**), while patient E has no asymmetry.

were short or asymmetric in seven children and had an abnormal orientation (purple/white colour on DEC maps) in eight cases. The superior cerebellar peduncles appeared normal in all children; however, their decussation (usually visible as a red spot on DEC maps in the mesencephalon)

appeared reduced in seven cases. The transverse pontine fibers (TPF) had an abnormal presentation in 13 of 15 subjects. The dorsal component of TPF was markedly reduced or absent in 12, while the anterior component was reduced in only one child. A thickened anterior component was detected in five children **(Fig.39)**.

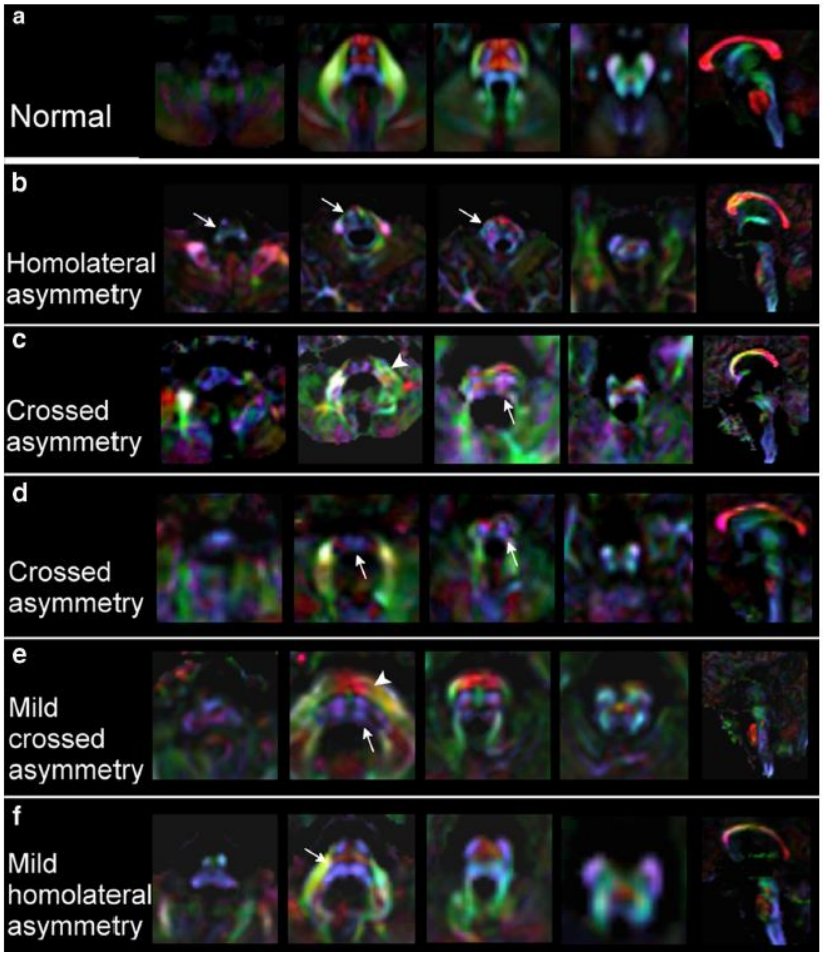

Fig.39. Directionally Encoded Colour maps of the malformed brainstems. Maps of five patients **(b-e)** with different patterns of brainstem malformation are compared to the maps obtained from the diffusion tensor imaging template of typically developing 4-year-old subjects from the NIH study **(a)** Lemnisci and corticospinal tracts can be enlarged/fused (arrows in **b**, **c** and **d**) or partially fused (arrows in **b**). Patients B, C and D show a thinning of anterior and a complete deletion of posterior transverse pontine fibers. In patient E, only an anterior thick component of transverse pontine fibers is present, whereas in patient F, the anterior component is nearly absent while the posterior is preserved (arrows in **f**). Asymmetry of middle cerebellar peduncles can be found (arrowhead in **c**).

(from Arrigoni *et al.* 2018)

The corticospinal tracts (CSTs) and the medial lemnisci appeared to be fused on axial DEC maps at the pontine level in nine children and reduced or asymmetric in four children. Asymmetry or hypoplasia and abnormal signal intensity of the CSTs at the level cerebral peduncles was evident in ten children **(Fig.39)**. Tractography performed on the CSTs and TPF showed several combinations of tract asymmetries, thinning and thickening, confirming the abnormalities detected on the DEC maps **(Fig.40)**.

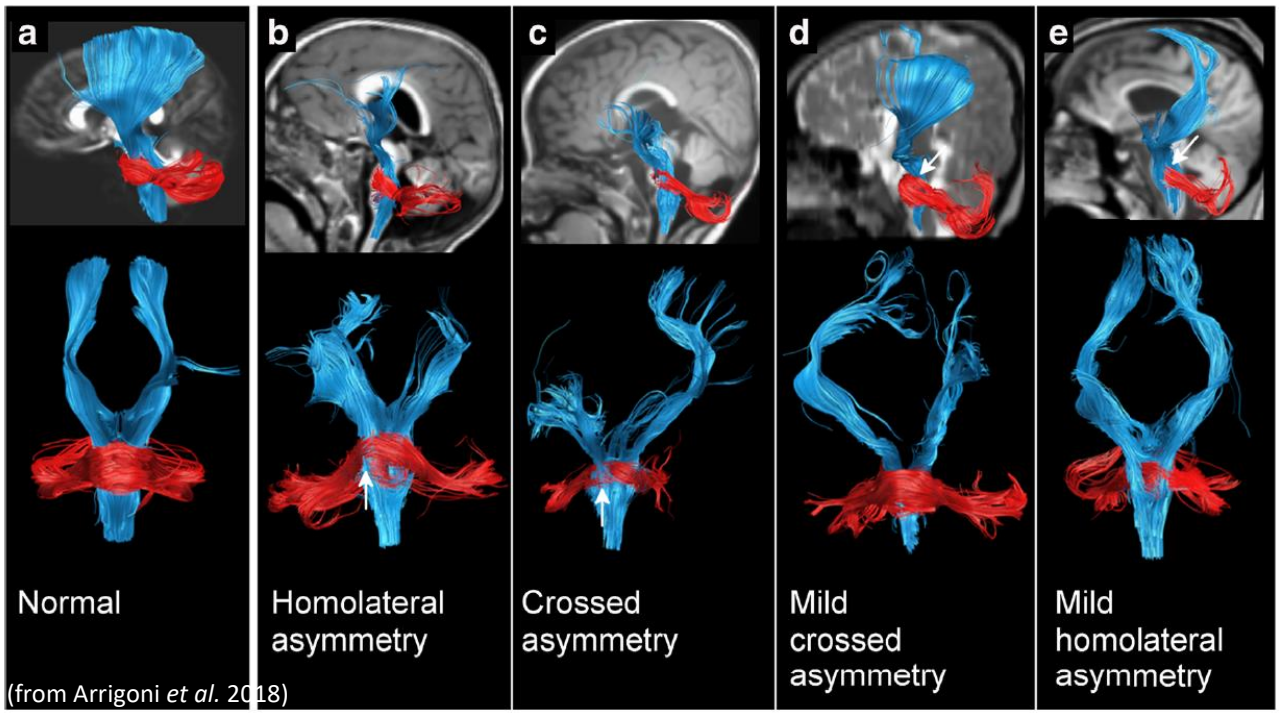

Fig.40. Tractography of corticospinal tracts and transverse pontine fibers. Brainstem tractography of four malformed patients **(b-e)** is compared to normal tracts reconstructed from a template of normal subjects **(a)**. Patients B and C (b and c in Fig. 39 as well) show a thinning of anterior transverse pontine fibers on the enlarged side of the pons, with corticospinal tracts that are close to the anterior bound of the brainstem. Patient D (e in Fig. DTI) has a thick anterior transverse pontine fiber component, while the posterior one is not properly reconstructed by the algorithm (arrow in **d**). Patient E (f in Fig. 39) shows only the posterior component of transverse pontine fibers. Corticospinal tracts are unilaterally thinned in c and d, while middle cerebellar peduncles are thinned in all cases.

Conventional/anatomical MRI and advanced/architectural DTI demonstrated a complex pattern of brainstem malformations in patients carrying mutations in *TUBA1A*, *TUBB2B* and *TUBB3* genes. The most frequent finding was an asymmetry (between the right and left side) of one or more segments of the brainstem (medulla, pons and mesencephalon), with either a consistently homolateral or crossed pattern. With “crossed pattern” abnormality we intend an abnormality that presents on one side at certain anatomical levels of the brainstem and then appears on the contralateral side at a different level (e.g. enlarged right medulla and left pons, or vice versa). With “homolateral pattern” we defined those cases where the hypertrophic (or hypotrophic) side of the brainstem is the same at different levels (e.g. enlarged right medulla and pons). The malformed shape of the brainstem corresponded to an altered organisation and representation of brainstem white matter tracts (mainly CSTs and TPF) more than to the presence of abnormal, ectopic tissue; as a proof of that, no focal signal alterations were detected on T1- and T2-weighted images and mean diffusivity maps. Specifically, the most relevant finding revealed by DTI analysis was the abnormal representation of, and irregular relationship between, CSTs and TPF. Such alterations may be the

results of: (1) thinning/atrophy of CST; (2) abnormal course of CST; (3) thinning/thickening of TPF; (4) irregular course of TPF; (5) a combination of the previous factors. However, histology or ultra-high resolution DTI may help to better characterise this finding. Anomalies in the course of CST were described or hypothesised in some malformative conditions like JS, horizontal gaze palsy and progressive scoliosis (HGPPS), Moebius syndrome and other disorders [155,162–165]. Anomalies in the orientation and organisation of TPF have initially been reported in the Dandy-Walker syndrome [152], where transverse fibers are vertically elongated and caudally displaced and in pontine tegmental cap dysplasia, where an abnormal transverse white matter bundle is present on the dorsal surface of the pons.

In this series, brainstem clefts were quite frequent (40%), usually involving one or two segments of the brainstem (medulla and pons) while sparing the mesencephalon. The presence of an anterior cleft in the brainstem is a rare condition, documented in few syndromes like HGPPS [156,166] or diencephalic-mesencephalic junction dysplasia [157,167,168]. Intriguingly, HGPPS is due to mutations in *ROBO3*, a gene involved in mechanisms of axonal guidance similar to the tubulin genes [169,170]. Even if the genetic mechanisms responsible for diencephalic-mesencephalic junction dysplasia have not been identified, previous data suggest the involvement of genes responsible of axonal guidance mechanisms [3,157].

We also observed pons hypoplasia, frequently associated with vermian hypoplasia and cortical cerebellar dysplasia (i.e. malorientation of cerebellar folia), suggesting that the whole hindbrain may be affected in tubulinopathies from a structural point of view. This is also supported by the altered orientation of MCP and the reduction of SCP decussation shown on the DEC maps.

Brainstem abnormalities in tubulinopathies have been reported previously by different authors [79,136,137,171]. Brainstem hypoplasia (in particular flattened pons) was the most reported finding, while asymmetries were described with a frequency of 37 to 100 % [136,171]. In line with the literature, our cohort showed a flattened and short pons in 67% of patients and asymmetries in 80%. A pontine cleft/indentation was described in 80% of patients by Oegema *et al* [136], while in our cohort brainstem clefts were detected in 40% of patients. A large tectum was described in 6/18 patients by Mutch *et al* [171], while we found it only in two cases.

Tab.10. Frequency of most relevant malformations per mutated gene

Finding	*TUBA1A* (8)	*TUBB2B* (4)	*TUBB3* (3)	All patients (15)
Brainstem asymmetry	75% (6)	100% (4)	67% (2)	80% (12)
Brainstem cleft	50% (4)	0% (0)	67% (2)	40% (6)
Pons hypoplasia on sagittal section	75% (6)	50% (2)	67% (2)	67% (10)
Abnormal size of MCPs	63% (5)	25% (1)	33% (1)	47% (7)
Small SCPs	50% (4)	25% (1)	67% (2)	47% (7)
Abnormal pontine transverse fibers	75% (6)	100% (4)	100% (3)	87% (13)
Fused corticospinal tracts/lemnisci	63% (5)	25% (1)	100% (3)	60% (9)

The number of affected patients is reported in brackets. MCPs: middle cerebellar peduncles: SCPs: superior cerebellar peduncles

The other features we reported (e.g. crossed pattern of asymmetries, abnormal size of MCP or DTI abnormalities) were not previously described and represent novel findings. Given the small number of patients per mutated gene, a statistical genotype-phenotype correlation has not been performed. However, when looking at the frequencies of malformations in the three genes **(Tab.10)**, we noticed some interesting elements that need further confirmation on larger samples. Brainstem abnormalities were detected in all mutated genes. In *TUBB2B* patients we did not find clefts and the frequency of SCP decussation thinning and fusion of CST with lemnisci was relatively low. The pattern of malformations was more similar between *TUBA1A* and *TUBB3* patients, except for abnormal MCP size that was particularly present in patients carrying mutations in *TUBA1A* gene.

Given the established role of tubulin genes in axonal guidance [148], we hypothesise that the altered representation of white matter tracts in our patients may be caused by an impairment of these mechanisms during embryogenesis and brain development. The constant presence of disorganised white matter tracts suggests that disruption of axon growth and guidance, in addition to defects in neuronal migration, represent the peculiar features of tubulin-related disorders and lead us to define tubulin related conditions as a primary axonal guidance disorder [140].

Among the limitations of this study, we did not provide quantitative measures of brainstem asymmetries because of the lack of reference standard measures for brainstem segments during childhood. However, asymmetries were carefully identified by experienced paediatric

neuroradiologists using different image weightings and planes. To be confirmed, the asymmetry should be present on three or more contiguous slices on the axial planes.

Given the retrospective nature of this study, we only had heterogeneous DTI protocols with maximum b values of 1,100 s/mm2 and no more than 32 directions. The limitations of DTI in resolving crossing fibers and the resolution used in these acquisitions did not allow us to go into further details in the characterisation of brainstem tracts. Different approaches may contribute to unravel the complexity of white matter reorganisation in these patients.

In conclusion, the present study expands the spectrum of malformations associated with tubulin genes mutations, revealing complex patterns of morphological and intrinsic white matter tracts anomalies at the level of the brainstem.

3.3 LOSS OF FUNCTION OF THE TUBULIN-MODIFYING ENZYME TTL CAUSES AUTOSOMAL RECESSIVE TUBULINOPATHY-LIKE DISORDER

Among patients with a neuroradiological phenotype suggesting for a tubulinopathy, a family has been selected and analysed through WES after excluding mutations in tubulin genes, leading to the identification of a new disease causative gene.

The analysis has been conducted on two affected sisters descending from Pakistani healthy consanguineous (first-cousin) parents **(Fig.41A)**.

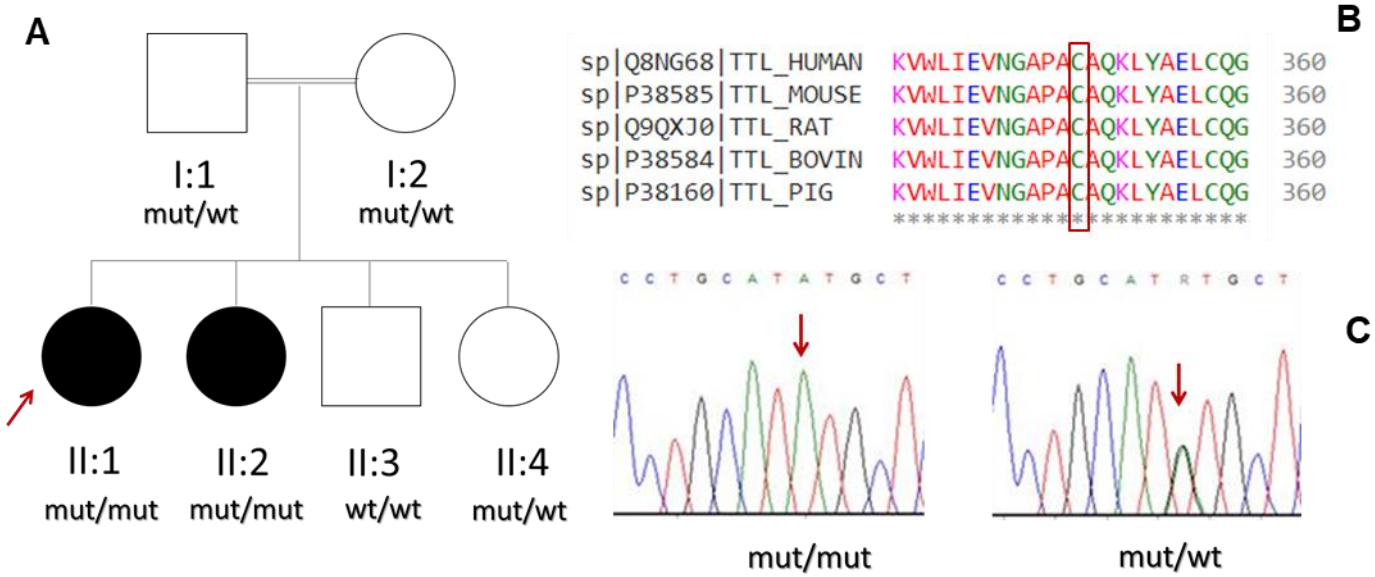

Fig.41. Genetic characterization of patients. (A) Family tree **(B)** Multiple sequence alignment of the TTL protein region flanking residue C338, demonstrating conservation of the affected amino acid residue in distinct species **(C)** Electropherograms showing c.1013G>A variant in the homozygous and heterozygous state.

Patient II:1 was found on prenatal ultrasound US examination with cerebellar vermis and corpus callosum hypoplasia, both confirmed at 24 weeks by fetal MRI. She was born at term by vaginal delivery and presented an Apgar score of 9 at both 1 and 5 minutes. Birth head circumference, weight and length were 32 cm, 3.32 kg and 49 cm, respectively. She acquired head control at 4 months of age, started rolling over at 15 months and sitting independently at 9 months. Autonomous walking was achieved at 4.1 years. Last follow-up dates back to 8.2 years. At that age, language was still completely lacking. In addition to global developmental delay, progressive microcephaly became evident (-3.3 SD), while objective examination showed generalized muscle hypotonia, gait ataxia, oculomotor apraxia and a lymphangioma of the chest wall (treated with sclerotherapy).

Patient II:2 showed cerebellar vermis hypoplasia and corpus callosum agenesis on prenatal US, subsequently confirmed on fetal MRI at 20 weeks. She was born at term by vaginal delivery, with Apgar score of 9 at both 1 and 5 minutes. Birth weight and length were 2.67 kg and 48 cm, respectively, while head circumference was 33 cm. Analogously to the older sister, she presented with neurodevelopmental delay, microcephaly (with brachycephalic skull and flat occiput) and non-progressive cerebellar signs. At the age of 6 years, she was able to sit autonomously, and to walk with support. Moreover, she could say a few words but she was not able to speak in sentences. Neurological assessment revealed marked muscle hypotrophy, central muscular hypotonia and distal hypertonia, hyperelicitable osteotendinous reflexes of lower limbs, drooling, left eye exotropia, and clubfoot.

Brain MRI examination (performed at 4.6 years in patient II:1 and 2.7 years in patient II:2) showed overlapping findings between the two sisters, consisting in commissural hypoplasia or agenesis, hypodysplastic cerebellar vermis, as well as dysplastic brainstem and basal ganglia, mimicking a tubulinopathy-like neuroimaging pattern **(Fig.42)**.

WES data were analyzed in accordance with the supposed autosomal recessive inheritance model. Among the biallelic variants shared by the two affected individuals, the homozygous missense c.1013G>A (p.(C338Y)) in *TTL* gene (NM_153712.4) was identified as a potential underlying cause of the disease. This conclusion was reached basing on biological function of the encoded protein, inheritance pattern, frequency data, scores for conservation and bioinformatic predictions of pathogenicity. In fact, *TTL* codes for tubulin-tyrosine ligase (TTL) protein, an enzyme involved in physiological cyclic tyrosination of the C-terminal region of α-tubulin. Moreover, the c.1013G>A

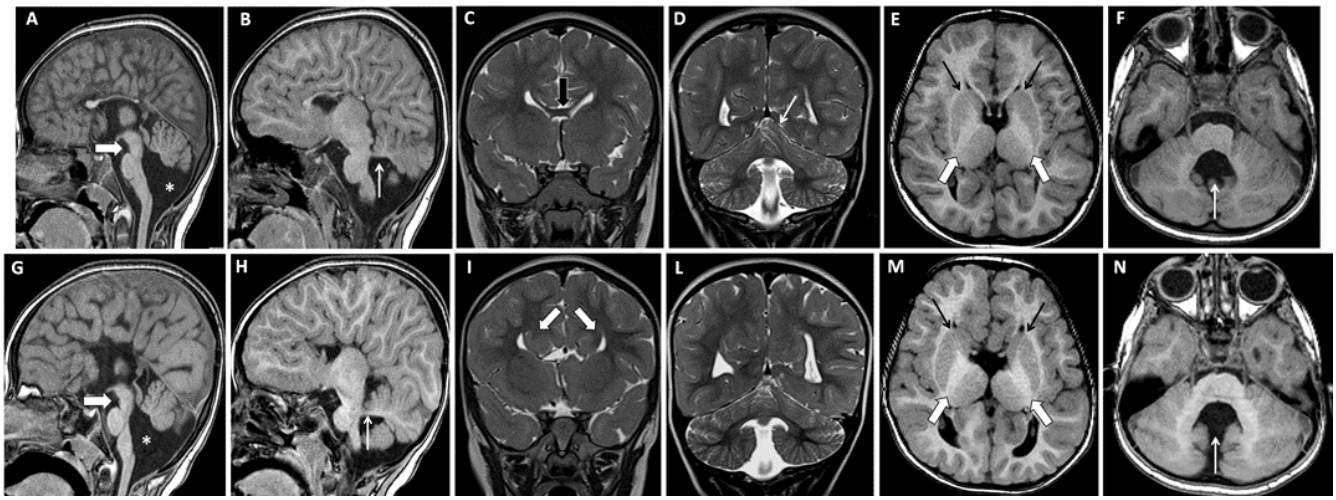

Fig.42. Brain MRI scans of patients II:1 (upper panels) and II:2 (bottom panels). (A-B-G-H) Sagittal T1-weighted images from volumetric GE sequence (3D MP-RAGE), showing complete commissural agenesis (corpus callosum, hyppocampal and anterior commissure) in II:2 or severe commissural hypoplasia in II:1, hypoplastic and counterclockwise rotated cerebellar vermis, dysplastic brainstem with elongated isthmus (thick white arrows) and slightly hypoplastic pons, enlarged 4th ventricle widely communicating with enlarged cisterna magna (asterisks) and horizontal course with normal thickness of the superior cerebellar peduncles (thin white arrows) **(C-D-I-L)** Coronal T2-weighted images, displaying typical "bull's head" appearance of the frontal horns of the lateral ventricles due to corpus callosum agenesis in II:2 (thick white arrows), hypoplastic genu of the corpus callosum in II:1 (thick black arrow) and slightly dysplastic superior vermis cortex ("rostral vermian cortical dysplasia") (thin white arrow) **(E-F-M-N)** Axial T1-weighted images from volumetric GE sequence (3D MP-RAGE), exhibiting enlarged "umbrella-shaped" 4th ventricle (thin white arrows), dysplastic internal capsule with hypoplastic anterior limb (thin black arrows) and "hyperplastic" posterior limb (thick white arrows) ("tubulin-like" appearance).

variant affects an amino-acid residue highly conserved across different species **(Fig.41B)** and is classified as deleterious by many *in silico* prediction tools **(Appendix, Tab.A10)**. Moreover, it has not been reported in gnomAD v2.1.1 spanning exomes of 141,456 unrelated individuals, neither in other consulted population databases. The variant was validated through Sanger sequencing and confirmed in a heterozygous state in both parents **(Fig.41C)**.

The pathogenic effect of the identified *TTL* variant has been confirmed through molecular dynamics simulation, enzymatic activity assays and cellular studies.

(i) The missense variant C338Y alters dynamic properties of TTL protein

TTL binds to a complex composed of two tubulin subunits and the stathmin-like domain of RB3 (T2R) [172], and tyrosinates tubulin in this complex to a similar extent as free tubulin **(Fig.43A)**. WT and mutant (mt) protein have been compared as previously described (see bioinformatic modeling performed for evaluating pathogenic effect of *SUFU* variants). Tubulin-stathmin-TTL-apo mt complex exhibited lower RMSD values with respect to WT **(Fig.43B)**, and appeared globally more

flexible in almost all protein regions, especially in those that are at the interface between TTL and one of the tubulin subunit, as shown by RMS fluctuation values **(Fig.43C)**. DCCMs of mt complex versus WT complex showed some changes in the atomic dynamics **(Fig.43D-E)**. In detail, the mt complex displayed a different distribution in the anti-correlated movements between the tubulin subunits. The perturbation of the binding between TTL and tubulin subunits, supposedly caused by p.(C338Y) mutation, was further studied by measuring the distance, the number of H-bonds, and the binding energy between TTL and tubulin subunits. It is worth noticing for the WT complex that the distance between TTL and tubulin subunits was fairly constant, while for the mt complex the distance constantly increased throughout the simulation **(Fig.43F)**. This evidence is further supported by the number of hydrogen bonds that decreased in mt complex throughout the simulation and by energy levels that were higher in mt complex compared to WT **(Fig.43G)**.

(ii) TTL missense variant C338Y lead to the absence of functional TTL

To evaluate if the missense mutation could affect the stability of the protein, we performed WB experiments on patients' fibroblasts and one healthy control. Results showed a decreased level of TTL mutant protein expression in both patients **(Fig.44A)**; this data goes in parallel with a higher detyrosinated tubulin expression in patients' fibroblasts with respect to control **(Fig.44B)**, suggesting a possible malfunction of the residual protein in the cells. To confirm this hypothesis, we tested the *in vitro* α-tubulin tyrosination activity of wild-type and mutant TTL by transfecting X-lenti HEK cells with either GFP alone, or GFP-tagged TTL (WT), TTL-E331Q, or TTL-C338Y. The results showed in **Fig.44C** revealed that both TTL mutants, the missense variant and the dominant negative form (E331Q) [173] used as negative control, are enzymatically inactive. After microtubule depolymerization, TTL tyrosinates α-tubulin, making tubulin detyrosination a cyclic event [174]. After nocodazole treatment, we do not observe a change in the timing of microtubules repolymerization in our patients **(Fig.44E)**; nevertheless, as shown in **Fig.44D**, the tyrosination curve is completely lost in patients' fibroblasts with respect to control. To analyze how the TTL C338Y variant could affect neuronal development we infected mouse hippocampal neurons with WT, C338Y and E331Q TTL variants. As shown in **Fig.45A and B**, expression of wild-type TTL at 4 d in culture (DIV4) leads to a reduction of axonal length while the expression of both E331Q and C338Y do not.

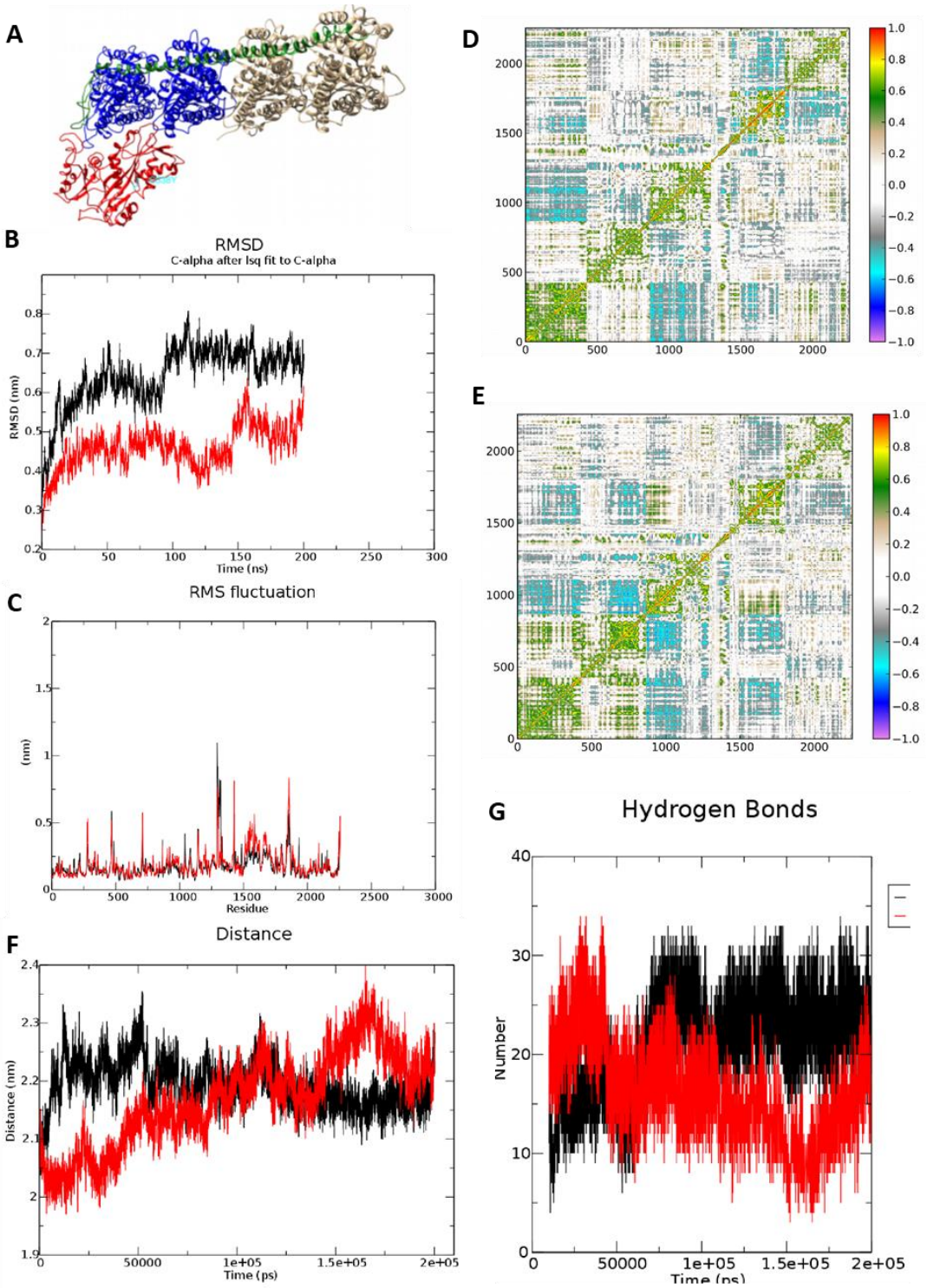

Fig.43. Dynamic properties of wild-type and mutant TTL. (A) 3D structure of TTL-tubulin complex **(B)** Root mean square deviation (RMSD) of heavy atoms in the wild-type (black) and mutated (red) complex. Wild-type complex maintains a stable state up to 91 ns, with RMSD ranging from 0.51 to 0.73 nm. RMSD peaks up to 0.8 nm around 110 ns and stabilizes around 0.7 nm for the remaining duration of the simulation. Mutant complex exhibited lower RMSD values for all simulation timespan. Similar to the wild-type complex, we observe an increase in RMSD values ranging from 0.40 to 0.64 nm between 144 and 156 ns, which are kept quite stable until the end of the simulation **(C)** Root mean square fluctuation (RMSF) of residue coordinates in the simulation of wild-type and mutated complex **(D-E)** Each matrix shows the covariance between atoms for wild-type (up) and mutant (down). Red means that two atoms move together, whereas blue means that they move in opposite directions. **(F)** Distance between amino acids forming interaction interface between TTL and tubulin subunit **(G)** Hydrogen bonds established during simulation.

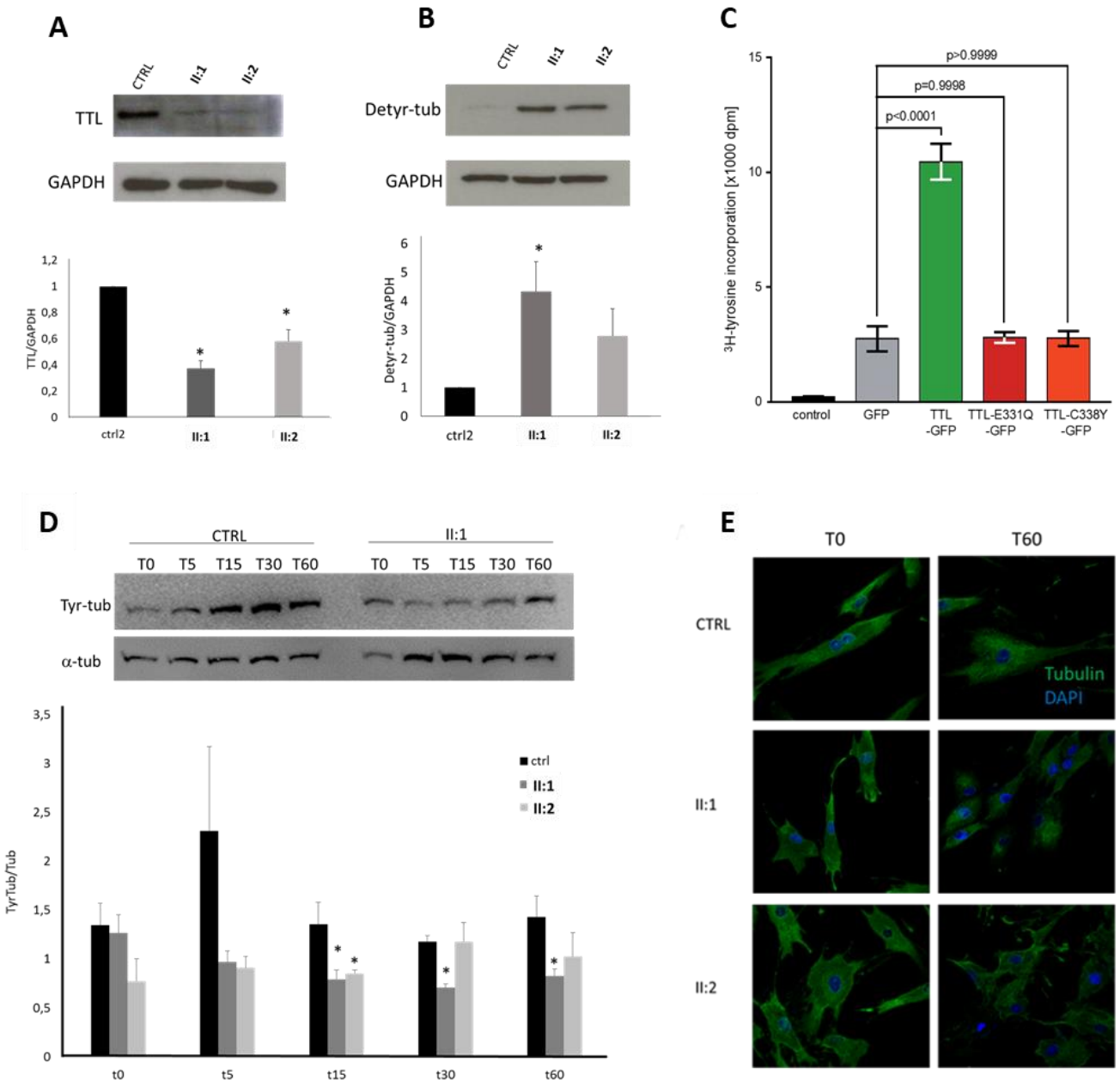

Fig.44. TTL expression, enzymatic activity and microtubules organization in mutant cells. (A) Western blot showing decreased levels of TTL mutant protein expression **(B)** Western blot showing higher detyrosinated tubulin expression in patients' fibroblasts with respect to one healthy control. Lower panels: histograms showing associated densitometric analysis for each Western blot experiment. Results are shown as mean± SE of at least three independent experiments; *p≤ 0.05 **(C)** *In vitro* α-tubulin tyrosination activity of wild-type and mutant TTL versions. Activities of the enzymes are represented as a bar graph of mean values +/-SEM of five independent experiments. Cell extracts expressing GFP were used as control. Note that the control represents a basal tyrosination activity that originates from endogenous TTL. Both TTL mutants (E331Q and C338Y) are enzymatically inactive **(D)** Western blot showing tyrosinated tubulin after nocodazole treatment at different time points. During the time course in control fibroblasts a tyrosination curve is evident while it is completely lost in patients' fibroblasts. Results are shown as mean± SE of at least three independent experiments; p≤ 0,05 respect to wild-type **(E)** Representative images of three independent Immunofluorescence experiments showing no differences in tubulin expression (green) and microtubules organization in patients and one healthy control fibroblasts after nocodazole treatment (T60). DAPI nuclear marker is shown in blue.

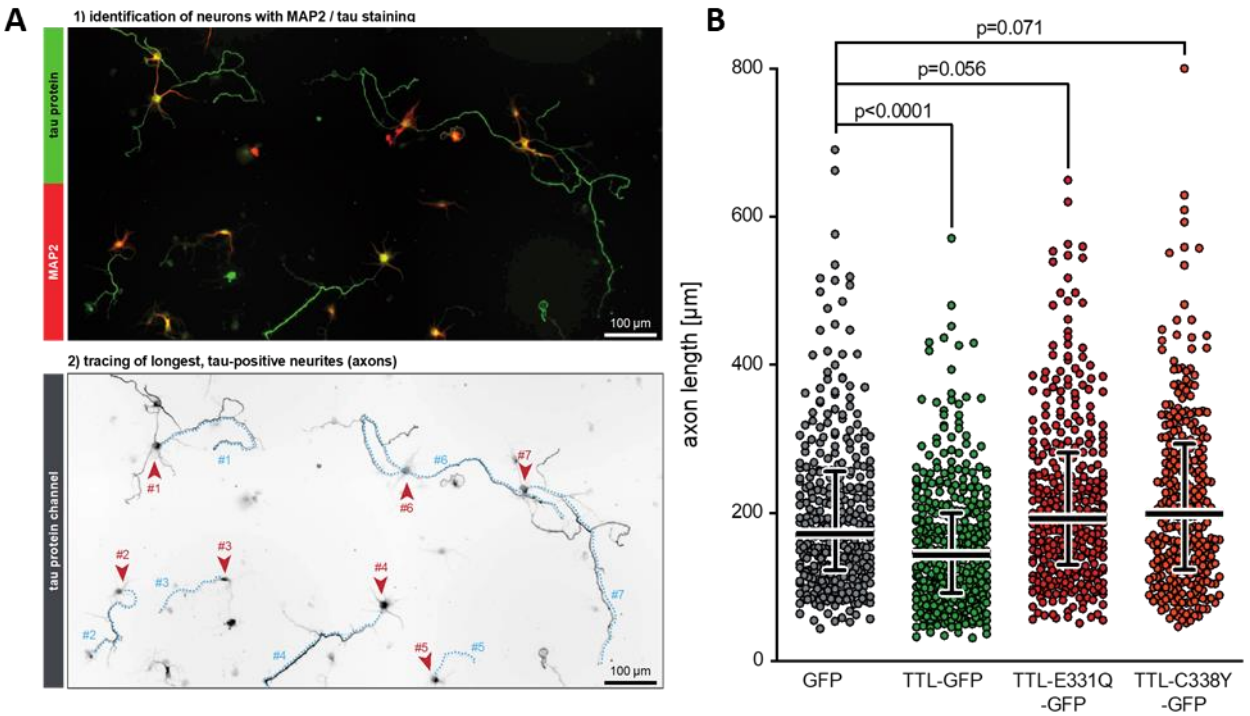

Fig.45. Representative images of neurons for axon length analyses. (A-1) A representative image showing DIV4 wild type neurons transduced with a lentivirus encoding GFP. Cell bodies and neurites are stained with MAP2 (red), and developing axons with Tau-1 (green) antibodies, respectively **(A-2)** Schematic representation of the axon-length analyses. For all cells in a field that can clearly be identified as neurons (arrow heads), the longest tau-positive neurite was identified and re-drawn using Fiji (blue dotted line). The length of all individual axons was measured and statistically analyzed in **(B)**.

Microtubules are fundamental elements of the cell cytoskeleton involved in cell division, morphogenesis and mobility, as well as in bidirectional motor-mediated trafficking of protein and vesicles along the axon [177]. Microtubules consist in polymers of α/β-tubulin heterodimers which expression differs among organs and cell types and is differentially regulated during development [178]. Moreover, they undergo many posttranslational modifications (PTMs) as acetylation, phosphorylation, polyglutamilation and detyrosination/tyrosination. In particular, tyrosination of the C-terminus of both α and β tubulin is believed to correlate with the dynamic properties of microtubules. Tyrosination is a cyclic enzymatic removal of the α-tubulin C-terminal tyrosine by a carboxipeptidase, which is re-added by TTL protein. This cyclic process is essential because mice lacking TTL died right after birth because of defective breathing and a massive accumulation of detyrosinated α-tubulin in the brain [175]. Furthermore, TTL has recently been demonstrated to be crucial for post-injury axon regeneration, increasing the levels of tyrosinated α -tubulin at the injury site [179]. In humans, TTL suppression correlates with poor prognosis in patients presenting with different forms of tumors, representing a strong selective advantage for cancer cells [180–182]. Moreover, since PTMs are enriched in neurons, mutations in α-tubulin residues that are involved in

the tubulin-TTL interaction correlate with neurodevelopmental disorders [183]. However, human disease linked to TTL had never been identified so far.

In this study, we demonstrate that loss of function biallelic variants in TTL gene, encoding the tubulin-modifying enzyme Tubulin Tyrosine Ligase, can be responsible for a tubulinopathy-like neurodevelopmental disorder. As opposed to most tubulinopathies [79], an autosomal recessive inheritance pattern has been observed in our family. The distinctive finding of the disease is a neuroimaging pattern characterized by commissural agenesis or hypoplasia, dysmorphic basal ganglia, and dysplasia of the cerebellar vermis and brainstem. In addition, clinical features of affected individuals include global developmental delay, intellectual disability, cerebellar ataxia, hypotonia and microcephaly. Despite the reporting of a single family, dynamic modelling and functional studies performed on both patients' fibroblasts and mouse hippocampal neurons provide strong evidence on the role of mutant TTL in determining the observed phenotype. Specifically, the Cys338Tyr variant is predicted to alter the dynamic properties and increase the flexibility of the protein, which could lead to defective interaction with α-tubulin. At the same time, the Cys338Tyr variant has been shown to cause the complete inactivation of TTL enzymatic activity (with both qualitative and quantitative impairment of α-tubulin tyrosination), resulting in abnormal neuronal development. Moreover, homozygous loss-of-function (LoF) variants were never observed in more than 141,000 individuals from the GnomAD database (LoF observed/expected score=0.23, 90% CI= 0.11-0.52), suggesting gene intolerance to LoF variation [127]. The TTL null mouse partially recapitulates our patients' features including ataxia, reduced expression of tyrosinated α-tubulin in skin fibroblasts, and augmented axon length of hippocampal neurons with respect to wild-type. In addition, TTL null mouse presents with a severe phenotype, characterized by defective breathing and disruption of the cortico-thalamic loop, leading to death 24 hours after birth [175]. Conversely, the affected children here reported show macroscopic brain malformations (not detected in mice) and clinical features apparently compatible with life. This divergence may be due to species differences or to other unknown reasons counterbalancing the loss of TTL function.

Taken together, our findings expand the spectrum of mendelian diseases caused by mutations in genes involved in tubulin PTMs [176], suggesting that molecular screening of TTL should be considered in individuals with a clinical picture resembling a tubulinopathy but with no identified variants in tubulin genes. However, the identification of additional cases will be necessary to investigate the phenotypic spectrum of the disease in more detail.

CHAPTER4: NON-PROGRESSIVE CONGENITAL ATAXIA

As part of NPCAs, two cases will be described, presenting with shrunken cerebellum due to mutations in distinct genes. In the first case, the existence of a mutation-specific atypical inheritance pattern has been ascertained; in the second case, an expansion of clinical and mutational spectrum has been observed. My personal contribution consisted in the assessment of clinical and neuroimaging data of patients, as well as in bioinformatic analysis and interpretation of NGS data.

4.1 BETWEEN SCA5 AND SCAR14: DELINEATION OF THE *SPTBN2* p.R480W ASSOCIATED PHENOTYPE[184]

As part of the CBCD research project, WES has been performed in a patient with congenital severe cerebellar ataxia and intellectual impairment showing no mutations after targeted resequencing analysis. The patient was a 2-year-old girl, the third child of healthy nonconsanguineous parents. She was born by cesarean section after an uncomplicated full-term pregnancy and was referred to the neuropsychiatric clinic because of generalized hypotonia, global developmental delay, and alternating esotropia. At age 12 months, she said her first words and got head control, but could not sit without support. Two months later, her developmental quotient was calculated to be 56. She progressively developed a cerebellar syndrome with gait ataxia and dysarthria. Brain MRI performed at age 1 year 10 months showed global cerebellar hypoplasia with enlarged interfolial spaces, in the absence of any brainstem or supratentorial abnormalities **(Fig.46A)**.

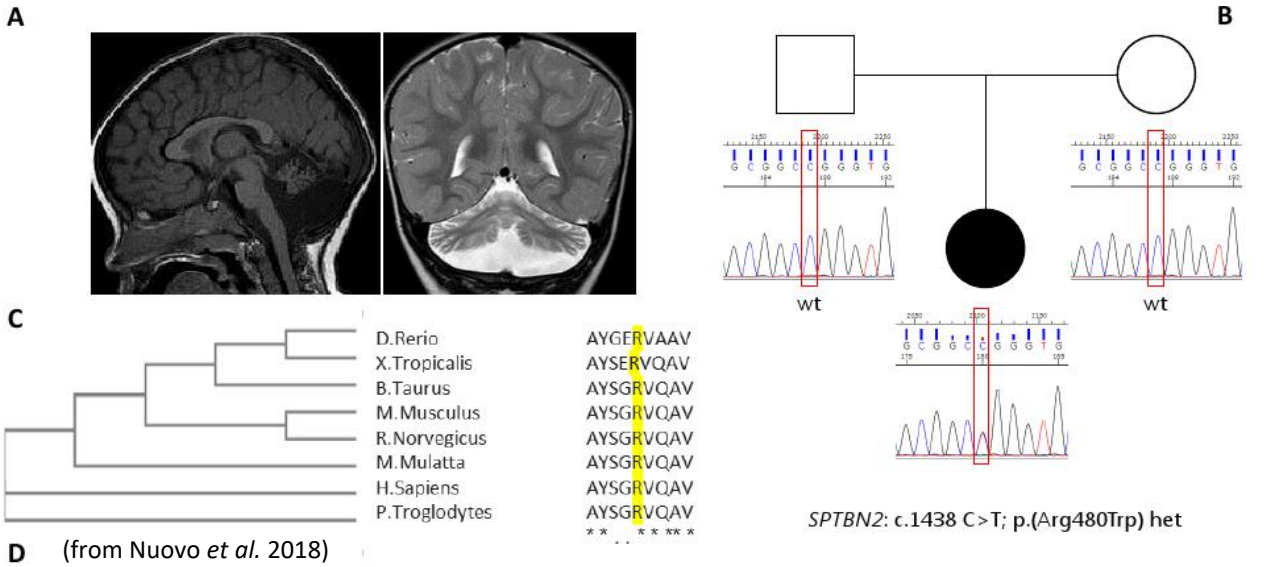

HGVSc	HGVSp	dbSNP	LOVD ID	gnomAD	EVS	SIFT	Polyphen	CADD	Condel	ClinVar
c.1438C>T	p.Arg480Trp	rs397514749	0000144051	0	0	Deleterious (0)	Probably_Damaging (0.999)	33	Deleterious	Pathogenic

Fig.46. Pedigree, imaging and genetic findings of the proband. (A) Brain MRI sections, showing global cerebellar hypoplasia associated with enlarged interfolial spaces **(B)** Pedigree and segregation analysis of Arg480Trp variant in *SPTBN2* gene (filled symbol represents the affected status) **(C)** Multiple sequence alignment of the *SPTBN2* region flanking residue Arg480, demonstrating conservation of the affected amino acid across species **(D)** Allele frequency and *in silico* pathogenicity prediction of Arg480Trp variant.

Molecular analysis identified a heterozygous genotype for the c.1438C>T (p.(R480W)) missense variant in the *SPTBN2* gene (NM_006946), encoding for a β3-spectrin with high expression in Purkinje cells that is involved in excitatory glutamate signaling through stabilization of the glutamate transporter EAAT4 at the membrane's surface. Potential heterozygous deletions involving one or more exons were ruled out using a custom script tool aimed at detecting significant differences in read depth from NGS data. The identified variant was not detected in either of the unaffected parents, suggesting *de novo* occurrence **(Fig.46B)**. Furthermore, it was not present in population databases, affects a highly conserved amino acid, and multiple *in silico* tools consistently predict it as deleterious on the gene product **(Fig.46C-D)**. Interestingly, Parolin-Schnekenberg and coworkers recently performed a genetic screening in a cohort of children diagnosed with ataxic cerebral palsy, and identified this same heterozygous variant in one case, confirming its pathogenicity using *in vitro* models [185]. Based on all these evidences, the variant can be classified as pathogenic according to ACMG guidelines [87].

In-frame heterozygous variants of *SPTBN2* had previously been identified as the cause of autosomal dominant adult-onset SCA5 (MIM#600224), a rare SCA subtype with a few mutations so far reported [186–189] **(Tab.11)**, a mean age of onset at 33 years and mostly normal lifespan. A recent work by Elsayed and colleagues [190] described a homozygous 5-bp deletion in *SPTBN2* in a consanguineous family with infantile ataxia, developmental delay and pyramidal signs that was unlinked to the known autosomal recessive cerebellar ataxia loci. The authors postulated the existence of *SPTBN2* genotype-phenotype correlates, suggesting that loss of function mutations would act recessively, producing a severe congenital ataxic phenotype associated with cognitive impairment and variable additional neurological signs. This hypothesis was partially supported by three subsequent studies, reporting homozygous missense, nonsense and splicing *SPTBN2* variants, all resulting in an analogous congenital ataxia syndrome, defined as SCAR14 (MIM#615386) **(Tab.11)** [191–193]. Elsayed and colleagues [190] also mentioned a previously reported patient affected by a severe infantile-onset cerebellar ataxia with developmental delay, carrying the heterozygous missense variant c.1438C>T (p.(R480W)) in the *SPTBN2* gene [188]. Based on previous literature data on heterozygous *SPTBN2* mutation carriers (presenting the typical SCA5 phenotype of adult-onset, slowly progressive pure cerebellar ataxia), they speculated that either a second-site SCA5 modifier or an undetected *SPTBN2* variant in trans (e.g., deep intronic or in a non-coding regulatory region) should contribute to the phenotypic manifestation.

Tab.11. Clinical features of all reported patients carrying heterozygous or homozygous *SPTBN2* variants

	SCA5					"R480W-phenotype"	SCAR14			
Reference	2	2	2	3	4	8, 9, present study	6	1	5	7
Genetic variant	c.1592_1630del p.E532_M544del	c.1886_1900del p.L629_R634 delinsW	c.758T>C p.L253P	c.1415 C>T p.T472M	c.2608_2610del p.E870del	c.1438C>T p.R480W	c.6375-1G>C	c.2864_2868del p.T955Sfs*120	c.1881C>A p.C627X	c.1572C>T p.R414C
Inheritance	het AD					het *de novo*	hom AR			
Exon	12	14	7	12	14	12	splice site	16	14	2
Domain	3rd SPEC	3rd SPEC	CH	2nd SPEC	6th SPEC	2nd SPEC	PH	6th SPEC	3rd SPEC	1st SPEC
N. of affected	90	6	12	3	5	3	9	3	3	2
Mean age of onset (years)	45	27	33	45	53	congenital	congenital			
Cerebellar syndrome	+	+	+	+	+	+	+	+	+	+
Abnormal ocular movements	-	+	+	-	-	+	-	-	+	+
Hypotonia	-	-	-	-	-	2/3	+	-	1/3	+
Pyramidal signs	4/90	5/6	-	-	1/5	1/3	-	+	-	-
Tremor	-	-	7/12	-	-	1/3	3/9	-	-	-
Focal dystonia	-	1/6	-	-	-	-	-	-	-	-

	SCA5					"R480W-phenotype"	SCAR14			
Facial myokymia	-	4/6	-	-	-	1/3	-	-	-	-
Bulbar dysfunction	2/90	-	-	-	1/5	-	-	-	-	-
DD/ID	-	-	-	-	-	+	+	+	+	+
Behavioral problems	-	-	-	-	-	-	8/8[c]	-	-	-
Cerebellar atrophy	+	+	+	+	+	+[a]	+	NA	2/3[e]	+
Clinical progression	+	+	+	+	+	1/2[b]	+[d]	no	no	no

Each column corresponds to a different *SPTBN2* variant. Clinical features are labeled as "+" (i.e. reported in all mutated patients) or "-" (i.e. absent in all mutated patients). For the remaining cases, the ratio of positive to total investigated patients for each feature is specified. AD: autosomal dominant; AR: autosomal recessive; CH: calponin homology; DD: developmental delay; het: heterozygous; hom: homozygous; ID: intellectual disability; PH: pleckstrin homology; SPEC: spectrin repeat. [a]in two out of three patients, enlarged interfolial spaces were present in association with cerebellar hypoplasia; [b]follow-up data were available only for two patients, with very mild clinical progression in one; [c]variable combination of attention deficit, hyperactivity and aggressive behavior; [d]more rapid progression compared to adult-onset SCA5 phenotype; [e]one out of three patients had normal cerebellum at age 5 years, but mild hypoplasia of the posterior corpus callosum.

Comparing the three reported cases heterozygous for *SPTBN2* p.R480W, a common phenotype of congenital ataxia emerged, closely resembling the SCAR14 phenotype. In particular, all three subjects presented in the neonatal age with abnormal ocular movements and developmental delay, later evolving into ataxia and intellectual disability. Additional neurological signs have been occasionally detected, including hyperreflexia, facial myokymia, and intention tremor **(Tab.11)**. Brain imaging was characterised by hypoplastic cerebellum with a shrunken appearance or overt cerebellar atrophy.

In the attempt to identify meaningful genotype-phenotype correlates, we compared the impact of p.R480W on β3-spectrin stability with that of SCA5-associated heterozygous missense variants p.L253P and p.T472M, by assessing their induced thermodynamic change with the FoldX algorithm [194]. Both p.R480W and p.T472M fall within the second spectrin repeat of the protein, which is thought to be involved in dimer formation needed for correct assembly of the tetrameric α-β-spectrin complex [185], while p.L253P resides in the calponin homology domain **(Fig.47)**.

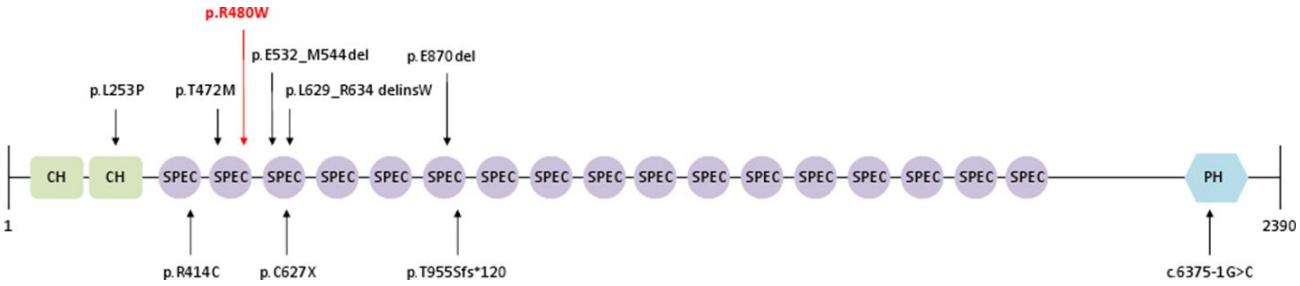

Fig.47. SPTNB2 domains and location of identified variants. Schematic structure of SPTNB2 protein, representing SMART-predicted domains. Variants above and below the panel represent heterozygous SCA5 variants and homozygous SCAR14 variants, respectively. The heterozygous p.R480W variant (LOVD Individual ID #00143194), associated to SCAR14-like phenotype, is highlighted in red.

Interestingly however, p.R480W is predicted to significantly increase protein stability (ΔΔG = −1.52 kcal/mol), while SCA5 missense variants were either destabilizing the protein (p.L253P, ΔΔG = 2.79 kcal/mol) or rather neutral (p.T472M, ΔΔG = −0.40 kcal/mol). The thermodynamic changes caused by these mutations may affect the overall dimerization capability of the protein by either stiffening or making excessively flexible the whole protein structure, yet the observation that SPTBN2 heterozygous p.R480W is able to produce such a severe clinical presentation compared to adult-onset SCA5 cases still remains to be understood.

In conclusion, the presented case further supports the existence of a specific SPTBN2 p.R480W-associated phenotype, which resembles SCAR14 but is associated to the *de novo* occurrence of this variant in the heterozygous state. These findings highlight the complexity of monogenic disorders, providing useful information for both clinical management and genetic counselling of *SPTBN2*-mutated patients.

4.2 THE MILD FORM OF *BRAT1*-RELATED DISORDER: REPORT OF THE FIRST ITALIAN FAMILY

Among NPCA patients, two brothers from Italian origin have been molecularly investigated through WES after negative result of targeted resequencing.

The index patient was a 12-year-old boy, first son of healthy non-consanguineous parents. He was referred to neurogenetics clinic at the age of seven years due to neurodevelopmental delay, mild-moderate intellectual disability and ataxia. Neurological assessment showed generalized hypotonia, bilateral pes planus, severe dysarthria, strabismus and nystagmus. His neuropsychological profile was characterized by global impairment of psychomotor functions, mainly affecting linguistic skills. Moderate-severe sensorineural hearing loss was detected by hearing tests (impedentiometry, brainstem auditory evoked potentials and otoacoustic emissions). A previous brain MRI (performed at 1.5 years of age) revealed a mildly shrunken cerebellum with enlarged interfolial spaces, in the absence of any brainstem or supratentorial abnormalities **(Fig.48a-b)**. The clinical course was stable, with mild improvement in relational, motor praxis and linguistic skills. Brain imaging, repeated five years later, remained unmodified **(Fig.48d)**.

The younger brother, currently aged 8 years, had similar presentation and clinical course, except for the lack of strabismus and hearing loss. Brain imaging at 1.5 years showed a shrunken cerebellum with enlargement of interfolial spaces **(Fig.48e-f)**.

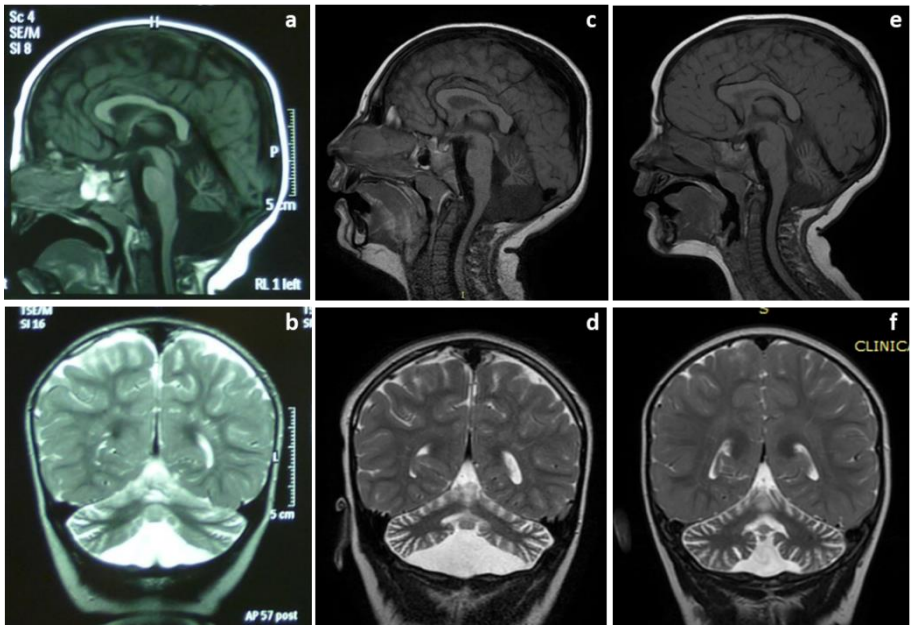

Fig.48. Brain MRI of the two brothers. a-b: Sagittal T1- and Coronal T2- weighted images of index patient at the age of 1.5 years, showing global cerebellar hypoplasia and enlarged interfolial spaces. **c-d**: Sagittal T1- and Coronal T2-weighted images of the same child at the age of 6.5 years, suggestive of stable cerebellar atrophy. **e-f**: Sagittal T1- and Coronal T2- weighted images of the younger brother at the age of 1.5 years, revealing marked enlargement of cerebellar interfolial spaces.

Annotation and filtering of variants shared by the two brothers led to the identification of the c.638dupA (p.(V214Gfs*189)) frameshift variant and the c.1395G>A (p.(T465T)) synonymous variant in the *BRAT1* gene (NM_152743.3), inherited from the unaffected father and mother, respectively **(Fig.49A)** predicted as pathogenic by different *in silico* tools **(Fig.49B)**. Fifteen additional predicted pathogenic variants were identified, none of which segregated with the disease in the family. The c.638dupA variant (rs730880324) has been already reported in several patients [195–199]. Conversely, the c.1395G>A variant (rs201855243) was reported with extremely low frequency in population databases (0.007% in EVS and 0.002% in GnomAD) and had not been previously associated to disease. This synonymous substitution involves the last nucleotide of exon 10 **(Fig.50b)** and is predicted to result in loss of the donor splice site **(Fig.49B)**. In order to assess the impact of this variant on splicing, RNA was extracted from fresh blood samples of the whole family. cDNA amplification and sequencing revealed an additional transcript in the samples of both brothers and their mother **(Fig.50a)**, corresponding to an alternatively spliced isoform produced by exon skipping. In particular, the resulting mRNA lacks the 73-bp-long exon 10 and contains a premature stop codon (p.(P442Sfs*23)) **(Fig.50 c)**.

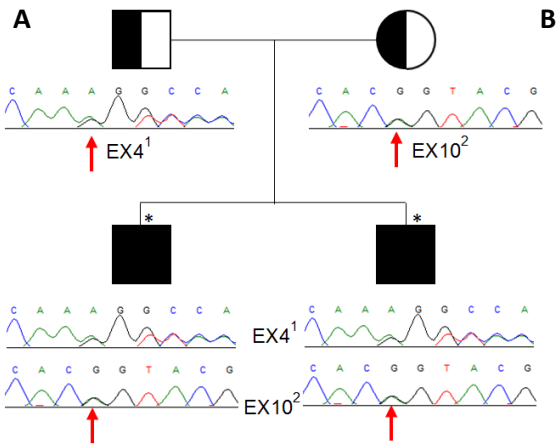

HGVS	c.638dupA p.Val214Glyfs*189	c.1395G>A p.Thr465Thr
dbSNP id	rs730880324	rs201855243
ClinVar	Pathogenic	.
GnomAD (%)	0.02	0.002
EVS (%)	0.05	0.007
CADD	26	11
PaPI	D (0.99)	.
DANN	.	0.63
GERP++	3.95	.
dbscSNV_AB	.	1
dbscSNV_RF	.	0.97
HSF	.	Probably affecting splicing
LOVD screening ID	0000169813-4	0000169813-4
LOVD individual ID	00168941-2	00168941-2

Fig.49. (A) Pedigree and electropherograms showing the results of segregation analysis of BRAT1 variants (red arrows). [1]EX4: c.638dupA (p.V214Gfs*189); [2]EX10: c.1395G>A (p.T465T); *individuals that underwent WES analysis. **(B)** Prediction of pathogenicity and frequency. Pathogenic cut-off scores are as follows: **CADD**: ≥ 15; PaPi_pred and **DANN_score**: range from 0 to 1 (higher is the score, higher is the probability to belong to damaging variant); **GERP++**: scores of > 2 are considered to be highly conserved; **AB**: adaptive boosting; **RF**: Random Forest; **dbscSNV**: range from 0 to 1, cut-off for prediction >0.6 (higher is the score, higher is the probability to the scSNV will affect splicing; **HSF**: Human Splicing Finder.

It has to be noted that the band corresponding to the exon 10-skipped transcript appears less intense compared to the full-length transcript, suggesting that alternative splicing could affect a small percentage of transcripts.

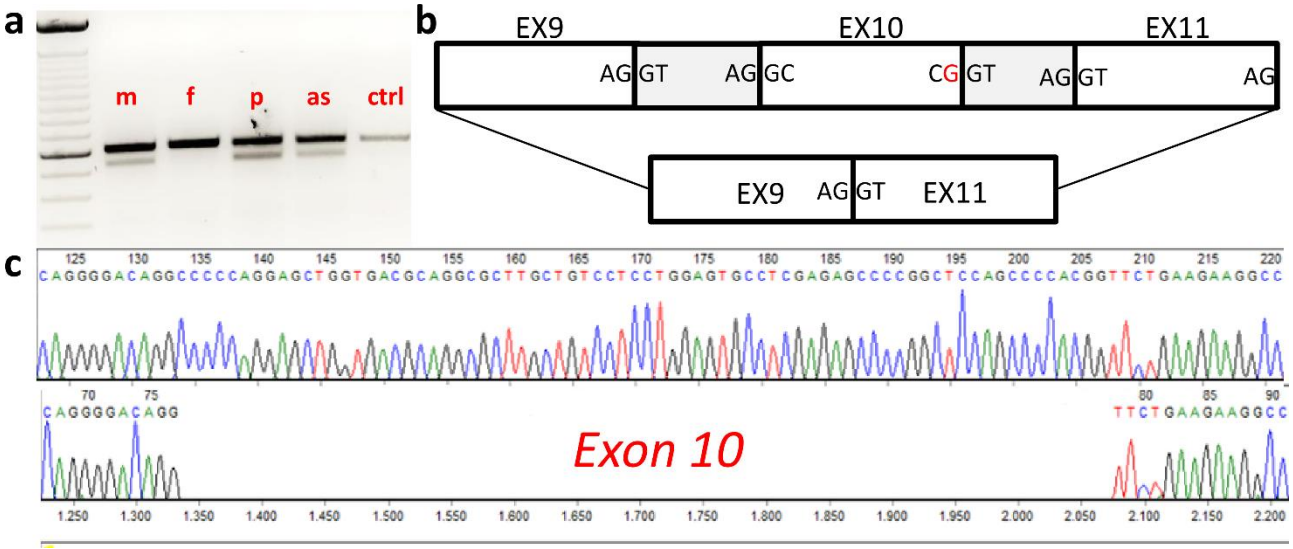

Fig.50. Characterization of BRAT1 synonymous variant p.T465T. a) agarose gel electrophoresis of cDNA amplified with primers flanking the supposed deletion breakpoints, showing the ~599 bp expected amplicon and the presence of a lower band in both patients and their mother **b)** schematic partial structure of BRAT1 (NM_152743.3) transcript (upper panel) and alternative splicing isoform (bottom panel) resulting from G to A substitution of the last nucleotide of exon 10 (highlighted in red). **c**: Sanger sequence of BRAT1 cDNA obtained from both the canonical transcript (upper panel) and the alternatively spliced isoform, (bottom panel), lacking the 73-bp-long exon 10.

BRAT1 encodes BRCA1-associated ATM (ataxia telangiectasia mutated) activator-1, which interacts with both the tumor suppressing BRCA1 and ATM proteins, playing an important role in cellular responses to DNA damage [200]. In addition, it is involved in p53-mediated apoptosis, cellular growth signaling, and mitochondrial homeostasis [200,201]. Recessive mutations in *BRAT1* were first reported to cause rigidity and multifocal seizure syndrome, lethal neonatal (RMFSL, OMIM#614498), a rare congenital disorder characterized by microcephaly, hypertonia, autonomic instability and intractable seizures, leading to death in the first 2 years of life [195–197,202–206]. Brain imaging was highly variable, ranging from normal findings to global atrophy [207]. Few patients presented a less severe presentation, with prolonged survival or a milder form of epilepsy [207–210]. Furthermore, few children showed milder phenotypes of ataxia, intellectual disability, and moderately progressive cerebellar atrophy, variably associated to microcephaly, hypertonia or retinal dystrophy [199,207,211,212]. Overall, 32 patients were identified carrying homozygous or compound heterozygous *BRAT1* mutations,

including frameshift, nonsense, missense, synonymous and splice site variants, as well as multi-exon deletions [195–197,199,202–213].

Smith and colleagues suggested that the observed phenotypic differences might relate to the functional consequences of the identified mutations, as variants leading to premature protein termination were more frequently associated with severe disease [206]. Nevertheless, genotype-phenotype correlations are not yet completely understood, and to predict the clinical outcome of patients carrying different combinations of compound heterozygous variants still remains challenging. As proof of that, the most commonly reported variant c.638dupA was identified in the homozygous or compound heterozygous state in patients with a wide spectrum of disease severity, ranging from mild to severe [195–197,199,207,212].

In this study, we expanded the allelic spectrum of *BRAT1* and describe two Italian siblings with a mild clinical course, confirming the inclusion of NPCA within the spectrum of "BRAT1-related neurodevelopmental disorders". Specifically, both siblings presented developmental delay, mild-moderate intellectual disability and slowly improving congenital ataxia. Brain imaging showed a shrunken cerebellum with enlarged interfolial spaces, which remained stable over time. The frameshift variant c.638dupA introduces a premature protein truncation, abolishing its nuclear localization and reducing stability, as confirmed by *in vitro* studies [195]. On the other hand, the synonymous variant c.1395G>A results in alteration of exon splice pattern. As hypothesized [207], the observed mild phenotype may be due to the occurrence of some normal splicing, leading to the presence of a quote of wild-type transcript. Interestingly, the homozygous c.1395G>C variant has recently been reported in a newborn female, leading to the same synonymous p.(T465T) change as in our family [213]. Yet, contrary to expectations, the resulting phenotype was extremely severe and characterised by hypertonia, dysmorphic features, progressive encephalopathy with refractory seizures, and worsening episodic apnea, leading to intubation and eventually death at 10 weeks of age. Despite the variant has been predicted to cause splice site disruption, further studies have not been performed to investigate the length and amount of alternatively spliced transcript.

All these evidences warn against the generalization of genotype-phenotype associations and demonstrate that genetic counselling of families at risk is still a challenging task. As for other rare disorders, the identification of additional patients and the results of functional studies (including minigene assays for the assessment of spicing variants) are needed to draw reliable associations between biallelic variants and clinical severity.

GENERAL DISCUSSION

In this thesis, clinical, neuroradiological and genetic features of selected CBCDs have been investigated. Because of the rareness of each distinct disorder, the creation of a European network involved in the study of CBCDs has represented a valuable strategy for collection of cases and phenotypic data.

The multistep molecular approach here proposed consists of many consequent analytic methods, which take into account the existence of recurrent variants or mutational mechanisms. This workflow has proved to be successful for the identification of the genetic cause in many different CBCDs, representing a time- and cost-effective strategy at the same time.

Furthermore, the involvement in this project of multiple specialists from different clinical and research institutes has permitted to take advantage of different expertise, required for both clinical-neuroradiological assessment of patients and functional validation of new candidate disease genes.

In Chapter 1, targeted resequencing conducted on both the European and Italian JS cohort has allowed to reach a genetic diagnosis in approximately 60% patients, in accordance with literature data [11]. Also the observed mutational frequency has resulted to be in line with the available studies describing large JS cohorts [11,105], suggesting the existence of a small group of genes (including *CPLANE1*, *CC2D2A*, *CEP290*, *AHI1* and *TMEM67*), accounting for more than one third of JS cases. On the other hand, the remaining portion of positive cases has resulted to be caused by a high number of less frequent genes, some of which occurring in single families, confirming the extreme genetic heterogeneity of the disease. Similar to previous works [11], NGS panel analysis has identified some cases harbouring monoallelic rare variants in one or more JS genes. In order to better elucidate their role, we focused on 43 variants predicted to be pathogenic or likely pathogenic according to ACMG criteria [87] and hypothesized the existence of a second variant on the other allele missed by NGS technique. The result of HD-CGH microarray analysis performed in these patients has proved that CNVs also contribute to JS and can explain a part of apparently negative cases, as recently demonstrated for other ciliopathies such as Bardet-Biedl Syndrome [55]. These findings highlight the need for considering HD-CGH microarray in the molecular diagnostic work-up of JS.

The strict cooperation with the Italian network including 46 different centers with proven experience in the field of JS has been crucial for estimating the prevalence of the disease and define its impact on the general population. As opposed to previous studies [27,91], both overall and sex/age-specific prevalence estimates have been ascertained. This approach has allowed to update the JS prevalence rate for the pediatric age, and to determine for the first time the prevalence of the

disease at later ages. Considering the clinical variability of JS, further epidemiological studies focusing on the distribution of specific sub-phenotypes within the recruited Italian cohort will be necessary in order to accurately define the healthcare needs of JS patients in Italy.

The existence of a national network for JS has also allowed to collect information on the natural history of the disease, in order to precisely quantify the frequency of organ injury and identify potential biomarkers. We specifically focused on kidney insufficiency, which may long remain unrecognized and is often diagnosed late, when renal function is impaired and complications such as anaemia and growth retardation have occurred and are only partially reversible. Studies describing the impact of renal failure in JS [11,94] are usually based on patient cohorts including many young children, at risk of developing kidney disease later in life. We have minimised this bias by following-up patients over time and by assessing the effectiveness of urine osmolality testing on a cohort not including pediatric patients with normal renal function. Our approach has led to the identification of a CKD frequency in JS higher than previously reported, allowing to identify urine osmolality as an early sensitive predictor of the risk of CKD progression.

Lastly, the use of WES analysis in two selected families has shown that germline recessive hypomorphic variants in SUFU are responsible for a phenotype sharing features of ciliopathies such as JS and of SHH-related disorders, including peculiar typical cranio-facial dysmorphisms, postaxial polydactyly and mild MTS.

In Chapter 2, a cohort of PCH patients has been deeply investigated. The detection rate of genetic testing was 73%, confirming that preliminary neuroradiological assessment is useful for increasing the probability of a positive genetic result. While many previous studies on large patient cohorts consisted in sequencing of selected genes in specific PCH subgroups, (identified according to both clinical and neuroimaging features) [68,75,131,132], we have performed NGS panel analysis in all patients showing a MRI pattern consistent with a diagnosis of PCH. This unbiased approach aimed at exploring the mutational frequency of each gene regardless of clinical presentation. *CASK* has resulted to be the most frequently mutated gene in the investigated cohort, explaining 43% of the screened probands. This figure is in contrast with data previously reported by Namavar and colleagues, showing *TSEN54* causative mutations in 59.2% of patients [73]. Since most of the PCH families described in this thesis are from Italy, our findings contribute to delineate the genetic architecture of PCH within the country. Approximately one third of *CASK*-mutated cases has been detected with an intragenic deletion or duplication, confirming the usefulness of MLPA assay as a first level analysis. Moreover, pathogenic mutations in CASK gene have been identified also in a

small percentage of male patients, with a clinical severity strictly dependent on the mutation type. All our *TSEN54* patients presented the c.919 G>T founder variant in a homozygous state. The predominance of this genotype is in line with previous works [73,131], highlighting the importance of searching this variant through Sanger sequencing before considering further genetic analyses.

The systematic assessment of clinical and neuroradiological features performed in a subset of patients allowed to investigate genotype-phenotype associations for the three most common PCH genes (*CASK*, *TSEN54* and *EXOSC3*) by using a cluster analysis approach, questioning the existence of clear boundaries between *CASK*- and *TSEN54*-related phenotypes.

In Chapter 3, the neuroradiological phenotype associated with mutations in tubulin genes has been assessed, with a special focus on CD and other PF morphological anomalies. Also in this case, the existence of a network involved in the study of CBCDs has been useful for ensuring a greater impartiality of the presented results, as all the identified malformations have been systematically reviewed by a team of experts and reported in consensus. Systematic evaluation of MRI images allowed to the identification of a well recognizable pattern, labelled as "tubulin-related CD" and characterised by asymmetrical involvement of the cerebellar hemispheres with possibly associated vermian dysplasia and regular aspect of the cerebellar cortex. Furthermore, conventional/anatomical MRI and DTI studies performed on patients presenting with tubulinopathy has revealed a complex pattern of brainstem malformations, including both morphological and intrinsic white matter tracts anomalies and consisting in brainstem hypoplasia, asymmetry or cleft, as well as anomalies in the orientation and organisation of CSTs and TPF. Among patients with neuroimaging features resembling a tubulinopathy, two affected sisters with no pathogenic mutations in tubulin genes have been selected and investigated with WES. By using this approach, a new disease-causing gene has been identified, coding for the tubulin-modifying enzyme TTL involved in the physiological tyrosination of the C-terminus of α tubulin. This finding expanded the spectrum of mendelian diseases caused by mutations in genes involved in tubulin PTMs, introducing the first recessively inherited tubulinopathy-like disorder.

In Chapter 4, clinical and molecular characterisation of two families with NPCA have been provided. In the first case, a heterozygous variant has been detected in *SPTBN2,* a gene causative for both SCA 5 (with late onset and autosomal dominant inheritance) and SCAR14 (with a more severe clinical presentation, onset in the pediatric age, and autosomal recessive inheritance pattern). Our patient presented with a severe pediatric phenotype caused by *de novo* R480W missense variant, showing features intermediate between SCA5 and SCAR14. A review of the literature led to the identification

of two additional cases sharing the same genotype and presenting with overlapping phenotype. This finding allowed to delineate a peculiar *SPTBN2* p.R480W-associated phenotype, highlighting the complexity of monogenic disorders and questioning the principles of Mendelian genetics.

In the second family, two compound heterozygous variants have been detected in *BRAT1* gene, typically causing a severe epileptic encephalopathy known as lethal neonatal rigidity and multifocal seizure syndrome, leading to intractable seizures and early lethality. The mild phenotype observed in our patients further confirmed the existence of a spectrum of "BRAT1-related neurodevelopmental disorders", also including congenital ataxias with stable course over time.

Furthermore, the positive result of genetic analysis in the two investigated families highlighted the importance of WES approach to facilitate molecular diagnosis of non-specific neurologic disorders such as NPCA.

CONCLUSIONS AND FUTURE PERSPECTIVES

The research findings described in this thesis clearly demonstrate that clinically oriented NGS-based genetic testing allows to get a molecular diagnosis for many rare neurogenetics disorders and lay the basis for the identification of new disease-causing genes. Delineation of the genetic architecture of molecularly heterogeneous conditions such as JS or PCH is essential for defining the most suitable diagnostic strategy, providing guidance for the laboratory workup. Furthermore, the identified genotype-phenotype associations could be translated into clinical practice, in order to prevent or precociously treat organ complications (especially in the case of JS) or to provide patients with a more accurate genetic counselling. On the other hand, our results open new perspectives for a deeper understanding of the investigated disorders. For example, considering the availability of effective treatment options for hepatic fibrosis, it would be desirable to identify precocious markers of liver disease in JS patients (in the same way as has happened for renal insufficiency). Analogously, the potential role of additional monoallelic variants affecting ciliary genes in molecularly confirmed JS patients need to be further elucidated, in order to unravel the mechanisms at the base of intrafamilial clinical variability. With regard to PCH and NPCA, additional efforts will be needed to expand the collected cohorts, in order to validate the obtained results on genotype-phenotype associations and better define the phenotypic spectrum associated with rare genes. Lastly, the identification of a new disease-causing mechanism for tubulinopathy, involving post-translational modifications of microtubules, could facilitate the development of targeted therapies for this disorder.

APPENDIX

CLINICAL QUESTIONNAIRE

General data

name and surname: _____ sex: M ☐ F ☐

date of birth: _____ date of last examination: _____

referral clinician: _____

Family history

Father (name): _____ place of birth/ethnicity: _____

Mother (name): _____ place of birth/ethnicity: _____

parents related: yes ☐ no ☐ possibly ☐ If yes, how are they related: _____

affected sibs: yes ☐ no ☐ if yes, how many brothers (____) and sisters (____) ages: _____

healthy sibs yes ☐ no ☐ if yes, how many brothers (____) and sisters (____) ages: _____

others affected: yes ☐ no ☐ *if yes, please attach pedigree*

family history of other genetic disorders: _____

blood for genetic study: yes ☐ no ☐

If yes, please specify on the pedigree which family members have submitted samples and whether this was blood, saliva, or other sample type. Please note any differences between affected persons, or fill out separate questionnaires for each affected family member.

Pregnancy and Delivery history

premature?: Yes ☐ No ☐ If yes, what gestational age: _____ delivery: vaginal ☐ C-section ☐

pregnancy (relevant events): _____

delivery (relevant events): _____

Apgar scores: 1': ____ 5': ____ birth weight _____ length _____ head circumference: _____

Measurements of head circumference (OFC) at birth and during the first several months are important.

Early development

Developmental milestones (age):

head control: _____ rolling: _____ sitting: _____ crawling: _____

walking: _____ first words: _____ sentences (structured language): _____

scholarship: normal ☐ aided ☐ impossible ☐

System 1: Cognitive and seizures

Development Quotient (DQ): _____ at age _____; _____at age _____; _____ at age _____

Intelligence Quotient (IQ): _____ at age _____; _____at age _____; _____ at age _____

if DQ or IQ performed, please specify test: _____

Seizures: yes ☐ no ☐

*If yes, describe type(s), onset and frequency:*_____

Electroencephalogram (EEG): date: _____ normal ☐ abnormal ☐ not performed ☐

if abnormal , please describe: _____

System 2: Eyes, vision and eye movements

strabismus: yes ☐ no ☐ *if yes, describe:* _____

ptosis: absent ☐ right eye ☐ left eye ☐ nystagmus: yes ☐ no ☐

oculomotor apraxia: yes ☐ no ☐ other abnormal ocular movements: yes ☐ no ☐

If yes, please describe: _____

ocular malformations / anomalies: yes ☐ no ☐ *(such as microphthalmia, colobomas, cataracts, etc)*

If yes, please describe (important):

_____

visual acuity: date: _____ right eye: _____ left eye: _____ not evaluated ☐

visual field: date: _____ right eye: _____ left eye: _____ not evaluated ☐

Fundus exam: date: _____ normal ☐ abnormal ☐ not evaluated ☐

Electroretinogram (ERG): date: _____ normal ☐ abnormal ☐ not performed ☐

if any of these is abnormal , please describe in detail:

_____

System 3: Hearing and balance

Hearing loss: yes ☐ no ☐ *If yes:* sensorineural ☐ conductive ☐ both ☐

if yes, describe: _____

Balance problems: yes ☐ no ☐

if yes, describe: _____

System 4: Heart and circulation

Heart malformation: yes ☐ no ☐ unknown ☐

Heart rhythm abnormality: yes ☐ no ☐ unknown ☐

Blood vessel anomalies: yes ☐ no ☐ unknown ☐

*if yes to any of the above, please describe in detail:*_____

System 5: Lungs and respiration

Lung malformation: yes ☐ no ☐ unknown ☐

Respiratory pattern abnormality: yes ☐ no ☐ unknown ☐

Recurrent respiratory infections: yes ☐ no ☐ unknown ☐

if yes, please describe: _____

System 6: Gastro-intestinal tract, liver and pancreas

situs inversus: yes ☐ no ☐ unknown ☐

GI malformation including Hirschsprung disease: yes ☐ no ☐ unknown ☐

congenital liver disease including biliary hypoplasia: yes ☐ no ☐ unknown ☐

later liver disease especially fibrosis or cysts: yes ☐ no ☐ unknown ☐

congenital pancreas disease including congenital diabetes: yes ☐ no ☐ unknown ☐

if any are abnormal, please describe in detail: _____

serum liver enzymes: date: _____ normal ☐ abnormal ☐ not evaluated ☐

liver ultrasound: date: _____ normal ☐ abnormal ☐ not performed ☐

liver biopsy: date: _____ normal ☐ abnormal ☐ not performed ☐

if any are abnormal, please describe in detail: _____

System 7: Reproductive

sex reversal: yes ☐ no ☐ ambiguous genitalia: yes ☐ no ☐ closest to: M ☐ F ☐

M: small penis: yes ☐ no ☐ undescended testes yes ☐ no ☐

F: menses age onset: _____ menstrual disorder yes ☐ no ☐

If any are abnormal, please describe in detail: _____

System 8: Kidney, ureters and bladder

Cystic kidney disease: yes ☐ no ☐ *if yes:* nephronophthisis ☐ PKD ☐ CDK ☐ unknown ☐

Other malformations: yes ☐ no ☐ polyuria: yes ☐ no ☐

renal failure: yes ☐ no ☐ if yes, age of diagnosis: _____

renal ultrasound: date: _____ normal ☐ abnormal ☐ not performed ☐

*if abnormal, please describe (very important):*_____

serum creatinine: _____ dates: _____ not evaluated ☐

urine specific gravity: _____ dates: _____ not evaluated ☐

DDAVP concentration test: _____ dates: _____ not performed ☐

other tests (describe): _____

PKD: Polycystic Kidney Disease; CDK: Cystic Disease of the Kidneys

System 9: Skeletal and limbs

scoliosis: yes ☐ no ☐ spine malformation: yes ☐ no ☐

polydactyly: yes ☐ no ☐ *If yes*: preaxial ☐ mesaxial ☐ postaxial ☐

syndactyly: yes ☐ no ☐ other limb anomaly: yes ☐ no ☐

if yes for any of above, please describe: _____

System 10: Face and dysmorphology

dysmorphic features: yes ☐ no ☐ not evaluated ☐

tongue hamartomas: yes ☐ no ☐ not evaluated ☐

multiple lingual frenula: yes ☐ no ☐ not evaluated ☐

cleft lip and palate: yes ☐ no ☐ lip only ☐ palate only ☐ not evaluated ☐

any other tumors: yes ☐ no ☐ not evaluated ☐

If yes to any, please describe in detail: _____

Growth and other:

Please list all available growth measurements (weight, height or length, head circumference) for the first two years of life, and the most recent available. Head circumference (OFC) is VERY IMPORTANT.

Weights: _____

Heights: _____

OFCs: _____

Neurological Examination

Nystagmus: yes ☐ no ☐ dysarthria: yes ☐ no ☐ drooling: yes ☐ no ☐

muscle strength, upper limbs: normal ☐ reduced -1 ☐ -2 ☐ -3 ☐ -4 ☐ (most severe)

muscle strength, lower limbs: normal ☐ reduced -1 ☐ -2 ☐ -3 ☐ -4 ☐ (most severe)

tone, axial (neck, trunk): normal ☐ hypotonia ☐ spastic ☐

tone, limbs: normal ☐ hypotonia ☐ spastic ☐ symmetric ☐

tendon reflexes, upper limbs: absent 0 ☐ low 1+ ☐ normal 2+ ☐ brisk 3+ ☐ clonus 4+ ☐

tendon reflexes, lower limbs: absent 0 ☐ low 1+ ☐ normal 2+ ☐ brisk 3+ ☐ clonus 4+ ☐

plantar responses (Babinski): normal ☐ abnormal ☐

*If any are abnormal, also describe:*_____

ataxia: yes ☐ no ☐ *If yes*: ocular ☐ speech ☐ arms ☐ legs ☐ gait ☐

dyskinesias: yes ☐ no ☐ *If yes:* athetosis ☐ chorea ☐ dystonia ☐ tremor ☐ other ☐

If yes to any of the above, please describe or specify as needed: _____

Blood/serum/CSF testing & biopsies

transferrin IEF: date: _____ normal ☐ abnormal ☐ not performed ☐

creatine kinase: date: _____ normal ☐ abnormal ☐ not evaluated ☐

muscle biopsy: date: _____ normal ☐ abnormal ☐ not performed ☐

plasma amino acids: date: _____ normal ☐ abnormal ☐ not evaluated ☐

plasma lactate levels: date: _____ normal ☐ abnormal ☐ not evaluated ☐

CSF lactate levels: date: _____ normal ☐ abnormal ☐ not evaluated ☐

*If ANY of the above are abnormal, please describe the results in detail:*_____

_____

IEF: isoelectric focusing.

Other relevant tests

Describe any other important test results.

_____

_____

_____

Brain MRI date (latest MRI): _____ not performed ☐

Cerebellar malformation: atrophy ☐ hypoplasia ☐ dysplasia ☐

vermis : total ☐ partial ☐ mild ☐ moderate ☐ severe ☐

left hemisphere: total ☐ partial ☐ mild ☐ moderate ☐ severe ☐

right hemisphere: total ☐ partial ☐ mild ☐ moderate ☐ severe ☐

if partial, describe (i.e. superior vermis): _____

_____

progression over time: yes ☐ no ☐ unknown ☐

other cerebellar malformations (i.e. rhomboencephalosynapsis, cortical heterotopia etc): yes ☐ no ☐

if yes, please describe: _____

_____

Extra-cerebellar involvement: yes ☐ no ☐

if yes:

IV ventricle: normal ☐ enlarged ☐ cystic dilatation ☐

tentorium: normal ☐ elevated ☐

pons: normal ☐ hypoplasia ☐ atrophy ☐

corpus callosum: normal ☐ hypoplasia ☐ absence ☐

Molar Tooth Sign: yes ☐ no ☐

encephalo-meningocele: yes ☐ no ☐

hydrocephalus: yes ☐ no ☐

pituitary / sella abnormality: yes ☐ no ☐

other brainstem malformations: yes ☐ no ☐

other malformations of the posterior fossa: yes ☐ no ☐

supratentorial abnormalities: yes ☐ no ☐

if yes to ANY of the above, please describe the MRI findings in detail: _____

FINAL DIAGNOSIS OF THE **TYPE OF CEREBELLAR MALFORMATION** (if reached):

_____

originals/copy available: yes ☐ no ☐

if yes from whom? _____

Genetic testing

Standard karyotype: date: _____ normal ☐ abnormal ☐ not performed ☐

FISH analysis: date: _____ normal ☐ abnormal ☐ not performed ☐

CGH-array: date: _____ normal ☐ abnormal ☐ not performed ☐

SNP-array: date: _____ normal ☐ abnormal ☐ not performed ☐

If ANY of the above are abnormal, please describe the results in detail: _____

_____

other genetic testing (please describe): _____

_____

Neurophysiologic studies

Nerve MCV date: _____ normal ☐ abnormal ☐ not evaluated ☐

Nerve SCV date: _____ normal ☐ abnormal ☐ not evaluated ☐

Muscle EMG date: _____ normal ☐ abnormal ☐ not evaluated ☐

Brainstem AER date: _____ normal ☐ abnormal ☐ not evaluated ☐

MEP date: _____ normal ☐ abnormal ☐ not evaluated ☐

SSEP date: _____ normal ☐ abnormal ☐ not evaluated ☐

VEP date: _____ normal ☐ abnormal ☐ not evaluated ☐

*if ANY of the above is "abnormal", please describe the results in detail:*_____

MCV-Motor Conduction Velocity; SCV-Sensory Conduction Velocity; EMG-Electromiography; AER-Auditory Evoked Responses; MEP-Motor Evoked Potentials; SSEP-SomatoSensory Evoked Potentials; VEP-Visual Evoked Potentials.

Comments and notes (i.e. stable or progressive course):

_____

_____

_____

_____ _____

physician's signature date

MRI ASSESSMENT SHEET

A – PRIMARY CEREBELLAR DIAGNOSIS (choose ONE option only and describe if necessary)

0. Normal cerebellum
1. Cerebellar agenesis
2. Isolated vermis hypoplasia
3. Whole cerebellar hypoplasia
4. Progressive cerebellar atrophy
5. "Shrunken" cerebellum
6. Cerebellar (hypo)dysplasia
7. Severe ponto-cerebellar hypoplasia (Barth, MEB etc…)
8. Romboencephalosynapsis
9. Pontine tegmental cap dysplasia
10. Dandy-Walker malformation
11. Molar tooth malformation
12. Unilateral hemispheric defect
13. Other primary diagnosis (Arnold-Chiari etc…)

B – ASSOCIATED INFRATENTORIAL ABNORMALITIES not included in previous categories (please describe below)

1. Mild pons hypoplasia (not fitting A7 diagnosis)
2. Occipital encephalocele
3. Mega cisterna magna / Blake's pouch / posterior fossa arachnoideal cyst
4. Cerebellar signal abnormalities
5. Intracerebellar cysts
6. Abnormally small posterior fossa
7. Primary brainstem defect
8. Other (including infratentorial anomalies or additional cerebellar anomalies associated with a primary diagnosis)

C – ASSOCIATED SUPRATENTORIAL ABNORMALITIES (please describe below)

1. Cerebral cortex
2. White matter
3. Basal ganglia
4. Commissures (corpus callosum, septum pellucidum, fornix)
5. Enlarged ventricles and/or CSF spaces
6. Other

COMMENTS

Likely primary

Likely acquired

Imaging insufficient / inadequate / poor quality

rev mar10

Legend

In box A, please choose ONE OPTION ONLY. In case of doubt, choose the most relevant "A" diagnosis and also select B8 (other) and describe the additional malformation in "comments".
A0 – normal: to be assigned in cases of normal cerebellum; it is possible to assign categories in boxes B and C
A4 – progressive cerebellar atrophy: to be assigned ONLY with proof of damage progression (at least 2 MRIs over time)
A5 – shrunken: to be assigned when cerebellum is clearly atrophic or there is a combination of atrophy and hypoplasia, but progression has been excluded or is unknown (i.e. only one MRI available)
A6 – cerebellar (hypo)dysplasia: to be assigned to all cases showing some evidence of bilateral cerebellar dysplasia (i.e. not only to classical forms of "cerebellar cortical dysplasia"), even if associated with hypoplasia
A7 – severe pontocerebellar hypoplasia: to be assigned to all cases showing severe pons hypoplasia (i.e. flat pons) associated with cerebellar hypoplasia (including not only typical "Barth" PCH but also other less specific conditions sharing these neuroradiological features)
A10 – Dandy-Walker malformation: to be assigned to typical DWM cases, in particular pay attention to vermis rotation to distinguish these cases from WCH with enlarged cisterna magna.
A12 – Unilateral hemispheric defect: to be assigned to all types of unilateral cerebellar defects (i.e. dysgenesis, schisis, hypoplasia, dysplasia), regardless whether it is supposed an acquired or genetic cause. Asymmetric bilateral defects should NOT be assigned this category.

In box B, multiple choices are possible. Please describe in "comments" when necessary (concise descriptions please!)
B1 – Mild pons hypoplasia (not fitting A7 diagnosis): to be assigned to all cases where a mildly hypoplastic pons is observed as an accessory feature in a patient with any other major defect (mainly A3 - WCH)
B6 – Abnormally small posterior fossa: to be assigned in all cases in which the posterior fossa seems abnormally small (i.e. verticalized tentorium), in association with any other A and B diagnosis.
B7 – Primary brainstem defect: to be assigned when a brainstem defect not fitting in other categories (e.g. A7 or A8) represents the major abnormality of the patient; it can be associated to a normal cerebellum (A0) or to other cerebellar abnormalities (e.g. A2 or A3)
B8 – Other: to be assigned in case of additional cerebellar defects that are associated with a major diagnosis (A), or to describe infratentorial abnormalities not included in B1-B7

In box C, multiple choices are possible. Please describe in "comments" when necessary (concise descriptions please!)

Comments: please avoid lengthy descriptions and try to comment only on particular features that cannot be appropriately described by the proposed categories

Please state if you think the defect to represent **a primary malformation** or to result from an **acquired lesion** by highlighting the relevant option

Tab.A1. List of genes causative for Joubert Syndrome and other ciliopathies analysed through targeted resequencing

Gene	NM accession number**	Gene	NM accession number**
AHI1	NM_001134830	*MKS1*	NM_017777
ARL13B	NM_001174150	*NPHP1*	NM_001128178.2
*B9D1**	NM_015681	*NPHP3**	NM_153240
B9D2	NM_030578	*NPHP4**	NM_015102
*C2CD3**	NM_015531.6	*OFD1**	NM_003611
CC2D2A	NM_001080522	*PDE6D**	NM_002601
CEP41	NM_018718	*PIBF1**	NM_006346
*CEP104**	NM_014704	*POC1B**	NM_172240
*CEP120**	NM_153223	*RPGRIP1L**	NM_015272
*CEP164**	NM_014956	*SCLT1**	NM_144643
CEP290	NM_025114	*SUFU*	NM_016169
CPLANE1 (C5orf42)	NM_023073	*TBC1D32**	NM_152730
CSPP1	NM_024790	*TCTN1*	NM_001082538
*DDX59**	NM_001031725	*TCTN2*	NM_024809
*EXOC8**	NM_175876	*TCTN3**	NM_015631
*GLI3**	NM_000168	*TMEM17*	NM_198276
*IFT172**	NM_015662	*TMEM67*	NM_153704
INPP5E	NM_019892	*TMEM107**	NM_032354
*INTU**	NM_015693	*TMEM138**	NM_016464
*INVS**	NM_014425	*TMEM216**	NM_001173991.2
*KIAA0556**	NM_015202	*TMEM231**	NM_001077416.2
KIAA0586	NM_001244189	*TMEM237*	NM_001044385
*KIAA0753**	NM_014804	*TTC21B**	NM_024753
*KIF7**	NM_198525	*WDPCP**	NM_015910
*KIF14**	NM_014875	*ZNF423**	NM_015069

*****: genes marked with asterisk have also been analysed through custom High Density Comparative Genomic Hybridisation microarray, in order to investigate intragenic deletions/duplications.

**: corresponding to canonical transcript

Tab.A2. List of genes causative for pontocerebellar hypoplasia and other cerebellar and brainstem congenital defects (including non-progressive congenital ataxia) analysed through targeted resequencing

Gene	NM accession number**	Gene	NM accession number
ABCB7	NM_004299	*LAMC1*	NM_002293
ADGRG1	NM_005682	*NEUROD1*	NM_002500
AMPD2	NM_004037	*NID1*	NM_002508
AP1S2	NM_001272071	*OPHN1*	NM_002547
ARHGEF2	NM_001162383	*PAX6*	NM_001258462
ATCAY	NM_033064	*PMM2*	NM_000303
ATP2B3	NM_001001344	*PMPCA*	NM_015160
ATP8A2	NM_016529	*PTF1A*	NM_178161
BRF1	NM_001519	*RARS2*	NM_020320
CA8	NM_004056	*ROBO3*	NM_022370
CAMTA1	NM_015215	*SIL1*	NM_022464
CASK	NM_003688	*TOE1*	NM_025077
CHMP1A	NM_002768	*TSEN2*	NM_001145392
CLP1	NM_006831	*TSEN34*	NM_001077446
COQ8A	NM_020247	*TSEN54*	NM_207346
CWF19L1	NM_018294	*VLDLR*	NM_003383
DKC1	NM_001363	*VRK1*	NM_003384
EXOSC3	NM_016042	*WASHC5*	NM_014846
EXOSC8	NM_181503	*WDR81*	NM_001163809
FOXC1	NM_001453	*WWOX*	NM_016373
GPSM2	NM_013296	*ZIC1*	NM_003412
KCNJ10	NM_002241	*ZIC4*	NM_001168378
LAMA1	NM_005559	*ZNF592*	NM_014630

**: corresponding to canonical transcript

Tab.A3. Genomic variants and clinical features identified in Joubert probands molecularly confirmed after NGS analysis

Family ID	Gene	Allele 1		Allele 2		phenotype					
		cDNA	protein	cDNA	protein	kidney	retina	eye_malform	liver	polydactyly	orofacial
COR07	*AHI1*	c.1997A>T	p.(Asp666Val)	c.1123A>C	p.(Thr375Pro)	-	+	-	-	-	-
COR11	*AHI1*	c.2168G>A	p.(Arg723Gln)	c.2168G>A	p.(Arg723Gln)	+	+	-	-	-	-
COR63	*AHI1*	c.630_633dup	p.(Leu212Glufs*17)	c.1900dup	p.(Tyr634Leufs*7)	na	na	na	na	-	-
COR72	*AHI1*	c.1328T>A	p.(Val443Asp)	c.1328T>A	p.(Val443Asp)	-	+	-	-	-	-
COR79	*AHI1*	c.2687A>G	p.(His896Arg)	c.2687A>G	p.(His896Arg)	-	+	-	-	-	-
COR135	*AHI1*	c.1981T>C	p.(Ser661Pro)	c.1981T>C	p.(Ser661Pro)	na	na	na	na	na	na
COR144	*AHI1*	c.1484G>T	p.(Arg495Leu)	c.2033C>A	p.(Ala678Asp)	-	na	-	-	-	-
COR147	*AHI1*	c.2493-1G>A		c.2493-1G>A		-	+	-	-	-	-
COR156	*AHI1*	c.1550G>A	p.(Trp517*)	c.1550G>A	p.(Trp517*)	+	+	-	-	-	-
COR177	*AHI1*	c.1828C>T	p.(Arg610*)	c.2266+1G>A		-	na	-	-	-	-
COR179	*AHI1*	c.1912+1G>A		c.1780-1G>C		-	-	-	na	-	-
COR182	*AHI1*	c.640G>T	p.(Glu214*)	c.640G>T	p.(Glu214*)	-	-	-	na	-	-
COR220	*AHI1*	c.985C>T	p.(Arg329*)	c.985C>T	p.(Arg329*)	-	+	-	-	na	-
COR224	*AHI1*	c.2687A>G	p.(His896Arg)	c.2687A>G	p.(His896Arg)	-	+	-	-	-	-
COR248	*AHI1*	c.787dup	p.(Gln263Profs*8)	c.787dup	p.(Gln263Profs*8)	-	+	-	-	-	-
COR296	*AHI1*	c.2156A>C	p.(Asp719Ala)	c.1474T>C	p.(Ser492Pro)	-	+	-	-	-	-
COR358	*AHI1*	c.1213A>C	p.(Thr405Pro)	c.1213A>C	p.(Thr405Pro)	-	na	-	na	-	-
COR399	*AHI1*	c.1151G>C	p.(Ser384Thr)	c.931G>A	p.(Val311Ile)	na	+	+	na	na	na
COR401	*AHI1*	c.2671C>T	p.(Arg891*)	c.1829G>C	p.(Arg610Pro)	-	+	-	-	-	-
COR402	*AHI1*	c.1780-1G>C		c.2765-1G>C		-	+	-	-	-	-
COR415	*AHI1*	c.2105C>T	p.(Thr702Met)	c.2167C>G	p.(Arg723Gly)	-	-	-	-	-	-
COR419	*AHI1*	c.2687A>G	p.(His896Arg)	c.2687A>G	p.(His896Arg)	-	+	-	-	-	-
COR434	*AHI1*	c.985C>T	p.(Arg329*)	c.1550G>A	p.(Trp517*)	na	na	na	na	na	na
COR436	*AHI1*	c.2687A>G	p.(His896Arg)	c.2009T>C	p.(Leu670Pro)	+	na	-	-	-	-
COR472	*AHI1*	c.2273A>C	p.(His758Pro)	c.2273A>C	p.(His758Pro)	na	na	na	na	na	na
COR478	*AHI1*	c.1328T>A	p.(Val443Asp)	c.1328T>A	p.(Val443Asp)		na	-	-	-	-
COR493	*AHI1*	c.2168G>A	p.(Arg723Gln)	c.2168G>A	p.(Arg723Gln)	-	+	na	-	-	-
COR578	*AHI1*	c.910dup	p.(Thr304Asnfs*6)	c.910dup	p.(Thr304Asnfs*6)	na	-	-	-	-	-
COR346	*B9D1*	c.95A>G	p.(Tyr32Cys)	c.520_522del	p.(Val174del)	-	-	-	-	-	-
COR363	*B9D1*	c.467G>A	p.(Arg156Gln)	c.467G>A	p.(Arg156Gln)	-	-	-	-	-	-
COR372	*B9D1*	c.467G>A	p.(Arg156Gln)	c.511_513del	p.(Phe171del)	-	+	-	na	-	-
COR06	*CC2D2A*	c.4669T>A	p.(Tyr1557Asn)	c.4669T>A	p.(Tyr1557Asn)	-	-	-	-	-	-
COR41	*CC2D2A*	c.4667A>T	p.(Asp1556Val)	c.3289del	p.(Val1097Phefs*2)	-	-	-	-	-	-

Tab.A3 (continued)											
COR68	*CC2D2A*	c.4667A>T	p.(Asp1556Val)	c.4256del	p.(Gly1419Aspfs*9)	-	+	-	-	-	-
COR75	*CC2D2A*	c.4136T>C	p.(Leu1379Pro)	c.4667A>T	p.(Asp1556Val)	-	-	-	-	-	-
COR86	*CC2D2A*	c.1252C>G	p.(His418Asp)	c.2999A>T	p.(Glu1000Val)	-	-	-	-	-	-
COR122	*CC2D2A*	c.4667A>T	p.(Asp1556Val)	c.4597_4598del	p.(Leu1533Valfs*12)	na	na	na	na	na	na
COR128	*CC2D2A*	c.3544T>C	p.(Trp1182Arg)	c.2996_3001del	p.(Glu999_Glu1000del)	na	na	na	na	na	na
COR149	*CC2D2A*	c.3364C>T	p.(Pro1122Ser)	c.3364C>T	p.(Pro1122Ser)	na	na	na	na	na	na
COR161	*CC2D2A*	c.3452T>C	p.(Val1151Ala)	c.4147G>C	p.(Ala1383Pro)	-	-	-	na	-	-
COR167	*CC2D2A*	c.4667A>T	p.(Asp1556Val)	c.1017+1G>A		na	-	-	na	-	-
COR185	*CC2D2A*	c.4220A>G	p.(Tyr1407Cys)	c.3341C>T	p.(Thr1114Met)	-	+	-	-	-	-
COR218	*CC2D2A*	c.3289del	p.(Val1097Phefs*2)	c.2996_3001del	p.(Glu999_Glu1000del)	-	-	-	-	-	-
COR239	*CC2D2A*	c.3195del	p.(Gln1065Hisfs*34)	c.4465G>C	p.(Asp1489His)	-	na	-	-	-	-
COR270	*CC2D2A*	c.3856T>C	p.(Cys1286Arg)	c.3856T>C	p.(Cys1286Arg)	-	-	-	-	-	-
COR285	*CC2D2A*	c.2848C>T	p.(Arg950*)	c.2848C>T	p.(Arg950*)	-	-	-	-	-	-
COR317	*CC2D2A*	c.4786G>A	p.(Ala1596Thr)	c.4786G>A	p.(Ala1596Thr)	-	-	-	-	-	-
COR342	*CC2D2A*	c.2999A>T	p.(Glu1000Val)	c.3638del	p.(Gly1213Alafs*8)	-	-	-	-	-	-
COR377	*CC2D2A*	c.3364C>T	p.(Pro1122Ser)	c.3364C>T	p.(Pro1122Ser)						
COR400	*CC2D2A*	c.4345C>A	p.(Pro1449Thr)	c.1558C>T	p.(Arg520*)	-	-	-	-	-	+
COR410	*CC2D2A*	c.3347C>T	p.(Thr1116Met)	c.4582C>T	p.(Arg1528Cys)	-	na	-	-	-	-
COR439	*CC2D2A*	c.2848C>T	p.(Arg950*)	c.2848C>T	p.(Arg950*)	na	na	na	na	na	na
COR449	*CC2D2A*	c.4667A>T	p.(Asp1556Val)	c.4844_4847del	p.(Ser1615Leufs*16)	na	na	na	na	na	na
COR481	*CC2D2A*	c.4102C>A	p.(His1368Asn)	c.3596T>C	p.(Ile1199Thr)	na	na	na	na	na	na
COR521	*CC2D2A*	c.879dup	p.(Val294Serfs*5)	c.4258C>A	p.(Gln1420Lys)	-	+	-	-	-	-
COR526	*CC2D2A*	c.4289T>C	p.(Val1430Ala)	c.4774G>T	p.(Glu1592*)	-	-	-	-	na	-
COR555	*CC2D2A*	c.4667A>T	p.(Asp1556Val)	c.4256del	p.(Gly1419Aspfs*9)	-	na	-	-	-	-
COR557	*CC2D2A*	c.3289del	p.(Val1097Phefs*2)	c.4667A>T	p.(Asp1556Val)	-	na	na	-	-	na
COR570	*CC2D2A*	c.2999A>T	p.(Glu1000Val)	c.3084del	p.(Lys1029Argfs*3)	na	na	na	na	na	na
COR576	*CC2D2A*	c.4667A>T	p.(Asp1556Val)	c.3976-2A>G		-	-	-	-	-	-
COR98	*CEP41*	c.423-2A>C		c.423-2A>C		-	+	-	-	+	-
COR297	*CEP104*	c.1485+1G>A		c.1485+1G>A		-	-	-	-	-	-
COR331	*CEP104*	c.375del	p.(Lys126Asnfs*2)	c.375del	p.(Lys126Asnfs*2)	-	na	-	-	na	+
COR391	*CEP120*	c.581T>C	p.(Val194Ala)	c.581T>C	p.(Val194Ala)	-	-	-	-	-	-
COR551	*CEP120*	c.2917C>T	p.(Arg973*)	c.2179G>C	p.(Ala727Pro)	-	-	-	-	-	-
COR03	*CEP290*	c.2086del	p.(Asp696Metfs*6)	c.5668G>T	p.(Gly1890*)	+	+	-	-	-	-
COR04	*CEP290*	c.3811C>T	p.(Arg1271*)	c.5734_5735del	p.(Trp1912Glyfs*4)	+	+	-	-	-	-
COR22	*CEP290*	c.21G>T	p.(Trp7Cys)	c.21G>T	p.(Trp7Cys)	+	+	-	-	-	-

Tab.A3 (continued)											
COR27	*CEP290*	c.4732G>T	p.(Glu1578*)	c.4732G>T	p.(Glu1578*)	-	+	+	-	-	-
COR31	*CEP290*	c.4723A>T	p.(Lys1575*)	c.4393C>T	p.(Arg1465*)	+	+	-	-	-	-
COR51	*CEP290*	c.5668G>T	p.(Gly1890*)	c.5668G>T	p.(Gly1890*)	+	+	-	-	-	-
COR83	*CEP290*	c.5163del	p.(Thr1722Glnfs*2)	c.5163del	p.(Thr1722Glnfs*2)	+	+	-	-	-	-
COR84	*CEP290*	c.4882C>T	p.(Gln1628*)	c.5941G>T	p.(Glu1981*)	na	na	na	na	na	na
COR105	*CEP290*	c.3176del	p.(Ile1059Lysfs*6)	c.3176del	p.(Ile1059Lysfs*6)	+	+	-	na	-	-
COR109	*CEP290*	c.3814C>T	p.(Arg1272*)	c.1683del	p.(Glu562Lysfs*11)	na	+	-	na	-	-
COR125	*CEP290*	c.5668G>T	p.(Gly1890*)	c.5434_5435del	p.(Glu1812Lysfs*5)	+	+	-	-	-	-
COR145	*CEP290*	c.1657_1666del	p.(Lys553Phefs*17)	c.6031C>T	p.(Arg2011*)	-	+	-	-	-	-
COR153	*CEP290*	c.4882C>T	p.(Gln1628*)	c.4882C>T	p.(Gln1628*)	+	+	-	-	-	-
COR165	*CEP290*	c.1823A>G	p.(Lys608Arg)	c.3894dup	p.(Lys1299*)	+	-	-	-	-	-
COR198	*CEP290*	c.5493del	p.(Ala1832Profs*19)	c.7341dup	p.(Leu2448Thrfs*8)	-	+	-	-	-	-
COR221	*CEP290*	c.5709+2T>G		c.2368-1G>A		-	na	-	-	-	-
COR300	*CEP290*	c.5995_5999del	p.(Asp1999Ilefs*23)	c.5995_5999del	p.(Asp1999Ilefs*23)	-	+	-	-	-	-
COR312	*CEP290*	c.5668G>T	p.(Gly1890*)	c.5668G>T	p.(Gly1890*)	-	-	-	-	-	-
COR320	*CEP290*	c.2086del	p.(Asp696Metfs*6)	c.1666del	p.(Ile556Phefs*17)	-	+	-	-	-	-
COR322	*CEP290*	c.4864C>T	p.(Arg1622Cys)	c.4864C>T	p.(Arg1622Cys)	+	+	+	-	+	+
COR333	*CEP290*	c.2306T>C	p.(Ile769Thr)	c.4966G>T	p.(Glu1656*)	na	+	-	-	-	-
COR378	*CEP290*	c.4771C>T	p.(Gln1591*)	c.3573+1G>T		+	+	-	-	-	-
COR379	*CEP290*	c.5668G>T	p.(Gly1890*)	c.5668G>T	p.(Gly1890*)	-	-	+	-	-	-
COR384	*CEP290*	c.2722C>T	p.(Arg908*)	c.7320_7324del	p.(Leu2441Argfs*13)	-	+	+	-	-	-
COR387	*CEP290*	c.6277del	p.(Val2093Serfs*4)	c.6277del	p.(Val2093Serfs*4)	+	-	-	-	-	-
COR390	*CEP290*	c.5668G>T	p.(Gly1890*)	c.5668G>T	p.(Gly1890*)	-	-	-	-	-	-
CR424	*CEP290*	c.4522C>T	p.(Arg1508*)	c.4394G>A	p.(Arg1465Gln)	na	na	na	na	na	na
COR431	*CEP290*	c.1078C>T	p.(Arg360*)	c.6919_6920del	p.(Glu2307Thrfs*4)	na	na	na	na	na	na
COR435	*CEP290*	c.1645C>T	p.(Arg549*)	c.1666del	p.(Ile556Phefs*17)	na	na	na	na	na	na
COR451	*CEP290*	c.5668G>T	p.(Gly1890*)	c.5668G>T	p.(Gly1890*)	-	-	-	na	-	-
COR455	*CEP290*	c.6072C>A	p.(Tyr2024*)	c.6072C>A	p.(Tyr2024*)	-	-	+	-	-	-
COR457	*CEP290*	c.5668G>T	p.(Gly1890*)	c.5668G>T	p.(Gly1890*)	-	+	-	-	-	+
COR525	*CEP290*	c.4882C>T	p.(Gln1628*)	c.6277del	p.(Val2093Serfs*4)	na	na	na	na	na	na
COR541	*CEP290*	c.3894dup	p.(Lys1299*)	c.5668G>T	p.(Gly1890*)	+	+	+	-	-	+
COR574	*CEP290*	c.4763T>G	p.(Leu1588*)	c.1909+2T>A		-	na	na	-	-	-
COR15	*CPLANE1*	c.1819del	p.(Tyr607Thrfs*6)	c.8406_8407del	p.(Phe2803Serfs*14)	na	na	na	na	na	na
COR42	*CPLANE1*	c.3868T>C	p.(Ser1290Pro)	c.7477C>T	p.(Arg2493*)	+	-	-	-	+	-
COR45	*CPLANE1*	c.3551G>A	p.(Arg1184His)	c.4034A>G	p.(Gln1345Arg)	na	na	na	na	+	+

Tab.A3 (continued)											
COR69	*CPLANE1*	c.4168_4177delinsGTTG	p.(Leu1390_Cys1393delinsValGly)	c.1214C>T	p.(Ala405Val)	-	-	-	-	-	-
COR77	*CPLANE1*	c.7429C>T	p.(Gln2477*)	c.3550C>T	p.(Arg1184Cys)	-	-	-	-	+	+
COR88	*CPLANE1*	c.7988_7989del	p.(Gly2663Alafs*40)	c.7988_7989del	p.(Gly2663Alafs*40)	-	-	-	-	-	-
COR102	*CPLANE1*	c.1784T>G	p.(Leu595*)	c.4634G>A	p.(Arg1545His)	-	-	-	-	+	-
COR120	*CPLANE1*	c.8608G>T	p.(Glu2870*)	c.4394_4397dup	p.(Asp1467Argfs*8)	-	-	-	-	-	-
COR126	*CPLANE1*	c.493del	p.(Ile165Tyrfs*17)	c.8608G>T	p.(Glu2870*)	-	-	-	-	-	-
COR134	*CPLANE1*	c.7988_7989del	p.(Gly2663Alafs*40)	c.7988_7989del	p.(Gly2663Alafs*40)	na	na	na	na	na	na
COR137	*CPLANE1*	c.817A>C	p.(Asn273His)	c.493del	p.(Ile165Tyrfs*17)	na	na	na	na	na	na
COR139	*CPLANE1*	c.3091T>C	p.(Ser1031Pro)	c.817A>C	p.(Asn273His)	na	na	na	na	+	na
COR140	*CPLANE1*	c.3998C>T	p.(Pro1333Leu)	c.3998C>T	p.(Pro1333Leu)	na	na	na	na	na	na
COR146	*CPLANE1*	c.3012T>A	p.(Tyr1004*)	c.8406_8407del	p.(Phe2803Serfs*14)	na	na	na	na	na	na
COR148	*CPLANE1*	c.3545del	p.(Asn1182Ilefs*26)	c.8406_8407del	p.(Phe2803Serfs*14)	-	-	-	-	-	-
COR151	*CPLANE1*	c.5733T>G	p.(Tyr1911*)	c.5348C>A	p.(Ala1783Asp)	-	-	-	na	na	na
COR168	*CPLANE1*	c.493del	p.(Ile165Tyrfs*17)	c.4643A>G	p.(Asp1548Gly)	na	na	na	na	+	-
COR172	*CPLANE1*	c.493del	p.(Ile165Tyrfs*17)	c.968C>T	p.(Thr323Met)	-	-	-	-	-	-
COR174	*CPLANE1*	c.7477C>T	p.(Arg2493*)	c.7477C>T	p.(Arg2493*)	+	-	-	-	-	-
COR184	*CPLANE1*	c.8810C>G	p.(Ser2937*)	c.2123_2124del	p.(Glu708Glyfs*7)	-	-	-	na	-	-
COR204	*CPLANE1*	c.8406_8407del	p.(Phe2803Serfs*14)	c.7234-2_7234delAGT		+	+	-	-	-	-
COR210	*CPLANE1*	c.2624C>T	p.(Ser875Phe)	c.5733T>G	p.(Tyr1911*)	-	-	-	-	+	-
COR215	*CPLANE1*	c.7817T>A	p.(Leu2606*)	c.2641C>T	p.(Leu881Phe)	-	-	-	-	-	-
COR246	*CPLANE1*	c.7400+1G>A		c.7400+1G>A		+	+	-	-	na	-
COR315	*CPLANE1*	c.3380C>T	p.(Ser1127Leu)	c.3380C>T	p.(Ser1127Leu)	-	-	-	-	+	-
COR316	*CPLANE1*	c.1784T>G	p.(Leu595*)	c.143G>A	p.(Gly48Glu)	-	-	-	-	-	-
COR348	*CPLANE1*	c.7477C>T	p.(Arg2493*)	c.3857G>A	p.(Arg1286His)	-	+	-	-	+	-
COR360	*CPLANE1*	c.455C>T	p.(Ser152Phe)	c.2334G>A	p.(Trp778*)	+	-	-	-	-	-
COR373	*CPLANE1*	c.3599C>T	p.(Ala1200Val)	c.7817T>A	p.(Leu2606*)	-	-	-	-	+	+
COR385	*CPLANE1*	c.7477C>T	p.(Arg2493*)	c.7477C>T	p.(Arg2493*)	-	-	-	-	-	na
COR452	*CPLANE1*	c.3820A>G	p.(Arg1274Gly)	c.3190C>G	p.(Pro1064Ala)	-	-	-	-	-	na
COR473	*CPLANE1*	c.4634G>A	p.(Arg1545His)	c.4634G>A	p.(Arg1545His)	+	-	-	-	+	-
COR474	*CPLANE1*	c.1784T>G	p.(Leu595*)	c.8884C>T	p.(Arg2962*)	na	na	na	na	+	na
COR486	*CPLANE1*	c.493del	p.(Ile165Tyrfs*17)	c.3577C>T	p.(Arg1193Cys)	na	na	na	na	na	na

Tab.A3 (continued)											
COR494	*CPLANE1*	c.1041_1044dup	p.(Thr349Alafs*27)	c.5348C>A	p.(Ala1783Asp)	-	-	-	-	-	-
COR506	*CPLANE1*	c.8263dup	p.(Thr2755Asnfs*8)	c.[1819del; 7817T>A]	p.[(Tyr607Thrfs*6; Leu2606*)]	na	na	na	na	na	na
COR510	*CPLANE1*	c.1819del	p.(Tyr607Thrfs*6)	c.5348C>A	p.(Ala1783Asp)	-	-	-	-	+	-
COR517	*CPLANE1*	c.2933G>A	p.(Arg978Gln)	c.[1819del; 7817T>A]	p.[(Tyr607Thrfs*6; Leu2606*)]	-	-	-	-	+	-
COR548	*CPLANE1*	c.8263insA	p.(Thr2755Asnfs*8)	c.[1819del; 7817T>A]	p.[(Tyr607Thrfs*6; Leu2606*)]	-	-	-	-	+	+
COR579	*CPLANE1*	c.4634G>A	p.(Arg1545His)	c.4634G>A	p.(Arg1545His)	-	-	-	-	+	-
COR582	*CPLANE1*	c.260T>G	p.(Leu87Arg)	c.[1036G>A; 994A>G]	p.[(Glu346Lys; Met332Val)]	-	-	-	-	-	-
COR24	*CSPP1*	c.432dup	p.(Asn145*)	c.432dup	p.(Asn145*)	-	+	-	-	+	-
COR118	*CSPP1*	c.2320C>T	p.(Arg774*)	c.2953+1G>A		na	na	na	na	na	na
COR171	*CSPP1*	c.2244_2245del	p.(Glu750Glyfs*30)	c.2869delinsTGT	p.(Ala957Cysfs*12)	-	+	-	+	-	-
COR187	*CSPP1*	c.950G>A	p.(Arg317Lys)	c.658C>T	p.(Arg220*)	-	-	-	-	-	-
COR197	*CSPP1*	c.2244_2245del	p.(Glu750Glyfs*30)	c.2244_2245del	p.(Glu750Glyfs*30)	-	+	+	-	-	+
COR418	*CSPP1*	c.1214+1G>A		c.2244_2245del	p.(Glu750Glyfs*30)	-	-	-	-	-	-
COR450	*CSPP1*	c.2506_2509del	p.(Ile836Glyfs*7)	c.2506_2509del	p.(Ile836Glyfs*7)	na	na	-	na	-	+
COR10	*INPP5E*	c.1132C>T	p.(Arg378Cys)	c.1132C>T	p.(Arg378Cys)	-	+	-	-	-	-
COR21	*INPP5E*	c.1132C>T	p.(Arg378Cys)	c.1132C>T	p.(Arg378Cys)	-	+	-	+	-	-
COR64	*INPP5E*	c.1277C>A	p.(Thr426Asn)	c.1277C>A	p.(Thr426Asn)	-	-	-	-	-	-
COR176	*INPP5E*	c.1629C>G	p.(Tyr543*)	c.874C>G	p.(Arg292Gly)	-	+	+	-	-	-
COR199	*INPP5E*	c.907G>A	p.(Val303Met)	c.1753C>T	p.(Arg585Cys)	-	+	+	-	-	-
COR327	*INPP5E*	c.1468G>T	p.(Asp490Tyr)	c.1718A>G	p.(Tyr573Cys)	-	-	-	-	-	-
COR393	*INPP5E*	c.1264A>G	p.(Thr422Ala)	c.907G>A	p.(Val303Met)	-	+	-	-	-	-
COR459	*INPP5E*	c.1064C>T	p.(Thr355Met)	c.1064C>T	p.(Thr355Met)	-	+	-	-	-	-
COR562	*INPP5E*	c.1106_1108dup	p.(Gly369dup)	c.874C>G	p.(Arg292Gly)	-	-	-	-	-	-
COR34	*KIAA0586*	c.428del	p.(Arg143Lysfs*4)	c.2209C>T	p.(Arg737*)	-	-	-	-	-	-
COR133	*KIAA0586*	c.428del	p.(Arg143Lysfs*4)	c.863_864del	p.(Gln288Argfs*7)	na	na	na	na	na	na
COR207	*KIAA0586*	c.428del	p.(Arg143Lysfs*4)	c.1815G>A	p.(Gln605=)	-	-	-	-	-	-
COR230	*KIAA0586*	c.428del	p.(Arg143Lysfs*4)	c.863_864del	p.(Gln288Argfs*7)	-	-	-	-	-	-
COR253	*KIAA0586*	c.428del	p.(Arg143Lysfs*4)	c.1658_1661delinsAAA	p.(Val553Glufs*79)	-	-	-	-	-	-
COR271	*KIAA0586*	c.428del	p.(Arg143Lysfs*4)	c.3040C>T	p.(Gln1014*)	-	-	-	-	-	-

Tab.A3 (continued)											
COR292	*KIAA0586*	c.428del	p.(Arg143Lysfs*4)	c.428del	p.(Arg143Lysfs*4)	na	na	-	-	na	na
COR350	*KIAA0586*	c.428del	p.(Arg143Lysfs*4)	c.1413-1G>C		na	na	na	na	-	-
COR354	*KIAA0586*	c.74del	p.(Lys25Argfs*6)	c.74del	p.(Lys25Argfs*6)	-	-	-	-	-	-
COR404	*KIAA0586*	c.74del	p.(Lys25Argfs*6)	c.3462del	p.(Gly1155Glufs*40)	-	-	-	-	-	-
COR414	*KIAA0586*	c.74del	p.(Lys25Argfs*6)	c.649C>T	p.(Gln217*)	-	-	-	-	-	-
COR467	*KIAA0586*	c.74del	p.(Lys25Argfs*6)	c.1006C>T	p.(Gln336*)	-	-	-	-	-	-
COR496	*KIAA0586*	c.74del	p.(Lys25Argfs*6)	c.74del	p.(Lys25Argfs*6)	na	na	na	na	-	-
COR518	*KIAA0586*	c.74del	p.(Lys25Argfs*6)	c.1006C>T	p.(Gln336*)	-	-	-	-	-	-
COR519	*KIAA0586*	c.74del	p.(Lys25Argfs*6)	c.790_793del	p.(Leu264Valfs*36)	-	-	-	-	-	-
COR251	*KIF7*	c.2335G>T	p.(Glu779*)	c.2335G>T	p.(Glu779*)	-	-	-	-	+	-
COR427	*KIF7*	c.434A>C	p.(Tyr145Ser)	c.434A>C	p.(Tyr145Ser)	+	-	-	-	-	+
COR458	*KIF7*	c.2473G>T	p.(Glu825*)	c.2473G>T	p.(Glu825*)	na	na	-	na	-	-
COR538	*KIF7*	c.62G>A	p.(Arg21Gln)	c.62G>A	p.(Arg21Gln)	-	na	na	-	-	-
COR584	*KIF7*	c.2896_2897del	p.(Ala966Profs*81)	c.2896_2897del	p.(Ala966Profs*81)	-	-	-	-	+	-
COR340	*MKS1*	c.1461-2A>G		c.1461-2A>G		-	+	-	-	-	-
COR341	*MKS1*	c.240G>T	p.(Trp80Cys)	c.1408-34_1408-6del		na	na	na	na	na	na
COR413	*MKS1*	c.1085_1087del	p.(Ser362del)	c.1558+1G>T		-	-	-	-	-	na
COR416	*MKS1*	c.800_801del	p.(Asn267Serfs*37)	c.1476T>G	p.(Cys492Trp)	-	-	-	-	-	-
COR440	*MKS1*	c.1085_1087del	p.(Ser362del)	c.1085_1087del	p.(Ser362del)	na	+	-	-	-	+
COR488	*MKS1*	c.1476T>G	p.(Cys492Trp)	c.370C>T	p.(Arg124*)	na	-	-	na	na	na
COR523	*MKS1*	c.378T>A	p.(Phe126Leu)	c.805T>C	p.(Ser269Pro)	-	-	-	-	-	-
COR534	*MKS1*	c.1115_1117del	p.(Ser372del)	c.1115_1117del	p.(Ser372del)	-	+	-	-	-	-
COR558	*MKS1*	c.[1476T>G;1388G>A]	p.[(Cys492Trp; Arg463Gln)]	c.1600C>T	p.(Arg534*)	-	-	-	na	-	-
COR560	*MKS1*	c.1476T>G	p.(Cys492Trp)	c.1408-34_1408-6del		-	+	-	-	+	-
COR597	*MKS1*	c.1476T>G	p.(Cys492Trp)	c.1024+1G>A		na	na	na	na	na	na
COR406	*NPHP1*	c.84_87del	p.(Ser29Argfs*4)	c.84_87del	p.(Ser29Argfs*4)	na	na	na	na	na	na
COR08	*NPHP4*	c.1804C>T	p.(Gln602*)	c.452+1G>T		+	-	-	-	-	-
COR35	*OFD1*	c.517+4_517+7del				-	-	-			
COR36	*OFD1*	c.92G>T	p.(Gly31Val)			na	na	na	na	na	na
COR211	*OFD1*	c.2315dup	p.(Pro773Thrfs*5)			na	na	na	-	+	+
COR244	*OFD1*	c.2488+5G>T				na	na	-	na	+	-
COR298	*OFD1*	c.2757+1G>A				-	na	na	-	-	-

Tab.A3 (continued)											
COR322	*OFD1*	c.2608_2609ins TCTA	p.(Gln870Leufs*2)			+	+	+	-	+	+
COR432	*OFD1*	c.2725C>T	p.(Arg909*)			-	+	-	-	-	-
COR520	*OFD1*	c.710dup	p.(Tyr238Valfs*2)			-	-	-	-	-	+
COR16	*RPGRIP1L*	c.1975del	p.(Ser659Leufs*40)	c.1843A>C	p.(Thr615Pro)	+	+	+	-	-	-
COR46	*RPGRIP1L*	c.2268_2269del	p.(Thr757Ilefs*4)	c.2268_2269del	p.(Thr757Ilefs*4)	+	-	-	-	+	-
COR50	*RPGRIP1L*	c.1843A>C	p.(Thr615Pro)	c.1843A>C	p.(Thr615Pro)	+	-	-	-	+	-
COR73	*RPGRIP1L*	c.2451C>A	p.(Tyr817*)	c.1843A>C	p.(Thr615Pro)	+	-	-	-	-	-
COR123	*RPGRIP1L*	c.1829A>C	p.(His610Pro)	c.1829A>C	p.(His610Pro)	na	na	na	na	na	na
COR129	*RPGRIP1L*	c.986_987del	p.(Lys329Thrfs*9)	c.881A>G	p.(Glu294Gly)	na	na	na	na	na	na
COR136	*RPGRIP1L*	c.1649A>G	p.(Gln550Arg)	c.1649A>G	p.(Gln550Arg)	-	na	na	-	-	-
COR186	*RPGRIP1L*	c.1649A>G	p.(Gln550Arg)	c.1649A>G	p.(Gln550Arg)	-	na	na	-	-	-
COR201	*RPGRIP1L*	c.2050C>T	p.(Gln684*)	c.2304+1G>T		+	-	-	-	+	-
COR405	*RPGRIP1L*	c.287G>A	p.(Gly96Asp)	c.3548C>G	p.(Ala1183Gly)	-	-	-	-	-	-
COR483	*RPGRIP1L*	c.1804C>T	p.(Arg602*)	c.1804C>T	p.(Arg602*)	+	+	+	-	+	+
COR556	*RPGRIP1L*	c.1843A>C	p.(Thr615Pro)	c.1843A>C	p.(Thr615Pro)	+	na	na	na	na	na
COR369	*SUFU*	c.1217T>C	p.(Ile406Thr)	c.1217T>C	p.(Ile406Thr)	-	-	-	-	+	-
COR29	*TCTN1*	c.262G>A	p.(Asp88Asn)	c.1775_1778del	p.(Val592Aspfs*106)	-	-	-	-	-	-
COR160	*TCTN1*	c.898C>T	p.(Arg300*)	c.290G>T	p.(Cys97Phe)	na	+	-	na	-	-
COR274	*TCTN2*	c.1235-1G>A		c.1235-1G>A		-	-	-	-	+	-
COR108	*TCTN3*	c.940G>A	p.(Gly314Arg)	c.940G>A	p.(Gly314Arg)	na	na	na	na	na	na
COR91	*TMEM17*	c.306C>A	p.(Asn102Lys)	c.306C>A	p.(Asn102Lys)	-	-	-	-	+	+
COR09	*TMEM67*	c.1769T>C	p.(Phe590Ser)	c.1961-2A>C		-	-	-	+	-	-
COR20	*TMEM67*	c.1769T>C	p.(Phe590Ser)	c.579_580del	p.(Gly195Ilefs*13)	-	-	-	+	-	-
COR32	*TMEM67*	c.1115C>A	p.(Thr372Lys)	c.2345A>G	p.(His782Arg)	+	+	+	+	-	-
COR47	*TMEM67*	c.370G>A	p.(Glu124Lys)	c.1073C>T	p.(Pro358Leu)	-	+	-	+	-	-
COR71	*TMEM67*	c.389C>G	p.(Pro130Arg)	c.675G>A	p.(Trp225*)	+	-	+	+	-	-
COR94	*TMEM67*	c.2182A>G	p.(Ser728Gly)	c.1319G>A	p.(Arg440Gln)	+	+	+	+	-	-
COR106	*TMEM67*	c.2439+5G>C		c.2439+5G>C		na	na	na	na	na	na
COR110	*TMEM67*	c.651+2T>G		c.1634G>A	p.(Gly545Glu)	na	na	na	na	na	na
COR113	*TMEM67*	c.1706G>A	p.(Gly569Asp)	c.1860+1G>A		-	+	+	-	-	-
COR143	*TMEM67*	c.1285C>T	p.(Gln429*)	c.1847C>T	p.(Ala616Val)	-	+	+	-	-	-
COR190	*TMEM67*	c.312+5G>A		c.2498T>C	p.(Ile833Thr)	+	+	-	+	-	-
COR212	*TMEM67*	c.2216T>G	p.(Leu739Arg)	c.1115C>A	p.(Thr372Lys)	+	+	+	+	-	-
COR240	*TMEM67*	c.1769T>C	p.(Phe590Ser)	c.1079_1080del	p.(Thr360Argfs*19)	-	-	-	+	-	-
COR254	*TMEM67*	c.903C>G	p.(Asp301Glu)	c.1538A>G	p.(Tyr513Cys)	na	-	-	na	-	-

Tab.A3 (continued)											
COR256	*TMEM67*	c.515G>A	p.(Arg172Gln)	c.769A>G	p.(Met257Val)	-	na	na	+	na	na
COR265	*TMEM67*	c.270T>G	p.(Asn90Lys)	c.755T>C	p.(Met252Thr)	-	+	+	+	+	-
COR266	*TMEM67*	c.2498T>C	p.(Ile833Thr)	c.300C>A	p.(Cys100*)	-	-	+	+	-	-
COR289	*TMEM67*	c.652-9T>A		c.652-9T>A		na	na	na	na	na	na
COR291	*TMEM67*	c.1607T>A	p.(Val536Asp)	c.619C>T	p.(Arg207Cys)	-	-	-	-	-	-
COR343	*TMEM67*	c.2086C>T	p.(Leu696Phe)	c.2086C>T	p.(Leu696Phe)	-	+	-	-	-	-
COR345	*TMEM67*	c.725A>G	p.(Asn242Ser)	c.224G>A	p.(Gly75Glu)	-	+	-	+	-	-
COR446	*TMEM67*	c.1843T>C	p.(Cys615Arg)	c.2907+1G>A		+	+	na	+	-	-
COR490	*TMEM67*	c.226A>G	p.(Thr76Ala)	c.226A>G	p.(Thr76Ala)	-	na	+	-	-	-
COR501	*TMEM67*	c.1769T>C	p.(Phe590Ser)	c.755T>C	p.(Met252Thr)	-	na	+	+	-	-
COR533	*TMEM67*	c.1843T>C	p.(Cys615Arg)	c.579del	p.(Gly195Aspfs*27)	+	-	+	-	-	-
COR542	*TMEM67*	c.1975C>T	p.(Arg659*)	c.1843T>C	p.(Cys615Arg)	+	+	-	na	-	-
COR544	*TMEM67*	c.1927C>T	p.(Arg643*)	c.2086C>T	p.(Leu696Phe)	-	+	-	+	-	-
COR575	*TMEM67*	c.1321C>T	p.(Arg441Cys)	c.515G>A	p.(Arg172Gln)	na	na	na	na	na	na
COR447	*TMEM138*	c.380C>T	p.(Ala127Val)	c.380C>T	p.(Ala127Val)	na	na	na	na	na	na
COR00	*TMEM216*	c.218G>T	p.(Arg73Leu)	c.218G>T	p.(Arg73Leu)	+	-	-	-	-	-
COR76	*TMEM216*	c.35G>T	p.(Gly12Val)	c.35G>T	p.(Gly12Val)	-	-	-	-	-	-
COR114	*TMEM216*	c.218G>T	p.(Arg73Leu)	c.218G>T	p.(Arg73Leu)	-	-	+	na	+	-
COR284	*TMEM216*	c.35G>T	p.(Gly12Val)	c.35G>T	p.(Gly12Val)	na	na	na	na	na	na
COR287	*TMEM216*	c.35G>T	p.(Gly12Val)	c.35G>T	p.(Gly12Val)	-	-	-	-	+	-
COR477	*TMEM231*	c.269A>C	p.(Asn90Thr)	c.269A>C	p.(Asn90Thr)	-	+	-	-	-	-
COR05	*TMEM237*	c.52C>T	p.(Arg18*)	c.553+1G>T		-	na	+	+	-	-
COR101	*TMEM237*	c.1066dup	p.(Gln356Profs*24)	c.1066dup	p.(Gln356Profs*24)	-	na	+	-	-	-
COR454	*TMEM237*	c.175C>T	p.(Arg59*)	c.175C>T	p.(Arg59*)	na	na	na	na	na	na
COR559	*TMEM237*	c.1066dup	p.(Gln356Profs*24)	c.1074G>T	p.(Trp358Cys)	na	na	na	na	-	-
COR225	*TTC21B*	c.3340C>T	p.(Gln1114*)	c.985G>A	p.(Glu329Lys)	+	-	-	+	na	-
COR464	*TTC21B*	c.626C>T	p.(Pro209Leu)	c.626C>T	p.(Pro209Leu)	-	+	-	na	-	-

Tab.A4. List of cases diagnosed trough the combined use of Next-generation Sequencing and High Density-Comparative Genomic Hybridization microarray analyses

Family_ID	Gene	Allele 1		Allele 2 (containing CNV)			
		cDNA	protein	CNV	Genomic coordinates (bp)(GRCh37/hg19)	Size (KB)	exons included
COR127	*AHI1*	c.1500C>G	p.(Tyr500*)	DEL 6q23.3	chr6:135,751,067-135,756,077	5	exons 14-16
COR01	*CEP290*	c.5493del	p.(Ala1832Profs*19)	DEL 12q21.32	chr12:88,433,351-88,468,144	35	exons 42-54
COR508	*CPLANE1*	c.3676C>T	p.(Arg1226*)	DUP 5p13.2	chr5:37117993-37206464	88,47	exons 19-49
COR130	*KIAA0586*	c.428del	p.(Arg143Lysfs*4)	DEL 14q23.1	chr14:58,910,526-58,917,507	7	exons 8-10
COR93	*KIAA0586*	c.428del	p.(Arg143Lysfs*4)	DEL 14q23.1	chr14:58,910,526-58,917,507	7	exons 8-10

Positive control					
Family_ID	Gene	Allele 1= Allele2 (HOMOZYGOUS GENOTYPE)			
		CNV	Genomic coordinates (bp)(GRCh37/hg19)	Size (KB)	exons included
COR17	*NPHP1*	DEL 2q13	chr2:110,873,992-110,969,198	95	whole gene

This sample (previously identified through real-time PCR) has been used as a positive control to assess the validity of High Density-Comparative Genomic Hybridization microarray method

Tab.A5. List of genomic variants identified in pontocerebellar hypoplasia probands molecularly confirmed after next-generation sequencing anaysis

Family_ID	Gene	Allele 1		Allele 2	
		cDNA	protein	cDNA	protein
BR1	*CASK*[m]	c.1852A>G	p.(Arg618Gly)		
CCM031	*CASK*	c.2206_2207insGTGTTTT CCTAAGACTAGTG	p.(T736Sfs*9)		
CCM041	*CASK*	dup exon 2			
CCM043	*CASK*	c.316C>T	p.(Arg106*)		
CCM086	*CASK*	c.1610del	p.(Arg537Glnfs*81)		
CCM115	*CASK*	c.996_997insT	p.(Glu333*)		
CCM157	CASK	c.372_373del	p.(Gln124Hisfs*10)		
CCM195	*CASK*[m]	c.82C>T[#]	p.(Arg28*)[#]		
CCM239	*CASK*	c.1501dup	p.(Met501Asnfs*9)		
CCM249	*CASK*	del exon 6			
CCM333	*CASK*	c.2302+1G>A			
CCM395	*CASK*[m]	del exons 9-10			
CCM411	*CASK*	c.2446G>T	p.(Glu816*)		
CCM433	*CASK*	del exon 1			
CCM457	*CASK*	c.1970G>A	p.(Trp657*)		
CCM509	*CASK*	del exons 4-5			
CCM510	*CASK*[m]	c.2174_2176del	p.(Glu725del)		
CCM515	*CASK*	c.1499_1500del	p.(Pro500Hisfs*9)		
CCM525	*CASK*	c.2221+1delGinsAT	p.G741Dfs*1		
CCM529	*CASK*	del exon 1			
CCM530	*CASK*	del exon 1			
CCM531	CASK	c.846C>G	p.(Tyr282*)		
CCM532	*CASK*	c.1015+1G>A			
CCM533	*CASK*	c.1609C>T	p.(Arg537*)		
CCM568	*CASK*	del exons 23-27			
CCM596	*CASK*	del exon 3			

CCM598	*CASK*	c.149C>A	p.(Ser50*)		
BR2	*EXOSC3*	c.395A>C	p.(Asp132Ala)	c.395A>C	p.(Asp132Ala)
CCM220	*EXOSC3*	c.545A>T	p.(Asp182Val)	c.395A>C	p.(Asp132Ala)
CCM248	*EXOSC3*	c.92G>C	p.(Gly31Ala)	c.92G>C	p.(Gly31Ala)
CCM422	*EXOSC3*	c.294_303del	p.(Val99Trpfs*11)	c.395A>C	p.(Asp132Ala)
CCM565	*EXOSC3*	c.395A>C	p.(Asp132Ala)	c.395A>C	p.(Asp132Ala)
CCM540	*PMM2*	c.368G>A	p.(Arg123Gln)	c.640G>A	p.(Gly214Ser)
CCM373	*RARS2*	c.1A>G	p.M1?	c.1327T>C	p.(Ser443Pro)
CCM336	*TOE1*	c.658G>A	p.(Glu220Lys)	c.658G>A	p.(Glu220Lys)
CCM216	*TSEN54*	c.919G>T	p.(Ala307Ser)	c.919G>T	p.(Ala307Ser)
CCM276	*TSEN54*	c.919G>T	p.(Ala307Ser)	c.919G>T	p.(Ala307Ser)
CCM325	*TSEN54*	c.919G>T	p.(Ala307Ser)	c.919G>T	p.(Ala307Ser)
CCM419	*TSEN54*	c.919G>T	p.(Ala307Ser)	c.919G>T	p.(Ala307Ser)
CCM430	*TSEN54*	c.919G>T	p.(Ala307Ser)	c.919G>T	p.(Ala307Ser)
CCM495	*TSEN54*	c.919G>T	p.(Ala307Ser)	c.919G>T	p.(Ala307Ser)
CCM516	*TSEN54*	c.919G>T	p.(Ala307Ser)	c.919G>T	p.(Ala307Ser)
CCM517	*TSEN54*	c.919G>T	p.(Ala307Ser)	c.919G>T	p.(Ala307Ser)
CCM543	*TSEN54*	c.919G>T	p.(Ala307Ser)	c.919G>T	p.(Ala307Ser)
CCM549	*TSEN54*	c.919G>T	p.(Ala307Ser)	c.919G>T	p.(Ala307Ser)
CCM409	*VLDLR*	c.1256G>A	p.(Cys419Tyr)	c.1256G>A	p.(Cys419Tyr)

[m]: male proband; [#]: variant identified in heterozygous state

Tab.A6. Clinical and genetic findings of the 28 patients mutated in tubulin genes

Patient	Genetic findings	Gender Age last exam	Development	Neurological examination	Intellectual disability	Congenital microcephaly	Neuro Ophthalmological findings	Epilepsy	Extra-cerebral findings
TUBA1A									
P89815	p.(R2S) *de novo*	F 5 mo	Delayed, Partial head control	Poor mimic and spontaneous movements	Severe	+	Nystagmus, CVI	Drug resistant focal seizures	Mild facial dysmorphisms
P113708 II-1 (proband)	p.(S54N)	F 22 y	Delayed	Spastic diparesis, ataxia	Mild (FIQ= 51)	+	Strabismus, LOH	-	-
P113708 II-2 (sibling)		F 22 y	Delayed	Spastic diparesis, ataxia	Mild (FIQ= 53)	+	Strabismus	-	Right lumbar scoliosis
P113708 I-3 (father)		M 52 y	Delayed	Spastic diparesis, ataxia	Mild (FIQ= 67)	+	Strabismus	-	Obesity, scoliosis
P78411	p.(G59S) *de novo*	M 4 y	Mildly delayed: trunk control at 7 mo	Mild asymmetry of spontaneous arm movem. (R<L)	Mild (GQ = 65)	-	Mild eyelid asymmetry (L < R); deficit of elevation in adduction (L)	-	-

Tab.A6 (continued)

Patient	Genetic findings	Gender Age last exam	Development	Neurological examination	Intellectual disability	Congenital microcephaly	Neuro Ophthalmological findings	Epilepsy	Extra-cerebral findings
TUB01	p.(V118L) *de novo*	M 2.5 y	Delayed	Spastic tetraparesis	Severe	+	-	Focal seizures	-
P34016	p.(R123H) *de novo*	M 18 mo	Mild delayed	Normal	Mild (FIQ= 67)	+	-	West syndrome	-
P46814 II-1 (proband)	p.(T150I) *de novo*	F 20 mo	Delayed: Sitting 12 mo	Diffuse hypotonia, Dystonia-dyskinesia	Severe, No expressive language	+	Strabismus, Nystagmus	-	Mild facial dysmorphisms
P46814 II-2 (identical twin sister)		F 20 mo	Delayed: Sitting 12 mo	Diffuse Hypotonia	Severe,no expressive language	+	Strabismus, Nystagmus	-	Mild facial dysmorphisms
TUB06	p.(R214H)*	F 3 y	Delayed: not able to sit or stand	Diffuse hypotonia	Severe	+	OH, CVI	West syndr, drug-resistant TC seizures	-
TUB07	p.(R264C)*	M 3.5 y	Delayed	Spastic tetraparesis	Moderate	+	-	-	-
P76111	p.(A387V) *de novo*	F 5 y	Delayed: walking unaided at 30 mo	Clumsiness, mild gait ataxia	Severe: poor skills/social interaction, No expressive language	+	Alternating strabismus	-	Mild facial dysmorphisms

Tab.A6 (continued)

Patient	Genetic findings	Gender Age last exam	Development	Neurological examination	Intellectual disability	Congenital microcephaly	Neuro Ophthalmological findings	Epilepsy	Extra-cerebral findings
21807	p.(R390H) *de novo*	M 3 y	Severely delay: not able to sit or stand	Profound motor delay	Severe: Language absent	-	Nystagmus, CVI	Myoclonic seizures	Facial dysmorphisms
17656	p.(R390H)*	M 11 y	Delayed	Spastic tetraparesis	Severe: No expressive language, Poor social interaction	+	Ptosis, strabismus, nystagmus	Focal seizures responsive to LEV	Facial dysmorphisms
TUBB2B									
P38408	p.(G140A) *de novo*	F 8 y	Delayed	Spastic tetraparesis	Severe: language absent, no Eye contact, poor social interaction	+	R ptosis, strabismus	Focal complex Seizures partially responsive to VPA and LTG (5 mo)	-
17897	p.(I210T) *de novo*	M 5 y	Delayed	Normal	NA	+	-	Focal seizures since birth, responsive to Treatment	Mild facial dysmorphisms

Tab.A6 (continued)

Patient	Genetic findings	Gender Age last exam	Development	Neurological examination	Intellectual disability	Congenital microcephaly	Neuro Ophthalmological findings	Epilepsy	Extra-cerebral findings
18912	p.(L228P) *de novo*	F 9 mo	Severely delayed: no sitting, no roll over	Hypotonia	NA	+	OH	+	Mild facial dysmorphisms
P58315	p.(D327G) *de novo*	M 15 days	NA	Normal	NA	+	-	-	-
P76712	p.(C354R) *de novo*	M 5 y	Delayed	Spastic tetraparesis (R>L)	Severe (GQ = 28)	+	-	Spasms	Cyclic vomiting
P78511#	p.(L361_ K362delinsHLQ) *de novo*	35 y	Severely delayed	Spastic tetraparesis	Severe: no expressive language, poor social interaction, self-harm	+ With deflection of head's growth curve	OH, OA (L>R)	West syndrome (7 mo); focal complex seizures responsive to treatment (12 mo)	Severe thoraco-lumbar scoliosis
14382	p.(R380C)**	M 7 y	Severely delayed: roll over at 2 y	Diffuse hypotonia	Severe	+	Mild ptosis, strabismus, OA, blindness	+	Facial dysmorphisms

Tab.A6 (continued)

Patient	Genetic findings	Gender Age last exam	Development	Neurological examination	Intellectual disability	Congenital microcephaly	Neuro Ophthalmological findings	Epilepsy	Extra-cerebral findings
P216	p.(E421K)*	M 3.5 y	Delayed	Left side spastic paresis	Mild	+	Ptosis	Focal seizures resp to treatment (LEV)	-
TUBB3									
P62715	p.(T238A) *de novo*	F 7 y	Delayed	Pyramidal signs (L>R)	Borderline	-	-	-	-
P7615	p.(E288K) *de novo*	F 2.5 y	Delayed: Sitting 12 mo; First words 18 mo	Diffuse hypotonia walk with aid, ataxia	Mild	- With deflection of head's growth curve	OMA	-	Right sensorineural deafness
P105814	p.(E288K) *de novo*	M 2 y	Delayed: Sitting 15 mo; bubbling 22 mo	Diffuse Hypotonia	Moderate (GQ < 50)	-	Strabismus, nystagmus, depigmented fundus oculi	-	-
P49016	p.(Q292E) *de novo*	M 8 m	Delayed	Axial hypotonia, distal hypertonia	NA	-	NA	-	-

Tab.A6 (continued)

Patient	Genetic findings	Gender Age last exam	Development	Neurological examination	Intellectual disability	Congenital microcephaly	Neuro Ophthalmological findings	Epilepsy	Extra-cerebral findings
TUB03	p.(R380C) *de novo*	F 23 mo	Delayed	Diffuse hypotonia, Dystonia	Moderate (FIQ = 50)	+	-	-	-
P17816	p.(E410K) *de novo*	F 13 mo	Delayed Trunk control, Not walking	Facial diplegia	Moderate (QG < 50)	-	Ptosis (R>L), strabismus (R>L), vertical nystagmus	-	Facial dysmorphisms

CVI: central visual impairment; F: female; FIQ: full intelligence quotient; GQ: general quotient; L: left; LEV: levetiracetam; LTG: lamotrigine; M: male; mo: months; NA: not available; OA: optic atrophy; OH: optic nerve hypoplasia; OMA: oculomotor apraxia; R: right; TC: tonic-clonic; *TUBA1A*: Tubulin α-1A; *TUBB2B*: Tubulin β-2B; *TUBB3*: Tubulin β-3; y: years; VPA: valproic acid; +: present; -: absent. *Parents not available; **Only mother tested (wild type)

Tab.A7. Neuroimaging findings of the 28 patients mutated in tubulin genes

Patient Gender/ Age	Cortical cerebellar dysplasia	Vermis	Ventral brainstem cleft	Pons	MCP	P-M junction	Mesencephalon	IV ventricle	Corpus callosum	Basal ganglia	MCD and other defects
TUBA1A											
P89815 F/5 mo	Malorientation L hemi	Hypoplastic	-	-	-	-	-	Mildly enlarged	Thin, partial agenesis	Absent/thin ALIC	PMG-multi
P113708 II-1 F/22 y	Malorientation Superior R hemi	Dysplastic	-	-	-	-	-	-	Thin	Absent/thin ALIC-rounded thalami	-
P113708 II-2 F/22 y	Malorientation superior R hemi	Dysplastic	-	-	-	-	-	-	Thin	Absent/thin ALIC - rounded thalami	Perisylvian-PMG
P113708 I-3 M/52 y	Malorientation superior R hemi	Dysplastic	-	-	-	-	-	-	Thin	Absent/thin ALIC - rounded thalami	-
P34016 M/18 mo	Malorientation posterior L hemi	-	-	Asymmetrical		Thick R	- Asymmetrical	Mildly enlarged	Thin	Absent/thin ALIC - rounded thalami	-

Tab.A7 (continued)

Patient Gender/ Age	Cortical cerebellar dysplasia	Vermis	Ventral brainstem cleft	Pons	MCP	P-M junction	Mesencephalon	IV ventricle	Corpus callosum	Basal ganglia	MCD and other defects
P46814 II-1 F/20 mo	Malorientation posterior R+L hemi	Hypoplastic	Yes	Hypoplastic asymmetrical	Short	-	-	Mildly enlarged	Thin	Absent/thin ALIC	Perisylvian-PMG
P46814 II-2 F/20 mo	Malorientation posterior R+L hemi	Hypoplastic	Yes	Hypoplastic asymmetrical	Short	-	-	Mildly enlarged	Thin	Absent/thin ALIC	Perisylvian-PMG
TUB06 F/3 y	Malorientation superior R hemi	Mildly rotated	Yes	Hypoplastic asymmetrical	Short	Thick	-	Enlarged	Thin, partial agenesis	Absent/thin ALIC - rounded thalami	-
21807 M/5 y	Malorientation postero-superior R+L hemi	Dysplastic rotated	Yes-small	Hypoplastic asymmetrical	Thick l	-	Asymmetrical	Enlarged	Partial agenesis	Absent/thin ALIC -rounded thalami	Perisylvian-PMG
17656 M/11 y	Malorientation superior R hemi	Dysplastic	Yes	Hypoplastic asymmetrical	Thick l	Narrow	Asymmetrical	Mildly enlarged	Partial agenesis	Absent/thin ALIC- rounded thalami	-
P78411 M/4 y	-	-	-	Regular	-	-	-	-	Irregular shape	Thalamic asymmetry	-

Tab.A7 (continued)

Patient Gender/ Age	Cortical cerebellar dysplasia	Vermis	Ventral brainstem cleft	Pons	MCP	P-M junction	Mesencephalon	IV ventricle	Corpus callosum	Basal ganglia	MCD and other defects
TUB01 M/2.5 y	-	Hypoplastic rotated	-	Asymmetrical	-	-	-	-	Agenesis	Absent/thin ALIC - rounded thalami	simp_Gyr_occipital
TUB07 M/3.5 y	-	-	-	Regular	-	-	-	-	Thin	Absent/thin ALIC - rounded thalami	Perisylvian-PMG+Pachy
P76111 F/5 y	-	Hypoplastic rotated	Yes-small	Hypoplastic	Short	Narrow	-	Mildly enlarged	Thin	Absent/thin ALIC	-
TUBB2B											
P38408	Malorientation posterior R hemi	Hypoplastic	-	-	-	Narrow	Thick	-	Agenesis	Absent/thin ALIC - rounded thalami	Generalized PMG+ SCH, L 3rd cn agenesis
P58315 M/15 d	Malorientation Superior R hemi	Dysplastic rotated	-	Hypoplastic	-	-	-	Enlarged	Dysgenesis	Absent/thin ALIC rounded Thalami	Perisylvian-PMG

Tab.A7 (continued)

Patient Gender/ Age	Cortical cerebellar dysplasia	Vermis	Ventral brainstem cleft	Pons	MCP	P-M junction	Mesencephalon	IV ventricle	Corpus callosum	Basal ganglia	MCD and other defects
P78511 F/35 y	Malorientation superior R hemi	Hypoplastic rotated	-	-	-	-	-	Mildly enlarged	-	Absent/thin ALIC	simp_Gyr, periventricular and subcortical heterotopia, small temporal lobes
P216 M/3.5 y	Malorientation superior R hemi	-	-	Hypoplastic asymmetrical	Thick L	-	-	Mildly enlarged	Thin	Absent/thin ALIC - rounded thalami	-
17897 M/5 y	-	Dysplastic rotated	-	Mildly hypoplastic	-	Shallow interped. Fossa	-	Mildly enlarged	Partial agenesis	Absent/thin ALIC - rounded thalami	Generalized PMG
18912 F/9 mo	-	Hypoplastic	-	Hypoplastic asymmetrical	-	Thick	-	Mildly enlarged	Agenesis	Absent/thin ALIC - rounded thalami	simp_Gyr_occipital
P76712 M/5 y	-	-	-	Short, thin, posterior cap	-	-	-	Enlarged	Irregular shape	Absent/thin ALIC - rounded thalami	Generalized PMG+SCH

Tab.A7 (continued)

Patient Gender/ Age	Cortical cerebellar dysplasia	Vermis	Ventral brainstem cleft	Pons	MCP	P-M junction	Mesencephalon	IV ventricle	Corpus callosum	Basal ganglia	MCD and other defects
14382 M/7 y	-	Hypoplastic rotated	-	Hypoplastic asymmetrical	-	-	Asymmetrical	Enlarged	Agenesis	Absent/thin ALIC - rounded thalami	Perisylvian-PMG, hypoplasia optic nerves and chiasm
TUBB3											
P62715 F/7 y	Malorientation R hemi	-	Yes	Hypoplastic	Thick L	-	-	Mildly enlarged	Dysgenesis	Absent/thin ALIC - rounded thalami	-
P62715 F/7 y	Malorientation superior R hemi	-	-	Asymmetrical	Thick L	-	-	Mildly enlarged	Thin	Absent/thin ALIC - rounded thalami	-
P62715 F/7 y	Malorientation R hemi	Hypoplastic rotated	Yes	Hypoplastic	Thick L	-	-	Enlarged	Short	Absent/thin ALIC - rounded thalami	-
P62715 F/7 y	Malorientation medial R hemi	Hypoplastic	Yes-small	Hypoplastic asymmetrical	-	-	-	-	Dysgenesis	Absent/thin ALIC - rounded thalami	-

Tab.A7 (continued)

Patient Gender/ Age	Cortical cerebellar dysplasia	Vermis	Ventral brainstem cleft	Pons	MCP	P-M junction	Mesencephalon	IV ventricle	Corpus callosum	Basal ganglia	MCD and other defects
P62715 F/7 y	-	Hypoplastic	-	Hypoplastic asymmetrical	-	-	-	-	Thin	Absent/thin ALIC - rounded thalami	-
P62715 F/7 y	-	-	-	-	-	Narrow	-	-	Thin	-	Bilateral 3rd cn agenesis; thin R 7th cn; doubt agenesis/hypoplasia of L 7th cn; no recognizable 4th cn; agenesis of olfactory bulbs and L olfactory sulcus

-: no abnormalities; ALIC: anterior limb internal capsule; cn: cranial nerve; F: female; hemi: hemisphere; L: left; M: male; MCD: malformations of cortical development; MCP: middle cerebellar peduncles; mo: months; y: years; P-M: junction ponto-mesencephalic junction; Pachy: pachygyria; PMG:-multi multifocal polymicrogyria; R: right; Simp_gyr_occipital: simplified gyral pattern occipital with focal polymicrogyria; SCH: schizencephaly; Simp_Gyr simplified: simplified gyral pattern with focal polymicrogyria

Tab.A8. Clinical and genetic data of the 15 patients mutated in tubulin genes

Patient	Genetic findings	Gender	Age at MR (years)	Age at last follow-up (years)	Microcephaly	Developmental delay	Motor functions	Epilepsy	Ocular findings
1	*TUBA1A*	m	0.1	2.5	Yes	Moderate	Bilateral spasticity	Focal seizures	No
2	*TUBA1A*	m	0.6	3.5	Yes	Moderate	Bilateral spasticity	No	No
3	*TUBA1A*	f	0.8	3	Yes	Moderate	Diffuse hypotonia	West syndrome, generalised seizures	ONH, visual impairment, nystagmus
4	*TUBA1A*	f	0.8	1.6	Yes	Severe	Diffuse hypotonia, dystonia-dyskinesia	No	Strabismus, nystagmus
5	*TUBA1A*	m	1.0	3.5	No	Mild	Mild impairment	No	Strabismus
6	*TUBA1A*	f	1.3	1.6	Yes	Severe	Diffuse hypotonia	No	Strabismus, nystagmus
7	*TUBA1A*	f	5.0	8.5	Yes	Severe	Clumsiness, mild gait ataxia	No	Strabismus
8	*TUBA1A*	f	11.5	11.6	NA	Severe	Clumsiness, gait ataxia	West syndrome, focal complex seizures	Strabismus, nystagmus, left ptosis
9	*TUBB2B*	m	1.1	3.5	Yes	Moderate	Unilateral spasticity (left)	Focal seizures	Ptosis
10	*TUBB2B*	m	4.5	4.9	Yes	Moderate	Bilateral spasticity	Spasms	No
11	*TUBB2B*	f	8.3	12.9	Yes	Severe	Bilateral spasticity	Focal complex seizures	Strabismus, right ptosis
12	*TUBB2B*	f	31.8	30.7	Yes	Severe	Bilateral spasticity	West syndrome, focal complex seizures	ONH, OA, strabismus, nystagmus
13	*TUBB3*	f	1.1	1.1	No	Moderate	Facial diplegia	No	Bilateral ptosis, strabismus, nistagmus paralysis of the 3rd, 4th, 7th Bilaterally
14	*TUBB3*	m	1.3	1.2	No	Moderate	Diffuse hypotonia	No	Strabismus, nystagmus, OA
15	*TUBB3*	f	2.0	4.5	Yes	Moderate	Diffuse hypotonia, dystonia	No	No

F: female; m: male; NA: not available; OA: optic atrophy; ONH: optic nerve hypoplasia

Tab.A9. Infra-tentorial MRI findings of the 15 patients mutated in tubulin genes

Patient	Brainstem symmetry	Brainstem cleft	Pons appearance midsagittal planes	MCP	P-M junction	Mesencephalon	Cranial nerves	IV ventricle	Vermis	Cerebellar cortex
1	Asymmetric pons (l > r)	No	Short and small	Regular	Regular	Regular. Thick tectum		Regular	Hypoplastic	Regular
2	No asymmetry	No	Regular	Regular	Regular	Regular		Regular	Regular	Regular
3	Asymmetric brainstem (r < l)	Anterior cleft in the medulla	Short and small	Short	Thick	Regular, Thick tectum		Dilated	Moderate vermis rotation	Malorientation of cerebellar folia (superior r hemisphere)
4	Asymmetric Brainstem (r > l in the medulla; l > r in the pons)	Anterior cleft in the medulla and pons	Short and small	Short	Regular	Asymmetric		Dilated	Hypoplastic and rotated	Cerebellar cortical dysplasia
5	Mild asymmetric Brainstem (r > l)	No	Regular	Regular	Regular	Regular		Regular	Regular	Regular
6	Asymmetric brainstem (r > l in the medulla; l > r in the pons)	Anterior cleft in the medulla and pons	Short and small	Short	Regular	Asymmetric		Mildly dilated	Hypoplastic and rotated	Cerebellar cortical dysplasia
7	No asymmetry	Small pontine cleft	Short and small	Short	Narrow	Regular		Mildly dilated	Hypoplastic and rotated	Maloriented hemispheres. No dysplasia
8	Asymmetric brainstem (r > l)	No	Short and small	Short	Narrow	Asymmetric		Regular	Hypoplastic	Malorientation of folia (r and l hemisphere)
9	Asymmetric pons (l >r)	No	Short and small	Thick left MCP	Regular	Regular		Mildly dilated	Regular	Malorientation of folia (superior r hemisphere)
10	Asymmetric Brainstem (r > l)	No	Short and thin pons. Posterior right "cap"	Regular	Regular	Regular		Dilated	Regular	Maloriented hemispheres. No dysplasia

Tab.A9 (continued)

Patient	Brainstem symmetry	Brainstem cleft	Pons appearance midsagittal planes	MCP	P-M junction	Mesencephalon	Cranial nerves	IV ventricle	Vermis	Cerebellar cortex
11	Mild asymmetric brainstem (r > l in the medulla; l > r in the pons)	no	Regular	Regular	Narrow	Thick	Thin right III nerve	Regular	Hypoplastic	Malorientation of folia (superior hemispheres r > l)
12	Mild asymmetric Brainstem (r > l)	No	Regular	Regular	Regular	Regular		Mildly dilated	Hypoplastic and rotated	Malorientation of folia (superior r hemisphere)
13	No asymmetry	No	Regular	Regular	Narrow	Regular	Agenesis of III pair of nerves. Agenesis of left VII nerve; thinning of right VII nerve. Agenesis of olfactory bulbs	Regular	Regular	Regular
14	Asymmetric brainstem (r > l in the medulla; l > r in the pons)	Anterior cleft (pons > medulla)	Short and small	Thick left MCP	Regular	Regular		Dilated	Hypoplastic and rotated	Malorientation of folia (r hemisphere)
15	Mild asymmetric brainstem (r > l in the medulla; l >r in the pons)	Small pontine cleft	Short and small	Regular	Regular	Regular		Regular	Mildly Hypoplastic	Malorientation of folia (medial r hemisphere)

MCP: middle cerebellar peduncles; P-M Junction: ponto-mesencephalic junction

Diffusion tensor imaging findings at the level of the brainstem in the 15 patients mutated in tubulin genes								
Patient	**ICP**	**MCP**	**SCP**	**SCP decussation**	**Pontine transverse fibers**	**Medial lemnisci**	**CSTs-pons**	**CSTs-mesencephalon**
1	n.a.	Regular	Regular	Regular	Reduced (the dorsal component is not clear)	Fused with CSTs	Fused with lemnisci	Small
2	Regular	Regular	Regular	Small	Regular	Regular	Regular	Regular
3	n.a.	Short, abnormal signal (red/white)	Regular	Small	Reduced (the dorsal component is not clear) + asymmetric	Fused with CSTs	Fused with lemnisci	Asymmetric
4	n.a.	Short, abnormal signal (white)	Regular	Small	Reduced (the dorsal component is not clear) + asymmetric	Fused with CSTs	Fused with lemnisci	Asymmetric
5	Regular	Abnormal signal (mild)	Regular	Regular	Regular	Regular	Mild asymmetry (l < r)	Regular
6	n.a.	Short, abnormal signal (white)	Regular	Small	Reduced (the dorsal component is not clear) + asymmetric	Fused with CSTs	Fused with lemnisci	Asymmetric
7	Regular	Short, abnormal signal (white)	Regular	Regular	Thick anterior component; dorsal component not clear	Regular	Reduced	Small
8	n.a.	Short, abnormal signal (red/white)	Regular	Regular	Thick anterior component; dorsal component not clear	Fused with CSTs	Fused with lemnisci	Asymmetric
9	Regular	Asymmetric (l > r)	Regular	Small	Thick anterior component; dorsal component not clear	Fused with CSTs	Reduced	Regular
10	Regular	Abnormal signal (red/white)	Regular	Regular	Reduced (the dorsal component is not clear)	Reduced	Reduced and asymmetric (l < r)	Asymmetric (l<<r)
11	Regular	Regular	Regular	Regular	Thick anterior component; dorsal component not clear	Regular	Regular	Bilateral abnormal signal
12	Regular	Regular	Regular	Regular	Reduced anterior component	Regular	Regular	Regular
13	Regular	Regular	Regular	Small	Thick anterior component; dorsal component not clear	Fused with CSTs	Fused with lemnisci	Regular
14	n.a.	Asymmetric (l > r) Right MCP looks white	Regular	Small	Reduced (the dorsal component is not clear) + asymmetric	Fused with CSTs	Fused with lemnisci	Small; pale colour
15	n.a.	Regular	Regular	Regular	Reduced (the dorsal component is not clear)	Fused with CSTs	Fused with lemnisci	Small; pale colour

ICP inferior cerebellar peduncles, MCP middle cerebellar peduncles, SCP superior cerebellar peduncles, CST corticospinal tract

Tab.A10. Frequencies and bioinformatic predictions of TTL c.1013G>A variant

gnomAD	-	**DANN_score**	1
1000G	-	**MutationAssessor prediction (score)**	M (2.27)
ESP	-	**MutationTaster prediction (score)**	D (1)
PolyPhen-2 prediction (score)	D (0.94)	**GERP++score**	5.58
SIFT prediction (score)	D (0.007)	**PhastCons100way score**	1
CADD prediction (phred-like score)	31	**PhyloP100way score**	9.36

D: Deleterious; M: Medium. Pathogenic cut-off scores are as follows: **PolyPhen-2**: D ≥0.9; **SIFT**: D≤0.05; **CADD**: ≥15 (for a more conservative estimate: ≥20); **DANN**: scores range from 0 to 1 (higher is the score, higher is the probability to belong to a damaging variant); **MutationAssessor**: scores range from -5.14 to 6.49 with higher scores indicating increasing likelihood of functional impact of a variant (score cutoff between "neutral", "low", "medium" and "high" predictions are 0.8, 1.94 and 3.50); **MutationTaster**: D>0.5; **GERP++**: estimates evolutionary constraint of specific positions in 36 mammalian species. Scores range from -12.36 to 6.18 with higher scores indicating more conserved sites; **PhastCons** and **PhyloP** conservation scores are based on multiple alignments of 100 vertebrate genomes. Scores range from 0 to 1 for PhastCons and from -20 to 9.87 for PhyloP with higher scores suggesting stronger conservation of the site

REFERENCES

1. Parisi MA, Dobyns WB. Human malformations of the midbrain and hindbrain: Review and proposed classification scheme. *Mol Genet Metab*. 2003;80(1-2):36-53. doi:10.1016/j.ymgme.2003.08.010

2. Doherty D, Millen KJ, Barkovich AJ. Midbrain and hindbrain malformations: Advances in clinical diagnosis, imaging, and genetics. *Lancet Neurol*. 2013;12(4):381-93. doi:10.1016/S1474-4422(13)70024-3

3. Poretti A, Boltshauser E, Huisman TA. Cerebellar and Brainstem Malformations. *Neuroimaging Clin N Am*. 2016;26(3):341-357. doi:10.1016/j.nic.2016.03.005

4. Santoro M, Coi A, Barišić I, et al. Epidemiology of Dandy-Walker Malformation in Europe: A EUROCAT Population-Based Registry Study. *Neuroepidemiology*. 2019;1-11. doi:10.1159/000501238

5. Howley MM, Keppler-Noreuil KM, Cunniff CM, Browne ML. Descriptive epidemiology of cerebellar hypoplasia in the National Birth Defects Prevention Study. *Birth Defects Res*. 2018;110(19):1419-1432. doi:10.1002/bdr2.1388

6. D'Antonio F, Khalil A, Garel C, et al. Systematic review and meta-analysis of isolated posterior fossa malformations on prenatal ultrasound imaging (part 1): Nomenclature, diagnostic accuracy and associated anomalies. *Ultrasound Obstet Gynecol*. 2016;47(6):690-697. doi:10.1002/uog.14900

7. Long A, Moran P, Robson S. Outcome of fetal cerebral posterior fossa anomalies. *Prenat Diagn*. 2006;26:707–710. doi:10.1002/pd.1485

8. Forzano F, Mansour S, Ierullo A, Homfray T, Thilaganathan B. Posterior fossa malformation in fetuses: a report of 56 further cases and a review of the literature. *Prenat Diagn*. 2007;27:495–501. doi:10.1002/pd.1722

9. Steinlin M. Cerebellar disorders in childhood: Cognitive problems. *Cerebellum*. 2008;7(4):607-610. doi:10.1007/s12311-008-0083-3

10. Pinchefsky EF, Accogli A, Shevell MI, Saint-Martin C, Srour M. Developmental outcomes in children with congenital cerebellar malformations. *Dev Med Child Neurol*. 2019;61(3):350-358. doi:10.1111/dmcn.14059

11. Bachmann-Gagescu R, Dempsey JC, Phelps IG, et al. Joubert syndrome: a model for untangling recessive disorders with extreme genetic heterogeneity. *J Med Genet*. 2015;52(8):514-522. doi:10.1136/jmedgenet-2015-103087

12. Aldinger KA, Timms AE, Thomson Z, et al. Redefining the Etiologic Landscape of Cerebellar Malformations. *Am J Hum Genet*. 2019;105(3):606-615. doi:10.1016/j.ajhg.2019.07.019

13. Sajan SA, Fernandez L, Nieh SE, et al. Both Rare and De Novo Copy Number Variants Are Prevalent in Agenesis of the Corpus Callosum but Not in Cerebellar Hypoplasia or Polymicrogyria. *PLoS Genet*. 2013;9(10). doi:10.1371/journal.pgen.1003823

14. D'Antonio F, Khalil A, Garel C, et al. Systematic review and meta-analysis of isolated posterior fossa malformations on prenatal imaging (part 2): neurodevelopmental outcome. *Ultrasound Obstet Gynecol*. 2016;48(1):28-37. doi:10.1002/uog.15755

15. Lei T, Feng JL, Xie YJ, Xie HN, Zheng J, Lin MF. Chromosomal aneuploidies and copy number variations in posterior fossa abnormalities diagnosed by prenatal ultrasonography. *Prenat Diagn*. 2017;37(11):1160-1168. doi:10.1002/pd.5159

16. Zou Z, Huang L, Lin S, et al. Prenatal diagnosis of posterior fossa anomalies: Additional value of

chromosomal microarray analysis in fetuses with cerebellar hypoplasia. *Prenat Diagn*. 2018;38(2):91-98. doi:10.1002/pd.5190

17. Grinberg I, Northrup H, Ardinger H, Prasad C, Dobyns WB, Millen KJ. Heterozygous deletion of the linked genes ZIC1 and ZIC4 is involved in Dandy-Walker malformation. *Nat Genet*. 2004;36(10):1053-1055. doi:10.1038/ng1420

18. Ballarati L, Rossi E, Bonati MT, et al. 13q Deletion and central nervous system anomalies: further insights from karyotype-phenotype analyses of 14 patients. *J Med Genet*. 2007;44(1):1-6. doi:10.1136/jmg.2006.043059

19. Aldinger KA, Lehmann OJ, Hudgins L, et al. FOXC1 is required for normal cerebellar development and is a major contributor to chromosome 6p25.3 Dandy-Walker malformation. *Nat Genet*. 2009;41(9):1037-1042. doi:10.1038/ng.422

20. Ferraris A, Bernardini L, Avramovska VS, et al. Dandy-walker malformation and wisconsin syndrome: Novel cases add further insight into the genotype-phenotype correlations of 3q23q25 deletions. *Orphanet J Rare Dis*. 2013;8(1):1-7. doi:10.1186/1750-1172-8-75

21. Patel S, Barkovich J. Analysis and Classification of Cerebellar Malformations. *Am J Neuroradiol*. 2002;23:1074–1087.

22. Barkovich AJ, Millen KJ, Dobyns WB. A developmental classification of malformations of the brainstem. *Ann Neurol*. 2007;62(6):625-639. doi:10.1002/ana.21239

23. Barkovich AJ, Millen KJ, Dobyns WB. A developmental and genetic classification for midbrain-hindbrain malformations. *Brain*. 2009;132(12):3199-3230. doi:10.1093/brain/awp247

24. Bosemani T, Orman G, Boltshauser E, Tekes A, Huisman TA, Poretti A. Congenital abnormalities of the posterior fossa. *Radiographics*. 2015;35(1):200-220. doi:10.1148/rg.351140038

25. Poretti A, Boltshauser E. Terminology in morphological anomalies of the cerebellum does matter. *Cerebellum & Ataxias*. 2015;2(1):4-9. doi:10.1186/s40673-015-0027-x

26. Romani M, Micalizzi A, Valente EM. Joubert syndrome: Congenital cerebellar ataxia with the molar tooth. *Lancet Neurol*. 2013;12(9):894-905. doi:10.1016/S1474-4422(13)70136-4

27. Parisi MA, Doherty D, Chance PF, Glass IA. Joubert syndrome (and related disorders) (OMIM 213300). *Eur J Hum Genet*. 2007;15(5):511-521. doi:10.1038/sj.ejhg.5201648

28. Dempsey JC, Phelps IG, Bachmann-Gagescu R, Glass IA, Tully HM, Doherty D. Mortality in Joubert syndrome. *Am J Med Genet Part A*. 2017;173(5):1237-1242. doi:10.1002/ajmg.a.38158

29. Musselman KE, Stoyanov CT, Marasigan R, et al. Prevalence of ataxia in children: A systematic review. *Neurology*. 2014;82(1):80-89. doi:10.1212/01.wnl.0000438224.25600.6c

30. Summers AC, Snow J, Wiggs E, et al. Neuropsychological phenotypes of 76 individuals with Joubert syndrome evaluated at a single center. *Am J Med Genet A*. 2017;173(7):1796-1812. doi: 10.1002/ajmg.a.38272.

31. Foell D, August C, Frosch M, Harms E, Zimmer KP. Early detection of severe cholestatic hepatopathy in COACH syndrome. *Am J Med Genet*. 2002;1(111):429-434. doi:10.1002/ajmg.10614.

32. Gentile M, Di Carlo A, Susca F, et al. COACH syndrome: report of two brothers with congenital hepatic fibrosis, cerebellar vermis hypoplasia, oligophrenia, ataxia, and mental retardation. *Am J Med Genet*. 1996;64(3):514-520. doi:10.1002/(SICI)1096-8628(19960823)64:3<514::AID-AJMG13>3.0.CO;2-O

33. Herzog D, Martin S, Yandza T, Alvarez F. Hepatic insufficiency and liver transplantation in a patient

with COACH syndrome. *Pediatr Transpl*. 2002;6(5):443-446. doi:10.1034/j.1399-3046.2002.02035.x

34. Uemura T, Sanchez EQ, Ikegami T, et al. Successful combined liver and kidney transplant for COACH syndrome and 5-yr follow-up. *Clin Transpl*. 2005;19(6):717-720. doi:10.1111/j.1399-0012.2005.00409.x

35. Coppola G, Vajro P, De Virgiliis S, Ciccimarra E, Boccone L, Pascotto A. Cerebellar vermis defect, oligophrenia, congenital ataxia, and hepatic fibrocirrhosis without coloboma and renal abnormalities: report of three cases. *Neuropediatrics*. 2002;33(4):180-185. doi:10.1055/s-2002-34492

36. Moscoso CG, Steer CJ. "Let my liver rather heat with wine" - a review of hepatic fibrosis pathophysiology and emerging therapeutics. *Hepat Med*. 2019;11:109-129. doi: 10.2147/HMER.S213397

37. Mitchison HM, Valente EM. Motile and non-motile cilia in human pathology: from function to phenotypes. *J Pathol*. 2016:294-309. doi:10.1002/path.4843

38. Vilboux T, Malicdan MC, Roney JC, et al. CELSR2, encoding a planar cell polarity protein, is a putative gene in Joubert syndrome with cortical heterotopia, microophthalmia, and growth hormone deficiency. *Am J Med Genet Part A*. 2017;173(3):661-666. doi:10.1002/ajmg.a.38005

39. Stephen J, Vilboux T, Mian L, et al. Mutations in KIAA0753 cause Joubert syndrome associated with growth hormone deficiency. *Hum Genet*. 2017;136(4):399-408. doi:10.1007/s00439-017-1765-z

40. Beck BB, Phillips JB, Bartram MP, et al. Mutation of POC1B in a severe syndromic retinal ciliopathy. *Hum Mutat*. 2014;35(10):1153-1162. doi:10.1002/humu.22618

41. Li C, Jensen VL, Park K, et al. MKS5 and CEP290 Dependent Assembly Pathway of the Ciliary Transition Zone. *PLoS Biol*. 2016;14(3):1-29. doi:10.1371/journal.pbio.1002416

42. Alkanderi S, Molinari E, Shaheen R, et al. ARL3 Mutations Cause Joubert Syndrome by Disrupting Ciliary Protein Composition. *Am J Hum Genet*. 2018;103(4):612-620. doi:10.1016/j.ajhg.2018.08.015

43. Shaheen R, Jiang N, Alzahrani F, et al. Bi-allelic Mutations in FAM149B1 Cause Abnormal Primary Cilium and a Range of Ciliopathy Phenotypes in Humans. *Am J Hum Genet*. 2019;104(4):731-737. doi:10.1016/j.ajhg.2019.02.018

44. Van De Weghe JC, Rusterholz TDS, Latour B, et al. Mutations in ARMC9, which Encodes a Basal Body Protein, Cause Joubert Syndrome in Humans and Ciliopathy Phenotypes in Zebrafish. *Am J Hum Genet*. 2017;101(1):23-36. doi:10.1016/j.ajhg.2017.05.010

45. Bruel AL, Levy J, Elenga N, et al. INTU-related oral-facial-digital syndrome type VI: A confirmatory report. *Clin Genet*. 2018. doi:10.1111/cge.13238

46. Brancati F, Iannicelli M, Travaglini L, et al. MKS3/TMEM67 Mutations Are a Major Cause of COACH Syndrome, a Joubert Syndrome Related Disorder with Liver Involvement. 2010;30(2):1-14. doi:10.1002/humu.20924.MKS3/TMEM67

47. Iannicelli M, Brancati F, Mougou-Zerelli S, et al. Novel TMEM67 Mutations and Genotype-phenotype Correlates in Meckelin-related Ciliopathies. *Hum Mutat*. 2010;31(5):E1319-31. doi:10.1002/humu.21239

48. Doherty D, Parisi MA, Finn LS, et al. Mutations in 3 genes (MKS3, CC2D2A and RPGRIP1L) cause COACH syndrome (Joubert syndrome with congenital hepatic fibrosis). *J Med Genet*. 2010;47(1):8-21. doi:10.1136/jmg.2009.067249

49. Brancati F, Barrano G, Silhavy JL, et al. CEP290 Mutations Are Frequently Identified in the Oculo-Renal Form of Joubert Syndrome–Related Disorders. *Am J Hum Genet*. 2007;81(1):104-113.

doi:10.1086/519026

50. Romani M, Mancini F, Micalizzi A, et al. Oral-facial-digital syndrome type VI: is C5orf42 really the major gene? *Hum Genet*. 2015;134(1):123-126. doi:10.1007/s00439-014-1508-3

51. Valente EM, Brancati F, Silhavy JL, et al. AHI1 gene mutations cause specific forms of Joubert Syndrome Related Disorders. *Ann Neurol*. 2006;59(3):527-534. doi:10.1002/ana.20749

52. Bachmann-Gagescu R, Ishak GE, Dempsey JC, et al. Genotype-phenotype correlation in CC2D2A-related Joubert syndrome reveals an association with ventriculomegaly and seizures. *J Med Genet*. 2012. doi:10.1136/jmedgenet-2011-100552

53. Valente EM, Logan CV, Mougou-Zerelli S, et al. Mutations in TMEM216 perturb ciliogenesis and cause Joubert, Meckel and related syndromes. *Nat Genet*. 2010;42(7):619-625. doi:10.1038/ng.594

54. Bachmann-Gagescu R, Dempsey JC, Phelps IG, et al. Joubert syndrome: A model for untangling recessive disorders with extreme genetic heterogeneity. *J Med Genet*. 2015;52(8):514-522. doi:10.1136/jmedgenet-2015-103087

55. Lindstrand A, Frangakis S, Carvalho CM, et al. Copy-Number Variation Contributes to the Mutational Load of Bardet-Biedl Syndrome. *Am J Hum Genet*. 2016;99(2):318-336. doi:10.1016/j.ajhg.2015.04.023

56. Mendes De Almeida R, Tavares J, Martins S, et al. Whole gene sequencing identifies deep-intronic variants with potential functional impact in patients with hypertrophic cardiomyopathy. *PLoS One*. 2017;12(8):1-19. doi:10.1371/journal.pone.0182946

57. Janin A, Bardel C, Faivre L, et al. Whole MYBPC3 NGS sequencing as a molecular strategy to improve the efficiency of molecular diagnosis of patients with hypertrophic cardiomyopathy. *Hum Mutat*. doi:10.1002/humu.23944

58. Rudnik-Schöneborn S, Barth PG, Zerres K. Pontocerebellar hypoplasia. *Am J Med Genet Part C Semin Med Genet*. 2014;166(2):173-183. doi:10.1002/ajmg.c.31403

59. Van Dijk T, Baas F, Barth PG, Poll-The BT. What's new in pontocerebellar hypoplasia? An update on genes and subtypes. *Orphanet J Rare Dis*. 2018;13(1):1-16. doi:10.1186/s13023-018-0826-2

60. van Dijk T, Ferdinandusse S, Ruiter JPN, et al. Biallelic loss of function variants in COASY cause prenatal onset pontocerebellar hypoplasia, microcephaly, and arthrogryposis. *Eur J Hum Genet*. 2018;26(12):1752-1758. doi:10.1038/s41431-018-0233-0

61. Sánchez-Albisua I, Frölich S, Barth PG, Steinlin M, Krägeloh-Mann I. Natural course of pontocerebellar hypoplasia type 2A. *Orphanet J Rare Dis*. 2014;9(1):1-11. doi:10.1186/1750-1172-9-70

62. Wambach JA, Wegner DJ, Yang P, et al. Functional characterization of biallelic RTTN variants identified in an infant with microcephaly, simplified gyral pattern, pontocerebellar hypoplasia, and seizures. *Pediatr Res*. 2018;84(3):435-441. doi:10.1038/s41390-018-0083-z

63. Accogli A, Russell L, Sébire G, et al. Pathogenic variants in AIMP1 cause pontocerebellar hypoplasia. *Neurogenetics*. 2019. doi:10.1007/s10048-019-00572-7

64. Gershlick DC, Ishida M, Jones JR, Bellomo A, Bonifacino JS, Everman DB. A neurodevelopmental disorder caused by mutations in the VPS51 subunit of the GARP and EARP complexes. *Hum Mol Genet*. 2019;28(9):1548-1560. doi:10.1093/hmg/ddy423

65. Uwineza A, Caberg JH, Hitayezu J, et al. VPS51 biallelic variants cause microcephaly with brain malformations: A confirmatory report. *Eur J Med Genet*. 2019;62(8):51-54. doi:10.1016/j.ejmg.2019.103704

66. Wojcik MH, Okada K, Prabhu SP, et al. De novo variant in KIF26B is associated with pontocerebellar hypoplasia with infantile spinal muscular atrophy. *Am J Med Genet Part A*. 2018;176(12):2623-2629. doi:10.1002/ajmg.a.40493

67. Najm J, Horn D, Wimplinger I, et al. Mutations of CASK cause an X-linked brain malformation phenotype with microcephaly and hypoplasia of the brainstem and cerebellum. *Nat Genet*. 2008;40(9):1065-1067. doi:10.1038/ng.194

68. Burglen L, Chantot-Bastaraud S, Garel C, et al. Spectrum of pontocerebellar hypoplasia in 13 girls and boys with CASK mutations: Confirmation of a recognizable phenotype and first description of a male mosaic patient. *Orphanet J Rare Dis*. 2012;7(1):18. doi:10.1186/1750-1172-7-18

69. Takanashi JI, Okamoto N, Yamamoto Y, et al. Clinical and radiological features of Japanese patients with a severe phenotype due to CASK mutations. *Am J Med Genet Part A*. 2012;158 A(12):3112-3118. doi:10.1002/ajmg.a.35640

70. Nakamura K, Nishiyama K, Kodera H, et al. A de novo CASK mutation in pontocerebellar hypoplasia type 3 with early myoclonic epilepsy and tetralogy of Fallot. *Brain Dev*. 2014;36(3):272-273. doi:10.1016/j.braindev.2013.03.007

71. Moog U, Bierhals T, Brand K, et al. Phenotypic and molecular insights into CASK-related disorders in males. *Orphanet J Rare Dis*. 2015;10(1). doi:10.1186/s13023-015-0256-3

72. Hayashi S, Uehara DT, Tanimoto K, et al. Comprehensive investigation of CASK mutations and other genetic etiologies in 41 patients with intellectual disability and microcephaly with pontine and cerebellar hypoplasia (MICPCH). *PLoS One*. 2017;12(8):1-18. doi:10.1371/journal.pone.0181791

73. Namavar Y, Barth PG, Kasher PR, et al. Clinical, neuroradiological and genetic findings in pontocerebellar hypoplasia. *Brain*. 2011;134(1):143-156. doi:10.1093/brain/awq287

74. Takanashi JI, Arai H, Nabatame S, et al. Neuroradiologic features of CASK mutations. *Am J Neuroradiol*. 2010;31(9):1619-1622. doi:10.3174/ajnr.A2173

75. Rudnik-Schöneborn S, Senderek J, Jen JC, et al. Pontocerebellar hypoplasia type 1: Clinical spectrum and relevance of EXOSC3 mutations. *Neurology*. 2013;80(5):438-446. doi:10.1212/WNL.0b013e31827f0f66

76. Ivanov I, Atkinson D, Litvinenko I, et al. Pontocerebellar hypoplasia type 1 for the neuropediatrician: Genotype–phenotype correlations and diagnostic guidelines based on new cases and overview of the literature. *Eur J Paediatr Neurol*. 2018;22(4):674-681. doi:10.1016/j.ejpn.2018.03.011

77. Eggens VR, Barth PG, Niermeijer JM, et al. EXOSC3 mutations in pontocerebellar hypoplasia type 1: Novel mutations and genotype-phenotype correlations. *Orphanet J Rare Dis*. 2014;9(1):1-10. doi:10.1186/1750-1172-9-23

78. Wan J, Yourshaw M, Mamsa H, et al. Mutations in the RNA exosome component gene EXOSC3 cause pontocerebellar hypoplasia and spinal motor neuron degeneration. *Nat Genet*. 2012;44(6):704-708. doi:10.1038/ng.2254

79. Bahi-Buisson N, Poirier K, Fourniol F, et al. The wide spectrum of tubulinopathies: What are the key features for the diagnosis? *Brain*. 2014;137(6):1676-1700. doi:10.1093/brain/awu082

80. Cushion TD, Paciorkowski AR, Pilz DT, et al. De novo mutations in the beta-tubulin gene TUBB2A cause simplified gyral patterning and infantile-onset epilepsy. *Am J Hum Genet*. 2014;94(4):634-641. doi:10.1016/j.ajhg.2014.03.009

81. Bertini E, Zanni G, Boltshauser E. Nonprogressive congenital ataxias. *Handb Clin Neurol*. 2018;155:91-103. doi:10.1016/B978-0-444-64189-2.00006-8

82. Feraco P, Mirabelli-Badenier M, Severino M, et al. The shrunken, bright cerebellum: A characteristic MRI finding in congenital disorders of glycosylation type 1a. *Am J Neuroradiol*. 2012;33(11):2062-2067. doi:10.3174/ajnr.A3151

83. Pierpaoli C,Walker L, Irfanoglu MO et al (2010) Tortoise: an integrated software package for processing of diffusion MRI data. In: Proceedings of the annual meeting of the International Society for Magnetic Resonance in Medicine (ISMRM 2010), 1–7 May 2010. Stockholm, Sweden, p. 1597

84. Basser PJ, Pierpaoli C. Microstructural and physiological features of tissues elucidated by quantitative-diffusion-tensor MRI. 1996. *J Magn Reson*. 2011;213(2):560-570. doi:10.1016/j.jmr.2011.09.022

85. Pajevic S, Pierpaoli C. Color schemes to represent the orientation of anisotropic tissues from diffusion tensor data: Application to white matter fiber tract mapping in the human brain. *Magn Reson Med*. 1999;42(3):526-540.

86. Chang LC, Jones DK, Pierpaoli C. RESTORE: Robust estimation of tensors by outlier rejection. *Magn Reson Med*. 2005;53(5):1088-1095. doi:10.1002/mrm.20426

87. Richards S, Aziz N, Bale S, et al. Standards and guidelines for the interpretation of sequence variants: A joint consensus recommendation of the American College of Medical Genetics and Genomics and the Association for Molecular Pathology. *Genet Med*. 2015;17(5):405-424. doi:10.1038/gim.2015.30

88. Morava É, Cser B, Kárteszl J, et al. Screening for CDG type Ia in Joubert syndrome. *Med Sci Monit*. 2004;10(8):CR469-72

89. Nuovo S, Bacigalupo I, Ginevrino M, et al. Age and sex prevalence estimate of Joubert Syndrome in Italy. *Neurology*. 2020;94(8):e797-e801. doi:10.1212/WNL.0000000000008996.

90. Schoenberg BS. Calculating confidence intervals for rates and ratios. Simplified method utilizing tabular values based on the Poisson distribution. *Neuroepidemiology*. 1983;2:257-265. doi.org/10.1159/000110529

91. Esscher E, Flodmark O, Hagberg G, Hagberg B. Non-progressive ataxia: origins, brain pathology and impairments in 78 swedish children. *Dev Med Child Neurol*. 1996;38:285–296. doi:10.1111/j.1469-8749.1996.tb12095.x

92. Nuovo S, Fuiano L, Micalizzi A, et al. Impaired urinary concentration ability is a sensitive predictor of renal disease progression in Joubert syndrome. *Nephrol Dial Transplant*. 2018:1-8. doi:10.1093/ndt/gfy333

93. Brancati F, Dallapiccola B, Valente EM. Joubert Syndrome and related disorders. *Orphanet J Rare Dis*. 2010;5:20. doi:10.1186/1750-1172-5-20

94. Fleming LR, Doherty DA, Parisi MA, et al. Prospective Evaluation of Kidney Disease in Joubert Syndrome. *Clin J Am Soc Nephrol*. 2017;12(12):1962-1973. doi:10.2215/CJN.05660517

95. Stokman M, Lilien M, Knoers N. Nephronophthisis. 2016 Jun 23. In: Adam MP, Ardinger HH, Pagon RA, Wallace SE, Bean LJH, Stephens K, Amemiya A, editors. GeneReviews® [Internet]. Seattle (WA): University of Washington, Seattle; 1993-2020. Available from http://www.ncbi.nlm.nih.gov/books/NBK368475/

96. Kidney Disease Improving Global Outcomes (KDIGO) CKD Work Group. KDIGO 2012 Clinical Practice Guideline for the Evaluation and Management of Chronic Kidney Disease. *Kidney Int Suppl*. 2013;3:1-150

97. Kidney Disease Improving Global Outcomes (KDIGO) CKD-MBD Update Work Group. KDIGO 2017 Clinical Practice Guideline Update for the Diagnosis, Evaluation, Prevention, and Treatment of

Chronic Kidney Disease–Mineral and Bone Disorder (CKD-MBD). *Kidney Int Suppl*. 2017;7: 1–59. doi: 10.1016/j.kisu.2017.04.001

98. Aronson AS, Svenningsen NW. DDAVP test for estimation of renal concentrating capacity in infants and children. *Arch Dis Child*. 1974;49(8):654-659. doi:10.1136/adc.49.8.654

99. Rees L, Brogan PA, Bockenhauer D et al. *Paediatric Nephrology*. 2nd edn. Oxford, UK: Oxford University Press, 2012

100. Schwartz GJ, Haycock GB, Edelmann CMJr et al. A simple estimate of glomerular filtration rate in children derived from body length and plasma creatinine. *Pediatrics*. 1976;58:259–263.

101. Schwartz GJ, Muñoz A, Schneider MF, et al. New Equations to Estimate GFR in Children with CKD. *J Am Soc Nephrol*. 2009;20:629-637. doi:10.1681/ASN.2008030287

102. National Kidney Foundation. https://www.kidney.org/content/mdrd-study-equation. (10 July 2018, date last accessed)

103. Firth D. Bias Reduction of Maximum Likelihood Estimates. *Biometrika*. 1993;80(1):27-38. doi: 10.1093/biomet/80.1.27

104. R Development Core Team. R: A language and environment for statistical computing. Vienna, Austria: R Foundation for Statistical Computing, 2017

105. Vilboux T, Doherty DA, Glass IA, et al. Molecular genetic findings and clinical correlations in 100 patients with Joubert syndrome and related disorders prospectively evaluated at a single center. *Genet Med*. 2017;19(8):875-882. doi:10.1038/gim.2016.204

106. Rinschen MM, Schermer B, Benzing T. Vasopressin-2 receptor signaling and autosomal dominant polycystic kidney disease: From bench to bedside and back again. *J Am Soc Nephrol*. 2014;25(6):1140-1147. doi:10.1681/ASN.2013101037

107. Adalat S, Woolf AS, Johnstone KA, et al. HNF1B Mutations Associate with Hypomagnesemia and Renal Magnesium Wasting. *J Am Soc Nephrol*. 2009;20(5):1123-1131. doi:10.1681/ASN.2008060633

108. De Mori R, Romani M, D'Arrigo S, et al. Hypomorphic Recessive Variants in SUFU Impair the Sonic Hedgehog Pathway and Cause Joubert Syndrome with Cranio-facial and Skeletal Defects. *Am J Hum Genet*. 2017;101(4):552-563. doi:10.1016/j.ajhg.2017.08.017

109. Hui CC, Angers S. Gli proteins in development and disease. *Annu Rev Cell Dev Biol*. 2011;27:513-537. doi:10.1146/annurev-cellbio-092910-154048

110. Tukachinsky H, Lopez L V, Salic A. A mechanism for vertebrate Hedgehog signaling: recruitment to cilia and dissociation of SuFu–Gli protein complexes. 2010;191(2):415-428. doi:10.1083/jcb.201004108

111. Ruat M, Roudaut H, Ferent J, Traiffort E. Hedgehog trafficking, cilia and brain functions. *Differentiation*. 2012;83(2):S97-104. doi:10.1016/j.diff.2011.11.011

112. Han YG, Spassky N, Romaguera-Ros M, et al. Hedgehog signaling and primary cilia are required for the formation of adult neural stem cells. *Nat Neurosci*. 2008;11(3):277-284. doi:10.1038/nn2059

113. Spassky N, Han YG, Aguilar A, er al. Primary cilia are required for cerebellar development and Shh-dependent expansion of progenitor pool. *Dev Biol*. 2008;317(1):246-259. doi:10.1016/j.ydbio.2008.02.026

114. Aguilar A, Meunier A, Strehl L, Martinovic J, Bonniere M. Analysis of human samples reveals impaired SHH-dependent cerebellar development in Joubert syndrome/Meckel syndrome. 2012;109(42). doi:10.1073/pnas.1201408109

115. Larkins CE, Aviles GD, East MP, Kahn RA, Caspary T. Arl13b regulates ciliogenesis and the dynamic localization of Shh signaling proteins. *Mol Biol Cell*. 2011;22(23):4694-703. doi:10.1091/mbc.E10-12-0994

116. Poretti A, Vitiello G, Hennekam RC, et al. Delineation and Diagnostic Criteria of Oral-Facial- Digital Syndrome Type VI. *Orphanet J Rare Dis*. 2012;7(1):4. doi:10.1186/1750-1172-7-4

117. Dixon-salazar T, Silhavy JL, Marsh SE, et al. Mutations in the AHI1 Gene, Encoding Jouberin, Cause Joubert Syndrome with Cortical Polymicrogyria. *Am J Hum Genet*. 2004;75(6):979-987. doi:10.1086/425985

118. Putoux A, Thomas S, Coene KL, et al. KIF7 mutations cause fetal hydrolethalus and acrocallosal syndromes. *Nat Genet*. 2011;43(6):601-606. doi:10.1038/ng.826.

119. Kiwilsza M, Sporniak-Tutak K. Gorlin-Goltz syndrome-a medical condition requiring a multidisciplinary approach. 2012;18(9):RA145-153. doi:10.12659/msm.883341

120. Pastorino L, Ghiorzo P, Nasti S, et al. Identification of a SUFU germline mutation in a family with Gorlin syndrome. *Am J Med Genet A*. 2009;149A(7):1539-1543. doi:10.1002/ajmg.a.32944

121. Brugières L, Pierron G, Chompret A, et al. Incomplete penetrance of the predisposition to medulloblastoma associated with germ-line SUFU mutations. *J Med Genet*. 2010;47(2):142-144. doi: 10.1136/jmg.2009.067751

122. Brugières L, Remenieras A, Pierron G, et al. High frequency of germline SUFU mutations in children with desmoplastic/nodular medulloblastoma younger than 3 years of age. *J Clin Oncol*. 2012;30(17):2087-2093. doi:10.1200/JCO.2011.38.7258

123. Aavikko M, Li S, Saarinen S, et al. Loss of SUFU Function in Familial Multiple Meningioma. 2012:520-526. doi:10.1016/j.ajhg.2012.07.015

124. Taylor MD, Liu L, Raffel C, et al. Mutations in SUFU predispose to medulloblastoma. *Nat Genet*. 2002;31(3):306-310. doi:10.1038/ng916

125. Teglund S, Toftgård R. Hedgehog beyond medulloblastoma and basal cell carcinoma. *Biochim Biophys Acta*. 2010;1805(2):181-208. doi:10.1016/j.bbcan.2010.01.003

126. Svärd J, Heby-Henricson K, Persson-Lek M, et al. Genetic elimination of Suppressor of fused reveals an essential repressor function in the mammalian Hedgehog signaling pathway. *Dev Cell*. 2006;10(2): 187-197. doi:10.1016/j.devcel.2005.12.013

127. Lek M, Karczewski KJ, Minikel EV, et al. Analysis of protein-coding genetic variation in 60,706 humans. *Nature*. 2016;536(7616):285-291. doi:10.1038/nature19057

128. Zhulyn O, Hui CC. Sufu and Kif7 in Limb Patterning and Development. *Dev Dyn*. 2015:468-478. doi:10.1002/DVDY.24249

129. Zhulyn O, Li D, Deimling S, et al. Short Article A Switch from Low to High Shh Activity Regulates Establishment of Limb Progenitors and Signaling Centers. *Dev Cell*. 2014;29(2):241-249. doi:10.1016/j.devcel.2014.03.002

130. Kim JJ, Gill PS, Rotin L, et al. Suppressor of Fused Controls Mid-Hindbrain Patterning and Cerebellar Morphogenesis via GLI3 Repressor. *J Neurosci*. 2011;31(5):1825-1836. doi:10.1523/JNEUROSCI.2166-10.2011

131. Budde BS, Namavar Y, Barth PG, et al. tRNA splicing endonuclease mutations cause pontocerebellar hypoplasia. *Nat Genet*. 2008;40(9):1113-1118. doi:10.1038/ng.204

132. Cassandrini D, Biancheri R, Tessa A, et al. Pontocerebellar hypoplasia: Clinical, pathologic, and

genetic studies. *Neurology*. 2010;75(16):1459-1464. doi:10.1212/WNL.0b013e3181f88173

133. R Core Team (2019). R: A language and environment for statistical computing. R Foundation for Statistical Computing, Vienna, Austria. URL https://www.R-project.org/.

134. Romaniello R, Arrigoni F, Panzeri E, et al. Tubulin-related cerebellar dysplasia: definition of a distinct pattern of cerebellar malformation. *Eur Radiol*. 2017;27(12):5080-5092. doi:10.1007/s00330-017-4945-2

135. Demaerel P. Abnormalities of cerebellar foliation and fissuration: classification, neurogenetics and clinicoradiological correlations. *Neuroradiology*. 2002;44(8):639-646. doi:10.1007/s00234-002-0783-1

136. Oegema R, Cushion TD, Phelps IG, et al. Recognizable cerebellar dysplasia associated with mutations in multiple tubulin genes. *Hum Mol Genet*. 2015;24(18):5313-5325. doi:10.1093/hmg/ddv250

137. Romaniello R, Arrigoni F, Bassi MT, Borgatti R. Mutations in α- and β-tubulin encoding genes: implications in brain malformations. *Brain Dev*. 2015;37(3):273-280. doi: 10.1016/j.braindev.2014.06.002

138. Bahi-Buisson N, Cavallin M. Tubulinopathies Overview. 2016 Mar 24. In: Adam MP, Ardinger HH, Pagon RA, Wallace SE, Bean LJH, Stephens K, Amemiya A, editors. GeneReviews® [Internet]. Seattle (WA): University of Washington, Seattle; 1993-2020. Available from http://www.ncbi.nlm.nih.gov/books/NBK350554/

139. Kumar RA, Pilz DT, Babatz TD, et al. TUBA1A mutations cause wide spectrum lissencephaly (smooth brain) and suggest that multiple neuronal migration pathways converge on alpha tubulins. *Hum Mol Genet*. 2010;19(14):2817-2827. doi:10.1093/hmg/ddq182

140. Romaniello R, Arrigoni F, Cavallini A, et al. Brain malformations and mutations in α- and β-tubulin genes: A review of the literature and description of two new cases. *Dev Med Child Neurol*. 2014;56(4):354-360. doi:10.1111/dmcn.12370

141. Jaglin XH, Poirier K, Saillour Y, et al. Mutations in the beta-tubulin gene TUBB2B result in asymmetrical polymicrogyria. *Nat Genet*. 2009;41(6):746-752. doi:10.1038/ng.380

142. Tischfield MA, Cederquist GY, Gupta ML Jr, Engle EC. Phenotypic spectrum of the tubulin-related disorders and functional implications of disease-causing mutations. *Curr Opin Genet Dev*. 2011;21(3):286-294. doi:10.1038/jid.2014.371

143. Romaniello R, Tonelli A, Arrigoni F, et al. A novel mutation in the β-tubulin gene TUBB2B associated with complex malformation of cortical development and deficits in axonal guidance. *Dev Med Child Neurol*. 2012;54(8):765-769. doi:10.1111/j.1469-8749.2012.04316.x

144. Keays DA, Tian G, Poirier K, et al. Mutations in α-Tubulin Cause Abnormal Neuronal Migration in Mice and Lissencephaly in Humans. *Cell*. 2007;128(1):45-57. doi:10.1016/j.cell.2006.12.017

145. Zanni G, Colafati GS, Barresi S, et al. Description of a novel TUBA1A mutation in Arg-390 associated with asymmetrical polymicrogyria and mid-hindbrain dysgenesis. *Eur J Paediatr Neurol*. 2013;17(4):361-365. doi:10.1016/j.ejpn.2012.12.006

146. Cushion TD, Dobyns WB, Mullins JG, et al. Overlapping cortical malformations and mutations in TUBB2B and TUBA1A. *Brain*. 2013;136(2):536-548. doi:10.1093/brain/aws338

147. Cederquist GY, Luchniak A, Tischfield MA, et al. An inherited TUBB2B mutation alters a kinesin-binding site and causes polymicrogyria, CFEOM and axon dysinnervation. *Hum Mol Genet*. 2012;21(26):5484-5499. doi:10.1093/hmg/dds393

148. Tischfield MA, Baris HN, Wu C, et al. Human TUBB3 Mutations Perturb Microtubule Dynamics,

Kinesin Interactions, and Axon Guidance. *Cell*. 2010;140(1):74-87. doi:10.1016/j.cell.2009.12.011

149. Arrigoni F, Romaniello R, Peruzzo D, et al. The spectrum of brainstem malformations associated to mutations of the tubulin genes family: MRI and DTI analysis. *Eur Radiol*. 2019;29(2):770-782. doi:10.1007/s00330-018-5610-0

150. Poirier K, Saillour Y, Bahi-Buisson N, et al. Mutations in the neuronal β-tubulin subunit TUBB3 result in malformation of cortical development and neuronal migration defects. *Hum Mol Genet*. 2010;19(22):4462-4473. doi:10.1093/hmg/ddq377

151. Kamiya K, Tanaka F, Ikeno M, Okumura A, Aoki S. DTI tractography of lissencephaly caused by TUBA1A mutation. *Neurol Sci*. 2014;35(5):801-803. doi:10.1007/s10072-014-1662-3

152. Poretti A, Meoded A, Rossi A, Raybaud C, Huisman TA. Diffusion tensor imaging and fiber tractography in brain malformations. *Pediatr Radiol*. 2013;43(1):28-54. doi:10.1007/s00247-012-2428-9

153. Rollins NK, Booth TN, Chahrour MH. Variability of Ponto-cerebellar Fibers by Diffusion Tensor Imaging in Diverse Brain Malformations. *J Child Neurol*. 2017;32(3):271-285. doi: 10.1177/0883073816680734

154. Poretti A, Boltshauser E, Loenneker T, et al. Diffusion tensor imaging in Joubert syndrome. *Am J Neuroradiol*. 2007;28(10):1929-1933. doi:10.3174/ajnr.A0703

155. Arrigoni F, Romaniello R, Peruzzo D, et al. Anterior mesencephalic cap dysplasia : novel brainstem malformative features associated with Joubert syndrome. 2018;38(12):2385-2390. doi:10.3174/ajnr.A5360.Anterior

156. Sicotte NL, Salamon G, Shattuck DW, et al. Diffusion tensor MRI shows abnormal brainstem crossing fibers associated with ROBO3 mutations. *Neurology*. 2006;67(3):519-521. doi: 10.1212/01.wnl.0000227960.38262.0c

157. Severino M, Tortora D, Pistorio A, et al. Expanding the spectrum of congenital anomalies of the diencephalic-mesencephalic junction. *Neuroradiology*. 2016;58(1):33-44. doi:10.1007/s00234-015-1601-x

158. Peruzzo D, Arrigoni F, Triulzi F, Parazzini C, Castellani U . Detection of corpus callosum malformations in pediatric population using the discriminative direction in multiple kernel learning. *Med Image Comput Comput Assist Interv*. 2014;17:300-307. doi:10.1007/978-3-319-10470-6_38

159. Kweldam CF, Gwynn H, Vashist A, Hoon AH Jr, Huisman TA, Poretti A. Undecussated superior cerebellar peduncles and absence of the dorsal transverse pontine fibers: a new axonal guidance disorder? *Cerebellum*. 2014;13(4):536-540. doi:10.1007/s12311-014-0562-7

160. Avadhani A, Ilayaraja V, Shetty AP, Rajasekaran S. Diffusion tensor imaging in horizontal gaze palsy with progressive scoliosis. *Magn Reson Imaging*. 2010;28(2):212-216. doi: 10.1016/j.mri.2009.10.004

161. Calloni SF, Cohen JS, Meoded A, et al. Compound Heterozygous Variants in ROBO1 Cause a Neurodevelopmental Disorder With Absence of Transverse Pontine Fibers and Thinning of the Anterior Commissure and Corpus Callosum. *Pediatr Neurol*. 2017;70:70-74. doi: 10.1016/j.pediatrneurol.2017.01.018

162. Friede RL, Boltshauser E. Uncommon syndromes of cerebellar vermis aplasia. I: Joubert syndrome. *Dev Med Child Neurol*. 1978;20(6):758-763. doi:10.1111/j.1469-8749.1978.tb15307.x

163. Ferland RJ, Eyaid W, Collura RV, et al. Abnormal cerebellar development and axonal decussation due to mutations in AHI1 in Joubert syndrome. *Nat Genet*. 2004;36(9):1008-1013. doi:10.1038/ng1419

164. Miyata H, Miyata M, Ohama E. Pyramidal tract abnormalities in the human fetus and infant with trisomy 18 syndrome. *Neuropathology*. 2014;34(3):219-226. doi:10.1111/neup.12081

165. ten Donkelaar HJ, Lammens M, Wesseling P, Hori A, Keyser A, Rotteveel J. Development and malformations of the human pyramidal tract. *J Neurol*. 2004;251(12):1429-1442. doi: 10.1007/s00415-004-0653-3

166. Chan WM, Traboulsi EI, Arthur B, Friedman N, Andrews C, Engle EC. Horizontal gaze palsy with progressive scoliosis can result from compound heterozygous mutations in ROBO3. *J Med Genet*. 2006;43(3):3-6. doi:10.1136/jmg.2005.035436

167. Jissendi-Tchofo P, Severino M, Nguema-Edzang B, Toure C, Soto Ares G, Barkovich AJ. Update on neuroimaging phenotypes of mid-hindbrain malformations. *Neuroradiology*. 2015;57(2):113-138. doi:10.1007/s00234-014-1431-2

168. Barkovich AJ. Developmental disorders of the midbrain and hindbrain. *Front Neuroanat*. 2012;6:7. doi:10.3389/fnana.2012.00007

169. Jen JC, Chan W, Bosley TM, et al. Mutations in a human ROBO gene disrupt hindbrain axon pathway crossing and morphogenesis. *Science*. 2004;304:1509-1513. doi:10.1126/science.1096437

170. Nugent AA, Kolpak AL, Engle EC. Human disorders of axon guidance. *Curr Opin Neurobiol*. 2012;22(5):837-43. doi:10.1016/j.conb.2012.02.006

171. Mutch CA, Poduri A, Sahin M, Barry B, Walsh CA, Barkovich AJ. Disorders of microtubule function in neurons: Imaging correlates. *Am J Neuroradiol*. 2016;37(3):528-535. doi:10.3174/ajnr.A4552

172. Prota AE, Magiera MM, Kuijpers M, et al. Structural basis of tubulin tyrosination by tubulin tyrosine ligase. 2013;200(3):259-270. doi:10.1083/jcb.201211017

173. van Dijk J, Rogowski K, Miro J, Lacroix B, Eddé B, Janke C. A Targeted Multienzyme Mechanism for Selective Microtubule Polyglutamylation. 2007:437-448. doi:10.1016/j.molcel.2007.04.012

174. Nieuwenhuis J, Brummelkamp TR. The Tubulin Detyrosination Cycle: Function and Enzymes. *Trends Cell Biol*. 2019;29(1):80-92. doi:10.1016/j.tcb.2018.08.003

175. Erck C, Peris L, Andrieux A, et al. A vital role of tubulin-tyrosine-ligase for neuronal organization. 2005;102(22). doi:10.1073/pnas.0409626102

176. Shashi V, Magiera MM, Klein D, et al. Loss of tubulin deglutamylase CCP1 causes infantile-onset neurodegeneration. 2018:1-12. doi:10.15252/embj.2018100540

177. Cai Q, Sheng ZH. Molecular motors and synaptic assembly. *Neuroscientist*. 2009;15(1):78-89. doi:10.1177/1073858408329511. doi:10.1177/1073858408329511

178. Fukushima N, Furuta D, Hidaka Y, Moriyama R, Tsujiuchi T. Post-translational modifications of tubulin in the nervous system. *J Neurochem*. 2009;109(3):683-693. doi:10.1111/j.1471-4159.2009.06013.x

179. Song W, Cho Y, Watt D, Cavalli V. Tubulin-tyrosine Ligase (TTL) -mediated Increase in Tyrosinated α-Tubulin in Injured Axons Is Required for Retrograde Injury Signaling and Axon Regeneration. 2015;290(23):14765-14775. doi:10.1074/jbc.M114.622753

180. Lafanechère L, Courtay-cahen C, Kawakami T, et al. Suppression of tubulin tyrosine ligase during tumor growth. 1998;181:171-181.

181. Mialhe A, Lafanechère L, Treilleux I, et al. Tubulin detyrosination is a frequent occurrence in breast cancers of poor prognosis. *Cancer Res*. 2001;61(13):5024-5027.

182. Whipple RA, Vitolo MI, Boggs AE, Charpentier MS, Thompson K, Martin SS. Parthenolide and

costunolide reduce microtentacles and tumor cell attachment by selectively targeting detyrosinated tubulin independent from NF-κB inhibition. 2013;15(5):1. doi:10.1186/bcr3477

183. Janke C, Kneussel M. Tubulin post-translational modifications: encoding functions on the neuronal microtubule cytoskeleton. *Trends Neurosci*. 2010;33(8):362-372. doi:10.1016/j.tins.2010.05.001

184. Nuovo S, Micalizzi A, D'Arrigo S, et al. Between SCA5 and SCAR14: Delineation of the SPTBN2 p.R480W-associated phenotype. *Eur J Hum Genet*. 2018;26(7):928-929. doi:10.1038/s41431-018-0158-7

185. Schnekenberg RP, Perkins EM, Miller JW, et al. De novo point mutations in patients diagnosed with ataxic cerebral palsy. 2015. doi:10.1093/brain/awv117

186. Ikeda Y, Dick KA, Weatherspoon MR, et al. Spectrin mutations cause spinocerebellar ataxia type 5. *Nat Genet*. 2006;38(2):184-190. doi:10.1038/ng1728

187. Cho E, Fogel BL. A family with spinocerebellar ataxia type 5 found to have a novel missense mutation within a SPTBN2 spectrin repeat. *Cerebellum*. 2013;12(2):162-164. doi:10.1007/s12311-012-0408-0.A

188. Jacob FD, Ho ES, Martinez-Ojeda M, Darras BT, Khwaja OS. Case of infantile onset spinocerebellar ataxia type 5. *J Child Neurol*. 2013;28(10):1292-1295. doi:10.1177/0883073812454331

189. Wang Y, Koh K, Miwa M, Yamashiro N, Shindo K, Takiyama Y. A Japanese SCA5 family with a novel three-nucleotide in-frame deletion mutation in the SPTBN2 gene: a clinical and genetic study. *J Hum Genet*. 2014;59(10):569-573. doi:10.1038/jhg.2014.74

190. Elsayed SM, Heller R, Thoenes M, et al. Autosomal dominant SCA5 and autosomal recessive infantile SCA are allelic conditions resulting from SPTBN2 mutations. 2014;(June 2013):286-288. doi:10.1038/ejhg.2013.150

191. Lise S, Clarkson Y, Perkins E, et al. Recessive Mutations in SPTBN2 Implicate b -III Spectrin in Both Cognitive and Motor Development. 2012;8(12). doi:10.1371/journal.pgen.1003074

192. Yıldız Bölükbaşı E, Afzal M, Mumtaz S, Ahmad N, Malik S, Tolun A. Progressive SCAR14 with unclear speech, developmental delay, tremor, and behavioral problems caused by a homozygous deletion of the SPTBN2 pleckstrin homology domain. *Am J Med Genet A*. 2017;173(9):2494-2499. doi:10.1002/ajmg.a.38332

193. Al-Muhaizea MA, AlMutairi F, Almass R, et al. A Novel Homozygous Mutation in SPTBN2 Leads to Spinocerebellar Ataxia in a Consanguineous Family: Report of a New Infantile-Onset Case and Brief Review of the Literature. *Cerebellum*. 2018;17(3):276-285. doi:10.1007/s12311-017-0893-2

194. Schymkowitz J, Borg J, Stricher F, Nys R, Rousseau F, Serrano L. The FoldX web server: An online force field. *Nucleic Acids Res*. 2005;33(SUPPL. 2):382-388. doi:10.1093/nar/gki387

195. Puffenberger EG, Jinks RN, Sougnez C, et al. Genetic mapping and exome sequencing identify variants associated with five novel diseases. *PLoS One*. 2012;7(1). doi:10.1371/journal.pone.0028936

196. Van De Pol LA, Wolf NI, Van Weissenbruch MM, et al. Early-Onset Severe Encephalopathy with Epilepsy: The BRAT1 Gene Should Be Added to the List of Causes. *Neuropediatrics*. 2015;46(6):392-400. doi:10.1055/s-0035-1564791

197. Horn D, Weschke B, Knierim E, et al. BRAT1 mutations are associated with infantile epileptic encephalopathy, mitochondrial dysfunction, and survival into childhood. *Am J Med Genet Part A*. 2016;170(9):2274-2281. doi:10.1002/ajmg.a.37798

198. Srivastava S, Olson HE, Cohen JS, et al. BRAT1 mutations present with a spectrum of clinical severity.

Am J Med Genet Part A. 2016;170(9):2265-2273. doi:10.1002/ajmg.a.37783

199. Fernández-Jaén A, Álvarez S, So EY, et al. Mutations in BRAT1 cause autosomal recessive progressive encephalopathy: Report of a Spanish patient. *Eur J Paediatr Neurol*. 2016;20(3):421-425. doi:10.1016/j.ejpn.2016.02.009

200. Aglipay JA, Martin SA, Tawara H, Lee SW, Ouchi T. ATM activation by ionizing radiation requires BRCA1-associated BAAT1. *J Biol Chem*. 2006;281(14):9710-9718. doi:10.1074/jbc.M510332200

201. So EY, Ouchi T. BRAT1 deficiency causes increased glucose metabolism and mitochondrial malfunction. *BMC Cancer*. 2014. doi:10.1186/1471-2407-14-548

202. Saunders CJ, Miller NA, Soden SE, et al. Rapid Whole-Genome Sequencing for Genetic Diseases in Neonatal Care Units. *Sci Transl Med*. 2012;4(154). doi:10.1126/scitranslmed.3004041.

203. Saitsu H, Yamashita S, Tanaka Y, et al. Compound heterozygous BRAT1 mutations cause familial Ohtahara syndrome with hypertonia and microcephaly. *J Hum Genet*. 2014;59(12):687-690. doi:10.1038/jhg.2014.91

204. Straussberg R, Ganelin-Cohen E, Goldberg-Stern H, et al. Lethal neonatal rigidity and multifocal seizure syndrome - Report of another family with a BRAT1 mutation. *Eur J Paediatr Neurol*. 2015;19(2):240-242. doi:10.1016/j.ejpn.2014.11.004

205. Celik Y, Okuyaz C, Arslankoylu AE, Ceylaner S. Lethal neonatal rigidity and multifocal seizure syndrome with a new mutation in BRAT1. *Epilepsy Behav Case Reports*. 2017;8:31-32. doi:10.1016/j.ebcr.2017.05.003

206. Smith NJ, Lipsett J, Dibbens LM, Heron SE. BRAT1-associated neurodegeneration: Intra-familial phenotypic differences in siblings. *Am J Med Genet Part A*. 2016;170(11):3033-3038. doi:10.1002/ajmg.a.37853

207. Srivastava S, Naidu S. Epileptic Encephalopathy Due to BRAT1 Pathogenic Variants. *Pediatr Neurol Briefs*. 2016;30(12):16452482. doi:10.15844/pedneurbriefs-30-12-1

208. Mundy SA, Krock BL, Mao R, Shen JJ. BRAT1-related disease-identification of a patient without early lethality. *Am J Med Genet Part A*. 2016;170(3):699-702. doi:10.1002/ajmg.a.37434

209. Hanes I, Kozenko M, Callen DJ. Lethal Neonatal Rigidity and Multifocal Seizure Syndrome - A Misnamed Disorder? *Pediatr Neurol*. 2015;53(6):535-540. doi:10.1016/j.pediatrneurol.2015.09.002

210. Rim JH, Kim SH, Hwang IS, et al. Efficient strategy for the molecular diagnosis of intractable early-onset epilepsy using targeted gene sequencing. *BMC Med Genomics*. 2018;11(1):1-10. doi:10.1186/s12920-018-0320-7

211. Oatts JT, Duncan JL, Hoyt CS, Slavotinek AM, Moore AT. Inner retinal dystrophy in a patient with biallelic sequence variants in BRAT1. *Ophthalmic Genet*. 2017;6810(March):1-3. doi:10.1080/13816810.2017.1290118

212. Valence S, Cochet E, Rougeot C, et al. Exome sequencing in congenital ataxia identifies two new candidate genes and highlights a pathophysiological link between some congenital ataxias and early infantile epileptic encephalopathies. *Genet Med*. 2019;21(3):553-563. doi:10.1038/s41436-018-0089-2

213. Van Ommeren RH, Gao AF, Blaser SI, Chitayat DA, Hazrati LN. BRAT1 Mutation: The First Reported Case of Chinese Origin and Review of the Literature. *Neuropathol Exp Neurol*. 2018;77(12):1071-1078. doi:10.1093/jnen/nly093

ACKNOWLEDGMENTS

Un sentito grazie ad Enza Maria, che mi ha seguito durante lo svolgimento di questo progetto, contagiandomi con il suo entusiasmo e amore per la scienza. Farò tesoro di tutti gli insegnamenti, dei consigli, e dei momenti di confronto che mi hanno permesso di crescere e di riscoprire la bellezza e la complessità delle neuroscienze. Grazie per avermi saputo indirizzare assecondando le mie inclinazioni, per aver dato spazio alle mie proposte e avere stimolato la mia curiosità con spunti di riflessione sempre nuovi.

Parte del lavoro presentato in questa tesi è stato svolto in collaborazione con il Dott. Emma e con i gruppi di ricerca del Dott. Bertini, del Dott. Borgatti e del Dott. Vanacore. In tutti loro ho trovato degli interlocutori motivati, disponibili e sempre pronti al dialogo. Grazie per avermi mostrato la ricchezza che scaturisce dal confronto delle idee e dalla pluralità dei punti di vista.

Un ringraziamento particolare è riservato al Prof. Boltshauser, per aver condiviso con tutti noi la sua esperienza decennale sulle patologie cerebellari e al caro Andrea Poretti, colonna portante di questo progetto, per avermi fatto avvicinare al mondo delle neuroimmagini con la dedizione, la gentilezza e l'umiltà che rendono le persone grandi.

Il mio Dottorato è stato finanziato dall'Associazione Italiana Sindrome di Joubert e Atassie Congenite, (AISJAC), a cui vanno i miei ringraziamenti. Le testimonianze dei pazienti e delle loro famiglie sono state e continuano ad essere fonte di ispirazione e guida per questo lavoro.

Un pensiero speciale va a Monia, Roberta, Silvia, Alessia, Cristina, Romina, Simona, Antonella, Elisa, Vanessa, Marianna e Danila, con le quali ho condiviso in questi anni momenti preziosi di lavoro e di vita e che hanno fatto sì che il Lab309 diventasse una seconda casa allegra e accogliente. Se questo dottorato ha rappresentato un'esperienza preziosa dal punto di vista umano oltre che professionale, il merito è soprattutto vostro.

Infine, un grazie di cuore ad Alessandro, ai miei genitori e al resto della mia famiglia, e a Margherita, che continuano a sostenermi e incoraggiarmi in ogni scelta, lasciandomi libera anche di commettere i miei errori.

PUBLICATIONS

PEER REVIEWED JOURNAL ARTICLES

1. Bachmann-Gagescu R, Dempsey JC, Bulgheroni S, Chen ML, D'Arrigo S, Glass IA, Heller T, Héon E, Hildebrandt F, Joshi N, Knutzen D, Kroes HY, Mack SH, **Nuovo S**, Parisi MA, Snow J, Summers AC, Symons JM, Zein WM, Boltshauser E, Sayer JA, Gunay-Aygun M, Valente EM, Doherty D. Healthcare recommendations for Joubert syndrome. *Am J Med Genet A*. 2020;182(1):229-249. doi: 10.1002/ajmg.a.61399

2. Ginevrino M, Battini R, **Nuovo S**, Simonati A, Micalizzi A, Contaldo I, Serpieri V, Valente EM. A novel *IRF2BPL* truncating variant is associated with endolysosomal storage. *Mol Biol Rep*. 2020;47(1):711-714. doi:10.1007/s11033-019-05109-7

3. **Nuovo S**, Bacigalupo I, Ginevrino M, Battini R, Bertini SE, Borgatti R, Casella A, Micalizzi A, Nardella M, Romaniello R, Serpieri V, Zanni G, Valente EM, Vanacore N. Age and sex prevalence estimate of Joubert Syndrome in Italy. *Neurology*. 2020;94(8):e797-e801. doi: 10.1212/WNL.0000000000008996

4. Brandsma R, Verschuuren-Bemelmans CC, Amrom D, Barisic N, Baxter P, Bertini E, Blumkin L, Brankovic-Sreckovic V, Brouwer OF, Bürk K, Catsman-Berrevoets CE, Craiu D, de Coo IFM, Gburek J, Kennedy C, de Koning TJ, Kremer HPH, Kumar R, Macaya A, Micalizzi A, Mirabelli-Badenier M, Nemeth A, **Nuovo S**, Poll-The B, Lerman-Sagie T, Steinlin M, Synofzik M, Tijssen MAJ, Vasco G, Willemsen MAAP, Zanni G, Valente EM, Boltshauser E, Sival DA. A clinical diagnostic algorithm for early onset cerebellar ataxia. *Eur J Paediatr Neurol*. 2019;23(5):692-706. doi: 10.1016/j.ejpn.2019.08.004.

5. **Nuovo S**, Fuiano L, Micalizzi A, Battini R, Bertini E, Borgatti R, Caridi G, D'Arrigo S, Fazzi E, Fischetto R, Ghiggeri GM, Giordano L, Leuzzi V, Romaniello R, Signorini S, Stringini G, Zanni G, Romani M, Valente EM, Emma F. Impaired urinary concentration ability is a sensitive predictor of renal disease progression in Joubert syndrome. *Nephrol Dial Transplant*. 2018 Nov 6. doi: 10.1093/ndt/gfy333. [Epub ahead of print]

6. Arrigoni F, Romaniello R, Peruzzo D, Poretti A, Bassi MT, Pierpaoli C, Valente EM, **Nuovo S**, Boltshauser E, Huisman TAGM, Triulzi F, Borgatti R.The spectrum of brainstem malformations associated to mutations of the tubulin genes family: MRI and DTI analysis. *Eur Radiol*. 2019;29(2):770-782. doi: 10.1007/s00330-018-5610-0.

7. **Nuovo S**, Micalizzi A, D'Arrigo S, Ginevrino M, Biagini T, Mazza T, Valente EM. Between SCA5 and SCAR14: delineation of SPTBN2 p.R480W-associated phenotype. *Eur J Hum Genet*. 2018;26(7):928-929. doi: 10.1038/s41431-018-0158-7.

8. De Mori R, Romani M, D'Arrigo S, Zaki MS, Lorefice E, Tardivo S, Biagini T, Stanley V, Musaev D, Fluss J, Micalizzi A, **Nuovo S**, Illi B, Chiapparini L, Di Marcotullio L, Issa MY, Anello D, Casella A, Ginevrino M, Leggins AS, Roosing S, Alfonsi R, Rosati J, Schot R, Mancini

GMS, Bertini E, Dobyns WB, Mazza T, Gleeson JG, Valente EM. Hypomorphic Recessive Variants in SUFU Impair the Sonic Hedgehog Pathway and Cause Joubert Syndrome with Cranio-facial and Skeletal Defects. *Am J Hum Genet*. 2017;101(4):552-63.doi: 10.1016/j.ajhg.2017.08.017.

9. Romaniello R, Arrigoni F, Panzeri E, Poretti A, Micalizzi A, Citterio A, Bedeschi MF, Berardinelli A, Cusmai R, D'Arrigo S, Ferraris A, Hackenberg A, Kuechler A, Mancardi M, **Nuovo S**, Oehl-Jaschkowitz B, Rossi A, Signorini S, Tüttelman F, Wahal D, Hehr U, Boltshauser E, Bassi MT, Valente EM, Borgatti R. Tubulin-related cerebellar dysplasia: definition of a distinct pattern of cerebellar malformation. *Eur Radiol*. 2017;27(12):5080-92. doi: 10.1007/s00330-017-4945-2.

BOOK CHAPTERS

1. Valente EM, **Nuovo S**, Doherty D. Genetics of cerebellar disorders. *Handb Clin Neurol*. 2018;154:267-286. doi: 10.1016/B978-0-444-63956-1.00016-3.